

VOLUME 79

JANUARY 30, 1975

NUMBER 3

JPCHAX

---

THE JOURNAL OF

PHYSICAL

CHEMISTRY

---

PUBLISHED BIWEEKLY BY THE AMERICAN CHEMICAL SOCIETY

# Keep up with today's

## 1. ADVANCES IN RADIATION CHEMISTRY, VOL. 4

Edited by **Milton Burton** and **John L. Magee**, both of University of Notre Dame

The volume reflects the current thrust toward refined elegance of understanding of the behavior of the displaced electron. Includes major contributions by prominent investigators.

Partial Contents: Ionization in Nonpolar Molecular Liquids by High-Energy Electrons. Electron Processes in Radiation Chemistry of Disordered Materials. Trapped Electrons in Organic Glasses. Radiation Chemistry of Polyethylene.

1974 410 pages \$31.50

## 2. FINITE GROUPS AND QUANTUM THEORY

By **D. B. Chesnut**, Duke University

Presents in a readable way the basic mathematical ideas and structure behind the theory of point groups, emphasizing its basic use and application in quantum mechanics.

Partial Contents: Sets. Groups. The Partitioning and Factoring of Groups. Mapping and Groups. Permutation Groups. Vectors, Matrices, and Transformations. Representations and Their Construction. Irreducible Representations.

1974 254 pages \$14.95

## 3. SOLID STATE AND MOLECULAR THEORY: A SCIENTIFIC BIOGRAPHY

By **John C. Slater**, University of Florida

The story of the development of the science and technology of the study of atoms, molecules and solids from 1923 to 1973 with particular attention to a very recent feature of the theory, the  $X\alpha$ -SCF method (self-consistent field method of approximation) as the author was associated with these advances. 1975 360 pages (approx.) \$18.95

## 4. WILLIAM DAVID COOLIDGE: A CENTENARIAN AND HIS WORK

By **Herman A. Liebhafsky**, Texas A & M University  
Tells the exciting story of the career of Coolidge, an early exponent of the experimental approach, and describes his work with ductile tungsten, which led to the world's first successful industrial research laboratory. 1974 96 pages \$6.95

## 5. ADVANCES IN CHEMICAL PHYSICS, VOL. 27: Aspects of the Study of Surfaces

Edited by **I. Prigogine**, University of Brussels, and **Stuart A. Rice**, The University of Chicago

Partial Contents: Determination of the Structure and Properties of Solid Surfaces by Electron Diffraction and Emission. Electron Spectroscopy of Chemisorption on Metals. Surface Plasma Oscillations and Related Surface Effects in Solids. Theory of Dynamical Properties of Dielectric Surfaces. Some Comments on the Electronic Properties of Liquid Metal Surfaces. 1974 668 pages (app.) \$32.50

## 6. THE EXCITED STATE IN CHEMICAL PHYSICS

Edited by **J. William McGowan**, The University of Ontario, Canada

Reflects the most recent developments in excited-state research, emphasizing neutral-neutral collisions.

Partial Contents: The Production of Excited Species in Simple Chemical Reactions. Potential Energy Surface Considerations for Excited State Reactions. Vibrational and Rotational Excitation in Gaseous Collisions. Sensitized Fluorescence and Quenching. 1975 432 pages (approx.) \$25.50

## 7. POLYMER HANDBOOK, 2nd Ed.

Edited by **Johannes Brandrup**, **Farbwerke Hoechst** and **E. H. Immergut**, with the collaboration of **W. McDowell**

A completely revised and updated edition of this comprehensive collection of data and constants needed by polymer chemists and physicists in the theoretical and experimental polymer work.

Contents: Fundamental Principles. The Bivalent Constitutional Repeating Unit. Bivalent Constitutional Repeating Units Having Two or More Substituents. Systematic and Source Name for Common Polymers.

1975 1408 pages (approx.) \$34.50

## 8. CLASSICAL DYNAMICS: A MODERN PERSPECTIVE

By **E. C. G. Sudarshan**, University of Texas, Austin and **N. Mukunda**, Indian Institute of Science, Bangalore

Incorporating insights gained over the past several decades, the authors present the essential principles of classical dynamics and demonstrate a number of key results originally considered only in the context of quantum theory and particle physics have their foundations in classical dynamics. 1974 615 pages \$24.95

## 9. ADVANCES IN PHOTOCHEMISTRY, VOL. 9

Edited by **J. N. Pitts, Jr.**, University of California, Riverside, **George S. Hammond**, University of California, Santa Cruz, and **Klaus Gollnick**, University of Munich

Exploring the frontiers of photochemistry through chapters written by its pioneers, this volume includes: Application of Electron Spin Resonance Spectroscopy to Photochemistry; Primary Processes and Energy Transfer: Consistent Terms and Definitions; Solution Phase Photochemistry of Cyclobutanones; Phosphorescence-Microwave Multiple Resonance Spectroscopy; and Photochemistry of the Troposphere.

1974 566 pages \$24.95

## 10. EQUILIBRIUM STATISTICAL MECHANICS, 2nd Ed.

By **Frank C. Andrews**, University of California, Santa Cruz

Clearly explains the fundamentals of statistical mechanics vital to all students of science and technology.

Partial Contents: Basic Theory. Quantum Statistics: Thermodynamics of Ideal Gases. General Quantum Statistical Thermodynamics. Semiclassical Statistical Mechanics.

1975 255 pages \$11.95

# breakthroughs in your field

Forthcoming:

## MEMBRANES, DISSIPATIVE STRUCTURES AND EVOLUTION

Edited by **G. Nicolis** and **R. Lefever**, both of the University of Brussels

Contains a number of original or review papers discussing the relationship between the biological order and thermodynamics, systematically presented in book form for the first time.

Partial Contents: Stability and Self-Organization in Open Systems. Dissipative Instabilities, Structure, and Evolution. Studies in Dissipative Phenomena with Biological Applications. Finite Fluctuations, Nonlinear Thermodynamics, and Far-From-Equilibrium Transitions between Multiple Steady States. 1975 464 pages (approx.) In Press

## EQUILIBRIUM AND NONEQUILIBRIUM STATISTICAL MECHANICS

By **Radu C. Balescu**, University of Brussels

Leads the professional or the student in statistical mechanics from elementary concepts to some of the most recent developments giving equal weight to both equilibrium and nonequilibrium theory.

Partial Contents: Review of Hamiltonian Dynamics. Statistical Ensembles. Reduced Distribution Functions. Equilibrium Ensembles and Thermodynamics. Equilibrium Properties of Ideal Systems. Slightly Nonideal Systems in Equilibrium. 1975 816 pages (approx.) \$29.95

## OPTICAL RESONANCE AND TWO-LEVEL ATOMS

By **L. Allen**, University of Sussex and **J. H. Eberly**, University of Rochester

Provides a coherent description of the various optical resonance phenomena developed from first principles within a single framework.

Partial Contents: Classical Theory of Resonance Optics. The Optical Bloch Equation. Two-Level Atoms in Steady Fields. Pulse Propagation. Pulse Propagation Experiments. Saturation Phenomena. Quantum Electrodynamics and Spontaneous Emission. 1975 224 pages (approx.) \$19.95

## COMPUTER AIDED EXPERIMENTATION: INTERFACING TO MINICOMPUTERS

By **Jules Finkel**, Weizmann Institute of Science, Israel

Will acquaint scientists and engineers with the basic concepts and techniques needed to specify, design, and implement experiments that are computer controlled.

Partial Contents: Analog Signals. Instrumentation Amplifiers. Analog to Digital Conversion. Telemetry: Remote Sensing. Position Encoding. Analog Recording. Interface Logic Design. Computer Digital Inputs. Digital Output. 1975 496 pages (approx.) \$24.95

Available at your bookstore or mail this coupon to:

WILEY-INTERSCIENCE, Dept. 552, Box 4569  
Grand Central Station, New York, N.Y. 10017  
In Canada: 22 Worcester Road, Rexdale, Ontario

Mail coupon to—

WILEY-INTERSCIENCE, Dept. 552, Box 4569  
Grand Central Station, New York, N.Y. 10017



Please send me the book(s) I have checked below to read and use free for 10 days. At the end of that time, if I am satisfied with my order and want to keep it, I will send you the amount indicated for each book received plus postage and handling. Otherwise, I will return the order and owe nothing.

- |   |  |
|---|--|
| <input type="checkbox"/> 1 (1 12543-1)  | <input type="checkbox"/> My check (money order) for \$_____ is enclosed.                 |
| <input type="checkbox"/> 2 (1 15445-8)  | <input type="checkbox"/> Please bill me. (Restricted to continental U.S.)                |
| <input type="checkbox"/> 3 (1 79681-6)  | <input type="checkbox"/> Please send me a list of local bookstores carrying your titles. |
| <input type="checkbox"/> 4 (1 53430-7)  | Name _____   |
| <input type="checkbox"/> 5 (1 69932-2)  | Affiliation _____  |
| <input type="checkbox"/> 6 (1 58425-8)  | Address _____  |
| <input type="checkbox"/> 7 (1 09804-3)  | City _____ State _____ Zip _____   |
| <input type="checkbox"/> 8 (1 83540-4)  |  |
| <input type="checkbox"/> 9 (1 69092-9)  | Please add state and local taxes where applicable.                                       |
| <input type="checkbox"/> 10 (1 03123-2) | Prices subject to change without notice.   |

092 A 4910-WI

# THE JOURNAL OF PHYSICAL CHEMISTRY

**BRYCE CRAWFORD, Jr.**, *Editor*  
**STEPHEN PRAGER**, *Associate Editor*  
**ROBERT W. CARR, Jr.**, **FREDERIC A. VAN-CATLEDGE**, *Assistant Editors*

**EDITORIAL BOARD:** C. A. ANGELL (1973-1977), F. C. ANSON (1974-1978), V. A. BLOOMFIELD (1974-1978), J. R. BOLTON (1971-1975), L. M. DORFMAN (1974-1978), H. L. FRIEDMAN (1975-1979), E. J. HART (1975-1979), W. J. KAUZMANN (1974-1978), R. L. KAY (1972-1976), D. W. McCLURE (1974-1978), R. M. NOYES (1973-1977), J. A. POPLER (1971-1975), B. S. RABINOVITCH (1971-1975), S. A. RICE (1969-1975), F. S. ROWLAND (1973-1977), R. L. SCOTT (1973-1977), A. SILBERBERG (1971-1975), J. B. STOTHERS (1974-1978), W. A. ZISMAN (1972-1976)

AMERICAN CHEMICAL SOCIETY, 1155 Sixteenth St., N.W., Washington, D.C. 20036

## Books and Journals Division

**JOHN K CRUM** *Director*  
**RUTH REYNARD** and **VIRGINIA E. STEWART** *Assistants to the Director*

**CHARLES R. BERTSCH** *Head, Editorial Processing Department*  
**D. H. MICHAEL BOWEN** *Head, Journals Department*  
**BACIL GUILLEY** *Head, Graphics and Production Department*  
**SELDON W. TERRANT** *Head, Research and Development Department*

©Copyright, 1975, by the American Chemical Society. Published biweekly by the American Chemical Society at 20th and Northampton Sts., Easton, Pa. 18042. Second-class postage paid at Washington, D.C., and at additional mailing offices.

All manuscripts should be sent to *The Journal of Physical Chemistry*, Department of Chemistry, University of Minnesota, Minneapolis, Minn. 55455.

*Additions and Corrections* are published once yearly in the final issue. See Volume 78, Number 26 for the proper form.

*Extensive or unusual alterations in an article after it has been set in type are made at the author's expense*, and it is understood that by requesting such alterations the author agrees to defray the cost thereof.

The American Chemical Society and the Editor of *The Journal of Physical Chemistry* assume no responsibility for the statements and opinions advanced by contributors.

Correspondence regarding accepted copy, proofs, and reprints should be directed to Editorial Processing Department, American Chemical Society, 20th and Northampton Sts., Easton, Pa. 18042. Department Head: CHARLES R. BERTSCH. Assistant Department Head: MARIANNE C. BROGAN. Assistant Editor: CELIA B. MCFARLAND. Editorial Assistant: JOSEPH E. YURVATI.

Advertising Office: Centcom, Ltd., 50 W. State St., Westport, Conn. 06880.

## Business and Subscription Information

Send all new and renewal subscriptions *with payment* to: Office of the Controller, 1155 16th Street, N.W., Washington, D.C. 20036. Subscriptions should be renewed promptly to avoid a break in your series. All correspondence and telephone calls regarding

changes of address, claims for missing issues, subscription service, the status of records, and accounts should be directed to Manager, Membership and Subscription Services, American Chemical Society, P.O. Box 3337, Columbus, Ohio 43210. Telephone (614) 421-7230. For microfiche service, contact ACS Journals Department, 1155 16th St. N.W., Washington, D.C. 20036. Telephone (202) 872-4444.

On changes of address, include both old and new addresses with ZIP code numbers, accompanied by mailing label from a recent issue. Allow four weeks for change to become effective.

Claims for missing numbers will not be allowed (1) if loss was due to failure of notice of change in address to be received before the date specified, (2) if received more than sixty days from date of issue plus time normally required for postal delivery of journal and claim, or (3) if the reason for the claim is "issue missing from files."

Subscription rates (hard copy or microfiche) in 1975: \$20.00 for 1 year to ACS members; \$80.00 to nonmembers. Extra postage \$4.50 in Canada and PUAS, \$5.00 other foreign. Supplementary material (on microfiche only) available on subscription basis, 1975 rates: \$15.00 in U.S., \$19.00 in Canada and PUAS, \$20.00 elsewhere. All microfiche airmailed to non-U.S. addresses; air freight rates for hard-copy subscriptions available on request.

Single copies for current year: \$4.00. Rates for back issues from Volume 56 to date are available from the Special Issues Sales Department, 1155 Sixteenth St., N.W., Washington, D.C. 20036.

Subscriptions to this and the other ACS periodical publications are available on microfilm. For information on microfilm write Special Issues Sales Department at the address above.

Notice to Authors last printed in the issue of January 16, 1975

# THE JOURNAL OF PHYSICAL CHEMISTRY

Volume 79, Number 3 January 30, 1975

JPCA<sub>x</sub> 79(3) 187-294 (1975)

ISSN 0022-3654

Direct and Triplet-Benzene-Sensitized Photolysis of Perfluorocyclobutanone at Low Pressures ..... Roger S. Lewis and Edward K. C. Lee*	187
Ring Opening and Isomerization of a Series of Chemically Activated Cycloalkyl Radicals ..... S. E. Stein and B. S. Rabinovitch*	191 ■
Phenolic-OH Torsional Frequency as a Probe for Studying $\pi$ -Electron Distortions in Aromatic Systems ..... William G. Fateley,* Gerald L. Carlson, and Freeman F. Bentley	199 ■
Thermal Dissociation of Cyanogen Bromide in Shock Waves ..... K. Tabayashi, O. Kajimoto, and T. Fueno*	204
Picosecond Pulse Radiolysis. V. Yield of Electrons in Irradiated Aqueous Solution with High Concentrations of Scavenger ..... R. K. Wolff, J. E. Aldrich, T. L. Penner, and J. W. Hunt*	210
An Infrared Study of the Photolysis of Trifluoromethyl Hypofluorite and Hypochlorite in Argon Matrices at 8°K ..... Richard R. Smardzewski and W. B. Fox*	219
The Lippmann Equation and the Ideally Polarizable Electrode ..... Jean-Pierre Badiali and Jerry Goodisman*	223
Conductivities and Thermodynamics of Dissociation of Fluorenyl Salts and Their Complexes with Dimethyldibenzo-18-crown-6 ..... T. E. Hogen-Esch and J. Smid*	233
Thermodynamics of Aggregation of Long Chain Carboxylic Acids in Benzene ..... O. Levy,* G. Y. Markovits, and I. Perry	239
Effect of Zinc, Gallium, and Germanium Ions on the Structural and Magnetic Properties of Nickel Ions Supported on Alumina ..... A. Cimino, M. Lo Jacono, and M. Schiavello*	243
Crystal Structures of Three Solid Solution Phases of Ammonium Nitrate and Potassium Nitrate ..... James R. Holden* and Charles W. Dickinson	249 ■
Electrical Conductances of Some Aqueous Rare Earth Electrolyte Solutions at 25°. III. The Rare Earth Nitrates ..... J. A. Reed and F. H. Spedding*	257 ■
A Limiting Law for the Conductance of the Rod Model of a Salt-Free Polyelectrolyte Solution ..... Gerald S. Manning	262
Electrical Conductivity of Aqueous Solutions of Salts of Polystyrenesulfonic Acid with Univalent and Divalent Counterions ..... Jan C. T. Kwak* and R. C. Hayes	265
Electrical Conductivity of Aqueous Solutions of Monovalent Salts of Polystyrenesulfonate ..... Janet Szymczak, Peter Holyk, and Paul Ander*	269 ■
Absolute Viscosity of D <sub>2</sub> <sup>18</sup> O between 15 and 35° ..... A. I. Kudish* and D. Wolf	272
Chemical Relaxation Studies of Micellar Equilibria ..... J. Lang, C. Tondre, R. Zana,* R. Bauer, H. Hoffmann, and W. Ulbricht	276
Depolarization Thermocurrents Study of Polymers above the Glass Transition Temperature ..... C. Lacabanne* and D. Chatain	283
A Multiple-Equilibrium Model for the Micellization of Ionic Surfactants in Nonaqueous Solvents ..... Norbert Muller	287

ห้องสมุด กรมวิทยาศาสตร์  
2.7 18.11.2518

## COMMUNICATIONS TO THE EDITOR

- Emission Spectra of Monochlorobenzene and Benzyl Chloride in Solid Matrix  
 . . . T. Ichimura,\* T. Hikida, and Y. Mori 291
- A Kinetics Study of the Reaction of the OH Free Radical with Aromatic Compounds. I.  
 Absolute Rate Constants for Reaction with Benzene and Toluene at 300°K  
 . . . D. D. Davis,\* W. Bollinger, and S. Fischer 293

■ Supplementary and/or miniprint material for this paper is available separately, in photocopy or microfiche form. Ordering information is given in the paper.

\*In papers with more than one author, the asterisk indicates the name of the author to whom inquiries about the paper should be addressed.

### AUTHOR INDEX

- |                       |                        |                         |                         |
|-----------------------|------------------------|-------------------------|-------------------------|
| Aldrich, J. E., 210   | Fueno, T., 204         | Lacabanne, C., 283      | Schiavello, M., 243     |
| Ander, P., 269        | Goodisman, J., 223     | Lang, J., 276           | Smardzewski, R. R., 219 |
| Badiali, J.-P., 223   | Hayes, R. C., 265      | Lee, E. K. C., 187      | Smid, J., 233           |
| Bauer, R., 276        | Hikida, T., 291        | Levy, O., 239           | Spedding, F. H., 257    |
| Bentley, F. F., 199   | Hoffmann, H., 276      | Lewis, R. S., 187       | Stein, S. E., 191       |
| Bollinger, W., 293    | Hogen-Esch, T. E., 233 | Lo Jacono, M., 243      | Szymczak, J., 269       |
| Carlson, G. L., 199   | Holden, J. R., 249     | Manning, G. S., 262     | Tabayashi, K., 204      |
| Chatain, D., 283      | Holyk, P., 269         | Markovits, G. Y., 239   | Tondre, C., 276         |
| Cimino, A., 243       | Hunt, J. W., 210       | Mori, Y., 291           | Ulbricht, W., 276       |
| Davis, D. D., 293     | Ichimura, T., 291      | Muller, N., 287         | Wolf, D., 272           |
| Dickinson, C. W., 249 | Kajimoto, O., 204      | Penner, T. L., 210      | Wolff, R. K., 210       |
| Fateley, W. G., 199   | Kudish, A. I., 272     | Perry, I., 239          | Zana, R., 276           |
| Fischer, S., 293      | Kwak, J. C. T., 265    | Rabinovitch, B. S., 191 |                         |
| Fox, W. B., 219       |                        | Rard, J. A., 257        |                         |

# THE JOURNAL OF PHYSICAL CHEMISTRY

Registered in U. S. Patent Office © Copyright, 1975, by the American Chemical Society

VOLUME 79, NUMBER 3 JANUARY 30, 1975

## Direct and Triplet-Benzene-Sensitized Photolysis of Perfluorocyclobutanone at Low Pressures

Roger S. Lewis and Edward K. C. Lee\*

Department of Chemistry, University of California, Irvine, California 92664 (Received July 18, 1974)

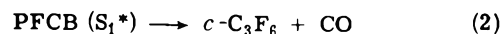
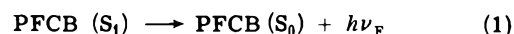
Publication costs assisted by the Office of Naval Research

Perfluorocyclobutanone (PFCB) has been produced in its triplet state ( $T_1$ ) by the triplet benzene ( $^3B_{1u}$ , 84.5 kcal/mol) sensitization method, and the  $T_1$  state decomposes mainly to  $c$ - $C_3F_6$  and CO. Investigation of the direct photolysis of PFCB at low pressure (<5 Torr) indicates that at low excitation energies,  $S_1 \rightarrow T_1$  intersystem crossing predominates and at high energies,  $S_1 \rightarrow S_0$  internal conversion predominates. The internally converted PFCB ( $S_0^*$ ) decomposes unimolecularly to  $C_2F_4$  and  $CF_2CO$ , and the latter product further decomposes to  $CF_2$  and CO. The total product quantum yield of the "primary" processes is unity at low pressure. Our new mechanism is similar to the mechanism proposed earlier for cyclobutanone photodecomposition but is not compatible with the singlet mechanism proposed by Phillips based on the photodecomposition study carried out at higher pressures.

### Introduction

The 0-0 band of the first singlet  $n-\pi^*$  transition is located at  $\sim 4100$  Å (70 kcal/mol), and the fluorescence decay time ( $\tau_F$ ) of an "isolated" molecule of perfluorocyclobutanone (PFCB) in its first excited singlet state ( $S_1$ ) with little vibrational excitation energy has been determined recently to be  $\sim 110$  nsec.<sup>1</sup> Both fluorescence quantum yield ( $\Phi_F$ ) and  $\tau_F$  at low pressure (<0.2 Torr) remain approximately constant from exciting wavelength ( $\lambda_{ex}$ ) of 4200 to 3800 Å. Below  $\lambda_{ex}$  3800 Å (75 kcal/mol), these quantities gradually decrease and they are diminished by a factor of 100 at  $\lambda_{ex}$  3480 Å (82 kcal/mol), indicating that a new nonradiative channel has become dominant. Since a qualitatively similar but more drastic effect of the excess vibrational energy was found for cyclobutanone,<sup>2</sup> we have decided to investigate the photodecomposition processes of PFCB at low pressures where an "isolated" molecule behavior can be maintained and to compare the decomposition mechanism of PFCB with that of cyclobutanone.<sup>2-4</sup> We believe that, in the earlier photolysis study of PFCB carried out at high pressures (<10 Torr) by Phillips,<sup>5</sup> the vibrationally hot PFCB ( $S_1^*$ ) and PFCB ( $S_0^*$ ) could easily have been collisionally quenched out unknowingly. On the basis of the fluorescence study of PFCB,<sup>1</sup> we expect that at low vibrational excitation energy, PFCB ( $S_1$ ) would undergo  $S_1 \rightarrow$

$T_1$  intersystem crossing and at high vibrational excitation energy PFCB ( $S_1^*$ ) would undergo  $S_1 \rightarrow S_0$  internal conversion in analogy with cyclobutanone.<sup>2-4</sup> On the contrary, Phillips had proposed earlier a primary photodecomposition mechanism involving only PFCB ( $S_1$ ) as shown by<sup>5</sup>



### Experimental Section

A sample of PFCB was provided by Dr. D. C. England of E. I. du Pont de Nemours and Co. It was stored with  $P_2O_5$  in an evacuated Pyrex sample tube at liquid nitrogen temperature. Samples were filled on a brass vacuum line equipped with a capacitance manometer (MKS Baratron pressure head Model No. 145 AHS-10) and a Bourdon gauge (Wallace and Tiernan Model No. 145). The sample was purified by pumping off volatile impurities at 2-propanol-liquid nitrogen slush temperatures. A barrel-shaped silica cell was used which had an optical pathlength of 14.7 cm, a 484-ml volume, two 5.0-cm diameter flat end windows, a cold finger, and a Teflon vacuum stopcock. In early experiments, the photolysis cell was used without an exter-

nal light shield, but it became necessary to paint the cell black. Photolysis was carried out with a Bausch and Lomb high-intensity monochromator and an Osram 200-W super-pressure mercury lamp at a spectral band width of 2 nm at 313, 334, 366, and 405 nm.

Photolysis at 325.0 nm was carried out with a He-Cd laser (Spectra Physics Model 185). A collimated light beam approximately 2 cm in diameter entered the photolysis cell. The intensity of the actinic light was measured with a thermopile detector system (Hewlett-Packard Models 3880A and 8334A), and the amount of the absorbed intensity was calculated from Beer's law, since the fraction of absorption was typically less than 1%. In order to double check the above actinometric technique, a chemical actinometer run was made with the photolysis of cyclobutanone at 305 nm which gives the total hydrocarbon quantum yield of  $C_2H_4$ ,  $C_3H_6$ , and  $c-C_3H_6$  to be unity.

After photolysis, fluorocarbons were condensed into an evacuated injection loop at liquid nitrogen temperature; or in some runs, CO was condensed into an injection loop containing activated silica gel at liquid nitrogen temperature while fluorocarbons were condensed in the cold finger of the photolysis cell at liquid nitrogen temperature.

Product analysis was carried out by conventional gas chromatography using a thermistor detector cell.<sup>3</sup> Fluorocarbons were separated on a 50-ft fluorolube column (0.25-in. o.d., stainless steel, 28% by weight of FS-5 oil on 30/60 mesh Chromosorb P-HMDS) at room temperature. The elution times of air,  $C_2F_4$ ,  $c-C_3F_6$ , and  $C_3F_6$  were 14.6, 20.0, 28.0, and 31.0 min, respectively. The molar sensitivity of  $C_2F_4$  and  $C_3F_6$  were  $3.0 \times 10^{10}$  and  $4.6 \times 10^{10}$  counts/mol, respectively, and we assumed that  $C_3F_6$  and  $c-C_3F_6$  have the same sensitivity. CO was analyzed on a 9-ft activated charcoal column (0.25-in. o.d.) at room temperature.

A Perkin-Elmer Hitachi MPF-2A spectrophotofluorimeter was employed to record fluorescence emission intensity in the benzene fluorescence quenching studies. Benzene photosensitization at 253.7 nm was obtained using a low-pressure mercury lamp (Mineralight Model R51, Ultraviolet Products, Inc.) with a Corning CS-7-54 filter and a 1.0-cm thick D<sub>3</sub>P solution filter to isolate the resonance line. However, an appreciable intensity of the 366-nm line (~5%) was transmitted. The same cell as used in direct photolysis experiments was used in this series of runs. The actinometry technique of Cundall<sup>6a</sup> was employed for quantum counting of the excited benzenes, and the quantum yield of *trans*-2-butene produced from the triplet benzene (<sup>3</sup>B<sub>1u</sub>) sensitized isomerization of *cis*-2-butene was taken as 0.36.<sup>6b</sup> Benzene and *cis*-2-butene pressure were both 1.0 Torr.

## Results

The direct photolysis product yields at  $\lambda_{ex}$  313, 334, 366, and 405 nm are tabulated as a function of pressure of PFCB in Table I. All photolyses in this series were carried out at constant light intensity with experimental error of ~5% for a period of 60 min at each wavelength. The relative quantum yields of  $c-C_3F_6$ ,  $\Phi_{rel}(c-C_3F_6)$ , can be obtained by dividing the observed yield of  $c-C_3F_6$  with the pressure of PFCB, and they are nearly independent of pressure over a wide range, since the fraction of light absorbed is nearly proportional to the pressure of PFCB below 5 Torr and the yield is roughly proportional to the pressure of PFCB. On the other hand, it is readily observable that at  $\lambda_{ex}$  366 and 405 nm the relative quantum yields of  $C_2F_4$ ,  $\Phi_{rel}(C_2F_4)$ , are

TABLE I: Product Distribution in Direct Photolysis of PFCB<sup>a</sup>

Run No.	P, Torr	Product yields, 10 <sup>-9</sup> mol		
		C <sub>2</sub> F <sub>4</sub>	c-C <sub>3</sub> F <sub>6</sub>	C <sub>3</sub> /C <sub>2</sub>
$\lambda_{ex}$ 313 nm; $I_0 = 2.9 \times 10^{14}$ photons/sec				
107	0.30	5.3	Trace	
101	1.00	17.5	4.6	0.27
105	3.0	47.7	8.0	0.17
102	5.0	77.9	18.9	0.24
$\lambda_{ex}$ 334 nm; $I_0 = 1.4 \times 10^{14}$ photons/sec				
129	0.20	4.6		
126	0.50	11.0	4.5	0.41
125	1.00	19.7	6.3	0.32
127	3.0	49.7	20.7	0.42
130	5.0	50.1		
$\lambda_{ex}$ 366 nm; $I_0 = 5.4 \times 10^{14}$ photons/sec				
80	0.030	7.9	4.0	0.51
79	0.050	13.6	6.5	0.48
77	0.100	24.0	12.2	0.51
76	0.20	33.6	19.7	0.59
75	0.50	61.6	70.3	1.14
71	1.00	63.5	145	2.28
74	1.00	72.7	146	2.01
78	5.0	92.3	760	8.2
$\lambda_{ex}$ 405 nm; $I_0 = 4.0 \times 10^{14}$ photons/sec				
111	0.050	Trace	4.0	
110	0.100	1.9	10.0	5.3
112	0.20	4.0	19.1	4.8
109	0.30	3.4	35.0	10.3
108	0.50	3.9	45.8	11.7
113	1.00	4.1	94.4	23.0

<sup>a</sup> The accuracy of the product yield measurement is  $\pm 1 \times 10^{-9}$  mol.

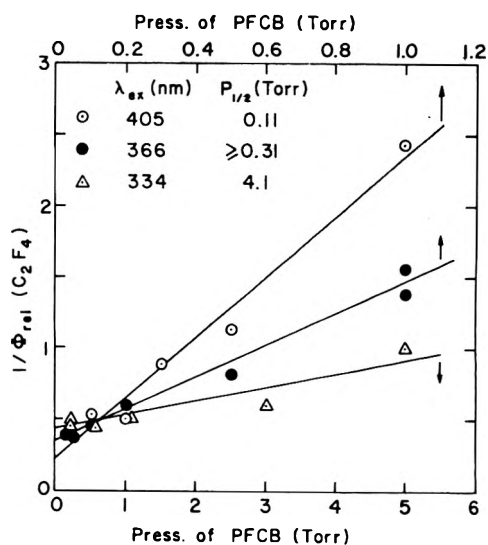


Figure 1. Stern-Volmer plot of the  $C_2F_4$  yield vs. pressure of PFCB.

monotonically decreasing at higher pressures of PFCB, although this pressure quenching effect is somewhat less obvious at  $\lambda_{ex}$  334 nm. The Stern-Volmer plots of  $C_2F_4$  yields in Figure 1 are linear within experimental error, and display an increasing half-pressure,  $P_{1/2}$ , with increasing pho-

toexcitation energy. Photolysis at  $\lambda_{\text{ex}}$  313 nm should show similar pressure dependence, if the measurements were made at much higher pressures of PFCB.

Absolute product quantum yields for  $\text{C}_2\text{F}_4$ ,  $c\text{-C}_3\text{F}_6$ , and CO are shown in Table II. The light intensities were measured before and after photolysis and were reproducible to  $\sim 3\%$ . Photolysis times of 180 min were used at all wavelengths except 60 min at 325.0 nm. The values listed in Table II have been normalized to the cyclobutanone actinometry standard<sup>8</sup> for which the total hydrocarbon product yields is known to be unity.<sup>9</sup> The quantum yield measured with the absolute power meter was about 7% too high, which is within the instrumental specification of the absolute error. Notice that the mass balance between the value of  $\Phi(\text{CO})$  and the value of  $[\Phi(c\text{-C}_3\text{F}_6) + \frac{2}{3}\Phi(\text{C}_2\text{F}_4)]$  is fair, agreeing to within the overall experimental error.

The technique of triplet benzene sensitization<sup>4,10</sup> was used to elucidate the decomposition mechanism of the triplet PFCB ( $T_1$ ). The experimental results are shown in Table III. Since the filter combination used affords a small "window" for 366-nm light ( $\sim 5\%$  of the mercury resonance line), the observed product yields were corrected for the direct photolysis contribution due to the 366-nm radiation and the true sensitized yields are displayed above. The Stern-Volmer plot of the benzene fluorescence intensity due to quenching of the singlet benzene ( $^1\text{B}_{2u}$ ) by PFCB is shown in Figure 2, indicating that the half-quenching pressure,  $P_{1/2}$ , is 1.0 Torr.

Therefore, at 1.0 Torr of PFCB, 50% of the  $^1\text{B}_{2u}$  benzene produced is quenched by PFCB ( $S_0$ ) to give PFCB ( $S_1^*$ ), which means that only 50% of the  $^1\text{B}_{2u}$  benzene is left to undergo its usual unimolecular relaxation processes.<sup>4,10</sup> These quantities of the singlet-singlet quenching quantum yield,  $\Phi_s(\text{calcd})$  in the presence of PFCB are listed in Table III. Since it is known that for  $^1\text{B}_{2u}$  benzene  $^1\text{B}_{2u} \rightarrow ^3\text{B}_{1u}$  intersystem crossing quantum yield is  $\sim 0.72$ ,<sup>6</sup> we expect that the quantum yield of the  $^3\text{B}_{1u}$  benzene in the presence of 1.0 Torr of PFCB is only 0.36. Therefore, this quantity is listed as  $\Phi_{T,\text{max}}$  in Table III, meaning that it is the upper limit of the quantum yield for PFCB ( $T_1$ ) which can be produced by a triplet-triplet energy transfer from the  $^3\text{B}_{1u}$  benzene in the presence of a given pressure of PFCB. Quantum yields due to sensitizations of  $\text{C}_2\text{F}_4$  and  $c\text{-C}_3\text{F}_6$ ,  $\Phi_{\text{sens}}(\text{C}_2\text{F}_4)$  and  $\Phi_{\text{sens}}(c\text{-C}_3\text{F}_6)$ , respectively, are shown also in Table III.

## Discussion

**Benzene Sensitization.** The energetics and kinetics of the singlet-singlet and the triplet-triplet energy transfer processes involving the electronically excited benzenes have been discussed in detail elsewhere,<sup>10</sup> and no repetition is necessary here. The energy of the singlet benzene ( $^1\text{B}_{2u}$ ) is 109 kcal/mol and the energy of the singlet PFCB ( $S_1$ ) is  $\sim 70$  kcal/mol.<sup>1</sup> If the average energy of the PFCB ( $S_1^*$ ) produced by the singlet-singlet energy transfer process is assumed to be  $\sim 90$  kcal/mol,<sup>4,10</sup> it corresponds to 313-nm photoexcitation. According to the results shown in Tables I and II, the  $\text{C}_3/\text{C}_2$  ratio at  $\lambda_{\text{ex}}$  313 nm is  $\sim 0.2$  and that ratio at  $\lambda_{\text{ex}}$  325 nm = 0.07 where the accuracy is somewhat better, indicating that about  $\frac{9}{10}$  of the product is  $\text{C}_2\text{F}_4$ . Hence, we expect  $\Phi_{\text{sens}}(\text{C}_2\text{F}_4)$  to be about  $\frac{9}{10}$  of the value of  $\Phi_s(\text{calcd})$  and this relationship is approximately obeyed within the uncertainty of experiment. This implies that nearly all of the sensitized yield of  $\text{C}_2\text{F}_4$  comes from the singlet-singlet energy transfer and only a tiny fraction of the sensi-

TABLE II: Product Quantum Yields<sup>a</sup>

$\lambda_{\text{ex}}$ , nm	$P$ , Torr	A $\Phi(\text{C}_2\text{F}_4)$	B $\Phi(c\text{-C}_3\text{F}_6)$	C $\Phi(\text{CO})$	$\left(\frac{A}{1.5}\right) + B$
325.0	0.30	1.46	0.10	1.05	1.07
366	0.30	0.73	0.47	0.84	0.96
366	10.0	0.046	0.65	0.69	0.68
405	0.30	0.14	1.06	1.08	1.15

<sup>a</sup> The probable accuracy is  $\sim 10\%$ .

TABLE III: Benzene Photosensitization Yields at Various Pressures of PFCB<sup>a</sup>

Run No.	$P$ , Torr	Sensitization yields, $10^{-3}$ mol <sup>b</sup>		$\Phi_s$ (calcd)	$\Phi_{\text{sens}}(\text{C}_2\text{F}_4)$	$\Phi_{\text{sens}}(c\text{-C}_3\text{F}_6)$	$\Phi_{T,\text{max}}$
		$\text{C}_2\text{F}_4$	$c\text{-C}_3\text{F}_6$				
120	0.020	1.7	57.4	0.020	0.016	0.54	0.71
119	0.030	3.8	58.8	0.029	0.036	0.55	0.70
118	0.050	7.2	64.6	0.048	0.068	0.61	0.69
116	0.100	8.2	56.7	0.091	0.077	0.53	0.65
121	1.00	41.8	50.9	0.50	0.39	0.48	0.36

<sup>a</sup> Pressure of  $\text{C}_6\text{H}_6 = 1.00$  Torr;  $t = 15$  min; absorbed intensity at 253.7 nm =  $116 \times 10^{-9}$  einstein. <sup>b</sup> Accuracy of the product yield measurement is  $\pm 1 \times 10^{-9}$  mol.

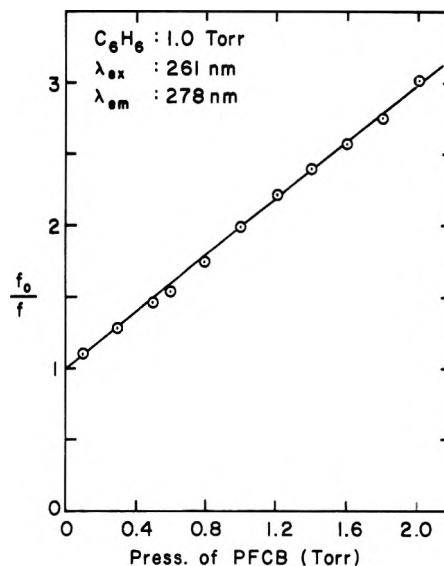


Figure 2. Stern-Volmer plot of the benzene fluorescence emission yield vs. pressure of PFCB.

tized yield of  $c\text{-C}_3\text{F}_6$  comes from the singlet-singlet energy transfer. Therefore, nearly all of the sensitized yield of  $c\text{-C}_3\text{F}_6$  is attributable to the triplet-triplet sensitization at pressures below 0.10 Torr, except at 1.0 Torr of PFCB where the contribution of the singlet-singlet energy transfer to the sensitized yield of  $c\text{-C}_3\text{F}_6$  is appreciable as expected.  $\Phi_{T,\text{max}}$  values listed in Table III represent the quantum yield of the triplet benzene ( $^3\text{B}_{1u}$ ) at the given pressures of PFCB and hence correspond to the maximum values of the triplet PFCB ( $T_1$ ) obtainable by the triplet-triplet energy transfer which are limited by the unimolec-

lar lifetime of the triplet benzene ( $^3B_{1u}$ ), the bimolecular rate constants of the triplet-triplet energy transfer process, and the pressure of PFCB.<sup>10</sup> The fact that  $\Phi_{\text{sens}}(c\text{-}C_3F_6)$  is lower than  $\Phi_{T,\text{max}}$  below 0.10 Torr of PFCB means that probably not all of the triplet benzene ( $^3B_{1u}$ ) is quenched by PFCB ( $S_1$ ) at these pressures.

The conclusions of the benzene photosensitization experiment are that (1) triplet PFCB ( $T_1$ ) dissociates efficiently to give  $c\text{-}C_3F_6$  and CO and (2) triplet PFCB ( $T_1$ ) which is the product of the  $S_1 \rightarrow T_1$  intersystem crossing is the most likely precursor of the decarbonylation products in direct photolysis below the "predissociation threshold" observed at  $\lambda_{\text{ex}}$  380 nm in our fluorescence lifetime and fluorescence excitation spectroscopy work.<sup>1</sup> This behavior is analogous to the behavior observed in cyclobutanone photochemistry.<sup>2,4</sup>

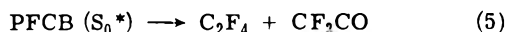
**Direct Photolysis.** In our forementioned fluorescence work,<sup>1</sup> it was observed that the emission yield vanished below  $\lambda_{\text{ex}}$  345 nm following its gradual diminution commencing at  $\lambda_{\text{ex}}$  380 nm (excess vibrational energy of  $\sim 7$  kcal/mol). Again in analogy to the case of cyclobutanone photochemistry,<sup>2,4</sup> we would expect a noticeable drop of the  $C_3/C_2$  product ratio obtainable at low pressures in this wavelength range. A 20-fold change in this ratio from  $\lambda_{\text{ex}}$  405 nm to  $\lambda_{\text{ex}}$  334 nm is readily observable in Table I. We will return later for further discussion of this point, and we will direct our attention to the pressure dependence of the  $C_2F_4$  yield now.

Again in analogy to cyclobutanone photochemistry,<sup>2,3</sup> we would expect that the pressure quenching of  $C_2F_4$  can be explained as the collisional deactivation of its precursor, vibrationally hot ground state PFCB ( $S_0^*$ ) which has a relatively long unimolecular lifetime for decomposition. A Stern-Volmer plot of the reciprocal quantum yield of  $C_2F_4$  vs. pressure of PFCB should be linear, if the PFCB ( $S_0^*$ ) has a narrow energy distribution due to monochromatic excitation in our experiment. Furthermore, the specific rate constant,  $k(E)$ , for its unimolecular decomposition should increase with the photoexcitation energy, and hence the half-quenching pressure,  $P_{1/2}$ , should increase accordingly. This expected behavior is well illustrated in Figure 1, showing a 40-fold change in  $k(E)$  from  $E \approx 73$  kcal/mol to  $E \approx 88$  kcal/mol, assuming  $E(\text{thermal})$  of  $\sim 2.5$  kcal/mol and  $E = E_{h\nu} + E_{\text{th}}$ . Certainly, the energy loss per collision cannot be more than a few kcal/mol, and an assumption of "strong collisions" cannot be valid. Therefore, we estimate that the unimolecular lifetime of PFCB ( $S_0^*$ ) in this energy range is a few times  $10^{-6}$  sec at  $\lambda_{\text{ex}}$  405 nm and  $\sim 1 \times 10^{-7}$  sec at  $\lambda_{\text{ex}}$  334 nm.

Now, it is certain that in the original photolytic work of Phillips<sup>5</sup> at high pressures the primary yields of the  $S_1 \rightarrow S_0$  internally converted product were collisionally suppressed unknowingly at  $\lambda_{\text{ex}}$  334, 366, and 405 nm; this would explain why the quantum yields of  $C_2F_4$  were extremely low at these wavelengths.

Let us now examine our quantum yield measurement shown in Table II.  $\Phi(c\text{-}C_3F_6)$  and  $\Phi(\text{CO})$  are nearly equal at  $\lambda_{\text{ex}}$  405 nm, but the former is too small by a factor of 10 than the latter at  $\lambda_{\text{ex}}$  325.0 nm. It is obvious that at shorter wavelengths, a stoichiometrically greater amount of CO is produced than  $c\text{-}C_3F_6$ . Furthermore, the quantum yield of  $C_2F_4$  exceeds unity,  $1.46 \pm 0.15$  at  $\lambda_{\text{ex}}$  325.0 nm. The apparent difficulty can be circumvented, if we assume that there is a new source of CO which is linked to the source of  $C_2F_4$ . We propose that the  $\text{CF}_2=\text{CO}$  produced together with

$C_2F_4$  from the unimolecular decomposition of PFCB ( $S_0^*$ ) undergoes secondary unimolecular decomposition to  $\text{CF}_2$  and CO and that the recombination of  $\text{CF}_2$  produces *extra*  $C_2F_4$ :



and



Inclusion of another reaction such as (2) will provide a test of the overall stoichiometry:  $\Phi(\text{CO})$  should equal  $\frac{2}{3}\Phi(C_2F_4) + \Phi(c\text{-}C_3F_6)$ . This relationship is well born out within the experimental uncertainty in the last column of Table II. It is probable that the  $\text{CF}_2=\text{CO}$  fragment is likely to possess some internal excitation energy due to energy partitioning of the excess energy available in dissociation reaction 5, and hence the unimolecular decomposition of  $\text{CF}_2=\text{CO}$  can be rapid compared to the collision rate. It has been proposed that  $\text{CF}_2=\text{CO}$  decomposes to  $\text{CF}_2$  and CO at  $35^\circ$  in solution.<sup>11</sup> Therefore, the facile decomposition of  $\text{CF}_2=\text{CO}$  in our system seems quite reasonable.

**Primary Processes.** The maximum fluorescence quantum yield from PFCB ( $S_1$ ) has been measured to be 0.021 by Phillips,<sup>5</sup> and therefore, it is a rather minor process. Since (1) the  $c\text{-}C_3F_6$  production is most important at long excitation wavelengths, (2) triplet benzene ( $^3B_{1u}$ ) sensitization gives predominantly  $c\text{-}C_3F_6$ , and (3) the fluorescence decay time ( $\sim 110$  nsec at long excitation wavelength)<sup>1</sup> is comparable to that of hexafluoroacetone (84 nsec)<sup>12</sup> which undergoes  $S_1 \rightarrow T_1$  intersystem crossing with a quantum yield of  $0.9 \pm 0.1$ ,<sup>13</sup> we propose that PFCB ( $S_1$ ) also intersystem crosses to the triplet state with a quantum yield of  $0.9 \pm 0.1$  at  $\lambda_{\text{ex}}$  405 nm. At shorter wavelengths, the  $S_1 \rightarrow S_0$  internal conversion begins to take place and becomes the dominant process eventually. It is difficult to assess whether or not a ring opening process precedes the production of the internally converted PFCB ( $S_0^*$ ) as in the photochemistry of cyclobutanone.<sup>2</sup> The following simplified primary mechanism supports our observation:



At low excitation energy the ratio of  $k_{10}/k_9$  is quite small and at high excitation energy some or all of  $c\text{-}C_3F_6$  could be coming directly from PFCB ( $S_1^*$ ). With this simple mechanism, we can interpret the ratio of  $(\frac{2}{3}C_2F_4)/(c\text{-}C_3F_6)$  extrapolated to zero pressure to be  $k_{10}/k_9$ . They are shown in Table IV.

It is interesting to note that thermal conversion of PFCB ( $S_0$ ) at  $298^\circ\text{K}$  to  $C_2F_4$  and  $\text{CF}_2\text{CO}$  is  $\sim 41$  kcal/mol endothermic and that to  $c\text{-}C_3F_6$  and CO is  $\sim 44$  kcal/mol endothermic according to the estimate by the group additivity procedure.<sup>14</sup> The decomposition of  $c\text{-}C_3F_6$  to  $C_2F_4$  and  $\text{CF}_2$  is 33 kcal/mol endothermic. Therefore, the secondary decomposition of the hot  $c\text{-}C_3F_6$  produced by energy partitioning cannot easily proceed at low excitation energies.

Our proposed mechanism above is not compatible with that proposed by Phillips<sup>5</sup> shown as reactions 1-4. Furthermore, his quantum yields of CO at  $\lambda_{\text{ex}}$  366 and 405 nm ap-

TABLE IV: Wavelength Dependence of Product Yields

$\lambda_{\text{ex}}$ , nm	$P_{1/2}$ of $\text{C}_2\text{F}_4$ , Torr	$(\text{C}_2\text{F}_4/c-\text{C}_3\text{F}_6)$ Phillips	$(\text{C}_2\text{F}_4/c-\text{C}_3\text{F}_6)_{P=0}$ This work	$k_{10}/k_9$
405	0.11	>0.01	0.4	0.3
366	$\geq 0.31$	$\sim 0.03$	2.2	1.4
334	4.4	1.2		
325			15	10
313	High	1.5	4	27.7

pear to be too high compared to our measured values. There are other minor discrepancies but it is probably not worthwhile to devote more space to them. The analogy between cyclobutanone and PFCB in their photochemical transformation mechanism is very impressive.

*Acknowledgment.* This research has been supported by the Office of Naval Research (Contract No. N00014-69A-0200-9005). We thank Dr. D. C. England (E. I. du Pont de

Neumours and Co.) for the generous gift of the perfluorocyclobutanone sample and also for pointing out the extreme reactivity of difluoroketene. We also thank Professor Alan S. Rogers (Texas A&M University) for providing us with the thermochemical information.

### References and Notes

- (1) R. S. Lewis and E. K. C. Lee, *J. Chem. Phys.*, **61**, 3434 (1974).
- (2) J. C. Hemminger and E. K. C. Lee, *J. Chem. Phys.*, **56**, 5284 (1972).
- (3) N. E. Lee and E. K. C. Lee, *J. Chem. Phys.*, **50**, 2094 (1969).
- (4) H. O. Denschlag and E. K. C. Lee, *J. Amer. Chem. Soc.*, **90**, 3628 (1968).
- (5) D. Phillips, *J. Phys. Chem.*, **70**, 1235 (1966).
- (6) (a) R. B. Cundall, F. J. Fletcher, and D. G. Milne, *Trans. Faraday Soc.*, **60**, 1146 (1964); (b) W. A. Noyes, Jr., and K. E. Al-Ani, *Chem. Rev.*, **74**, 29 (1974).
- (7) At 5 Torr, 14.7-cm path length, and 366 nm where the extinction coefficient is highest, only 11% of the actinic light is absorbed.
- (8) See, for example, R. G. Shortridge, Jr., and E. K. C. Lee, *J. Amer. Chem. Soc.*, **92**, 2228 (1970).
- (9) T. H. McGee, *J. Phys. Chem.*, **72**, 1621 (1968).
- (10) E. K. C. Lee in "Excited State Chemistry," J. N. Pitts, Jr., Ed., Gordon and Breach, New York, N.Y., 1970, p 59.
- (11) D. C. England and C. G. Kaspan, *J. Org. Chem.*, **33**, 816 (1968).
- (12) A. M. Halpern and W. R. Ware, *J. Chem. Phys.*, **53**, 1969 (1970).
- (13) A. Gandini, D. A. Whytock, and K. O. Kutschke, *Proc. Roy. Soc., Ser. A*, **300**, 529 (1968).
- (14) A. S. Rogers, private communication.

## Ring Opening and Isomerization of a Series of Chemically Activated Cycloalkyl Radicals<sup>1a</sup>

S. E. Stein<sup>1b</sup> and B. S. Rabinovitch\*

Department of Chemistry, University of Washington, Seattle, Washington 98195 (Received August 16, 1974)

Publication costs assisted by the Office of Naval Research

Unimolecular reactions of a series of chemically activated ( $\sim 40$  kcal mol<sup>-1</sup>) cycloalkyl radicals, vibrationally excited to the region of  $\sim 45$  kcal mol<sup>-1</sup>, were studied in the gas phase. Cyclopropylethyl, cyclobutyl, cyclopentyl, and cyclohexyl radicals were produced by H-atom addition to the appropriate olefin. Straight chain ring-opened products were observed for the first three of these radicals, while cyclopentylmethyl was the major product of the fourth. Critical threshold energies,  $E_0$ , for these reactions have been deduced.  $E_0$  for cyclopropylethyl ring opening is  $\approx 16$  kcal mol<sup>-1</sup>, which is less than that for the other reactions by at least 10 kcal mol<sup>-1</sup>; this indicates that for this reaction the ring strain in the activated complex is much less than that in the molecule and the findings can be related to studies on homoallylic rearrangements. For the other cyclic radicals,  $E_0$  is much closer to values found for corresponding acyclic processes, *i.e.*, 31–33 kcal mol<sup>-1</sup>.

### Introduction

The elucidation of the role of ring strain energy in the ring opening of cyclic radicals as well as its reverse, the intramolecular addition of a radical function to a double bond, has received considerable attention in recent years.<sup>2</sup> Gaseous cyclopentyl,<sup>3</sup> methylcyclobutyl-1,<sup>3a</sup> and, perhaps, cyclobutyl<sup>4</sup> radicals have been found to undergo ring opening with a threshold energy,  $E_0 \sim 30$ –35 kcal mol<sup>-1</sup>. In addition, the thermal  $A$  factor for the ring opening of the cyclopentyl radical has been calculated to be  $10^{14.0}$  from a comparison of the rates of ring rupture and ring formation at two different levels of vibrational excitation.<sup>3a</sup> Thermal

studies of the ring opening of cyclopropyl radical<sup>5a,b</sup> gave  $E_a \approx 20$  kcal mol<sup>-1</sup> which indicates that the activated complex for this reaction is loosened and is considerably less strained than the molecule. Due to inconsistencies in the cyclobutyl work,<sup>4b,c</sup> it is uncertain whether this result represents a break from the cyclobutyl behavior. Gordon<sup>3c</sup> has postulated that cyclopentyl may decompose directly to ethylene and propyl radical. No quantitative results for the ring opening of radicals larger than the cyclopentyl radical have been reported.

In order to clarify the effect of ring size on kinetic parameters for ring opening, we have examined a series of

chemically activated cyclic radicals having ring sizes from three to six members. Radicals were produced by H-atom addition to the appropriate cyclic olefin. The ring opening of activated *sec*-cyclopropylethyl radical (SCE $\cdot$ ) has been studied. This was the only radical investigated in the study in which the unpaired electron was not on the ring, and an activated complex somewhat different from that for a substituted cyclopropyl radical could result. This system is relevant to the kinetics and mechanism of homoallylic rearrangement.

Ring opening of chemically activated cyclobutyl (CB $\cdot$ ) and cyclopentyl (CPr $\cdot$ ) radicals was studied in order to clarify the nature of these reactions.

The unimolecular reaction of activated cyclohexyl radicals (CHx $\cdot$ ) has been investigated quantitatively. The larger size of this radical may result in an increased probability for a new reaction path, the intramolecular ring contraction to a five-membered ring.<sup>2c</sup>

During the late stages of the work, a preprint of ref 3a was received in which the chemically activated ring opening of CPn $\cdot$  and methylcyclobutyl-1 radicals was described.

### Experimental Section

**Materials.** Ultrapure Airco H<sub>2</sub> was further purified by passage through silica gel at liquid nitrogen temperature and through a column containing BTS catalyst. Vinylcyclopropane, cyclobutene, cyclopentene, and cyclohexene were obtained from Chemical Samples Co. and were further purified by gas-liquid-phase chromatography. High-purity Phillips ethylene was similarly purified.

**Apparatus and Procedure.** This chemical activation technique has been used in the past for a large number of studies.<sup>6</sup> Experiments were made with a conventional high vacuum Pyrex vacuum system fitted with Teflon stopcocks containing Viton O rings. Three different size reaction vessels were used: a Pyrex 12-l. vessel fitted with a quartz window for low pressures (<10 Torr), a 500-cc quartz vessel for medium pressures (10 to 100 Torr) and a 50-cc quartz vessel for high pressures (>100 Torr). A G.E. 8-W germicidal lamp fitted with a filter of variable intensity was used for the Hg photosensitization of H<sub>2</sub>. Pressures were measured with a Hg manometer, and the vacuum was checked periodically with Pirani and thermocouple gauges.

In all runs, the ratio of H<sub>2</sub> to substrate was greater than 50 to 1. Reaction mixtures were made up in the following way. A measured amount of olefin was frozen into the reaction vessel which was then pressurized with H<sub>2</sub>; in some runs, a mixture of olefin and H<sub>2</sub> was made up and then was transferred to the reactor.

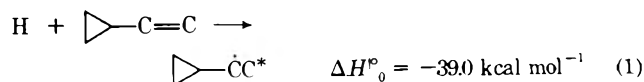
Reaction times varied from 10 min to 2 hr. The percentage reaction varied from 0.2 to 1.5%. After low pressure runs, the reaction vessel was pressurized with H<sub>2</sub> to facilitate collection by pumping through a glass wool packed trap at -195°. The condensate was then transferred to the injection trap of the chromatograph in a slow flow of H<sub>2</sub>.

**Analysis.** The products were separated on a 100-ft. SCOT squalane column and were identified by calibration with authentic compounds. The identity of some peaks was checked with a AgNO<sub>3</sub>-glycol column in series with the squalane column to characterize the olefinic nature of the unknown. A flame ionization detector was used. Peak areas were proportional within 5% to their concentration corrected for carbon number.

### Results

***sec*-Cyclopropylethyl Radical.** Hydrogen atoms were

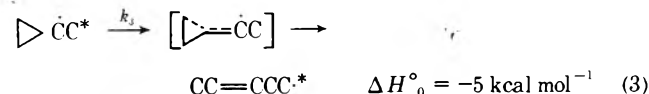
found to give 97.5% terminal addition to vinylcyclopropane:



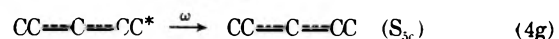
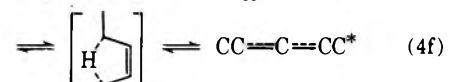
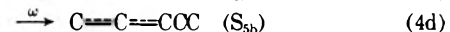
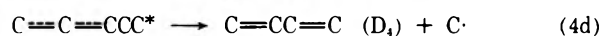
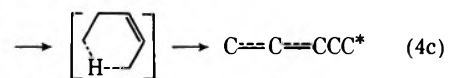
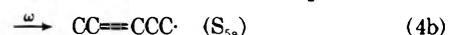
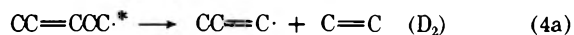
Vibrational deexcitation (stabilization) by a bath molecule (M  $\equiv$  H<sub>2</sub>) can occur



Exothermic ring opening may also occur

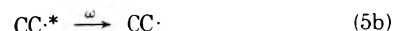


This ring-opening reaction was found to be so fast that S/D could be measured at the highest pressures only (Table I). No clear dependence of S/D on pressure could be measured. Aside from the reverse of reaction 3, the excited pent-2-en-5-yl radical may undergo the following unimolecular decomposition and isomerization or collisional stabilization



Because of the low activation energy of reaction 3 (relative to the ring-opening activation energies for most  $\beta$ -C bond rupture in radicals), it was necessary to work at relatively high pressure ( $p > 200$  Torr) before the apparent stabilization of SCE $\cdot$  became measurable. At these pressures, the amounts of D<sub>2</sub> and D<sub>4</sub> were negligible relative to S<sub>5a</sub> and S<sub>5b</sub>. It is uncertain how much S<sub>5c</sub> was produced by reaction 4f (see below).

Runs were carried out with ethyl radical-getting in reaction mixtures having ethylene: *c*-C<sub>3</sub>H<sub>5</sub>C=C ratios of  $\geq 8:1$ . The results are shown in Table I. Ethyl radicals were produced by



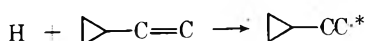
The reverse of (5a) is negligible at the pressures used. Ethyl-getting was used in order to check the results in self-getted systems as well as to eliminate decane or higher products which were difficult to handle. Ethyl-getting was preferable to self-getting in this system, also, because S/D was <0.002 and any disproportionated stabilization product *c*-C<sub>3</sub>H<sub>5</sub>CC would be obscured in analysis by disproportionated ring-opened products.

Since disproportionation involving ethyl radicals is a minor process, S/D could be accurately measured by determining the amount of *c*-C<sub>3</sub>H<sub>5</sub>C(C)CC(S<sub>7</sub>), relative to the decomposition products, *cis*- and *trans*-CC=CCCC(D<sub>7a</sub>), C=CC(CC)CC(D<sub>7b</sub>), and *cis*- and *trans*-CCC=CCCC(D<sub>7c</sub>), and then correcting for disproportionation.<sup>7</sup> About 10% of the C<sub>7</sub> product was determined to be *cis*- and *trans*-CC=CC(C)CC, which must have resulted from the ethyl

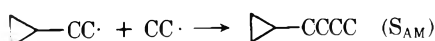
addition reaction,  $\text{CC}=\text{C}=\text{CC} + \text{CC}\cdot \rightarrow \text{CC}=\text{CC}(\text{C})\text{CC}\cdot$ . The origin of this allylic radical is uncertain because of its lack of dependence on pressure in the range where the ratio  $D_{7a}/(D_{7b} + D_{7c})$  increased with increasing pressure; thus, this product appears not to have been an eventual result of reaction 4. Some unknown alternate route may also exist which accounts for this allylic radical: thus, the presence of a *trans*- $\text{C}=\text{CC}=\text{CC}$  impurity in the reaction mixture (whose retention time happens to coincide almost exactly the same as that of *c*- $\text{C}_3\text{H}_5\text{C}=\text{C}$  on the squalane columns used) could have resulted in the production of the same allylic radical.

The rate of isomerization of vibrationally excited pent-2-en-5-yl to allylic pent-2-en-1-yl (first reaction of 4c provides no insight *per se* into the nature of the ring-opening process and is discussed elsewhere.<sup>7</sup>

The anti-Markovnikov addition



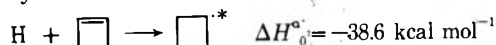
was monitored by the quantity of *c*- $\text{C}_3\text{H}_5\text{CCCC}$ ,  $S_{AM}$ , produced



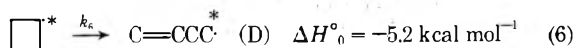
the decomposition of the excited primary cyclopropylethyl radical is much slower than its stabilization; therefore, the ratio  $S_{AM}/(D_{7a} + D_{7b} + D_{7c})$  remained very constant ( $2.5 \pm 0.1\%$ ) with pressure (see Table I). This value is somewhat lower than anti-Markovnikov addition (5–6%)<sup>8</sup> to terminal olefins, and the value may be modified by the homoallylic nature of the product SCE.

With the cyclic  $\text{C}_5$  and  $\text{C}_6$  olefins, allylic H abstraction is ~10% (see later) of H-atom addition and was expected to occur to a lesser extent in this system. The presumed ethyl-getted product, 1,1-ethylvinylcyclopropane, was not available as a standard, nor could its boiling point be found. One unidentified  $\text{C}_7$  peak (~2% of the total product  $\text{C}_7$ ) may have corresponded to this compound.<sup>9</sup>

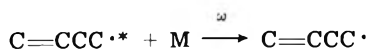
*Cyclobutyl Radical.* The activated  $\text{CB}\cdot$  radical was generated by



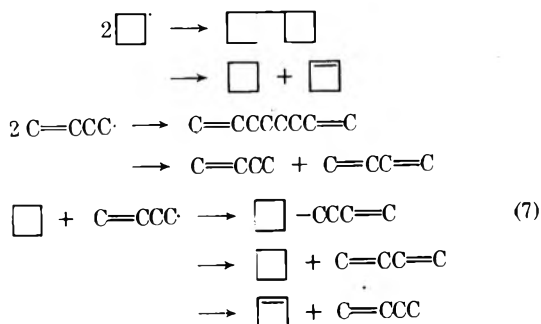
and was either stabilized or underwent ring opening



followed by stabilization



The following reactions occurred in the self-getted system



All of these products were detected (Table IIa). However, since authentic samples of *c*- $\text{C}_4\text{H}_7$ -*c*- $\text{C}_4\text{H}_7$  and *c*- $\text{C}_4\text{H}_7$ - $\text{CCC}=\text{C}$  were not available, their identity was deduced

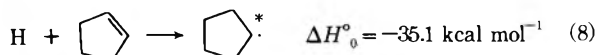
from (a) the expected dependence on pressure, (b) the change in retention time on an  $\text{AgNO}_3$ -glycol column, and (c) the deduced approximate boiling points for bicyclo and alkylcyclo compounds.<sup>10</sup> The disproportionation-combination ratios<sup>7</sup> were also useful in the estimation of combination products of higher radicals (*e.g.*, of  $\text{CPn}\cdot$  and  $\text{CHx}\cdot$ ).

Runs were also carried out with ethyl radical-getting (Table IIb). The rate parameters were in substantial agreement with those of the self-getted system.

No evidence was found here for the presence of the cyclobutenyl-3 radical resulting from H abstraction. This may be due to the instability of this species or of its products.

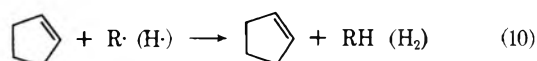
No other types of isomerization or decomposition products were found to be appreciable at pressures above 100 Torr; at lower pressures,  $\text{C}_6$  products appeared in the self-getted system and may have been due to decomposition of the excited product radical, *e.g.*,  $\text{C}=\text{CCC}\cdot^* \rightarrow \text{C}=\text{C}\cdot + \text{C}=\text{C}$ , followed by  $\text{C}=\text{C}\cdot + \text{C}=\text{CCC}\cdot \rightarrow \text{C}=\text{CCCC}=\text{C}$ . Since these reactions were not directly relevant to the ring-opening reaction at higher pressures, they were not examined in detail.

*Cyclopentyl Radical.* Chemically activated  $\text{CPn}\cdot$  undergoes ring opening

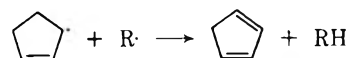


or is deactivated by collisions. Carter and Tardy (CT)<sup>3a</sup> investigated this system using ethyl and methyl radical-getting. Both self-getting and ethyl-getting (with a somewhat larger proportion of ethyl than was used by TC, in order to minimize self-getting) were employed here. The disproportionation products in the self-getted system were measured and combination amounts were calculated for the evaluation of S/D. Results are shown in Tables IIIa,b.

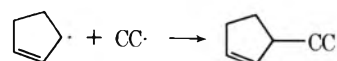
The allylic cyclopentyl radical, presumably formed by abstraction



arose in appreciable amounts (~9% of the reaction yield in the ethyl-getted system) as inferred from the production of 1,3-cyclopentadiene in the self-getted system



and of 3-ethylcyclopentene in the ethyl-getted system



The invariance with pressure of the ratio of allylic cyclopentyl products to H-addition products, in the range where S/D varied rather linearly with pressure ( $p = 0.6$ – $120$  Torr), indicates that the elimination reaction<sup>3c</sup>

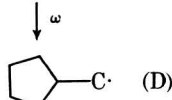
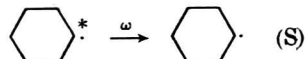
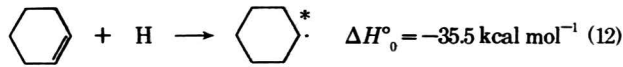


was not important under our conditions. It has been found<sup>4a</sup> that  $k_9/k_{11} \sim 10$ ; thus, this path cannot account for the large amount of allylic cyclopentyl, relative to pent-1-en-5-yl, found at higher pressures. The apparent increase in the amount of 3-ethylcyclopentene at the lowest pressures ( $p = 0.32$  Torr) may be due to the occurrence of reaction 11, or may be due to the increased proportion of pri-

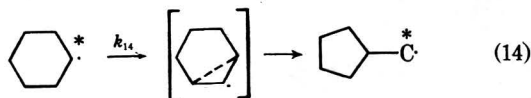
many ring-opened radicals, which would be better H-atom abstractors<sup>11</sup> in reaction 10.

No evidence for the appreciable occurrence of the decomposition or isomerization of  $C=CCCC^*$  was found in the pressure range studied.

**Cyclohexyl Radical Activation** was followed by stabilization, or isomerization



The formation of cyclopentylmethyl radical may have been due to direct isomerization *via* a tight transition state, as suggested by Gordon<sup>2c</sup>



or to the ring-opening, ring-closing sequence

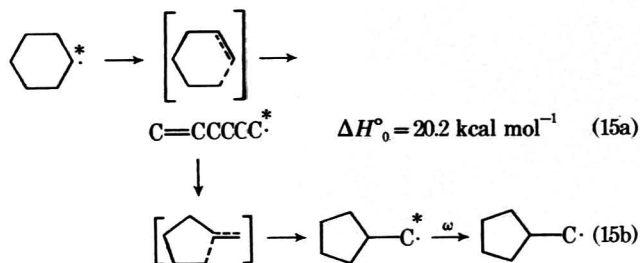


Table I. Product<sup>a</sup> Analysis for SHCP-Ethyl-Getted System

	Pressure (torr)									
	10.0	47.2	105	224	549	1023	1132	1133	1617	1840
$D_2/S_2 (10^{-3})^b$						2.1	4.6		2.1	
$D/S (10^{-3})^c$						1.6	3.5		1.6	
$k_{14}^d (10^{13} \text{ sec}^{-1})^d$	e	e	e	e	e	8.0	19	f	13	g
I reaction	~ 5	8.1	5.6	9.4	9.0	3.0	1.6	1.3	6.1	15.6
c,t-Melise-2/D <sub>2</sub>	~ 0.14	0.096	0.089	0.103	0.094	0.107	0.106	0.087	0.092	0.102
S/C-Hpe-2 c,t-Hpe-3-3-EtFe-1	0.033	0.237	0.653	1.25	2.73	8.54	4.72	3.18	3.02	4.22
C=C <sub>2</sub> -C <sub>2</sub> <sup>h</sup> /D <sub>2</sub>	0.0306	0.0192	0.0240	0.0203	0.0120	0.0714	0.180	0.164	0.022	0.0141
D-CCCC/D <sub>2</sub>	0.0257	0.0237	0.0209	0.0259	0.0250	0.0260	0.0247	0.0208	0.0260	0.0289
c,t-Fe-2/D <sub>2</sub>	—	0.0734	0.0908	0.0802	0.0951	0.102	0.0940	0.0923	0.0929	0.0982
c-1,3-Pnde/D <sub>2</sub>	—	0.0177	0.0324	0.0177	0.0189	0.0615	0.0107	0.0123	0.0215	0.0112
t-Fe-2/c-Fe-2	—	3.75	3.57	3.58	3.42	3.78	3.90	3.48	3.73	3.62
t-Hpe-3/c-Hpe-3	2.07	2.66	4.95	2.88	2.08	1.87	2.52	1.91	2.36	2.67
t-Hpe-2/c-Hpe-2	5.31	4.92	4.92	4.36	3	4.64	4.64	4.51	4.44	4.42
[ $\square$ ] <sup>1</sup>	7.17	13.1	19.6	16.8	32.1	16.4	9.1	1.1	26.8	74.5

a) Abbreviations used are: 4-Melise-2, 4-methyl hexene-2; Hpe-2, heptene-2;

Hpe-3, heptene-3; 3-EtFe-1, 3-ethyl pentene-1; Fe-2, pentene-2;

1,4-Pnde, 1,4-pentadiene.

b)  $D_2 = 3\text{-EtFe-1} + \text{c,t-Hpe-3} + \text{c,t-Hpe-2}$ ;  $S_2 = \text{D-CCC}$ .

c)  $D/S = \text{ratio of ring-opened to stabilized radicals} = D_2/(1.30S_2)$ .

Factor 1.30 is disproportionation correction, see ref. 7.

d)  $\omega = 4.87 \times 10^7 \text{ p}_{\text{corr}}$

e)  $S_2$  could not be detected because of lower pressure complications.

f)  $S_2$  was not detected because of relatively small amount of reaction products.

g)  $S_2$  was obscured by secondary reaction products due to high percent reaction.

h) This is the assumed compound corresponding to a measured peak whose identity has not been directly established (see text).

i) Relative measure of the total decomposition yield in arbitrary units.

A 500 cc reaction vessel was used for the four lowest pressure runs;

a 50 cc vessel was used for six highest pressure runs.

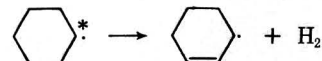
No evidence for the presence of the stabilized  $C=CCCC$ -radical was found. This system gave combination and disproportionation products analogous to those in other systems (Tables IVa,b).

At the lower pressures, partial equilibration between the CHx- and cyclopentylmethyl radicals resulted in a decrease of  $\omega D/S$ .

As in the CPn- system, H abstraction leads to a cyclic allylic radical. An appreciable amount of 3-ethylcyclohexene (13% of the total C<sub>8</sub> products at pressures above 10 Torr) was found in the ethyl-getted system

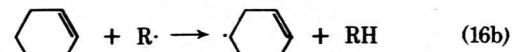
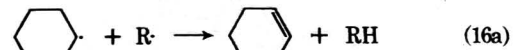


At lower pressures ( $p < 1$  Torr), the relative proportion of 3-ethylcyclohexene increased to ~25%, suggesting that the reaction



occurred to an appreciable extent.

Ethyl radicals are relatively more efficient abstractors of H atoms than are the parent radicals. The formation of large amounts of cycloallylic radical present may explain the production of benzene in especially large proportions (up to ~30% of the disproportionation products) in the ethyl-getted system, at all pressures



In order to clarify the mechanism of benzene production in this system, the mixture H<sub>2</sub>/1,3-cyclohexadiene (1,3-

Table IIa. Product<sup>a</sup> Analysis for Self-Getted C<sub>8</sub>-System

Products	p(torr)					
	115	229	430	815	1220	1680
$\frac{\text{C}=\text{CCCC} + \text{C}=\text{CCCC}}{\text{C}=\text{CCCC}}$	1.58	0.806	0.882	0.594	0.733	0.644
$\frac{\text{C}=\text{CCCC} + \text{C}=\text{CCCC}}{1,7 \text{ Ode}}$	1.81	3.53	5.47	5.42	6.30	11.2
Cha / D-CCCC	0.746	1.07	1.90	2.68	4.30	5.54
Cha / [□]	2.89	1.81	1.77	1.35	1.35	1.33
[□] / D-CCCC	0.487	0.403	0.462	0.477	0.300	0.494
1,7Ode / D-CCCC	0.467	0.332	0.374	0.456	0.325	0.485
S/D <sup>b</sup>	0.750	2.03	3.25	5.84	7.34	11.8
$k_{14}^c (10^7 \text{ sec}^{-1})^c$	6.19	4.55	5.35	5.65	6.85	5.75

a) The following abbreviations are used: 1,7Ode, 1,7-octadiene; Cha, cyclohexane.

b)  $S/D = 1.4 ([\square] + 2[\text{C}=\text{CCCC}]) / ([\text{C}=\text{CCCC}] + [\text{C}=\text{CCCC}] + [1,7 \text{ Octadiene}] + [\text{C}=\text{CCCC}])$

Factor 1.4 takes into account  $\square$  formed by H-abstraction from  $\square$ .

c)  $\omega = 4.0 \times 10^7 \text{ p(torr) sec}^{-1}$

Table IIb. Product<sup>a</sup> Analysis for Ethyl-Getted C<sub>8</sub>-System

p(torr)	$\frac{\text{C}=\text{C}}{\square}$	EtCha Hpe-1	$\frac{\text{EtCha}}{\text{Cha}}$	$\frac{1,3\text{-Hpe}}{\text{C}=\text{CCCC}}$	$\frac{S}{D}$	$k_{14}^c (10^7 \text{ sec}^{-1})^c$
312	9.4	1.82	4.46	2.65	2.03	5.21
610	8.5	3.40	3.52	2.94	3.81	5.47
1260	10.0	6.75	4.62	4.26	7.55	6.77
1710	9.2	10.1	4.36	< 8.8	11.3	6.19

a) The following abbreviations apply: EtCha, ethyl cyclohexane; Hpe-1, hexene-1.

b)  $\frac{S}{D} = \frac{[\text{C}=\text{C}](1 + \text{fraction } \square \text{ disprop. by CC})}{[\text{C}=\text{CCCC}](1 + \text{fraction C=CCC disprop. by CC})} = \frac{[\text{C}=\text{C}](1.45)}{[\text{C}=\text{CCCC}](1.3)} = 1.12 \frac{[\text{C}=\text{C}]}{[\text{C}=\text{CCCC}]}$

c)  $\omega = 4.0 \times 10^7 \text{ p(torr) sec}^{-1}$ .

CHxd)/ethylene ([ethylene]/[1,3-CHxd] > 5) was Hg photo-sensitized. Benzene constituted 30–40% of the disproportionated products, somewhat more than is produced in the CHx· system. Experiments of James, *et al.*,<sup>5c</sup> indicate that H atoms largely add to 1,3-CHxd (84%) and thus large quantities of benzene are not produced, which accords with our self-gettered CHx· runs where much smaller quantities of benzene were produced (<5%). Thus ethyl radicals appear to be a major factor in the production of benzene through their participation in one or more steps of reaction 16. This probably is due to their lower reactivity toward olefins relative to H atoms, and their larger steady-state concentration.

Methyl radicals may be formed *in situ* at low pressures by the decomposition of chemically activated butyl-2 radicals



However, attempts to use methyl radical-getting at pressures below 1 Torr were unsuccessful. Large (somewhat variable) amounts of benzene were formed. Only small amounts (<10%) of combination products relative to disproportionation products were observed, so that the disproportionation is highly favored.

## Discussion

Critical reaction threshold energies,  $E_0$ , and frequency factors have been well established for  $\beta\text{C}-\text{C}$  bond scission of a number of chemically activated acyclic radicals.<sup>6,12</sup>  $E_0$  is in the region 30–33 kcal mol<sup>-1</sup> for straight chain species,

and the activated complex is only a little loosened,<sup>13</sup> with  $A \approx 10^{14}$  sec<sup>-1</sup>. The reverse reaction, radical addition to a double bond, has  $E_0 \approx 8$  kcal mol<sup>-1</sup>. In the cyclic radical ring-opening reaction, which is analogous to the acyclic  $\beta\text{C}-\text{C}$  bond scission, two opposing effects may alter ring-opening energetics from acyclic values. There can be ring strain energy,  $E_{\text{RS}}$ , which is relieved in the activated complex if the ring is loosened, *i.e.*,  $|E_{\text{RS}}^{\ddagger}| < |E_{\text{RS}}|$ ; this change,  $\Delta E_{\text{RS}}$ , lowers  $E_0$ . On the other hand, the reaction coordinate in these systems is not simple bond scission because the final product is an olefinic monoradical. The new radical site is the  $\gamma$  carbon of the original center. The preferred configuration of the transition state has maximum overlap of the electrons of the nascent  $\pi$  bond. Since the radical site on the ring is relatively planar,<sup>14</sup> development of overlap in the transition state introduces some local orientation strain ( $E_{\text{LS}}$ ) which tends to increase  $E_0$ . These effects are illustrated qualitatively in Figures 1a,b.

As the ring is loosened, or strain in the cyclic species decreases, so do many of its frequencies.<sup>15</sup> In rate calculations, this implies increased sums and densities of vibrational eigenstates. The decomposition rate is enhanced on that account, apart from the direct effect of lowering  $E_0$ . This corresponds to an increased preexponential factor in thermal reactions. Thus, one expects the frequency factor to monotonically increase with decrease of  $E_0$ . We will revert to these principles in the discussion of the results for the several systems.

The experimentally observed specific rates in the present weak collisional systems were obtained from the relation,

 Table IIIa. Product<sup>a</sup> Analysis for Self-Gettered Cp<sup>•</sup> System

p (torr)	1-Pe 1,4-Pe <sub>2</sub>	Cp <sub>2</sub> C <sub>5</sub> <sup>b</sup>	2-Cp <sub>2</sub> C <sub>5</sub> <sup>b</sup>	1-Pe C <sub>5</sub> <sup>b</sup>	C <sup>c</sup>	$k_{\text{d}}^{\text{C}} (10^6 \text{ sec}^{-1})^d$
0.0928	3.32	9.97	15.7	1.02	0.41	0.425
0.133	2.93	26.0	15.2	2.75	0.50	0.591
0.566	3.61	43.5	43.9	1.60	0.53	0.927
1.54	3.90	41.9	60.3	1.04	0.73	1.04
7.83	2.99	42.9	220	0.293	0.51	2.41
10.13	3.52	31.0	223	0.208	0.60	3.05
18.78	4.08	61.9	495	0.191	0.46	2.56

- a) The following abbreviations apply: 1-Pe, 1-pentene; 1,4-Pe<sub>2</sub>, 1,4-pentadiene; Cp<sub>2</sub>, cyclopentane.  
 b)  $D_2 = \text{Pe}^{-1} + 1,4 \text{ Pe}_2 \approx 1.29 \text{ 1-Pe}$ ;  $C_5 = 2\text{Cp}_2$   
 c) Empirical combination correction factor, C, at a specific pressure such that  $\text{C}_5/D_2$  determined from the ratio of disproportionation products in self-gettered system equals S/D from ethyl-gettered system.  
 d)  $u = 4.75 \times 10^7 \text{ p (torr) sec}^{-1}$ ;  $D/S = D_2 / (\text{C}_5 \cdot C)$  where C as in footnote c is 0.544, as derived from the CB<sup>•</sup> system; see ref. [7].

 Table IIIb. Product<sup>a</sup> Analysis for the Ethyl-Gettered Cp<sup>•</sup> System

p (torr)	ECp <sub>2</sub> 1-Npe	ECp <sub>2</sub> C-C	$k_{\text{d}}^{\text{C}} (10^6 \text{ sec}^{-1})^a$
0.132	7.6	4.50	0.635
0.671	23.1 21.0	9.82 10.98	0.763 1.17
0.996	23.8	9.85	1.26
3.43	71.4	10.20	1.76
6.38	103 98.6	8.68 9.28	2.33 2.37
10.34	125	5.44	3.02
20.0	247 235	8.84 8.09	2.96 2.86
43.6	495	8.93	3.22
119	1461	9.80	3.10

- a) Abbreviations used are: ECp<sub>2</sub>, ethyl cyclopentane; 1-Npe, 1-heptene;  
 $u = 4.75 \times 10^7 \text{ p (torr) sec}^{-1}$   
 b) If  $(R_1/R_2) =$  probability of  $R_1$  abstracting H from  $R_2$  relative to combination with  $R_1$ .  
 $x = (\text{CC}/\text{Cp}_2) + (\text{Pe}/\text{C-C}) = 0.53$   
 $y = (\text{CC}/\text{C-C}) + (\text{C-C}/\text{C-C}) = 0.18$   
 $S/D = \left( \frac{1-x}{1-y} \right) \left[ \frac{\text{ECp}_2}{1-\text{Npe}} \right] \left[ \frac{1-x}{1-y} \right] = 1.30$

 Table IVa. Product<sup>a</sup> Analysis for the Self-Gettered C<sub>6</sub><sup>•</sup> System

p (torr)	MCp <sub>2</sub> C-C	C <sub>6</sub> MCp <sub>2</sub>	$k_{\text{d}}^{\text{C}} (10^6 \text{ sec}^{-1})^b$
0.0072	22.6	1.47	0.255
0.026	43.2	2.53	0.535
0.0668		3.60	0.965
0.0833	9.25	2.96	1.46
0.138	16.2	5.49	1.31
0.418	20.4	11.6	1.87
0.707	35.2	17.4	2.11
3.45	16.3	57.9	3.12
9.84	8.07	183.	2.80
45.07	3.72	770.	3.05
120.0		2026.	3.08

- a) Abbreviations used are: MCp<sub>2</sub>, methyl cyclopentane;  
 C<sub>6</sub>, cyclohexane  
 b)  $u = 5.29 \times 10^7 \text{ p (torr) sec}^{-1}$ ;  $2C[\text{C}_6]/1.07 [\text{MCp}_2]$ , where  $C = 0.544$  as in the CB<sup>•</sup> self-gettered system

Table VIII. Heats of Formation at 0°K of Cyclic Olefins and Alkanes

Molecule	$\Delta H_{\text{f}}^{\circ}$ (kcal mole <sup>-1</sup> )	Ref.
	8.8	a
	38.1	b
	11.8	c
	41.8	c
	-10.7	d
	13.8	d
	-20.01	d
	5.76	d

- a) Estimated from  $\Delta H_{\text{f}}^{\circ}$  group values in Benson, *Thermochemical Kinetics* (J. Wiley and Sons, New York, 1968), and corrected to 0°K using corrections by J. L. Franklin, *Ind. and Eng. Chem., Anal. Ed.*, **41**, 1070 (1949).  
 b) Derived from  $\Delta H_{\text{f}}^{\circ}$  of  $\Delta^{\text{C-C}}$  by analogy with  $\text{C-C-C}$  and  $\text{C-C-C}$ , and corrected to 0°K as in (a).  
 c)  $\Delta H_{\text{f}}^{\circ}$  values from P. R. Schleyer, J. E. Williams and K. R. Blanchard, *J. Amer. Chem. Soc.*, **92**, 2377 (1970), corrected to 0°K as in (a).  
 d) Directly from ref. 24.

 Table IVb. Product<sup>a</sup> Analysis for the Ethyl-Gettered C<sub>6</sub><sup>•</sup> System

p (torr)	EC <sub>6</sub> C <sub>6</sub>	EC <sub>6</sub> C-C	EC <sub>6</sub> C-C-C	$k_{\text{d}}^{\text{C}} (10^6 \text{ sec}^{-1})^b$
0.931	0.0321	7.76	0.230	17.4
0.936	0.0165	8.02	0.293	22.7
3.82	0.0124	1.00	0.184	64.2
3.92		0.92	0.172	91.1
9.48	0.0175	0.656	0.181	147.2
11.3	0.0444	0.683	0.121	
25.2	0.0158	0.633	0.170	
34.0		0.399	0.125	704
51.0		0.359	0.126	
59.6	0.0273	0.481	0.131	
93.2	0.0668	0.341	0.148	

- a) Abbreviation used is: EC<sub>6</sub>, ethyl cyclohexane  
 b)  $u = 5.29 \times 10^7 \text{ p (torr) sec}^{-1}$ ;  $S/D = 1.30 [\text{EC}_6]/[\text{C-C-C}]$  where factor 1.30 was derived from results from the Cp<sup>•</sup> system; see reference 7.

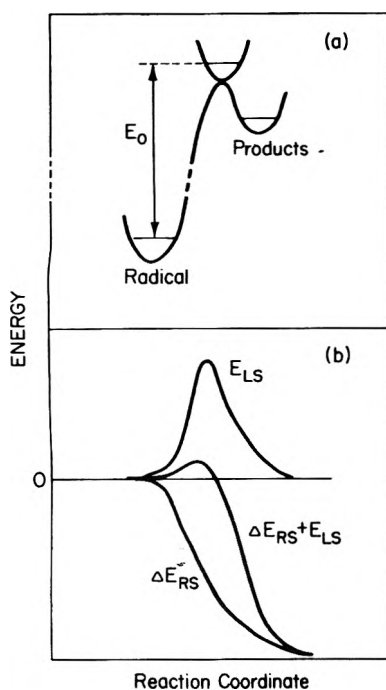


**Figure 1.** (a) Potential energy profile for acyclic radical decomposition via  $\beta$ C-C scission. (b) The variation of strain parameters along the reaction coordinate for cyclic radical ring opening. In order to obtain the potential energy profile for cyclic radical ring opening, a curve similar to the  $(\Delta E_{RS} + E_{LS})$  curve is added to the contour of Figure 1a. This representation is qualitative only; the shapes and activated complex position vary from system to system.

$k_a^{wc} = \omega D/S$ , where  $\omega$  is the specific collision rate (see Appendix), and  $D/S$  is the ratio of decomposed (ring-opened) radicals relative to collisionally stabilized cyclic radicals. The ratio may be determined from the relative amount of products resulting from the disproportionation and combination of the corresponding radical species if no correction is necessary for back-cyclization (none is necessary at high pressures except, perhaps, for the  $\text{CH}_x\cdot$  system). In this system,  $k_a^{wc}$  is expected to increase at both low and high pressures; at high pressures, a small increase is due to a spread of energies of the activated reactants;<sup>16</sup> this effect is minor for these systems; at low pressures, turn-up of  $k_a^{wc}$  is due to the inherently weak collisional nature of  $\text{H}_2$  bath gas. The true unimolecular rate of ring opening may be expressed as  $k_a = \beta k_a^{wc} = \beta \omega D/S$ , where  $\beta$  is a collisional inefficiency correction factor which may be calculated theoretically from the appropriate collisional transition probability model.

In order to apply Rice-Ramsperger-Kassel-Marcus (RRKM) rate theory, it is necessary to calculate<sup>17</sup> the energy distribution of the chemically activated radicals. Thermodynamic parameters are cited in the Appendix. An appropriate value of  $E_0$  may be fitted to the observed  $k_a^{wc}$  by adopting a set of frequencies for the internal degrees of freedom of the activated complex. Two models were considered: by assuming a "tightest" complex, whose frequencies were those of the parent cyclic radical, and a "loosest" complex, which corresponded to the frequencies of the ring-opened radical, extremes of possible values of  $E_0$  were found which gave calculated  $k_a^{wc}$  equal to the experimental value. In both models, a C-C stretch was deleted for the reaction coordinate. The reminder should be given that the tight complex (increased frequencies) corresponds to a

lower value of  $E_0$ , and *vice versa* for a loose complex model.

Because the bath gas  $\text{H}_2$  is a weak collider, it was necessary to assume an appropriate collisional deactivation model. A simple 400- $\text{cm}^{-1}$  stepladder model, found to be useful in related studies,<sup>18</sup> was used for this purpose. A more correct 450- $\text{cm}^{-1}$  exponential collisional deactivation model<sup>18</sup> was also used in the SCE $\cdot$  system (in which  $k_a^{wc}$  is most strongly affected by the specific deactivation model); this model results in only a 0.5 kcal mol<sup>-1</sup> increase in the fitted  $E_0$  values (Table VI). Experimental parameters and calculated rates are given in Table V along with pertinent thermochemical values.  $E_0$  values are summarized in Table VI as well as  $E_0$  and  $E_{act}$  values for cyclic radical ring opening from the literature.

SCE $\cdot$ . The apparent experimental rate constant for reaction of SCE $\cdot$  was  $k_a^{wc} \sim 1.2 \times 10^{14}$  sec<sup>-1</sup> at about 1600 Torr (Table Ia). This unusually large value is due both to a very low threshold energy and to a dramatic increase ("turn-up") of  $k_a^{wc}$  at low S/D values. Correction for the latter gives a true unimolecular rate of  $\sim 10^{11}$  sec<sup>-1</sup> (Table V). The possible range of  $E_0$  values is 14.0–18.5 kcal mol<sup>-1</sup> (Table VI). This value is 18–13.5 kcal mol<sup>-1</sup> less than  $E_0$  (acyclic), and thus the complex is much less strained than the radical (the strain energy in cyclopropane is  $\geq 22$  kcal mol<sup>-1</sup>);  $E_0 = 16$  kcal mol<sup>-1</sup> was adopted as an appropriate value. It should be mentioned that since no clear dependence of S/D on pressure was evident at the small S/D values involved, the stabilized SCE $\cdot$  detected may have been in thermal equilibrium with the ring-opened homoallylic radical. If this were true, the above value of  $E_0$  is simply an upper limit.

In SCE $\cdot$  ring opening the radical site is off the ring, and the orbital is free to align with the incipient free-electron orbital on the  $\beta$ -breaking carbon to give a more stable transition state. By contrast, in the  $\text{C}_3\text{H}_5$  cyclopropyl radical reaction ( $E_{act} = 19$ –22 kcal mol<sup>-1</sup> from thermal data, Table VI), the radical p orbital is roughly perpendicular to the plane of the breaking bond, thus a larger value of  $E_{LS}$  in the complex is expected as a concomitant of incipient double bond formation. The specific magnitude of this larger value of  $E_{LS}$  for the cyclopropyl reaction depends on the degree of loosening in the transition state. If the value of  $E_{act}$  from thermal systems is correct, then the transition state is quite loose, though not as loose as in the SCE $\cdot$  case, and  $E_{LS}$  is quite small for cyclopropyl opening.

CB $\cdot$ . The ring opening of CB $\cdot$ , as well as of CPn $\cdot$  and  $\text{CH}_x\cdot$ , was studied in a higher region of S/D ( $\geq 1$ ). In this region, the weak collisional behavior of  $\text{H}_2$  is such that  $\beta$  is semiconstant relative to  $\omega$ , and any error in the assumed collisional energy transfer model results in relatively small error in  $k_a$ .

The range of  $E_0$  which provides agreement with experiment is 27–31 kcal mol<sup>-1</sup> (Table V) for tight to loose complexes. This magnitude is  $\sim 13$  kcal mol<sup>-1</sup> greater than for SCE $\cdot$ . This difference is due to a much tighter complex for the CB $\cdot$  opening, i.e., a smaller  $\Delta E_S = \Delta E_{RS} + E_{LS}$ . Even so, this range of threshold energies is several kcal mol<sup>-1</sup> below  $E_0$  (acyclic);  $\Delta E_S \geq -5$  kcal mol<sup>-1</sup>, and a complex which is a little loosened is indicated. If  $\Delta E_{RS}$  is  $-15$  kcal mol<sup>-1</sup> as in SCE $\cdot$  ring opening (see Table V), then  $E_{LS} \sim 12$  kcal mol<sup>-1</sup>.

Our values of  $E_0$  for CB $\cdot$ , along with those of CT for methylcyclobutyl-1 (Table VI) differ markedly from Gordon's<sup>4a</sup> value of 18 kcal mol<sup>-1</sup>. Our values are several kcal mol<sup>-1</sup> below the range suggested by Walsh.<sup>4b</sup>

TABLE V: Selected Thermochemical, Experimental and Kinetic Values

Radical	$\Delta H_{298RS}^\circ$ , <sup>a</sup> kcal mol <sup>-1</sup>	$\Delta H_0^\circ$ , <sup>b</sup> kcal mol <sup>-1</sup>	Press range, Torr	S/D (max)	$k_a^{wc}$ , <sup>c</sup> sec <sup>-1</sup>	$k_a$ , <sup>d</sup> sec <sup>-1</sup>	
						Tight	Loose
	≥22.0 (27.6)	-6.0	1000-2000	~0.002	1.2 (14) <sup>e,f</sup>	6.6 (10)	1.2 (11)
	28.0	-5.2	100-1700	12	5.9 (9)	4.9 (8)	6.5 (8)
	6.1	15.5	0.1-120	1800	3.1 (6)	3.4 (5)	4.0 (5)
	0.7	20.2 (6.1) <sup>g</sup>	0.01-120	2100	2.6 (6)	2.2 (5) <sup>h</sup>	

<sup>a</sup> Values mainly from ref 19. Strain values for radicals are the average ring strain for the cyclic olefin and paraffin. <sup>b</sup> Enthalpy of reaction. <sup>c</sup> At highest pressures corresponding to S/D (max). <sup>d</sup> These are energy averaged theoretical RRKM values which when treated on a stochastic weak collider model basis (see text), in conjunction with the associated  $E_0$  values in Table VI, and when multiplied by 2 to allow for reaction path degeneracy give back the experimental  $k_a^{wc}$  value. <sup>e</sup> ( $n$ ) =  $10^n$ . <sup>f</sup> Determined at  $\omega = 7(10)$  sec<sup>-1</sup> and affected by "turn-up;" see text. <sup>g</sup> This parenthetic value for direct isomerization to product cyclo-C<sub>5</sub>. <sup>h</sup> Assumes that the amount of  $\cdot\text{CH}_2$ -cyclopentyl is equal to the total amount of unimolecular reaction products.

TABLE VI: Ring-Opening Activation Energies (kcal mol<sup>-1</sup>)

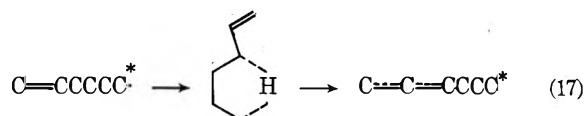
Radical	Thermal $E_{act}$	Chemical activation		
		$E_0$ (ref 3a)	$E_0$ (this work) <sup>a</sup>	
			Tight	Loose
	20 (5a) 19.1 (5b) 22 (4b)			
			13.8 <sup>b</sup> (13.5) <sup>c</sup> (14.3) <sup>d</sup>	18.5 <sup>b</sup> (18.1) <sup>c</sup> (19.0) <sup>d</sup>
	18 (4a) 35 ± 5 (4b)		27.0	30.9
		32.0		
	36.9 (3b) 37.7 (3c) ≤32.5 (4b)		30.8	35.8
		34.3		
			30.8 <sup>e</sup>	

<sup>a</sup> Assuming a 400-cm<sup>-1</sup> stepladder deactivation model (except where noted). <sup>b</sup> At  $\omega = 7(10)$  sec<sup>-1</sup>; all values for SCE<sup>-</sup> may be an upper limit (see text). <sup>c</sup> At  $\omega = 9(10)$  sec<sup>-1</sup>. <sup>d</sup> At  $\omega = 7(10)$  sec<sup>-1</sup>, with a 450-cm<sup>-1</sup> exponential deactivation model. <sup>e</sup> This value corresponds to the reaction threshold energy for Gordon's direct (tight) isomerization mechanism, if it were the only major reaction path. This value also corresponds to the threshold energy for the ring-opening reaction if the reaction path involves a "tight" transition state, and all ring-opened products cyclize to form CH<sub>2</sub>-cyclopentyl radical. If a portion of the ring-opened radicals recycles to form CH<sub>x</sub>, this  $E_0$  would be an upper limit. This value is a lower limit if a loose ring-opening model applies (with no recyclization).

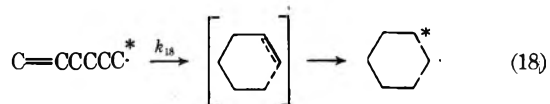
**CPn.** For the decomposition of CPn,  $k_a^{wc} = 3.1 \times 10^6$  sec<sup>-1</sup> and is somewhat lower than for CB<sup>-</sup>. This appears to be due not only to the increased number of atoms in CPn and to lower excitation energy, but also to a larger  $E_0$  value (Table VI). The strain energy of CPn is ~6.1 kcal mol<sup>-1</sup>, so that the possible lowering of  $E_0$  is much less than for the C<sub>3</sub> and C<sub>4</sub> cyclic radicals. The calculated range of  $E_0$  for tight to loose complexes is 30.8-35.8 kcal mol<sup>-1</sup>. This region indicates a complex which is somewhat strained;  $E_0 = 32$  kcal mol<sup>-1</sup> is a reasonable estimate.

**CH<sub>x</sub>.** In thermal systems, cyclopentylmethyl was observed as a major product of CH<sub>x</sub> at higher tempera-

tures.<sup>2c,21</sup> The assumed<sup>2c</sup> path for the formation of this product was a direct one through a tight transition state (reaction 14); it was argued that if ring opening did occur, the reaction



would proceed as fast or faster than the competing five-membered ring reaction (15b), or six-membered ring closing



(the reverse of the original ring opening). No evidence for occurrence of either of the acyclic radicals of reaction 17 could be found despite strenuous efforts.

Calculations were performed for a direct isomerization mechanism.  $E_0$  was required to be 30.8 kcal mol<sup>-1</sup> (Table VI). This value is ~1 kcal mol<sup>-1</sup> less than for CPn, and since it is not apparent why ring opening of CH<sub>x</sub> should not occur relative to CPn, we believe that opening does occur, and that the steady-state concentration of acyclic radicals is too low to be detected.

Reaction 14 which leads to a radical with more strain energy than reaction 18 may actually proceed faster because, in this case, the radical center is off the ring; although  $|\Delta E_{RS}|$  is greater for the five-membered ring transition state than for the six-membered transition state, the situation is reversed for the relative values of  $E_{LS}$ . In fact, reaction 14 has been found to be faster than reaction 18 in liquid phase cyclizations.<sup>22</sup> If all of the product radical cyclized *via* reaction 14, and if the direct isomerization were not important,  $E_0$  would be ~32 kcal mol<sup>-1</sup>, by analogy to CPn. If  $k_{18}/k_{14}$  were not close to zero, the measured rate would be too small, and the corresponding deduced value of  $E_0$  too high.

#### Appendix. Calculation of Unimolecular Rate Constants

**Cross Sections.** Effective collision cross sections,  $s^2$ , were derived from the Lennard-Jones parameters  $\sigma$  and  $\epsilon/k$

$$s^2 = (\sigma_{CO}^2 + \sigma_{H_2}^2)(\Omega^{(2,2)}(T^*))^2/2$$

where

$$T^* = T/[(\epsilon/k)_{CO}(\epsilon/k)_{H_2}]^{1/2}$$

**TABLE VII: Effective Collision Cross Section Data for Cyclic Olefins in H<sub>2</sub> Bath<sup>a</sup>**

Species	$\sigma, \text{\AA}^b$	$\epsilon/k, ^\circ\text{K}^b$	$s, \text{\AA}$
SCE•	5.27	310	4.24
CB•	4.7	244	3.87
CPn•	5.20	320	4.20
CHx•	5.67 <sup>b</sup>	325 <sup>b</sup>	4.44

<sup>a</sup>  $\sigma$  and  $\epsilon/k$  values for all species except CHx• were estimated by comparison with linear hydrocarbons from ref 23. <sup>b</sup> From value for CHx in ref 23.

and  $\Omega^{(2,2)}(T^*)$  values were obtained from standard tables;<sup>23</sup> the CO subscript represents the cyclic olefin. The values used are given in Table VII.

**Thermochemical Parameters.**  $\Delta H_f^\circ$  values for the cyclic radicals, as well as their minimum vibrational excitation energies, were calculated using  $\Delta H_f^\circ$  values where available from the literature<sup>24</sup> or estimated using appropriate corrections (see Table VIII). C–H dissociation energies were assumed to be as follows:<sup>25</sup>  $D^\circ_0$ (secondary C–H), 92.8;  $D^\circ_0$ (primary C–H) = 96.2;  $D^\circ_0$ (CB–H) = 94.6;  $D^\circ_0$ (CPn–H) = 92.6;  $D^\circ_0$ (CHx–H) = 93.5 kcal mol<sup>-1</sup>. An activation energy of 2 kcal mol<sup>-1</sup> was assumed for H-atom addition to a double bond.

**Miniprint Material Available.** Full-sized photocopies of the miniprinted material from this paper only (Tables I–IV and VIII) or microfiche (105 × 148 mm, 24× reduction, negatives) containing all of the miniprinted and supplementary material for the papers in this issue may be obtained from the Journals Department, American Chemical Society, 1155 16th St., N.W., Washington, D. C. 20036. Remit check or money order for \$3.00 for photocopy or \$3.00 for microfiche, referring to code number JPC-75-191.

## References and Notes

- (1) (a) This work was supported by the Office of Naval Research. (b) NSF Predoctoral Trainee

- (2) (a) M. Julia, *Pure Appl. Chem.*, **15**, 167 (1967); (b) *Accounts Chem. Res.*, **4**, 386 (1971); (c) A. S. Gordon, *Pure Appl. Chem.*, **5**, 441 (1962).
- (3) (a) W. P. L. Carter and D. W. Tardy, *J. Phys. Chem.*, **78**, 2201 (1974); (b) H. E. Gunning and R. L. Stock, *Can. J. Chem.*, **42**, 357 (1964); (c) A. S. Gordon, *ibid.*, **43**, 570 (1965).
- (4) (a) A. S. Gordon, S. R. Smith, and C. M. Drew, *J. Chem. Phys.*, **36**, 824 (1962); (b) R. Walsh, *Int. J. Chem. Kinet.*, **2**, 71 (1970); (c) A. S. Gordon, *ibid.*, **2**, 75 (1970). The critical threshold from experiments of ref 4a gave 18 kcal mol<sup>-1</sup>, which was argued to be ~35 kcal mol<sup>-1</sup> in ref 4b.
- (5) (a) G. Greig and J. C. J. Thynne, *Trans. Faraday Soc.*, **62**, 3338 (1966); (b) J. A. Kerr, A. Smith, and A. F. Trotman-Dickinson, *J. Chem. Soc. A*, 1400 (1969); (c) K. Furukawa, D. G. L. James, and M. M. Papic, *Int. J. Chem. Kinet.*, **6**, 337 (1974).
- (6) See, e.g., D. C. Tardy, B. S. Rabinovitch, and C. W. Larson, *J. Chem. Phys.*, **45**, 1163 (1966); **47**, 4570 (1967); E. W. Hardwidge, B. S. Rabinovitch, and R. C. Ireton, *ibid.*, **58**, 340 (1973).
- (7) S. E. Stein and B. S. Rabinovitch, *Int. J. Chem. Kinet.*, submitted for publication; S. E. Stein, Ph.D. Thesis, University of Washington, Seattle, 1974.
- (8) R. J. Gvetanovic, *Advan. Photochem.*, **1**, 115 (1963).
- (9) The boiling point of 1,1-diethylcyclopropane is ~89°, and the unidentified peak has a boiling point of ~88°. Generally, the substitution of a vinyl for an ethyl group lowers the boiling point and thus the unknown peak may be 1,1-ethylvinylcyclopropane. See ref 10.
- (10) See, e.g., S. W. Ferris, "Handbook of Hydrocarbons," Academic Press, New York, N.Y., 1955.
- (11) See, e.g., A. F. Trotman-Dickinson and G. S. Milne, *Nat. Stand. Ref. Data Ser., Nat. Bur. Stand.*, No. 9 (1967).
- (12) M. J. Pearson and B. S. Rabinovitch, *J. Chem. Phys.*, **42**, 1624 (1965).
- (13) B. S. Rabinovitch, R. F. Kubin, and R. E. Harrington, *J. Chem. Phys.*, **38**, 405 (1963).
- (14) See, e.g., W. A. Pryor, "Free Radicals," McGraw-Hill, New York, N.Y., 1966.
- (15) As the strain of a compound increases, the effective force constants for some of its modes increases, thereby increasing some frequency values.
- (16) B. S. Rabinovitch and R. W. Diesen, *J. Chem. Phys.*, **30**, 735 (1959).
- (17) R. E. Harrington, B. S. Rabinovitch, and R. W. Diesen, *J. Chem. Phys.*, **32**, 1245 (1960).
- (18) J. H. Georgakakos, B. S. Rabinovitch, and E. J. McAlduff, *J. Chem. Phys.*, **52**, 2143 (1970).
- (19) S. W. Benson, "Thermochemical Kinetics," Wiley, New York, N.Y., 1967.
- (20) S. Arai, S. Sata, and S. Shida, *J. Chem. Phys.*, **33**, 1277 (1960).
- (21) R. C. Lamb, P. W. Ayers, and M. K. Toney, *J. Amer. Chem. Soc.*, **85**, 3483 (1963).
- (22) C. W. Larson, Ph.D. Thesis, University of Washington, Seattle, Washington, 1970.
- (23) J. O. Hirschfelder, C. F. Curtiss, and R. B. Bird, "Molecular Theory of Gases and Liquids," Wiley, New York, N.Y., 1967.
- (24) F. D. Rossini, "Selected Values of Physical and Thermodynamic Properties of Hydrocarbons," Carnegie, Pittsburgh, Pa., 1953.
- (25) Secondary and primary C–H dissociation energies are as used in similar work, see, e.g., ref 22. C–H dissociation energies for the cyclic hydrocarbons are assumed to be as follows:  $D^\circ_0$ (cyclic paraffin C–H) =  $D^\circ_0$ (sec-acyclic C–H) + [ $E_{RS}$ (cyclic olefin) –  $E_{RS}$ (cyclic paraffin)]/2.

## Phenolic-OH Torsional Frequency as a Probe for Studying $\pi$ -Electron Distortions in Aromatic Systems

William G. Fateley,\*

Department of Chemistry, Kansas State University, Manhattan, Kansas 66506

Gerald L. Carlson,

Mellon Institute of Science, Carnegie-Mellon University, Pittsburgh, Pennsylvania 15213

and Freeman F. Bentley

Air Force Materials Laboratory/LPH, Wright-Patterson Air Force Base, Ohio 45433 (Received July 25, 1974)

Publication costs assisted by Kansas State University

The phenolic-OH torsional frequencies for a large number of substituted phenols have been obtained. For the monosubstituted phenols, the shift of the torsional frequency from its position in phenol itself is found to be directly related to the electron-donating or -withdrawing power of the substituent group. This has led to the derivation of a new parameter,  $\Delta\omega_t$ , which is suggested to be a direct measure of the effect of a substituent on the  $\pi$ -electron density of the aromatic ring, and  $\Delta\omega_t$  values are presented for a variety of substituent groups in the ortho, meta, and para positions. For multisubstituted phenols, it is found that the torsional frequency can often be predicted using the  $\Delta\omega_t$  value for each substituent. This indicates that, in the absence of steric effects, the inductive and/or mesomeric effects of substituents are additive until the ring becomes almost fully substituted.

### Introduction

A large amount of effort encompassing many types of physicochemical techniques has gone into the measurement of substituent effects on the  $\pi$ -electron system in aromatic compounds. The goal of this work has been the determination of electronic interactions in aromatic molecules for the purpose of correlating structure and reactivity and predicting properties and reactions rates. An excellent review of this topic has been given by Katritzky and Topsom.<sup>1</sup>

In 1967, Miller, Fateley, and Witkowski<sup>2</sup> examined the effect of para substituents on the CHO torsional barrier in benzaldehyde and attempted to correlate the barrier potential ( $V_2$ ) with the double bond character of the C-CHO bond, and, hence the electron donor or acceptor properties of the 4 substituent. Although these authors concluded that there was no correlation of the torsional barrier with the Hammett  $\sigma$  constants of the substituent groups, Campagnaro and Wood<sup>3</sup> later showed that if substituents with large donor or acceptor powers were used, a correlation with various Hammett and Taft  $\sigma$  parameters, and in particular with <sup>19</sup>F shielding parameters, could be derived. These workers also proposed that a similar correlation could be made for 4-substituted phenols.

In a previous publication,<sup>4</sup> it was shown that the effect of 4 substituents on the barrier to internal rotation about the C-O bond in phenol as determined by far-infrared studies of the torsional frequencies was in excellent agreement with results obtained by *ab initio* molecular orbital calculations. This work showed definitively that substituents which are  $\pi$ -electron donors lower the observed barrier while  $\pi$ -electron acceptors raise the barrier, and that the phenolic-OH torsional frequency is a direct measure of the double bond character of the phenolic C-O bond.

In the present study, we have measured the phenol-OH torsional frequency in a large number of substituted phe-

nols. The results obtained suggest that the torsional frequency can be used as a sensitive probe for measuring the effect of substituents, including multiple substitution, on the  $\pi$ -electron density in aromatic systems.

### Experimental Section

The phenol samples studied were obtained from a variety of sources. Commercially available phenols were purchased in the highest available purity, and in most cases were confirmed by comparison of their infrared spectra with published reference spectra. A large number of phenol samples were also made available to us through the courtesy of Dr. A. W. Baker of the Dow Chemical Co. In general, the purity of the samples was probably better than 95%; in a few cases purification by distillation or recrystallization was required.

Low-frequency infrared spectra were obtained with a Digilab FTS-14 Fourier transform spectrometer. Both 3-(600-100-cm<sup>-1</sup> range) and 6- $\mu$  (450-75-cm<sup>-1</sup> range) beam splitters were employed in conjunction with a global source. A resolution of 4 cm<sup>-1</sup> and a triangular apodization function were generally used.

Spectra were obtained using dilute (0.01-0.06 M) cyclohexane solutions and polypropylene or polyethylene cell windows. Path length was generally 5 mm; for a few samples of very low solubility, a 10-mm path was required. Spectra of the analogous phenol-OD compounds were obtained by deuteration of the sample directly in the cyclohexane solution.<sup>5</sup>

For a few compounds whose torsions fell above 500 cm<sup>-1</sup>, iso-octane was used in place of cyclohexane as the solvent.

### Results

*Validity of Torsional Frequencies Measured in Cyclohexane Solution.* It is well known that phenols are strongly associated in the liquid and also undergo hydrogen bonding

**TABLE I: Comparison of Cyclohexane Solution and Vapor Phase Torsional Frequencies for Phenols**

Phenol	OH torsional frequency, $\text{cm}^{-1}$	
	Cyclohexane solution	Vapor <sup>a</sup>
Phenol	310	310
<i>p</i> -Fluorophenol	280	280
<i>p</i> -Chlorophenol	303	302
<i>m</i> -Fluorophenol	318	318.5
<i>m</i> -Chlorophenol	312	312.5
<i>m</i> -Bromophenol	312	314
<i>m</i> -Methylphenol	312	311
<i>m</i> -CF <sub>3</sub>	317	315.5
<i>o</i> -Fluorophenol (cis)	366	379
<i>o</i> -Chlorophenol (cis)	396	407

<sup>a</sup> References 9–10.

with many solvents. With cyclohexane, there seems little possibility of hydrogen bonding with the solvent, but solute-solvent interactions have been reported. von Keussler<sup>6</sup> has shown that phenol in cyclohexane at a concentration of  $3 \times 10^{-4} M$  is completely monomeric, but is 52% associated at a concentration of 0.15 *M*. Dearden and Forbes<sup>7</sup> noted a shift between the ultraviolet spectra of phenol vapor and  $2.3 \times 10^{-4} M$  cyclohexane solutions which they attributed to solute-solvent interaction because phenol should be completely monomeric at this concentration. Furthermore, Evans<sup>8</sup> found that the positions of some of the infrared bands of phenol are dependent on the degree of association.

To determine whether the association of phenols at the concentrations required for this study would influence the torsional frequency, a dilution study on phenol in cyclohexane solution was carried out. Over the concentration range 0.02–0.001 *M*, which is the lower limit of detection with a 1-cm path length, the torsional frequency did not shift by more than 1  $\text{cm}^{-1}$ . This study indicates that association effects at the concentrations employed should be negligible.

To test the effect of interaction of phenols with cyclohexane, we have also compared the torsional frequencies of several phenols with their available gas-phase frequencies.<sup>9–11</sup> This comparison is given in Table I. In the case of meta- and para-substituted phenols, the solution frequencies are in excellent agreement with the vapor. For the ortho-halophenols, a vapor solution shift is found which is reflecting a change in the strength of the intramolecular hydrogen bond<sup>9</sup> and such a shift is not unexpected.

Both of these studies give confidence that by employing cyclohexane solutions, we can obtain valid torsional frequency data for the isolated, monomeric phenol molecule free of association and solvent effects. It should, however, be noted that this is not true for many other solvents. For example, Green, *et al.*,<sup>12a</sup> have pointed out that the torsional frequency for *p*-fluorophenol shifts from  $\sim 283 \text{ cm}^{-1}$  in cyclohexane to  $290 \text{ cm}^{-1}$  in CS<sub>2</sub> and to  $350 \text{ cm}^{-1}$  in benzene.

These observations are in agreement with the conclusion of Woolley and Hepler<sup>12b</sup> that cyclohexane is a (nearly) inert solvent while there is considerable specific interaction between phenol and benzene.

**Presentation of Data.** Although complete far-infrared spectra were obtained for all of the phenols studied as well

as the analogous phenol-OD compounds, because of the large number of compounds included, only the torsional frequencies are presented.

Torsional frequency data for 45 monosubstituted phenols are given in Table II. The data are presented both as the torsional frequency and as the shift ( $\Delta\omega_t$ ) from the unsubstituted phenol torsion at  $310 \text{ cm}^{-1}$ . Torsional frequencies for di-, tri-, tetra-, and pentasubstituted phenols are given in mini print.<sup>22</sup>

The assignment of the torsional frequencies was generally straightforward. The phenolic-OH torsion is usually the strongest band in the far-infrared solution spectrum and can be readily verified by its disappearance on deuteration of the O-H group. In a few cases, the O-H torsion was overlapped by other intramolecular bands, but these were considerably weaker and presented no particular problem in identifying the torsion. For phenol itself and several of the substituted phenols, including all of the meta-substituted phenols, the O-D torsion undergoes Fermi resonance with another mode in the vicinity of  $235 \text{ cm}^{-1}$  and appears as two bands of about equal intensity. The torsion for *o*-cyanophenol-OH also is split, presumably due to Fermi resonance, and its actual position was deduced from the frequency of the O-D torsion.

Additional torsional frequency data for a few substituted phenols not available in this study were obtained from the literature.<sup>13–15</sup> Some of these frequencies were measured at relatively high concentrations and in solvents other than cyclohexane and probably are somewhat influenced by solvent and/or association effects.

## Discussion

**Monosubstituted Phenols.** It has been shown from both theory<sup>18</sup> and experiment<sup>19</sup> that the phenol molecule is planar. The planar structure is favored because in this configuration the maximum delocalization of the p-type lone pair electrons on the oxygen atom can occur. The extent of this delocalization determines the energy difference between the planar and orthogonal forms, and hence the barrier to internal rotation (and the torsional frequency) of the O-H group. For phenol, the torsional frequency in cyclohexane solution is  $310 \text{ cm}^{-1}$  yielding a barrier ( $V_2$ ) of  $1240 \text{ cm}^{-1}$  (3.54 kcal/mol).

Substitution at the 4 position of the phenol ring results in changes in the  $V_2$  barrier, and the direction and magnitude of these changes has been accurately predicted by *ab initio* molecular orbital calculations from the electron-withdrawing or -donating power of the substituent group.<sup>4</sup> For a  $\pi$ -donating group,  $\pi$ -electron donation by OH decreases, the double bond character in the C-O bond decreases, and the barrier (and the torsional frequency) decreases. Conversely, a  $\pi$  acceptor will cause an increase in the O-H torsional frequency. Thus, we are proposing that the phenolic-OH torsional frequency is a sensitive probe for determining the effect of a 4 substituent on the electron density at the 1 position of the aromatic ring.

The  $\Delta\omega_t$  values listed in Table II are then proposed as a parameter which measures the electron-donating ( $\Delta\omega_t$  negative) or -withdrawing ( $\Delta\omega_t$  positive) power of the substituent group relative to hydrogen in phenol itself. To be strictly correct, we should use the change in the  $V_2$  barrier as our parameter; however, in the case of para-substituted phenols where the barrier must be twofold, the torsional frequency exactly parallels the barrier and we use the frequency or change in frequency for convenience.

TABLE II: Torsional Frequencies of Monosubstituted Phenols in Cyclohexane Solution

Phenol	Concn, <i>M</i>	Torsional freq ( $\omega_t$ ), $\text{cm}^{-1}$			$\Delta\omega_t^a$	Phenol	Concn, <i>M</i>	Torsional freq ( $\omega_t$ ), $\text{cm}^{-1}$			$\Delta\omega_t^a$
		OH	OD					OH	OD		
Phenol	0.01	310	{247 <sup>b</sup> 212}	0	<i>m</i> -Methyl	0.01	312	{248 211}	+2		
<b>Para substituted</b>					<i>m</i> -CHO	Satd	312		+2		
<i>p</i> -Nitro	Satd	350		+40	<i>m</i> -Phenyl	0.03	311	{248 215}	+1		
<i>p</i> -CHO	Satd	349	253	+39	<i>m-tert</i> -Butyl	0.03	308	{247 212}	-2		
<i>p</i> -Cyano	Satd	343	241	+33							
<i>p</i> -CF <sub>3</sub>	0.02	334	{267 225}	+24	<b>Ortho substituted</b>						
<i>p</i> -Iodo	0.02	313	233	+3	<i>o</i> -CHO <sup>e</sup>	0.80	713 <sup>c</sup>		+403		
<i>p</i> -Phenyl	Satd	310	232	0	<i>o</i> -Nitro	0.07	675	495	+365		
<i>p</i> -CH <sub>3</sub> S	Satd	307	224	-3	<i>o</i> -CH <sub>3</sub> S <sup>e</sup>	0.70	537 <sup>c</sup>		+227		
<i>p</i> -Chloro	0.015	303	227	-7	<i>o</i> -C <sub>2</sub> H <sub>5</sub> S <sup>e</sup>	0.70	537 <sup>c</sup>		+227		
<i>p</i> -Bromo	0.03	303	228	-7	<i>o</i> -Ethoxy, cis	0.03	432	{329 294}	+122 +76		
<i>p-tert</i> -Butyl	0.015	301	214	-9	trans		386	{326 297}	+118 +78		
<i>p</i> -Methyl	0.01	298	219	-12	<i>o</i> -Methoxy, cis	0.015	428	{312 297}	+111 +86		
<i>p</i> -Fluoro	0.01	280	214	-30	trans		388	{300 261}	+86 +51		
<i>p</i> -Methoxy	Satd	269	198	-41	<i>o</i> -Hydroxy	Satd	411	312	+111		
<i>p-n</i> -Butoxy	0.03	268	201	-42	<i>o</i> -Chloro, cis	0.008	396	{300 261}	+86 +51		
<i>p</i> -Hydroxyl	Satd	266		-44	trans		361	{298 252}	+85 +51		
<b>Meta substituted</b>					<i>o</i> -Bromo, cis	0.02	395	{288 240}	+73 +9		
<i>m</i> -Nitro	Satd	321	{253 220}	+11	trans		361	{290 240}	+72 +9		
<i>m</i> -Fluoro	0.01	318	{225 212}	+8	<i>o</i> -Phenyl, cis	0.03	383	288	+73		
<i>m</i> -Hydroxyl	Satd	318		+8	trans		319 ?	240 ?	+9		
<i>m</i> -Methoxy	0.06	317	{250 216}	+7	<i>o</i> -Cyano, cis	Satd	{392 376}	290	~+72		
<i>m</i> -CF <sub>3</sub>	0.01	317	{250 217}	+7	trans		343	261	+33		
<i>m</i> -Cyano	Satd	316	{250 214}	+6	<i>o</i> -Iodo, cis	0.02	378	285	+68		
<i>m</i> -Iodo	0.02	313	{249 216}	+3	trans		345	246	+35		
<i>m</i> -Chloro	0.008	312	{250 218}	+2	<i>o</i> -Fluoro, cis	0.01	366	269	+56		
<i>m</i> -Bromo	0.006	312	{248 216}	+2	trans		332		+22		
					<i>o-tert</i> -Butyl, trans	0.02	307	227	-3		
					cis		277 ?		-33 <sup>e</sup>		
					<i>o</i> -Isopropyl <sup>f</sup>		301 <sup>d</sup>		-9		
					<i>o</i> -CF <sub>3</sub>	0.01	300	{245 202}	-10		
					<i>o</i> -Methyl	0.01	297	224	-13		

<sup>a</sup>  $\Delta\omega_t = \omega_{t\text{subst phenol}} - \omega_{t\text{phenol}}$ . <sup>b</sup> Bracketed frequencies indicate Fermi resonance pairs. <sup>c</sup> CS<sub>2</sub> solution values. <sup>d</sup> Polyethylene matrix. <sup>e</sup> Reference 15. <sup>f</sup> Reference 14. <sup>g</sup> Reference 16.

In the case of the meta-substituted phenols, the presence of the meta substituent removes the twofold symmetry of the ring and introduces additional terms in the potential function for internal rotation. However, these additional terms have been shown to be very small<sup>11</sup> and the torsional frequency again parallels the  $V_2$  barrier to a good approximation.

For the ortho-substituted phenols, the barrier becomes considerably more complicated. Steric effects and intramolecular hydrogen bonding result in the existence of cis and trans isomers and perhaps even nonplanarity of the O-H group in the case of large bulky groups. In these cases, the  $V_1$  potential term becomes appreciable<sup>9,16</sup> and the correlation between the  $V_2$  barrier and the torsional frequency should no longer hold. However, we have found empirically that the  $\Delta\omega_t$  values for the ortho substituents is still a useful parameter as will be shown below. In cases where the torsional frequencies for both the cis and trans forms could be observed,  $\Delta\omega_t$  values for both forms are given.

Campagnaro and Wood<sup>3</sup> pointed out that the torsional parameters they obtained for 4-substituted benzaldehydes and for a limited number of 4-substituted phenols correlated well with the various Hammett type parameters for the substituents and particularly with the <sup>19</sup>F shielding parameter derived from nmr data on fluorobenzene. The comparison of our  $\Delta\omega_t$  values with appropriate Hammett  $\sigma$  values and with available <sup>19</sup>F shielding parameters is given in Table III. Examination of the data in Table III shows no good correlation between our  $\Delta\omega_t$  values and the <sup>19</sup>F parameters. Although the correlation for the most powerful electron-withdrawing substituents is reasonable (*e.g.*, NO<sub>2</sub> and OH for para substituents; NO<sub>2</sub> and *t*-Bu for meta substituents), there are many substituents for which the agreement is very poor, and it would appear that the conclusions reached by Campagnaro and Wood are not substantiated by our data.

The lack of agreement between our  $\Delta\omega_t$  substituent values and the corresponding Hammett substituent con-

TABLE III: Comparison of  $\Delta\omega_t$  ( $\text{cm}^{-1}$ ) Values with Substituent Constants for Substituted Phenols<sup>a</sup>

Substituent	Para substituents				Meta substituents				Ortho substituents		
	$\Delta\omega_t, \text{cm}^{-1}$	$\sigma_{\text{para}}$	$^{19}\text{F}_{\text{para}}$	$(^{19}\text{F}_{\text{para}} - ^{19}\text{F}_{\text{meta}})$	Substituent	$\Delta\omega_t, \text{cm}^{-1}$	$\sigma_{\text{meta}}$	$^{19}\text{F}_{\text{meta}}$	Substituent	$\Delta\omega_t, \text{cm}^{-1c}$	$\sigma_{\text{ortho}}^b$
$\text{NO}_2$	+40	+1.24 <sup>b</sup>	-9.3	-5.8	$\text{NO}_2$	+11	+0.71	-3.5	$\text{CHO}$	+403 c	+0.75
$\text{CHO}$	+39	+1.03 <sup>b</sup>	-9.4	-8.1	$\text{F}$	+8	+0.34	-1.3	$\text{NO}_2$	+365 c	+1.24
$\text{CN}$	+33	+0.88 <sup>b</sup>	-9.2	-6.4	$\text{OH}$	+8	+0.10	-1.3	$\text{CH}_3\text{O}$	{+118 c +78 t}	0
$\text{CF}_3$	+24	+0.54	-5.1	+3.0	$\text{OCH}_3$	+7	+0.14	-1.1	$\text{Cl}$	{+86 c +51 t}	+0.68
$\text{I}$	+3	+0.30	+1.5	+3.9	$\text{CF}_3$	+7	+0.47	-2.1			
$\text{C}_6\text{H}_5$	0	+0.01	+2.9		$\text{CN}$	+6	+0.61	-2.8	$\text{Br}$	{+85 c +51 t}	+0.70
$\text{H}$	0	0	0		$\text{I}$	+3	+0.35	-2.4			
$\text{CH}_3\text{S}$	-3	+0.21			$\text{Cl}$	+2	+0.37	-2.0	$\text{C}_6\text{H}_5$	{+73 c +9 ? c}	0
$\text{Cl}$	-7	+0.23	+3.1	+5.1	$\text{Br}$	+2	+0.39	-2.3	$\text{I}$	{+68 c +35 t}	+0.63
					$\text{CH}_3$	+2	-0.07	+1.2			
$\text{Br}$	-7	+0.27	+2.5	+4.8	$\text{CHO}$	+2	+0.36	-1.3	$\text{F}$	{+56 c +22 t}	+0.54
<i>t</i> -Bu	-9	-0.20									
$\text{CH}_3$	-12	-0.17	+5.4	+4.2	$\text{C}_6\text{H}_5$	+1	+0.06		<i>t</i> -Bu	-3 t	-0.52
$\text{F}$	-30	+0.06	+6.8	+9.8	<i>t</i> -Bu	-2	-0.10		$\text{CH}_3$	-13	-0.13
$\text{CH}_3\text{O}$	-41	-0.11 <sup>b</sup>	+11.5	+12.6							
$\text{OH}$	-44	-0.37	+10.8	+12.1							

<sup>a</sup>  $\sigma$  values from ref 20. <sup>19</sup>F values from ref 21. <sup>b</sup> Indicates special values for phenols. <sup>c</sup> c and t refer to cis and trans forms.

stants may not be unexpected. The  $\Delta\omega_t$  parameter is reflecting the effect of a ring substituent on the  $\pi$ -electron density at the 1 position of the aromatic ring of the phenol molecule while the Hammett  $\sigma$  constant is a measure of the substituent effect on the ionization of the proton from the -OH group in benzoic acid or phenol. On the other hand, the <sup>19</sup>F shielding parameter depends upon electron density in the very close vicinity of the <sup>19</sup>F nucleus<sup>21</sup> and should perhaps correlate better with the  $\Delta\omega_t$  values.

It is, however, not the purpose of this paper to resolve the relationship between substituent effects on  $\pi$ -electron density in the aromatic ring and on reactivity constants. We feel, and calculation has shown,<sup>4</sup> that the new parameter we are presenting is an accurate measure of the effect of substituents on the  $\pi$ -electron density in the aromatic ring.

**Multisubstituted Phenols.** In order to study the effect of multiple substitution on the electron density in the aromatic ring, the phenolic-OH torsional frequency was measured for a large number of substituted phenols.<sup>22</sup> The results of this study indicate that, in the absence of steric effects, the net effect of several ring substituents can be predicted from the  $\Delta\omega_t$  value for each substituent.

If the substituents exert linear mesomeric and inductive effects, *i.e.*, if each substituent in a given position always influences the  $\pi$ -electron density with the same magnitude, then it should be possible to use the  $\Delta\omega_t$  values in Table II to predict the torsional frequencies and barriers for multisubstituted phenols. For example, the torsional frequency of 2-chloro-4-fluorophenol should be the linear combination of the  $\Delta\omega_t$  values of the 2-chloro and 4-fluoro substituents. To predict the torsional frequency for this molecule, it is only necessary to add these  $\Delta\omega_t$  values to the torsional frequency of phenol:

$$\omega_t^{\text{calcd}} = \omega_t^{\text{phenol}} + (\Delta\omega_t)_{\text{Cl}}^{\text{ortho}} + (\Delta\omega_t)_{\text{F}}^{\text{para}}$$

Since *o*-chlorophenol has cis and trans isomeric forms, it should also be possible to use  $(\Delta\omega_t)_{\text{Cl}}^{\text{ortho}}$  values for the cis and trans forms to predict both torsional frequencies for the 2-chloro-4-fluorophenol molecule: cis form  $\omega_t^{\text{calcd}} = 310 + (+86) + (-30) = 366 \text{ cm}^{-1}$ ; trans form  $\omega_t^{\text{calcd}} = 310 + (+51) + (-30) = 331 \text{ cm}^{-1}$ . The observed torsional frequencies for this molecule are 370 (cis) and 336 (trans)  $\text{cm}^{-1}$ . Thus in the case of a substituted phenol free of steric effects, we find good agreement between observation and prediction.

A similar calculation has been carried out for all of the phenols given<sup>22</sup> and the calculated torsional frequencies are compared with the observed. For many of the phenols, the agreement between calculation and observation is quite good.

One problem which has not yet been resolved is the calculation of the torsional frequency for 2,6 or 3,5 disubstitution. To illustrate, consider the following examples.

(1) 2,6-Dibromophenol

$$\omega_t^{\text{calcd}} = \omega_t^{\text{phenol}} + (\Delta\omega_t)_{\text{Br}}^{\text{ortho}}$$

Here we would not know whether to add the  $\Delta\omega_t$  contribution of one Br, both Br's, or the cis  $\Delta\omega_t$  value for one Br and the trans of the other. Since the observed torsion is at 395  $\text{cm}^{-1}$ , in order to bring our calculated value into agreement we only can use the  $\Delta\omega_t$  value (+85  $\text{cm}^{-1}$ ) of a single cis bromine substituent. This same result appears to hold for all cases of symmetrical 2,6 disubstitution.

(2) 2-Methyl-6-*tert*-butylphenol. In this case, it would appear that we should combine the contribution of the 2-methyl group with the trans  $\Delta\omega_t$  value of the *tert*-butyl group because steric factors would favor the O-H being trans to the bulkier group:

$$\omega_t^{\text{calcd}} = \omega_t^{\text{phenol}} + (\Delta\omega_t)_{\text{CH}_3}^{\text{ortho}} + (\Delta\omega_t)_{\text{t-Bu}}^{\text{ortho,trans}}$$

$$\omega_t^{\text{calcd}} = 310 + (-13) + (-3) = 294 \text{ cm}^{-1}$$



**Acknowledgment.** Partial support for this work was provided by the United States Air Force, Wright-Patterson Air Force Base, Contract No. F 33615-71-C-1157, and Carnegie-Mellon University. One of the authors (W.G.F.) acknowledges NSF Grant No. 1275 in support of this research. The authors are also grateful to Dr. A.W. Baker of the Dow Chemical Co. for providing some of the samples used in this study.

**Miniprint Material Available.** Full-sized photocopies of the miniprinted material from this paper only or microfiche (105 × 148 mm, 24× reduction, negatives) containing all of the miniprinted and supplementary material for the papers in this issue may be obtained from the Journals Department, American Chemical Society, 1155 16th St., N.W., Washington, D. C. 20036. Remit check or money order for \$3.00 for photocopy or \$2.00 for microfiche, referring to code number JPC-75-199.

## References and Notes

- (1) A. R. Katritzky and R. D. Topsom, *Angew. Chem., Int. Ed. Engl.*, **9**, 87 (1970).
- (2) F. A. Miller, W. G. Fateley, and R. E. Witkowski, *Spectrochim. Acta, Sect. A*, **23**, 891 (1967).

- (3) G. E. Campagnaro and J. L. Wood, *J. Mol. Structure*, **6**, 117 (1970).
- (4) L. Radom, W. J. Hehre, J. A. Pople, G. L. Carlson, and W. G. Fateley, *J. Chem. Soc., Chem. Commun.*, 308 (1972).
- (5) G. L. Carlson, W. G. Fateley, and F. F. Bentley, *Spectrochim. Acta, Sect. A*, **28**, 177 (1972).
- (6) V. von Keussler, *Z. Electrochem.*, **58**, 136 (1954).
- (7) J. C. Dearden and W. F. Forbes, *Can. J. Chem.*, **37**, 1294 (1959).
- (8) J. C. Evans, *Spectrochim. Acta*, **16**, 1382 (1960).
- (9) G. L. Carlson, W. G. Fateley, A. S. Manocha, and F. F. Bentley, *J. Phys. Chem.*, **76**, 1553 (1972).
- (10) W. G. Fateley, F. A. Miller, and R. E. Witkowski, Technical Documentary Report No. AFML-TR-66-408, Jan 1967.
- (11) A. S. Manocha, G. L. Carlson, and W. G. Fateley, *J. Phys. Chem.*, **77**, 2094 (1973).
- (12) (a) J. H. S. Green, D. J. Harrison, and W. Kynaston, *Spectrochim. Acta, Sect. A*, **27**, 2199 (1971); (b) E. M. Woolley and L. G. Hepler, *J. Phys. Chem.*, **76**, 3058 (1972).
- (13) J. H. S. Green, D. J. Harrison, and W. Kynaston, *Spectrochim. Acta, Sect. A*, **28**, 33 (1972).
- (14) R. J. Jakobsen and J. W. Brasch, *Spectrochim. Acta*, **21**, 1753 (1965).
- (15) R. A. Nyquist, *Spectrochim. Acta*, **19**, 1855 (1963).
- (16) G. L. Carlson and W. G. Fateley, *J. Phys. Chem.*, **77**, 1157 (1973).
- (17) H. D. Bist, J. C. D. Brand, and D. R. Williams, *J. Mol. Spectrosc.*, **24**, 402 (1967).
- (18) W. J. Hehre, L. Radom, and J. A. Pople, *J. Amer. Chem. Soc.*, **94**, 1496 (1972).
- (19) T. Kojima, *J. Phys. Soc. Jap.*, **15**, 284 (1960).
- (20) G. B. Barlin and D. D. Perrin in "Elucidation of Organic Structures by Physical and Chemical Methods," Part I, Wiley-Interscience, New York, N.Y., 1972, Chapter IX, pp 638-639.
- (21) R. W. Taft, Jr., *J. Phys. Chem.*, **64**, 1805 (1960).
- (22) See paragraph at end of text regarding miniprint material.

## Thermal Dissociation of Cyanogen Bromide in Shock Waves

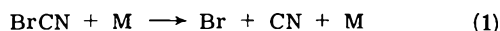
K. Tabayashi, O. Kajimoto, and T. Fueno\*

Department of Chemistry, Faculty of Engineering Science, Osaka University, Toyonaka, Osaka 560, Japan  
(Received September 4, 1973; Revised Manuscript Received August 22, 1974)

The thermal dissociation of cyanogen bromide diluted in argon was studied behind incident shock waves over the temperature range 2200–3600°K. The course of the dissociation was followed for 0.2–1% BrCN by monitoring the CN (0–1) violet absorption centered at 4216 Å. The initial slopes of absorption gave the bimolecular dissociation rate constants which are represented by  $k = [1.84 \times 10^{12}/1.5!]T^{1/2}(E/RT)^{1.5} \exp(-E/RT) \text{ cm}^3 \text{ mol}^{-1} \text{ sec}^{-1}$ , with  $E = D_0(\text{Br-CN}) = 81.6 \text{ kcal/mol}$ . The overall absorption profile was somewhat complex at lower temperatures, indicating the occurrence of a rapid homorecombination of CN to form  $\text{C}_2\text{N}_2$  as well as chain reactions involving Br and CN as chain carriers. Plausibility of the overall reaction scheme assumed was checked by computer integrations of a set of relevant rate equations. It was confirmed that the initial slope for the time-concentration curves of CN radicals is least affected by the various subsidiary reactions.

### I. Introduction

Kinetics of the bimolecular dissociation of cyanogen bromide in shock waves



has already been investigated by three groups of workers.<sup>1-3</sup> Patterson and Greene<sup>1</sup> first determined the dissociation rate of BrCN in argon, by monitoring the CN (0–1)  $\text{B}^2\Sigma^+ \rightarrow \text{X}^2\Sigma^+$  emission at temperatures between 2600 and 4200°K. They obtained second-order rate constants  $k_1$  which were fitted by a simple collisional expression having the activation parameter  $E_a = 90.5 \text{ kcal/mol}$ . Kayes and

Levitt<sup>2</sup> reinvestigated profiles of the same CN emission in greater detail and showed that, over the temperature range 2000–4000°K, their values of  $k_1$  are nearly two orders of magnitude greater than those reported by Patterson and Greene. Further, the temperature coefficient ( $E_a$ ) of  $k_1$  was found to be  $1.5RT$  less than the bond dissociation energy,  $D_0(\text{Br-CN}) = 82 \text{ kcal/mol}$ .

Recently, Clark, Dove, and Finkelman<sup>3</sup> studied the BrCN decomposition in neon and krypton, by means of the time-of-flight mass-spectrometric determination of the BrCN concentrations. The  $k_1$  values which they suggested for the BrCN-Kr system at 2100–2900°K were of the same order of magnitude as those obtained by Kayes and Levitt

for BrCN-Ar mixtures. However, the temperature coefficient of  $k_1$  was as low as 50 kcal/mol.

The overall decomposition kinetics of cyanogen halides seems to be more or less complicated by the operation of chain reactions involving halogen atoms and cyano radicals as chain carriers.<sup>2-4</sup> Under certain circumstances, the situation could even be more complex because of the possible intermediacy of vibrationally excited cyanogen  $C_2N_2^*$ , as has been claimed by Kayes and Levitt.<sup>2</sup> None the less, the afore-mentioned disagreements among the previous kinetic results do indicate that the kinetics of reaction 1 itself still remains to be settled.

We have thus undertaken to measure the dissociation rates of BrCN in Ar, adopting the CN  $X^2\Sigma^+ \rightarrow B^2\Sigma^+$  absorption technique which was successfully used in our previous work on the  $C_2N_2$  dissociation.<sup>5</sup> The rate constants  $k_1$  were obtained for 0.2–1% BrCN-Ar mixtures over the temperature range 2200–3600°K. They were found to agree fairly well with the afore-mentioned emission rate data reported by Kayes and Levitt.<sup>2</sup> The absorption study was complemented with computer tracings of the time history of CN radical concentration. The overall reaction scheme which was assumed to consist of reaction 1, homorecombinations of Br and CN, and chain reactions, was found to suffice to reproduce the observed concentration profiles of CN.

## II. Experimental Section

(A) *Material.* Cyanogen bromide with a minimum purity of 97.0% was purchased from the Nakarai Chemical Co. Ltd. Mass spectrometric analysis revealed the presence of slight amounts of HCN and CO as impurities. BrCN was distilled<sup>6</sup> and only the middle fraction was collected, bp 62°. The sample was then degassed at the temperature of a Dry Ice-acetone bath (−78°) and further purified by bulb-to-bulb distillation. Ultrapure argon (from the Takachiho Shoji Corp.), having a stated purity of 99.999%, was used as the carrier gas. Mixtures of 0.2, 0.5, and 1.0% BrCN in Ar were prepared in 10-l. glass flasks. They were allowed to stand for more than 12 hr before use.

(B) *Procedure.* Experiments were carried out in a stainless-steel cylindrical shock tube having an internal diameter of 10.4 cm. Details of the apparatus have been described previously.<sup>5</sup>

Considerable precautions were taken to minimize impurities due to the residue of air in the shock tube. The driven section was evacuated down to  $10^{-4}$  Torr, purged with the test gas, and then reevacuated to a pressure less than  $5 \times 10^{-6}$  Torr before each run. The leak rate was no greater than  $10 \times 10^{-6}$  Torr/min. The initial pressure,  $P_1$ , of the gas mixture was varied from 6.0 to 33.0 Torr to produce a given temperature condition for operation. The diaphragms were Mylar; their thickness ranged from 0.1 to 0.2 mm, which corresponded to the driver bursting pressure of 4 and 8 kg/cm<sup>2</sup>, respectively.

The absorption intensity was measured at the (0–1) band (P branch, head at 4216 Å) of the CN  $X^2\Sigma^+ \rightarrow B^2\Sigma^+$  system. The grating monochromator with 300- $\mu$  entrance and exit slits was set to isolate the spectral bandwidth 4213–4217 Å. This region encompasses the overlapping rotational lines  $J = 10$ –35 of the ground state CN ( $X^2\Sigma^+, v = 1$ ).

The state parameters of the shock-heated gas immediately behind the shock front were calculated from the measured shock velocity and initial gas pressure. No temperature correction for the heats of reaction was practiced.

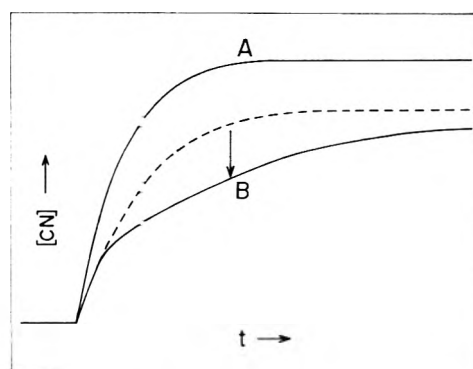


Figure 1. Characteristic patterns of the CN absorption profiles behind the incident shock wave: A,  $T > 3000^\circ\text{K}$ ; B,  $T < 3000^\circ\text{K}$ .

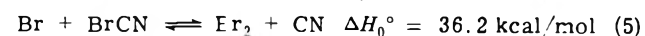
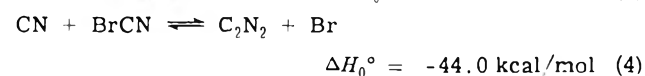
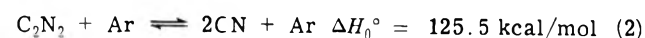
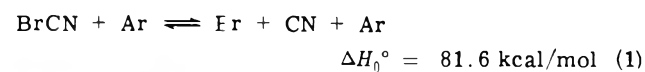
Boundary layer effects<sup>7</sup> on gas properties were estimated to be unimportant in the initial portion of absorption and assumed to be negligible over the time region of our interest. All calculations were carried out on an NEAC N-700 digital computer.

## III. Results

(A) *Qualitative Features of the Absorption Profile.* Absorption curves were oscillographically recorded for the 0.2, 0.5, and 1.0% BrCN-Ar mixtures. The total pressure of the shock-heated samples ranged from 0.37 to 1.20 atm, and the temperature ranged from 2200 to 3600°K.

Figure 1 illustrates the characteristic features of the CN absorption records. At temperatures above 3000°K, the absorption profile was simply of the form of exponential relaxation to an equilibrium value (curve A). At lower temperatures (and especially at higher pressures), however, it generally showed a nonexponential increase which involves an initial rapid rise, followed by a gradual rise to a final constant value (curve B). At any event, the absorbance was found to reach a steady level eventually.

It appears that the above features could be accounted for by assuming the following reaction scheme similar to that proposed by Schofield, Tsang, and Bauer for the ClCN pyrolysis.<sup>4</sup>



The backward processes of reactions 2 and 3 are homorecombinations of CN and Br, respectively. The forward processes of reactions 4 and 5 constitute a cycle of chain reactions by which BrCN is converted to  $C_2N_2$  and  $Br_2$ . Reaction 6 is a (concerted) bimolecular exchange reaction.

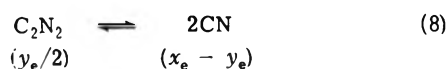
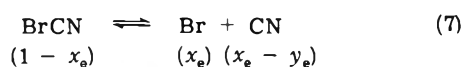
According to the above mechanism, the initial rise of the CN absorption should correspond to the production of CN by reaction 1. The fate of the CN radicals so produced should depend on the relative rates of the subsequent reactions. Thermodynamical considerations based on the available data<sup>8,9</sup> for the free-energy change of reactions  $\Delta G^\circ$  suggest that below 3000°K a considerable portion of the

TABLE I: BrCN Dissociation Rate Data

$n$ , mol %	$P$ , Torr	$U_s$ , mm/ $\mu$ sec	$\rho_{21}$	$T_2$ , °K	$[\text{Ar}]_0$ , $10^{-6}$ mol/cm <sup>3</sup>	$x_e$	$x_e - y_e$	$k_1$ , cm <sup>3</sup> mol <sup>-1</sup> sec <sup>-1</sup>
0.201	29.3	1.53	3.54	2363	5.72	0.996	0.219	$1.22 \times 10^8$
0.201	19.6	1.69	3.62	2826	3.91	0.999	0.862	$1.73 \times 10^9$
0.502	31.5	1.50	3.53	2279	6.11	0.992	0.0913	$8.89 \times 10^7$
0.501	30.3	1.53	3.54	2363	5.89	0.993	0.144	$1.09 \times 10^8$
0.500	27.2	1.58	3.55	2506	5.15	0.995	0.287	$3.95 \times 10^8$
0.500	20.4	1.61	3.57	2604	3.89	0.997	0.450	$5.37 \times 10^8$
0.500	20.4	1.66	3.59	2749	3.90	0.998	0.651	$1.41 \times 10^9$
0.500	18.9	1.71	3.61	2893	3.64	0.999	0.821	$2.54 \times 10^9$
0.501	8.73	1.79	3.65	3143	1.75	1.000	0.976	$7.47 \times 10^9$
0.502	8.25	1.86	3.67	3364	1.65	1.000	0.993	$1.69 \times 10^{10}$
0.975	33.3	1.48	3.51	2235	6.24	0.987	0.0511	$5.48 \times 10^7$
1.01	14.9	1.56	3.55	2442	2.88	0.994	0.208	$2.64 \times 10^8$
1.02	16.3	1.58	3.55	2502	3.06	0.995	0.265	$3.03 \times 10^8$
0.975	23.8	1.63	3.58	2668	4.53	0.995	0.407	$6.10 \times 10^8$
0.989	8.47	1.69	3.62	2826	1.68	0.999	0.768	$2.20 \times 10^9$
0.989	8.08	1.79	3.65	3144	1.60	1.000	0.958	$8.52 \times 10^9$
0.960	9.33	1.85	3.66	3334	1.79	1.000	0.983	$1.63 \times 10^{10}$
0.960	7.98	1.91	3.68	3553	1.54	1.000	0.995	$2.18 \times 10^{10}$

CN radicals should exist in the form of  $\text{C}_2\text{N}_2$  because of reactions 2 and 4. It is well conceivable that these reactions should affect the kinetic history of the CN radicals.

(B) *Pseudoequilibrium*. The final constancy of CN absorption suggests the existence of pseudoequilibrium of the reactions within the observation time. Under the condition at which data were taken, bromine should be dissociated into atoms almost completely, and hence reaction 3 can be neglected. Reactions 4–6 are stoichiometrically related to reaction 1 plus reaction 2 and/or 3, and hence can also be ignored for equilibrium considerations. The overall equilibrium is thus simplified into the scheme as follows:



The degrees of dissociation at equilibrium,  $x_e$  and  $y_e$ , which are defined as in eq 7 and 8, can be obtained by solving the following set of simultaneous equations:

$$K_1 = \frac{nx_e(x_e - y_e)P}{(1 - x_e)(1 + nx_e - ny_e/2)} \quad (9)$$

$$K_2 = \frac{2n(x_e - y_e)^2P}{y_e(1 + nx_e - ny_e/2)} \quad (10)$$

where  $K_1$  and  $K_2$  are the pressure-based equilibrium constants for reactions 1 and 2, respectively;  $n$  is the initial concentration (molar fraction) of BrCN; and  $P$  is the total pressure of the shock-heated gas mixture. Manipulation of eq 9 and 10 leads to a cubic equation with respect to  $x_e$ , viz.

$$f(x_e) = c_1x_e^3 + c_2x_e^2 + c_3x_e + c_4 = 0 \quad (11)$$

with

$$c_1 = n(P + K_1 - K_1K_{12})$$

$$c_2 = K_1(1 - n - 2K_{12} + 2nK_{12})$$

$$c_3 = -K_1(1 - 4K_{12} + nK_{12}) \quad (12)$$

$$c_4 = -2K_1K_{12}$$

and

$$K_{12} = K_1/K_2 \quad (13)$$

The value of  $x_e$ , i.e., the degree of dissociation of BrCN at equilibrium, is obtained as a positive root ( $0 \leq x_e \leq 1$ ) of eq 11. The corresponding fraction of the CN radicals, i.e.,  $x_e - y_e$  is related with  $x_e$  and  $K_{12}$  by

$$x_e - y_e = x_e^2/[x_e + 2K_{12}(1 - x_e)] \quad (14)$$

The values of  $x_e$  and  $x_e - y_e$  calculated as above<sup>11</sup> for some representative runs are shown in Table I. It is seen that, under our experimental conditions, BrCN is dissociated almost completely but that the fraction of free CN radicals diminishes appreciably as the temperature is lowered.

The predicted variation in the equilibrium concentration of CN radicals with temperature can be tested experimentally. The observed absorbance at equilibrium is related to the equilibrium concentration  $[\text{CN}]_e$  by<sup>5</sup>

$$\ln(I_0/I)_e = \beta l F_{\text{ab}}(T)[\text{CN}]_e \quad (15)$$

where  $\beta$  is the effective absorption coefficient for the CN radicals in the absorbing levels;  $l$  is the optical path length; and  $F_{\text{ab}}(T)$  is the fractional population of the absorbing  $\text{CN}(X^2\Sigma^+)$  radicals at temperature  $T$ . It is expected that the absorption coefficient  $\beta$  thus related with the absorbance should be least temperature dependent.<sup>5</sup>

Combining the observed absorbance at the final constant region with the calculated values of  $[\text{CN}]_e$  and  $F_{\text{ab}}(T)$ , one can evaluate  $\beta$  for each run. The  $\beta$  values thus obtained are plotted against the reaction temperature in Figure 2. Although the plotted points are scattered, they show no apparent temperature dependence. The results indicate that the assumption of the simple equilibrium scheme as expressed by eq 7 and 8 is basically correct. The most probable value of  $\beta$  in our present experimental settings was  $(4.91 \pm 0.76) \times 10^6$  cm<sup>2</sup>/mol.<sup>12</sup>

(C) *Dissociation Kinetics*. The bimolecular dissociation rate constants  $k_1$  were determined from the initial slopes of the absorption traces. Because relatively dilute sample mixtures were used, other processes of disappearance of BrCN than reaction 1 could be neglected immediately be-

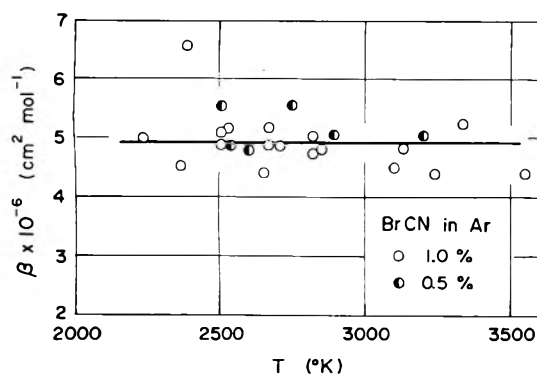


Figure 2. Temperature variation of the CN absorption coefficient at 4216 Å.

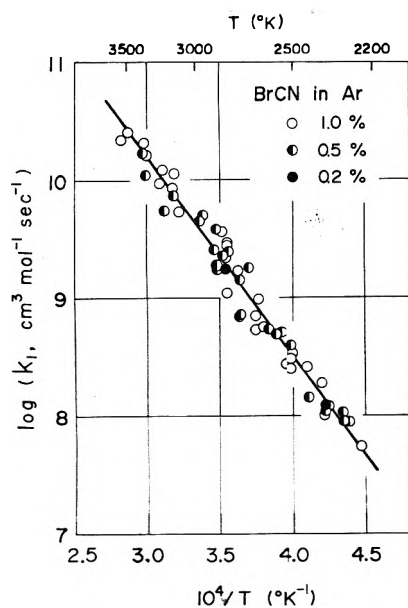


Figure 3. Arrhenius plots of  $k_1$ .

hind the shock front. Thus,  $k_1$  can be evaluated from the expression

$$\begin{aligned} k_1 &= (d[\text{CN}]/dt)_0 / [\text{BrCN}]_0 [\text{Ar}]_0 \\ &= r_0 / \beta I F_{\text{ab}}(T) [\text{BrCN}]_0 [\text{Ar}]_0 \end{aligned} \quad (16)$$

where  $r_0$  is the initial slope of absorbance

$$r_0 = \left\{ \frac{d \ln(I_0/I)}{dt} \right\}_0 \quad (17)$$

and where  $[\text{BrCN}]_0$  and  $[\text{Ar}]_0$  are the concentrations of cyanogen bromide and argon at zero time. We set  $\beta = 4.91 \times 10^6 \text{ cm}^2/\text{mol}$  as determined in the preceding section. The values of  $k_1$  thus obtained for representative runs are listed in Table I.

Figure 3 shows the Arrhenius plots of  $k_1$  obtained for a total of 57 experiments. It can be seen that a single straight line fits the plots, irrespective of the BrCN/Ar ratio. Least-squares treatment of the linearity led to the Arrhenius expression

$$k_1 = (1.60 \pm 0.36) \times 10^{15} \exp\left[\frac{-76,600 \pm 1200}{RT}\right] \text{ cm}^3 \text{ mol}^{-1} \text{ sec}^{-1} \quad (18)$$

In Figure 4, our rate constants  $k_1$  obtained by absorption spectroscopy are compared with the results which previous

TABLE II: Rate Constants Selected for Curve Fittings

Reaction	Rate constant, $\text{cm}^3 \text{ mol}^{-1} \text{ sec}^{-1}$	Ref
1	$k_1 = 1.60 \times 10^{15} \exp(-76,600/RT)$	This work
2	$k_2 = 6.66 \times 10^{16} \exp(-98,640/RT)$	5
3	$k_3 = 2.14 \times 10^{11} T^{1/2} \exp(-31,300/RT)$	14
4	$k_4 = 4.0 \times 10^{11}$	
5	$k_5 = 2.0 \times 10^{14} \exp(-23,000/RT)$	
6	$k_6 = 5.0 \times 10^{14} \exp(-65,000/RT)$	a

<sup>a</sup> Assumed equal to the rate constant reported for  $2\text{CF}_3\text{CN} \rightarrow \text{C}_2\text{F}_6 + \text{C}_2\text{N}_2$  (D. J. Perette and G. J. Janz, *J. Amer. Chem. Soc.*, **91**, 6590 (1969)).

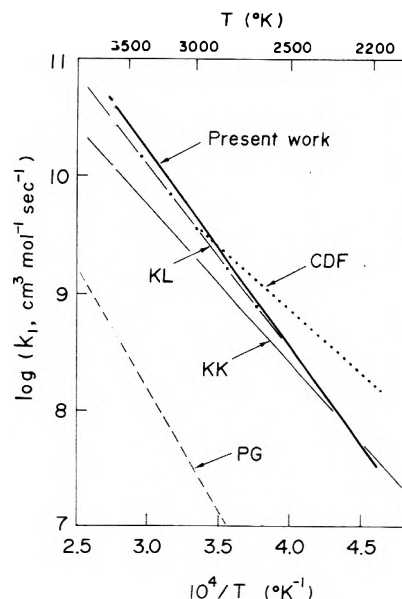


Figure 4. Comparison of the rate constants for the dissociation of BrCN in Ar: PG (Patterson and Greene),<sup>1</sup> emission study,  $k_1 = 10^{12.3} T^{0.5} \exp(-90,500/RT) \text{ cm}^3 \text{ mol}^{-1} \text{ sec}^{-1}$ ; KL (Kayes and Levitt),<sup>2</sup> emission study,  $k_1 = 10^{20.7} T^{-1.5} \exp(-82,500/RT) \text{ cm}^3 \text{ mol}^{-1} \text{ sec}^{-1}$ ; CDF (Clark, Dove, and Finkelman),<sup>3</sup> mass spectroscopy, in Kr,  $k_1 = 10^{13.7} \exp(-50,000/RT) \text{ cm}^3 \text{ mol}^{-1} \text{ sec}^{-1}$ ; KK (Keck and Kalelkar),<sup>13</sup> RRKM theory,  $k_1 = 10^{13.97} \exp(-63,030/RT) \text{ cm}^3 \text{ mol}^{-1} \text{ sec}^{-1}$ .

workers obtained by different experimental techniques.<sup>1-3</sup> The rate constants which were predicted theoretically by Keck and Kalelkar<sup>13</sup> are also included for comparison. Our results are found to be in close agreement with the emission results of Kayes and Levitt.<sup>2</sup>

(D) Computer Tracing of the Kinetic Histories of CN Radicals. In order to understand the absorption profile quantitatively, the rate equations for the entire mechanism consisting of reactions 1-6 were subjected to numerical (Runge-Kutta-Gill) integration on a computer.

Table II presents the rate parameters used for computations. The rate constants  $k_1$ ,  $k_2$ , and  $k_3$  are those determined experimentally.<sup>5,14</sup> For the remaining forward reactions (4-6), no rate data are available. Hence, the values of  $k_4$ ,  $k_5$ , and  $k_6$  were estimated by requiring the best overall fit of the calculated CN concentration profiles to the observed absorption curves. The rate constants of the reverse reactions were all calculated from those of the forward reactions and the equilibrium constants. The time step used for integration was 0.25  $\mu\text{sec}$ . In what follows, we will be concerned with the concentration profile of the CN radicals only.

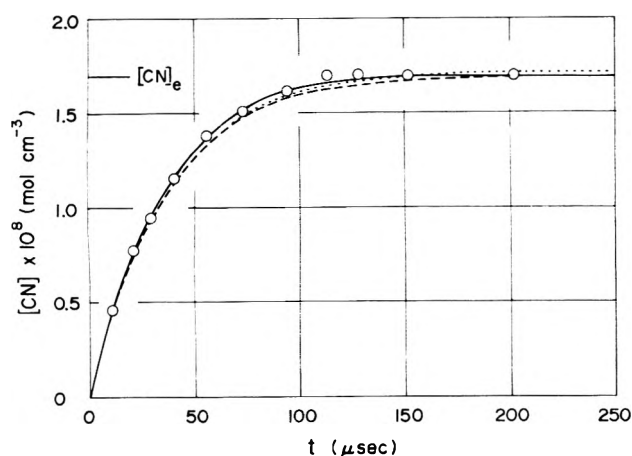


Figure 5. Comparison of the computed CN profiles with observed:  $T_2 = 3334^\circ\text{K}$ ;  $n = 1.0\%$ ;  $[\text{CN}]_e = 1.71 \times 10^{-8} \text{ mol/cm}^3$ ; (—) complete mechanism, reactions 1–6; (---) reactions 4 and 5 excluded; (· · ·) reaction 1 alone; (O) experimental.

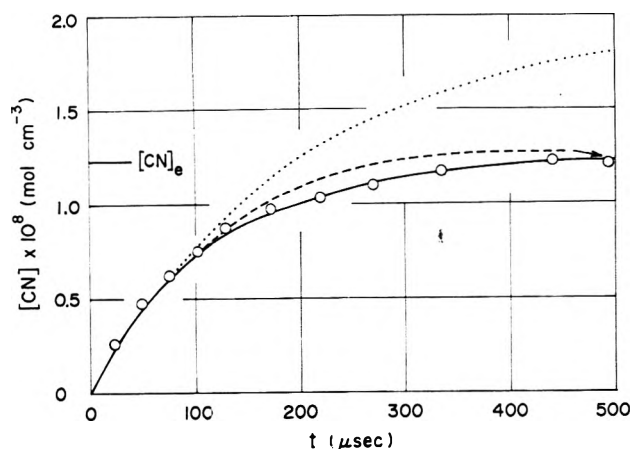


Figure 6. Comparison of the computed CN profiles with observed:  $T_2 = 2749^\circ\text{K}$ ;  $n = 0.5\%$ ;  $[\text{CN}]_e = 1.28 \times 10^{-8} \text{ mol/cm}^3$ . The lines and circles are the same as used in Figure 5.

The results of calculations for the cases of  $T_2 = 3334$ , 2749, and  $2506^\circ\text{K}$  are shown in Figures 5–7, respectively, where the abscissa is  $[\text{CN}]$  while the ordinate is the particle time. The solid line curves represent the results obtained for the complete mechanism, reactions 1–6. Broken lines are those for the cases in which reactions 4 and 5 have been omitted. Because both reactions 3 and 6 are least important under the present conditions, these latter results are essentially those for a two-step scheme comprising reactions 1 and 2 only. The dotted line curves show how  $[\text{CN}]$  should vary if only reaction 1 is responsible. The experimental concentrations read from the absorption records are indicated with open circles.

It is apparent from Figures 5–7 that reaction 1 is of importance only at high temperatures, where dissociation process 1 permits a nearly perfect description of the entire kinetic history of CN radicals. When the temperature is lowered, the CN concentration is suppressed considerably by reaction 2 as has been mentioned in a previous section. The influence of the chain reactions 4 and 5 on  $[\text{CN}]$  becomes marked only at relatively low temperatures.

At this point, it should be emphasized that reactions 2, 4, and 5 exert virtually no influence to the kinetics in the initial 20–30% region of dissociation. By sharp contrast, a

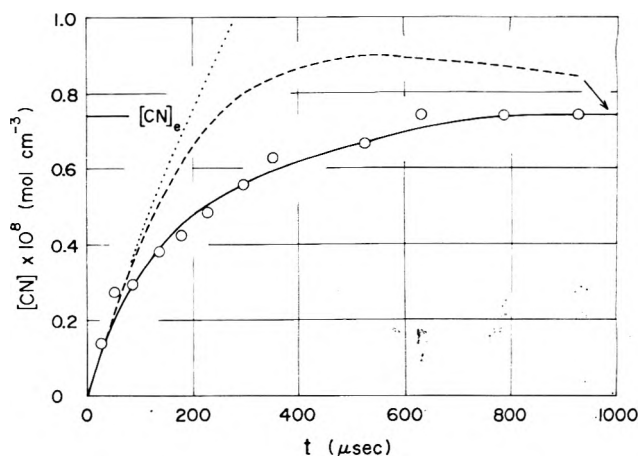


Figure 7. Comparison of the computed CN profiles with the observed:  $T_2 = 2506^\circ\text{K}$ ;  $n = 0.5\%$ ;  $[\text{CN}]_e = 7.40 \times 10^{-9} \text{ mol/cm}^3$ . The lines and circles are the same as used in Figure 5.

variation in  $k_1$  by a certain factor effected a change in the calculated rate by approximately the same factor. These results have an important implication that, even though the subsequent reactions 2, 4, and 5 may influence the overall kinetics, they do not affect the initial slope of the CN concentration profile. Evaluation of the dissociation rate constant from the initial slope of absorption thus proves to be perfectly legitimate.

#### IV. Discussion

The rate constant  $k_4$  which was estimated by curve fittings indicated no apparent activation energy under the conditions studied. The forward reaction is exothermic and should, as a consequence, exhibit only a small activation energy, if any. The same will be true with the backward process of reaction 5, so that the activation energy found for  $k_5$  (23 kcal/mol), which is somewhat smaller than  $\Delta H^\circ_0$  (36.2 kcal/mol), is reasonable. Further, a survey of the kinetic data<sup>15</sup> for bimolecular exchange reactions has shown that the Arrhenius  $A$  factors for atom-molecule reactions such as reaction 5 are generally of the order of  $10^{14} \text{ cm}^3 \text{ mol}^{-1} \text{ sec}^{-1}$  while those for radical(nonatom)-molecule reactions such as reaction 4 are approximately  $10^{11.5} \text{ cm}^3 \text{ mol}^{-1} \text{ sec}^{-1}$ . On all these grounds, the rate constants  $k_4$  and  $k_5$  given in Table II appear to be reasonable. Incidentally, our  $k_5$  is in good agreement with the expression,  $k_5 = 10^{13.0} T^{1/2} \exp(-29,010/RT) \text{ cm}^3 \text{ mol}^{-1} \text{ sec}^{-1}$ , which was estimated by Kayes and Levitt.<sup>2</sup> For reaction 4, however, their estimation  $k_4 = 10^{11.7} T^{1/2} \exp(-1990/RT) \text{ cm}^3 \text{ mol}^{-1} \text{ sec}^{-1}$  provides the  $k_4$  values about an order of magnitude greater than ours.

That the reactions other than (1) do not affect the initial slope of absorption has already been confirmed by the curve-fitting analysis (Figures 5–7). This was further corroborated by the observation that the gas samples having different molar ratios of BrCN to Ar gave  $k_1$  values which were fitted by a single Arrhenius expression (Figure 3). Had the chain reactions 4 and 5 or the (concerted) exchange reaction 6 affected the initial slope, the rate constants derived from eq 16 would have shown apparent dependence on the initial concentration of BrCN.

The experimental activation energy for the dissociation reaction 1 found in this study is 76.6 kcal/mol, which is less than the dissociation energy by 5 kcal/mol. The results

imply that the internal degrees of freedom of BrCN contribute energy to its dissociation process. Most likely, the Fowler-Guggenheim expression<sup>16</sup> is applicable to our results.

$$k_1 = \lambda(Z/n!)(E/RT)^n \exp(-E/RT) \quad (19)$$

When  $E$  is assumed to be equal to  $D_0(\text{Br-CN}) = 81.6$  kcal/mol, the temperature variation of eq 18 is best fitted to that of eq 19 by assigning  $n$  a value of 1.5. Least-squares fit of eq 19 with  $n = 1.5$  to the experimental  $k_1$  values led to the expression:

$$k_1 = [(1.84 \pm 0.52) \times 10^{12}/1.5!] \times T^{1/2}(E/RT)^{1.5} \exp(-E/RT) \text{ cm}^3 \text{ mol}^{-1} \text{ sec}^{-1} \quad (20)$$

The reduction that  $n = 1.5$  indicates that the number of "effective" oscillators participating in the activation process is 2.5, which does not appear to be unusual for a linear three-atom molecule. Taking a mean BrCN-Ar collision diameter as 3.9 Å, we get the steric factor  $\lambda = 0.24$ , a value which does not seem to be unreasonable either.

The Kayes-Levitt values of  $k_1$  shown in Figure 4 are those that they obtained with relatively rich BrCN-Ar mixtures ( $n \geq 0.05$ ). With lean mixtures ( $n \leq 0.01$ ), they observed higher overall rates of decomposition having a much lower activation energy (28 kcal/mol). In order to reconcile the significantly different kinetic behaviors of rich and lean mixtures, they broached the concept that the initial product formed by reaction 4 is vibrationally excited cyanogen,  $\text{C}_2\text{N}_2^*$ .<sup>17</sup> The same reasoning was employed by Clark, Dove, and Finkelman,<sup>3</sup> to account for the contrasting kinetic behaviors of BrCN decompositions in Kr and Ne.

The results of our *absorption* studies with lean mixtures were entirely free from the peculiarity as observed by Kayes and Levitt. So far as our absorption data are concerned, the overall kinetics is simple enough to permit full rationalization in terms of reactions 1, 2, 4, and 5 only. No sign of the intermediacy of  $\text{C}_2\text{N}_2^*$  was perceivable.

It should be noted, however, that in our data treatments no allowance was made for the change in gas temperature due to the thermochemistry of reactions and the boundary layer effects. The simplifications used may well be a source

of some systematic errors in our rate data, thus placing a certain limitation on the accuracy of the final results. Nevertheless, these errors do not seem to be so large as to affect our main conclusion. Absorption studies strongly indicate that the main kinetic features can most adequately be described by reactions 1, 2, 4, and 5.

## References and Notes

- (1) W. L. Patterson and E. F. Greene, *J. Chem. Phys.*, **36**, 1146 (1962).
- (2) P. J. Kayes and B. P. Levitt, *J. Chem. Soc., Faraday Trans. 1*, **69**, 1415 (1973); P. J. Kayes and B. P. Levitt in "Proceedings of the 9th International Shock Tube Symposium," D. Bershader and W. Griffith, Ed., Stanford University Press, Stanford, Calif., 1973, p 395.
- (3) T. C. Clark, J. E. Dove, and M. Finkelman in "Proceedings of the 9th International Shock Tube Symposium," D. Bershader and W. Griffith, Ed., Stanford University Press, Stanford, Calif., 1973, p 196.
- (4) D. Schofield, W. Tang, and S. H. Bauer, *J. Chem. Phys.*, **42**, 2132 (1965).
- (5) T. Fueno, K. Tabarashi, and O. Kajimoto, *J. Phys. Chem.*, **77**, 575 (1973).
- (6) C. S. Marvel, Ed., "Organic Syntheses," Vol. 11, Wiley, New York, N.Y., 1931, p 30.
- (7) R. L. Belford and F. A. Strehlow, *Annu. Rev. Phys. Chem.*, **20**, 247 (1969).
- (8) D. R. Stull, Ed., "JANAF Thermochemical Tables," Dow Chemical Co., Midland, Mich., 1965.
- (9) The free-energy data given in ref 8 were corrected for the heats of formation of CN and BrCN, i.e.,  $\Delta H_f^\circ(\text{CN}) = 99.5$  kcal/mol<sup>9</sup> and  $\Delta H_f^\circ(\text{BrCN}) = 46.1$  kcal/mol.<sup>10</sup> Least-squares fits of the corrected data to a linear equation in  $T$  over the relevant temperature range resulted in the following expressions (in kcal/mol):  $\Delta G_1^\circ = -3.051 \times 10^{-2}T + 82.19$ ;  $\Delta G_2^\circ = -3.546 \times 10^{-2}T + 122.23$ ;  $\Delta G_3^\circ = -2.801 \times 10^{-2}T + 49.89$ ;  $\Delta G_4^\circ = 4.097 \times 10^{-3}T - 40.04$ ;  $\Delta G_5^\circ = -2.539 \times 10^{-3}T + 32.42$ ;  $\Delta G_6^\circ = 2.368 \times 10^{-3}T - 7.62$ .
- (10) D. D. Davis and H. Ckabe, *J. Chem. Phys.*, **49**, 5526 (1968).
- (11) Both  $K_1$  and  $K_2$  at varying temperature were evaluated from the corrected  $\Delta G^\circ$  values.<sup>3</sup>
- (12) In preliminary studies in which the setting of the monochromator slit widths was kept unaltered from that used in a previous study on the  $\text{C}_2\text{N}_2$  dissociation,<sup>5</sup> we obtained  $\beta = 8.16 \times 10^6$  cm<sup>2</sup>/mol, which compared well with  $\beta = 9.16 \times 10^6$  cm<sup>2</sup>/mol observed in the  $\text{C}_2\text{N}_2$  case. In the present study, the slit setting was modified so as to better suit the recording of absorption curves. However, it was confirmed that both sets of experiments led to essentially the same kinetic results.
- (13) J. Keck and A. Kalekar, *J. Chem. Phys.*, **49**, 3211 (1968).
- (14) M. Warshay, *J. Chem. Phys.*, **54**, 4060 (1971).
- (15) S. W. Benson, "Thermochemical Kinetics," Wiley, New York, N.Y., 1968, p 99.
- (16) R. Fowler and E. A. Guggenheim, "Statistical Thermodynamics," Cambridge University Press, Cambridge, Mass., 1952, pp 495-499.
- (17) On subsequent collisions, the species  $\text{C}_2\text{N}_2^*$  could be either deactivated to  $\text{C}_2\text{N}_2$  (leading to the simple chain reaction scheme) or dissociated into CN radicals (giving rise to chain branching). According to Kayes and Levitt,<sup>2</sup> BrCN is capable of deactivating  $\text{C}_2\text{N}_2^*$  much more effectively than Ar. Thus, there would be more branching and hence a higher overall rate of decomposition in the lean mixture.

## Picosecond Pulse Radiolysis. V. Yield of Electrons in Irradiated Aqueous Solution with High Concentrations of Scavenger

R. K. Wolff, J. E. Aldrich, T. L. Penner, and J. W. Hunt\*

Ontario Cancer Institute and Department of Medical Biophysics, University of Toronto,

Toronto, Ontario Canada, M4X 1K9 (Received February 1, 1974; Revised Manuscript Received October 24, 1974)

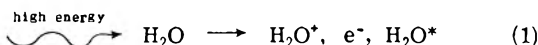
Publication costs assisted by the Ontario Cancer Institute

The stroboscopic pulse radiolysis, spr, system has been used to determine the yield of electrons in aqueous solution 30 psec after irradiation in the presence of high concentrations of scavenger. Using  $\text{Cd}^{2+}$  and cystamine as efficient electron scavengers a yield,  $G$  (product), of at least 4.8 molecules/100 eV is found for electrons compared to a  $g(e_{\text{aq}}^-)_{30 \text{ psec}}$  of 4.0. The yield of  $e_{\text{aq}}^-$  has also been investigated in high concentration of base. There is found to be very little, if any, increase in initial yield at concentrations up to 1 M NaOH. Small increases ( $\sim 13\%$ ) are noted in initial yield at concentrations up to 5 M which are attributed to recombination of species in the radiation "spurs" or to hole reactions. Very little increase in yield was noted when high concentrations (5 M) of NaCl were used ( $\sim 3\%$ ). By taking into account both the fast electron addition to scavengers observed in this paper and assuming the spur yield can be given by a simple equation,  $g(e_{\text{aq}}^-)_t = 2.7 + 1.3 \exp(-10^8 t)$ , excellent agreement was obtained between these pulse radiolysis studies and steady-state yields. The total yield of electrons can be described by the equation,  $G(\text{product}) = 4.8(1 - \exp(-[S]/C_{37}) + \exp(-[S]/C_{37})(2.7 + 1.3k[S])/(10^8 + k[S]))$ , again in agreement with other product yield studies.

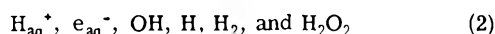
### Introduction

The yield of electrons in pure  $\text{H}_2\text{O}$  following exposure to ionizing radiation has been a subject of some controversy in recent years. The only well established yield has been that of the solvated electron  $e_{\text{aq}}^-$  after a few microseconds in very pure  $\text{H}_2\text{O}$ . In a very careful experiment Fielden and Hart<sup>1</sup> determined the  $g$  value<sup>2</sup> to be  $2.7 \pm 0.1$  molecules/100 eV of absorbed dose by direct measurement of the  $e_{\text{aq}}^-$  absorption  $\sim 1 \mu\text{sec}$  after irradiation using pulse radiolysis. Several steady-state studies show that yields of products in more concentrated solutions cannot be explained by the homogeneous yield of  $e_{\text{aq}}^-$  of 2.7, and suggests the initial yields of electrons are much higher, probably a  $g$  value of 4.8 or higher.<sup>3-7</sup>

The initial ionizing processes in water ( $< 10^{-13}$  sec) are thought to be



and followed by interactions of the initial radiation species in the medium to form the more stable radicals and molecular products



in times shorter than  $10^{-7}$  sec. In the time period from  $10^{-13}$  to  $10^{-7}$  sec, the radiation-induced species are clustered around tracks of the high energy particles, and this initial inhomogeneous distribution is called a spur.

The spur diffusion model assumes that significant recombination and radical-radical reactions take place quickly in the neighborhood of the original ionization events. This initial inhomogeneous distribution expands from the origin as the radicals diffuse out into the bulk of solution until a homogeneous distribution occurs. The steady-state yield of  $e_{\text{aq}}^-$  of 2.7/100 eV thus represents the number of  $e_{\text{aq}}^-$  which have escaped the spur. Higher yields are expected at early times since fewer  $e_{\text{aq}}^-$  will have disap-

peared by reaction in the spur. Pulse radiolysis determinations of  $e_{\text{aq}}^-$  yield with improving time resolution have indeed observed a higher yield at early times, decaying to the steady-state yield  $g(e_{\text{aq}}^-)$  of 2.7 after  $10^{-7}$  to  $10^{-6}$  sec. Thomas and Bensasson<sup>8</sup> measured a  $g(e_{\text{aq}}^-)$  of 3.2 after  $\sim 10$ -15 nsec and Buxton<sup>9</sup> has measured 3.6 after 7.5 nsec. More recently the experiments of Hunt, Wolff, Bronskill, Jonah, Matheson, and Hart<sup>10-12</sup> have established a consistent value for the initial yield  $g(e_{\text{aq}}^-)_{30 \text{ psec}}$  which is  $4.0 \pm 0.2/100$  eV.

This paper is an attempt to integrate the yield of  $e_{\text{aq}}^-$  in picosecond (psec) times, the total yield of electron adducts of different scavengers, and the steady-state products. Five somewhat different models of the early events of the radiation processes are discussed here: the normal diffusion model, Hamill's dry electron-dry hole model, time-dependent rate reactions, and two quantum mechanical electron tunnelling models.

(a) Many calculations have been done using the spur diffusion model,<sup>3,13-15</sup> the most comprehensive having been done by Schwarz<sup>3</sup> using well-known yields and rate constants. The calculations assume an initial gaussian distribution of  $\cdot\text{OH}$ ,  $\cdot\text{H}$ , and  $\text{H}_{\text{aq}}^+$  in the core of the spur with an average radius of 7.5 Å, and a wider gaussian distribution of  $e_{\text{aq}}^-$  with a radius of 23 Å. As these reactive species expand away from the origin, radical-radical and radical-scavenger reactions will occur. After about  $10^{-7}$  sec a homogeneous distribution of the reactive species will be found in the medium. The prescribed diffusion kinetic theory<sup>13</sup> assumes that the gaussian distribution of reactive species is not greatly disturbed by the recombination reactions in the spurs. Schwarz's calculations predict that  $e_{\text{aq}}^-$  will have an initial yield,  $g(e_{\text{aq}}^-)_0$  of 4.8, and decreasing to 3.5 at 1 nsec, 3.0 at 10 nsec, and 2.8 at 100 nsec.

(b) Hamill's model is that  $e^-$  and  $\text{H}_2\text{O}^+$ , the two initial products of the original ionization event<sup>6,16a,b</sup> known as the "dry" electron and "dry" hole, can take part in reactions.

With no scavengers present, these electrons can recombine in the spur, or form the observed normal  $g(e_{aq}^-)$  of 2.7. Hamill has predicted that the yield of dry electron  $g(e_e^-)$  could be 4.5–5.0<sup>6</sup> and the measured yield is at least 3.9.<sup>16a,b</sup> The properties of the hypothetical “dry” electron are not well known, therefore it is intentionally not defined at present. Because of this, the authors in this paper designate the dry electrons as the low-energy electrons whose energies are below the lowest electronic excited states of the medium, but the electrons have not formed their stable solvated traps. The dry electrons would include the subexcited, quasifree epithermal, and thermal electrons.

(c) A change of the rate of reactions for reactive species in early times might alter the spur kinetics as suggested by the fast electron reactions described by Wolff, *et al.*,<sup>17</sup> and Aldrich, *et al.*<sup>18</sup> Schwarz has suggested that a time-dependent factor<sup>19,20</sup> could explain some of the fast kinetics. The rate of reaction is not constant, but instead could be described by

$$k(t) = k(\infty)(1 + R/(\pi Dt)^{1/2}) \quad (1)$$

in which  $k(t)$  is the time-dependent rate constant,  $k(\infty)$  is the normal rate constant at infinite times,  $R$  is the reaction radius, and  $D$  is the sum of the diffusion coefficients of the reacting species. Under certain conditions,  $k(t)$  could alter the rate of reaction in the times from  $10^{-12}$  to  $10^{-10}$  sec.

(d) A quite different mechanism is to assume a long-range interaction between the electrons and the scavengers. Miller<sup>21,22</sup> has studied the electron attachment processes in cold glasses, and has proposed an electron quantum mechanical tunnelling process to explain his results. The electron first forms a shallow trap in the medium, and does not diffuse but instead there is a long-range interaction (*i.e.*, tunnelling) between the near neighbor reactants. In polar solvents a similar fast process could occur to near neighbor scavenger, but would be truncated by the formation of a deeper trap in the medium.

(e) In a somewhat different model, Czapski and Peled<sup>23</sup> suggest a similar large effective reaction radius of  $e_{aq}^-$  and different scavengers described by Anbar and Hart<sup>24a</sup> in microsecond reactions might also be valid in concentrated solutions. Czapski and Peled point out that as the concentration of solute increases, a large fraction of  $e_{aq}^-$  can be formed within the reaction radius of scavenger. These encounter pairs react very quickly and could explain the reduced yield of  $e_{aq}^-$  in concentrated solutions of scavenger.<sup>17,18</sup> This model requires a large effective reaction radius for the scavenging process. The tunnelling models of Anbar and Hart<sup>24b</sup> or Miller<sup>21</sup> would also provide an explanation for these observed results.

Models a and c could result in some effects which should be observable using the stroboscopic pulse radiolysis system with its time resolution of 24 psec described by Bronskill, *et al.*<sup>25</sup> Models b, d, and e would give rise to effects within the time resolution of the system and so could not be directly observed at present. For the purpose of this paper these latter categories of presolvated electrons are lumped under the general heading of “dry” electrons.

Models a, c, and e assume that all electron reactions are initiated by fully solvated electrons while models b and d assume a presolvated dry electron can react. This paper discusses the two possibilities by considering electron reactions in high concentration of scavenger.

Models a, c, and e assume that all electron products must come from  $e_{aq}^-$  so that the maximum yield for an electron

attachment product is the initial yield of  $e_{aq}^-$ . Therefore, in high concentrations of scavenger the maximum yield of electron product would be  $g(e_{aq}^-)_0$ . This value of initial solvated electron yield is assumed to be 4.0 according to the measured value of Wolff, *et al.*<sup>11</sup> There is no obvious spur decay in the initial 30–350-psec time interval. For these reasons, the initial yield of solvated electrons is assumed to be 4.0. At low concentrations of electron scavenger the yield of product will be 2.7, the steady-state yield of  $e_{aq}^-$ .

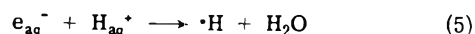
Hamill's model b predicts that the electron products in concentrated solution can be the result of reaction with a dry electron (reaction 3) competing with recombination with the dry hole (reaction 4). As recombination may take



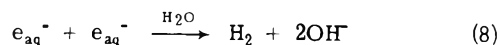
place in times shorter than  $10^{-11}$  sec, the number of dry electrons can be greater than the number of solvated electrons and so the maximum electron product yield may be greater than 4.0. Fast recombination of  $e^-$  with  $H_2O^+$  (or  $\cdot OH$ ) may also occur by the long-range interactions discussed in models d and e. As well, the fast process may be qualitatively described by the hypothesis of Hamill in which his “dry” model might predict higher electron product yield.

In this paper studies were carried out using high concentrations of  $Cd^{2+}$  and cystamine (RSSR). These solutes are excellent electron scavengers and give rise to easily observable electron reaction products  $Cd^+$  and  $RSSR^-$ . The description of electron product data is divided into two parts. Section I confirms the fast electron attachment process suggested by earlier work<sup>17,18</sup> on  $e_{aq}^-$  yield reduction. Section II measures the yield of electron product,  $Cd^+$  and  $RSSR^-$ , determining the total yield of electrons and relating these yields to the models mentioned above.

The situation with respect to solvated electron yields when high concentration of base is added is as follows. In the normal spur theory, the recombination between



and



will explain the higher initial yields of products. When  $OH^-$  is added as a scavenger of  $H_{aq}^+$  in the spur, a higher yield is expected. Scavengers which react with  $\cdot OH$  or  $H_{aq}^+$  will be referred to as spur scavengers. These scavenger reactions take place very quickly in the spur but might be observed using the stroboscopic pulse radiolysis system. High concentrations of  $OH^-$  should increase  $g(e_{aq}^-)$  at later times but not the absolute initial  $g(e_{aq}^-)_0$ . Thus if the observed  $g(e_{aq}^-)_{30 \text{ psec}}$  is the true initial yield it should not increase in the presence of high concentration of  $OH^-$  and a yield of 4.0 would be expected.

Hamill, *et al.*,<sup>6,16</sup> has studied the competition in concentrated solutions and predicts that an increase in  $g(e_{aq}^-)$  should occur by the reaction



The  $OH^-$  might react with the dry hole  $H_2O^+$ , and block the neutralization reaction 4. Thus  $g(e_{aq}^-) > 4.0$  in high

concentrations of  $\text{OH}^-$ . Other ion scavengers such as  $\text{Cl}^-$  should act in the same manner.

To differentiate these models the study described in section III was conducted to determine the initial solvated electron yield with high concentrations of  $\text{OH}^-$  and  $\text{Cl}^-$  using the stroboscopic pulse radiolysis system.

### Experimental Section

The stroboscopic pulse radiolysis, spr, technique used to observe transients in the 30–350-psec time period has been described in detail previously.<sup>25–27</sup> A series of electron pulses was obtained from the 40-MeV University of Toronto linac at a rate of 60 Hz. The pulse had a half-width of  $\sim 6$  nsec, and irradiated the solutions with doses in the range 3–8 krads per pulse depending on the experiment. Each 6-nsec pulse consisted of a train of fine structure pulses with a width of  $\sim 8$  psec which produced the radiation species studied, and also generated a Čerenkov analysis light beam to detect these changes.<sup>25</sup> The time resolution of this technique is limited mainly by the light path of the irradiated solutions; most of the experiments were carried out with a 2-cm cell, and the time resolution was 24 psec, but in certain experiments, a 1-cm cell with a time resolution of 18 psec was used.<sup>25,26</sup>

The spectra of species were obtained using the automatic scanning technique described by Aldrich, *et al.*<sup>27</sup> A typical time sweep giving a step trace is shown in Figure 1c. The absorption signal  $H$  is obtained by stopping the carriage of the movable mirrors at one fixed position, which is equivalent to stopping the time sweep: the subsequent spectrum is obtained by driving the wavelength control of the monochromator. In this technique  $H$  is the absorption integrated over the macropulse of 6 nsec. These spectra are averaged for  $\sim 5$  min at the 60-Hz rate and errors of only 1–2% result. They are obtained as absorptions from an on-line PDP-8 computer and then later converted to absorbances. These smooth spectra are referred to as the “6-nsec integrated spectra.”

A conventional pulse radiolysis system described by Hunt, Greenstock, and Bronskill<sup>28</sup> using single radiation pulses with a 35-nsec half-width, and radiation doses from 1 to 1.5 krads, was used to complement the stroboscopic results.

**Chemicals.** All chemicals were used as obtained from the supplier without further purification. The  $\text{Cd}(\text{ClO}_4)_2$  obtained from G. F. Smith was used to avoid complexing problems which were encountered with other cadmium salts. Cystamine hydrochloride (RSSR) was obtained from Sigma. Other chemicals were Fisher ACS grade. All solutions were prepared using four times quartz distilled water with no buffering or pH adjustment. The unbuffered cystamine solutions were at pH 3.7.

**Procedure.** For all conventional pulse radiolysis experiments the solutions were bubbled with argon but they were left open to the air for the spr experiments since no effect of oxygen concentration in the 30–350-psec time range has been observed.<sup>26</sup>

Conventional pulse radiolysis was used to obtain the extinction coefficient of  $\text{Cd}^+$ . Using  $2 \times 10^{-4} M$   $\text{Cd}^{2+}$  the formation of  $\text{Cd}^+$  at 310 nm and the decay of  $e_{\text{aq}}^-$  at 575 nm were simultaneously observed using a split light beam and two monochromators. The yield of  $\text{Cd}^+$  was equated to the initial yield of  $e_{\text{aq}}^-$  using an  $\epsilon_{575}$  of  $1.04 \times 10^4 M^{-1} \text{cm}^{-1}$ .<sup>1</sup> The extinction coefficient of  $\text{Cd}^+$  was  $1.1 \times 10^4 M^{-1} \text{cm}^{-1}$  at 310 nm. This value is somewhat higher than that of  $7.5 \times$

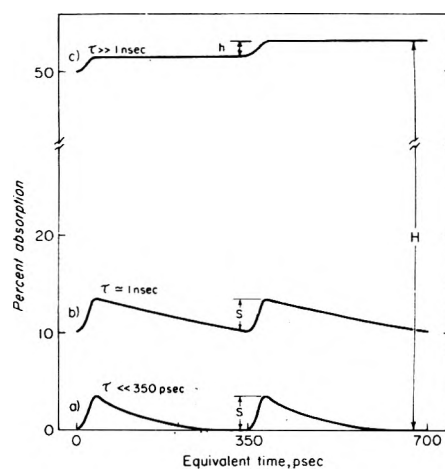


**Figure 1.** Idealized representation of 30–350-psec kinetic traces obtained using the stroboscopic pulse radiolysis system as the decay time,  $\tau$ , lengthens from (a) less than 350 psec to (b)  $\sim 1$  nsec to (c) much greater than 1 nsec. The peak height  $S$  and the step height  $h$  corresponding to 30-psec yields and the absorption  $H$  corresponding to absorption integrated over the 6-nsec pulse.

$10^3 M^{-1} \text{cm}^{-1}$  obtained by Baxendale.<sup>29</sup> This discrepancy may result from the extremely narrow absorption spectrum of  $\text{Cd}^+$  so that a wide band pass through the monochromators might affect the extinction obtained. Careful studies were done using a narrow wavelength band to obtain the extinction of  $\text{Cd}^+$ . The extinction coefficient used in this laboratory gave consistent yields as a function of concentration in a number of experiments as shown later in Figure 9 and also, results were always related to the solvated electron absorption to maintain consistency. The molar extinction coefficient, at 410 nm, used for  $\text{RSSR}^-$  was  $9.4 \times 10^3 M^{-1} \text{cm}^{-1}$  obtained by Adams.<sup>30</sup> The extinction was corrected to  $8.2 \times 10^3$  for pH 3.7 because of the pH dependence of  $\epsilon$ . This value for the extinction coefficient was confirmed in our laboratory.

**Dosimetry.** All yields have been obtained using  $e_{\text{aq}}^-$  dosimetry assuming an  $\epsilon_{575 \text{ nm}}(e_{\text{aq}}^-)$  of  $1.04 \times 10^4 M^{-1} \text{cm}^{-1}$  and  $g$  values appropriate to the time of observation as outlined below. The dose is corrected by the number of electrons per gram of the solution.<sup>31</sup> As well, an important correction, the density ( $\text{gm}/\text{cm}^3$ ) of the solution, was also applied. All quoted yields have been corrected for both of these factors lumped as electron density (number of electrons/ $\text{cm}^3$ ).

(a) **30-psec Yields.** Figure 1 shows the types of traces derived from the stroboscopic system which are obtained from the 30–350-psec time regions. The amplitude of the signals,  $S$ , and  $h$ , corrected for the absorption of the signals, give a measure of the yield of the products. The signal  $S$  is designated for the yields in which fast decays are present and little correction is necessary. The “step height” signals,  $h$ , describe the traces in which the decays of the signals are very small. Here, a large correction for the absorption signal  $H$  is made to obtain the true yield of the products. This analysis is described in papers by Wolff, *et al.*,<sup>11</sup> and Aldrich, *et al.*<sup>18</sup> The dosimetry was obtained by observing the relative step traces of the product under study at its  $\lambda_{\text{max}}$  and  $e_{\text{aq}}^-$  in pure  $\text{H}_2\text{O}$  at 575 nm, and assuming  $g(e_{\text{aq}}^-)$  at 30 psec is 4.0.<sup>10–12</sup> The “30-psec spectra” used in this paper were obtained from the 30-psec absorption signals at different wavelengths.

(b) **6-nsec Integrated Yields.** The 6-nsec integrated

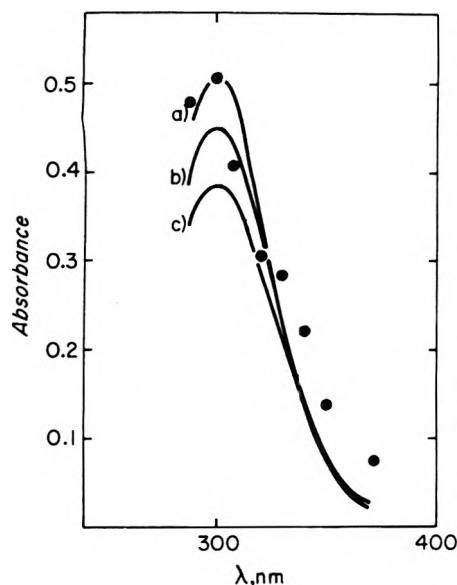


**Figure 2.** Spectra of  $\text{Cd}^+$  (—) are the 6-nsec integrated spectra in (a) 1.0 M  $\text{Cd}^{2+}$ , (b) 0.1 M  $\text{Cd}^{2+}$ , and (c) 0.025 M  $\text{Cd}^{2+}$ . The 30-psec values in 1.0 M  $\text{Cd}^{2+}$  are obtained from the fast component in the 30–350-psec traces shown in Figure 1.

yields are obtained from the spectra which plot out  $H$ , the absorption integrated over the pulse length. The procedure was to take a spectrum of  $e_{\text{aq}}^-$  in pure  $\text{H}_2\text{O}$ , and then take a product spectrum such as in Figure 2. The yield of product was determined by taking the absorbance at  $\lambda_{\text{max}}$  and using the  $e_{\text{aq}}^-$  absorbance at 575 nm as a dosimeter. As time proceeds the  $g$  value of the solvated electron decreases. Using the decay behavior observed by Jonah, *et al.*,<sup>12</sup> to account for the decay over the 6-nsec pulse,  $g(e_{\text{aq}}^-)$  in pure  $\text{H}_2\text{O}$  as measured by the 6-nsec integrated spectrum has been calculated to be 3.8.

(c) *100-nsec Yields.* The 100-nsec yields were obtained using the conventional pulse radiolysis system. In this case the absorbance of product and  $e_{\text{aq}}^-$  were compared and a  $g(e_{\text{aq}}^-)_{100 \text{ nsec}} = 2.8$  was assumed. In both cases the absorbances were extrapolated to the middle of the pulse.

## Results and Discussion

(I) *Evidence for Fast Electron Attachment.* One way to observe the yield of electrons is to use a solute which reacts efficiently with electrons and has an observable product spectrum. Two such solutes are  $\text{Cd}^{2+}$  and RSSR. They react with electrons ( $k_{e_{\text{aq}}^- + \text{Cd}^{2+}} = 5 \times 10^{10} \text{ M}^{-1} \text{ sec}^{-1}$ ,<sup>29</sup>  $k_{e_{\text{aq}}^- + \text{RSSR}} = 4 \times 10^{10} \text{ M}^{-1} \text{ sec}^{-1}$ ,<sup>32</sup> to give rise to  $\text{Cd}^+$  ( $\lambda_{\text{max}} 300 \text{ nm}$ <sup>29</sup>) and  $\text{RSSR}^-$  ( $\lambda_{\text{max}} 410 \text{ nm}$ <sup>30</sup>). The spectra for these electron adducts are shown in Figures 2 and 3.

In previous studies,<sup>17,18</sup> we have found that  $\text{Cd}^{2+}$  is an excellent electron scavenger, in which different concentrations reduce the initial yields of  $e_{\text{aq}}^-$  at 30 psec (including corrections for the decays of the signals during the resolution of the system). The  $C_{37}$  value, the concentration required to reduce  $e_{\text{aq}}^-$  yield to 37% of the value in pure  $\text{H}_2\text{O}$ , was 0.39 M. Therefore, the product should also show a fast formation ( $e^-$  component) within 30 psec, and then the normal first-order formation from the solvated electron ( $e_{\text{aq}}^-$  component).

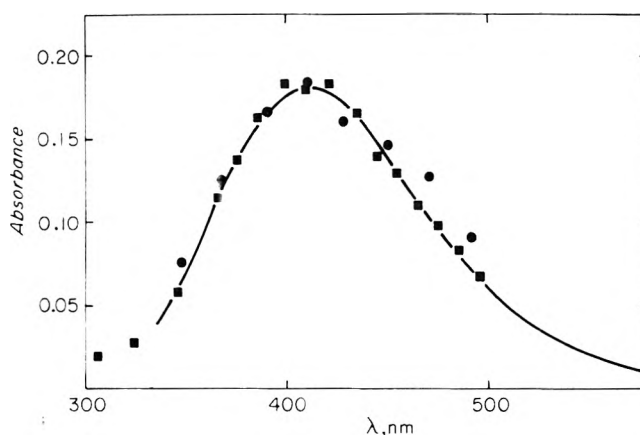
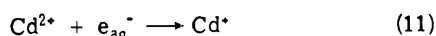
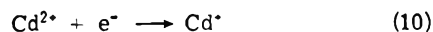


**Figure 3.** Spectrum of  $\text{RSSR}^-$  (—) in 6-nsec integrated spectrum in 0.5 M cystamine. The 30-psec values (●) are obtained in 1.0 M cystamine. The values (■) were obtained from Adams, *et al.*,<sup>30</sup> renormalized in solutions of  $10^{-2}$  to  $10^{-3}$  M cystamine and absorbance measured at the end of an 0.2- $\mu\text{sec}$  pulse.

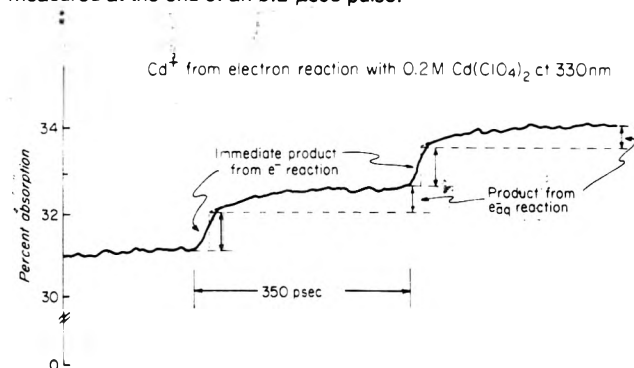


**Figure 4.** Formation of  $\text{Cd}^+$  at 330 nm in 0.2 M  $\text{Cd}^{2+}$  showing the  $e^-$  component and the  $e_{\text{aq}}^-$  component. The  $e_{\text{aq}}^-$  component is extrapolated to the middle of the rise time.

Figure 4 shows the formation of  $\text{Cd}^+$  in a 0.2 M  $\text{Cd}^{2+}$  solution which shows these two components resulting from reactions 10 and 11.

Figure 5a shows a sequence of traces for increasing concentration of scavenger. As scavenger concentration increases the  $e^-$  component increases and the  $e_{\text{aq}}^-$  component decreases until at 1 M it is essentially all  $e^-$  component. Figure 5b shows the data for the formation of  $\text{RSSR}^-$  which shows the same behavior.

Rate constants were obtained from the formation times of the products. These values are shown in Table I and it can be seen that they agree quite well with rate constants obtained from observing  $e_{\text{aq}}^-$  decay with these scavengers present. The large errors in the formation values result from a lack of a plateau level in the low concentration cases and from small  $e_{\text{aq}}^-$  components at the high concentrations. The rate constant for cystamine decreases quite substantially from  $3.2 \times 10^{10}$  at 0.1 M to  $0.7 \times 10^{10} \text{ M}^{-1} \text{ sec}^{-1}$  at 1 M. This decrease is consistent with that reported earlier for reactions between oppositely charged species in high concentrations<sup>18</sup> (cystamine is doubly positively charged at pH 3.7). The rate constant obtained at the lowest concentration of 0.1 M agrees well with the rate constant of  $4 \times 10^{10} \text{ M}^{-1} \text{ sec}^{-1}$  obtained by Braams.<sup>32</sup>

It was stated earlier that the loss in solvated electron yield in the presence of high concentration of scavenger should be reflected in a fast  $e^-$  component of product formation. Figures 6a and 6b illustrate this fact very clearly.

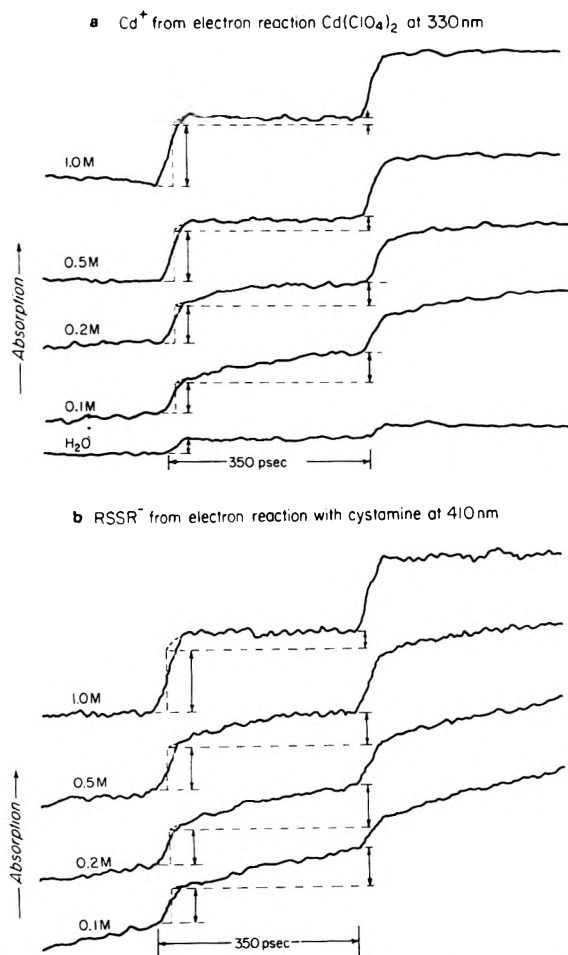
**TABLE I: Rate Constants of Reaction of  $e_{aq}^-$  with  $Cd^{2+}$  and RSSR**

$Cd(ClO_4)_2$ concn, $M$	Formation rate $\times 10^{10}$ , $M^{-1} \text{ sec}^{-1}$ (330 nm)	$e_{aq}^-$ decay rate $\times 10^{10}$ , $M^{-1} \text{ sec}^{-1}$ (575 nm)
0.1	$4.7 \pm 1.5$	$4.0 \pm 0.5^a$
0.2	$4.2 \pm 2.0$	$4.0 \pm 0.5^a$
0.5	$4.2 \pm 2.0$	$3.5 \pm 0.5^a$

Cystamine concn, $M$	Formation rate $\times 10^{10}$ , $M^{-1} \text{ sec}^{-1}$ (330 nm)	$e_{aq}^-$ decay rate $\times 10^{10}$ , $M^{-1} \text{ sec}^{-1}$ (575 nm)
0.1	$3.3 \pm 1.5$	
0.2	$2.3 \pm 1.0$	
0.5	$1.5 \pm 0.5$	$1.0 \pm 0.3$
1.0		$0.7 \pm 0.3$

<sup>a</sup> From previous work, ref 17.



**Figure 5.** Kinetic 30–350-psec traces of the formation of (a)  $Cd^+$  in 0.1 to 1.0  $M$   $Cd^{2+}$  at 330 nm (The light intensity was not sufficient to make observations at the  $\lambda_{max}$  of 300 nm.) (b) RSSR<sup>-</sup> in 0.1–1.0  $M$  RSSR at 410 nm. The  $e^-$  and  $e_{aq}^-$  yields are indicated as per Figure 4. The lowest trace in a shows the solvated electron absorption in pure  $H_2O$  at 330 nm.

The  $e^-$  yield is plotted as a function of concentration and compared to the initial loss of  $e_{aq}^-$  yield at 575 nm. The absorbance of the  $e_{aq}^-$  species has been subtracted out of

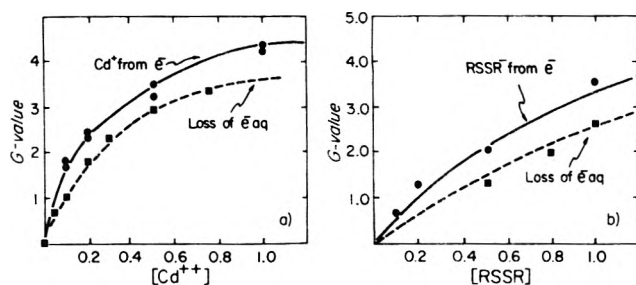


**Figure 6.** A comparison of the initial (30 psec) yield of solvated electron measured at 575 nm and the  $e^-$  yield (30 psec) as functions of scavenger concentration. Scavengers were (a)  $Cd^{2+}$  with  $e^-$  yield measured at 310 nm and (b) cystamine with yield measured at 410 nm.

these yields. It can be seen that an increase in initial  $e_{aq}^-$  loss is reflected in an increase in  $e^-$  yield. It can also be seen that the  $e^-$  yield is greater than the loss in  $e_{aq}^-$  yield indicating that the electron attachment occurs in times shorter than the  $e_{aq}^-$  formation.

(II) *Yield of Electron Products.* At high concentration of scavenger the electron products are formed mainly from the  $e^-$  reactions and so a good estimate of the total yield of electrons can be obtained. Four methods were used to determine the yield of  $Cd^+$  in 1  $M$   $Cd(ClO_4)_2$  solution and the yield of RSSR<sup>-</sup> in 2  $M$  RSSR. Electron density corrections ((electrons/gm)(gm/cm<sup>3</sup>) as discussed in the Experimental Section) of 1.18 for  $Cd^{2+}$  and 1.06 for cystamine have been made. Extinction coefficients of  $1.1 \times 10^4$  and  $0.82 \times 10^4 M^{-1} \text{ cm}^{-1}$  were used for  $Cd^+$  and RSSR<sup>-</sup> respectively.

(1) The 30-psec yield of  $Cd^+$  was obtained as 1.21g ( $e_{aq}^-$ ) at 30 psec and the yield of RSSR<sup>-</sup> was 1.22g ( $e_{aq}^-$ ). Using  $g(e_{aq}^-)_{30 \text{ psec}} = 4.0$  the  $G$  values of both are 4.8.

(2) The 6-nsec integrated yields were 1.22g ( $e_{aq}^-$ ) and 1.23g ( $e_{aq}^-$ ) giving  $G$  values 4.6 for both  $Cd^+$  and RSSR<sup>-</sup> using  $g(e_{aq}^-)_{6 \text{ nsec integrated}} = 3.8$ .

(3) The 100-nsec yields obtained using conventional pulse radiolysis were 1.56g ( $e_{aq}^-$ ) and 1.72g ( $e_{aq}^-$ ) giving  $G$  values of 4.4 and 4.8 for  $Cd^+$  and RSSR<sup>-</sup>, respectively, assuming  $g(e_{aq}^-)_{100 \text{ nsec}} = 2.8$ .

(4) The last method consists of comparing the 6-nsec  $Cd^+$  spectra at low  $Cd^{2+}$  concentration when the product is mostly from  $e_{aq}^-$  with that at high concentration when the product is almost entirely from  $e^-$ . Figure 2 indicates that  $Cd^+$  spectra in 0.025  $M$   $Cd^{2+}$  and 1.0  $M$   $Cd^{2+}$ . These spectra were taken within minutes of each other and were found to be very reproducible so that dose variation can be ruled out. The yield in 0.025  $M$   $Cd^{2+}$  should correspond to  $e_{aq}^-$  and that in 1  $M$   $Cd^{2+}$  to  $e^-$ . The yield of  $Cd^+$  in 1  $M$  solution was 1.15 times that in 0.025  $M$   $Cd^{2+}$  after electron density corrections. However, the yield in 0.025  $M$   $Cd^{2+}$  solution does not correspond exactly to that of  $e_{aq}^-$ . The product yield comes 95% from  $e_{aq}^-$  and 5% from  $e^-$ . These estimates are made from the fact that there is a 5%  $e_{aq}^-$  loss in 0.025  $M$   $Cd^{2+}$ . Correcting for this fact the yield in 1  $M$   $Cd^{2+}$  was 1.19g ( $e_{aq}^-$ ). Since it is the 6-nsec yield data that is being used  $g(e_{aq}^-) = 3.8$  and a yield of 4.6 is obtained for  $Cd^+$ . Using a similar procedure a  $G$  value of 4.6 was also obtained for RSSR<sup>-</sup>.

These yield values are summarized in Table II. All the yield values are very consistent giving an average  $G$  value of  $4.6 \pm 0.2$  for  $Cd^+$  in 1  $M$   $Cd^{2+}$  and  $4.7 \pm 0.2$  for RSSR<sup>-</sup> in 2  $M$  RSSR. The only value which seems slightly out of line is the 100-nsec yield for  $Cd^+$ . The decay of  $Cd^+$  is quite

TABLE II: Dry Electron Yield as Measured by  $G$ -Values of  $\text{Cd}^+$  and  $\text{RSSR}^-$  <sup>a</sup>

	(1) 30 psec	(2) 6-nsec integrated spectra	(3) 100 nsec	(4) Comparative $\text{Cd}^+$ (0.025 → 1 M)
$G(\text{Cd}^+)$	$4.8 \pm 0.2$ (3)	$4.6 \pm 0.2$ (3)	$4.1 \pm 0.3$ (2)	$4.6 \pm 0.3$ (2)
$G(\text{RSSR}^-)$	$4.8 \pm 0.2$ (2)	$4.6 \pm 0.2$ (2)	$4.7 \pm 0.3$ (2)	$4.6 \pm 0.2$ (3)
$g(e_{\text{aq}}^-)$	4.0	3.8	2.8	3.8

<sup>a</sup> The number in parentheses is the number of different experiments.

fast in 1 M  $\text{Cd}^{2+}$  solution,  $\sim 0.5 \mu\text{sec}$ , so that there is a large error on extrapolating yield to the middle of the pulse. If there were a fast decay of  $\text{Cd}^+$  of the order of 10–30 nsec, it would probably not be resolved by the conventional pulse radiolysis system. The rate constant  $k_{\text{Cd}^+ + \text{H}_{\text{aq}}^+}$  was measured to be  $\sim 10^5 \text{ M}^{-1} \text{ sec}^{-1}$  and so an acid spur mechanism seems unlikely.

Other studies done in this lab using sodium salicylate as a dry electron scavenger have shown an initial yield of electron product of 4.8<sup>33</sup> at high scavenger concentration. The 30-psec determination should be the most reliable of the methods quoted above, as it is measured at the earliest time possible, while other methods provide corroborating evidence. As the initial 30-psec yield was 4.8 for all three scavengers  $\text{Cd}^{2+}$ ,  $\text{RSSR}$ , and salicylate this value has been chosen as the initial yield of total electrons. This value represents the minimum yield as the full electron density corrections have been applied in all cases. Using the competition plot of the form  $1/G(\text{product})$  vs.  $1/[\text{S}]$ , an electron yield can be obtained by extrapolation to infinite concentrations: a  $G$  value ranging from 5.6 to 6.0 was obtained. It is not certain, however, that this plot is valid in such concentrated solutions, but does suggest that an even higher initial yield of electrons is possible.

Reactions with the hydrogen atom,  $\cdot\text{H}$ , were excluded as contributors to the measured product yields. The rate  $k_{\text{Cd}^{2+} + \cdot\text{H}}$  is less than  $10^5 \text{ M}^{-1} \text{ sec}^{-1}$ <sup>34</sup> and so there should be a negligible contribution within the first 30 psec after the pulse. Also, the experiments of Adams, *et al.*,<sup>30</sup> indicated that the attack of  $\text{RSSR}^-$  by  $\cdot\text{H}$  atoms does not give rise to  $\text{RSSR}^-$ .

(III) Yield of  $e_{\text{aq}}^-$  in the Presence of High Concentrations of  $\text{OH}^-$  and  $\text{Cl}^-$ . As discussed in the Introduction, the  $\text{OH}^-$  and  $\text{Cl}^-$  might alter the normal spur reactions, reactions 5 and 6. Similarly,  $\text{OH}^-$  and  $\text{Cl}^-$  might also block the geminate recombination  $\text{H}_2\text{O}^+ + e^-$  as shown in reactions 4 and 9. These suggested reactions might increase the observed yield of  $e_{\text{aq}}^-$  in which the  $\text{OH}^-$  ion should react with both  $\text{H}_{\text{aq}}^+$  and  $\text{H}_2\text{O}^+$  in the spur, while  $\text{Cl}^-$  should react only with  $\text{H}_2\text{O}^+$  and not with  $\text{OH}^-$  or  $\text{H}_{\text{aq}}^+$ .<sup>6,16,35,36</sup>

Figure 7 shows the 6-nsec integrated spectra of  $e_{\text{aq}}^-$  observed with 5 M NaOH and NaCl, respectively. It is immediately evident that there is a large increase in absorbance with high concentrations of these solutes. It is also evident that the spectra are blue shifted, an effect noted by Anbar and Hart<sup>37</sup> in 16 M NaOH. The data in this paper show a 20-nm shift for 5 M NaOH and a 25-nm shift for 5 M NaCl. An approximately linear shift with increasing concentration in the 0 → 5 M range was noted for both solutes.

The absorbances at  $\lambda_{\text{max}}$  for each concentration were calculated and then corrected for the electron density of the solution (electron density correction for 5 M NaOH was 1.08, 1.17 for 5 M NaCl). Table III shows the results of these yields were correlated to the  $g(e_{\text{aq}}^-)$  at 6 nsec of 3.8 which was used to calculate the absolute yields.

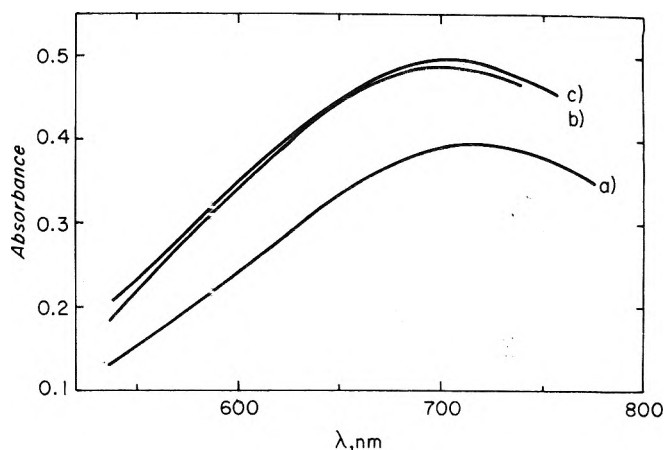
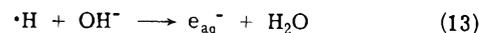


Figure 7. The 6-nsec integrated spectra of  $e_{\text{aq}}^-$  in (a) pure  $\text{H}_2\text{O}$ , (b) 5 M NaCl, and (c) 5 M NaOH. The 30-psec spectra obtained were very similar to these and so there are no apparent shifts from 30 psec to 10 nsec.

The 30-psec yields were obtained from kinetic traces at 575 nm and corrected for the amount of spectral shift obtained from the 5-nsec integrated spectra. These yields were also corrected for electron density and correlated with  $g(e_{\text{aq}}^-)$  at 30 psec of 4.0. It can be seen that the increase in initial  $e_{\text{aq}}^-$  yield is small with  $\text{OH}^-$  as a scavenger ( $1.3 \pm 5\%$  increase at 5 M) and almost zero for NaCl ( $3 \pm 5\%$  at 5 M) after electron density corrections are made. In 1 M solutions the increase in initial yield is essentially zero in both cases ( $2 \pm 5\%$  for NaOH,  $0 \pm 5\%$  for NaCl). A similar conclusion was reached by Jonah, *et al.*<sup>12</sup>

It is possible that reaction 13 may contribute some of the



increased yield of  $e_{\text{aq}}^-$  in alkaline solutions. The rate constant of reaction 13 is  $2.3 \times 10^7 \text{ M}^{-1} \text{ sec}^{-1}$ <sup>38</sup> which means that formation time of the reaction would be 10 nsec in a 5 M solution. Therefore, a small increased yield of the component of  $e_{\text{aq}}^-$  ( $g \approx 0.2$ ) in 6-nsec integrated yields shown in Table III can be explained from this reaction.

The small increase in  $e_{\text{aq}}^-$  when  $\text{Cl}^-$  is present agrees with results obtained by Peled, *et al.*,<sup>39</sup> and Buxton.<sup>9</sup> Buxton has also studied the effect of added  $\text{OH}^-$ . His results indicate  $g(e_{\text{aq}}^-) = 4.45$  in a 1 M NaOH solution compared to the values of 4.0 and 4.1 obtained in this paper. It seems that most of the discrepancy between the laboratories is due to the blue shift in the  $e_{\text{aq}}^-$  spectrum in 1 M NaOH, and the absorption  $e_{\text{aq}}^-$  signals are sensitive at the critical wavelength of 575 nm, and this was not corrected.<sup>9</sup> The data in this present paper were corrected for the blue shift.

Buxton has also obtained a  $g(e_{\text{aq}}^-)$  of 5.05 in a solution of 1 M NaOH + 1 M  $\text{CH}_3\text{OH}$ . The  $\text{CH}_3\text{OH}$  is present to compete with reaction 6 and NaOH to compete with reaction 5 and so fewer solvated electrons will be lost in radical-

TABLE III:

Solute	Concn, <i>M</i>	30-psec yield		6-nsec yield	
		Relative	Absolute	Relative	Absolute
H <sub>2</sub> O	Pure	1.0	4.0	1.0	3.8
NaOH	1	1.02 ± 0.05	4.1	1.07 ± 0.02	4.1
	2	1.07	4.3	1.09	4.2
	3	1.13	4.5	1.16	4.4
	4	1.12	4.5	1.17	4.5
	5	1.13	4.5	1.185	4.5
NaCl	1	1.0	4.0	1.0	3.8
	2	1.0	4.0	1.0	3.8
	3	1.01	4.04	1.04	4.0
	4	1.03	4.12	1.05	4.0
	5	1.03	4.12	1.06	4.0

radical reactions and the yield should increase as he has observed. However, in this laboratory using the 6-nsec integrated spectral data a *g* value of only 4.1 was obtained in 1 *M* NaOH + 1 *M* CH<sub>3</sub>OH.

The increases in initial yield of  $e_{aq}^-$  are very small (2 ± 5%) at scavenger concentrations up to 1 *M* NaOH or 1 *M* CH<sub>3</sub>OH substantiating the view that the true initial yield of  $e_{aq}^-$  is 4.0 as indicated by the observations in pure H<sub>2</sub>O.<sup>10</sup> There is almost no increase in  $e_{aq}^-$  yield even with these high concentrations of spur scavengers. The increases in initial yield at higher concentrations seem to be the result of hole reactions. It is possible that the increases are due to competition with spur reactions 5 and 6. However, these hypotheses are unlikely as these would have to spur reactions complete in 30 psec and the direct observations of  $e_{aq}^-$  decay do not indicate any fast spur reactions over the time region from 30 to 350 psec.<sup>11</sup> The spur decay of  $e_{aq}^-$  has been observed with a lifetime of ~10 nsec<sup>12</sup> in pure H<sub>2</sub>O. There are also no observable changes in the kinetics of  $e_{aq}^-$  formation or decay in this 30–350-psec time region for 0.1–5 *M* NaOH, or 1 *M* CH<sub>3</sub>OH. It is possible, however, that the formations would be too fast for our system to reliably resolve given the rate of  $1.4 \times 10^{11} M^{-1} sec^{-1}$ <sup>40</sup> for the  $H_{aq}^+ + OH_{aq}^-$  reaction in 1 *M* OH<sup>-</sup> solution.

Careful studies have been done on the initial yield of  $e_{aq}^-$  in high concentrations of spur scavengers. As discussed earlier, at concentrations up to 1 *M* NaOH or CH<sub>3</sub>OH the observed  $g(e_{aq}^-)_{30 \text{ psec}}$  is 4.0–4.1, essentially the same as in pure H<sub>2</sub>O and only at higher concentrations does the yield increase. The small increase in  $e_{aq}^-$  yield which is observed at the higher concentrations is tentatively attributed to hole trapping since no kinetic evidence has been seen for spur reactions at the earliest times. The fact that Cl<sup>-</sup> does not release more  $e_{aq}^-$  (except as expected from electron density considerations) is not entirely surprising. Although there is some evidence that Cl<sup>-</sup> ions might react with the "dry hole," H<sub>2</sub>O<sup>+</sup>,<sup>16,36</sup> a back reaction, between ClOH<sup>-</sup> and Cl<sub>2</sub><sup>-</sup> and e<sup>-</sup> might give the same yield,  $g(e_{aq}^-)_{30 \text{ psec}} = 4.0$ . It has been assumed that electron yield will be proportional to electron density per unit volume. At high concentrations of solute this assumption may break down and serve to change our calculated yields at concentrations greater than 1 *M*. At present, there is no data, however, which suggest that the assumption is not valid.

## Conclusions

(I) *Fast Formation of Electron Adducts.* The total yield of electron adduct products, P, scavenged by the solute

molecules, is  $G(P) \geq 4.8$ , which is 20% higher than the solvated electron yield  $g(e_{aq}^-)_{30 \text{ psec}} = 4.0 \pm 0.2$ . It should be emphasized that the picosecond product yields have been measured relative to the solvated electron yield, so that it is a 20% increase of  $G(P)_{30 \text{ psec}}$  over  $g(e_{aq}^-)_{30 \text{ psec}}$ . This increase has been demonstrated in a large number of experiments using different experimental setups (see Table II). The observed results presented in this paper show that in concentrated solutions of electron scavengers there is an inverse relation between the loss of the initial yield of  $e_{aq}^-$ ,<sup>17,18</sup> and the fast formation of the products, Cd<sup>+</sup> and RSSR<sup>-</sup>. The difference between the two yields,  $g(e_{aq}^-)_{30 \text{ psec}}$  and  $G(P)$  suggests that a fraction of the initial electrons (~20%) quickly recombine with the reactive species in the radiation spur. There is little increase of  $e_{aq}^-$  in solutions with Cl<sup>-</sup>, and a 10% increase with OH<sup>-</sup>, so that these results cannot directly differentiate between spur and hole models for the initial recombination of radiation products. That is, the neutralization reaction,  $e^- + H_2O^+ \rightarrow H_2O$ , *vs.* the normal spur reactions,  $e_{aq}^- + H_{aq}^+ \rightarrow H^+$  and  $e_{aq}^- + \cdot OH \rightarrow OH^-$ , should change the yield of  $e_{aq}^-$  in the same way. Our experiment, therefore, cannot prove or disprove the model of Hamill,<sup>5,16a,b</sup> that the initial positive hole, H<sub>2</sub>O<sup>+</sup>, can react with neighboring molecules. There are certain recent results of Wolff<sup>36</sup> that suggest that the reactions of H<sub>2</sub>O<sup>+</sup> may explain some of the unusual results for the oxidizing reactions in the spurs.

Several models of the fast electron attachment processes have been summarized in the Introduction and also in a recent paper of Lam and Hunt.<sup>41</sup> Two models which best describe the observed results are the "dry" electron models,<sup>16–18</sup> and a long-range interaction between the electron and the scavenger.<sup>21–23</sup> Both models predict the observed fast scavenging relationship in concentrated solutions found by Wolff, *et al.*,<sup>17</sup> Aldrich, *et al.*,<sup>18</sup> and Lam, *et al.*<sup>42</sup>

$$[e_{aq}^-]/[e_{aq}^-]_0 = \exp(-[S]/C_{37}) \quad (II)$$

in which  $[e_{aq}^-]_0$  is the initial concentration of  $e_{aq}^-$  in pure water, [S] is the concentration of the scavenger, and  $C_{37}$  is the concentration of the scavenger to reduce the ratio  $[e_{aq}^-]/[e_{aq}^-]_0$  to a value of 37%. The detailed mechanism of the processes is not finalized, but recent studies in alcohols<sup>33,41,42</sup> indicate that precursors of the solvated electrons are needed to explain the fast electron process. In the rest of this paper, the fast electron attachment process is assumed to be due to the mobile "dry" electron, e<sup>-</sup>. However, the identical mathematical analysis can also be used for the long-range models.

(II) *Yield vs. Scavenger Distribution for the Radiation Spurs.* The experimental results of this paper, and those of other papers<sup>10–12</sup> are at variance with the yield and time relationship for the spur diffusion model. The theoretical spur diffusion kinetics predict a fast decay: the initial yield of  $g(e_{aq}^-)_0 = 4.8^3$  decays to  $g(e_{aq}^-)_{1 \text{ nsec}} = 3.5$ . Wolff, *et al.*, have obtained a value of  $g(e_{aq}^-)_{30 \text{ psec}} = 4.0 \pm 0.2$  and very little decay over the initial 350-psec interval.<sup>11</sup> Excellent agreement of the yields of  $e_{aq}^-$  were found by the group in Argonne,<sup>10,12</sup> and a yield of  $g(e_{aq}^-)_{1 \text{ nsec}} = 4.1 \pm 0.2$  was obtained. Buxton,<sup>9</sup> Hunt, *et al.*,<sup>10</sup> and Jonah, *et al.*,<sup>12</sup> have followed the decay of  $e_{aq}^-$  with an apparent lifetime of 10 nsec relative to the steady-state value of 2.7. Therefore, the yield of the solvated electron in pure water at any time, *t*, is simplified by the equation

$$g(e_{aq}^-)_t = 2.7 + 1.3 \exp(-10^8 t) \quad (III)$$

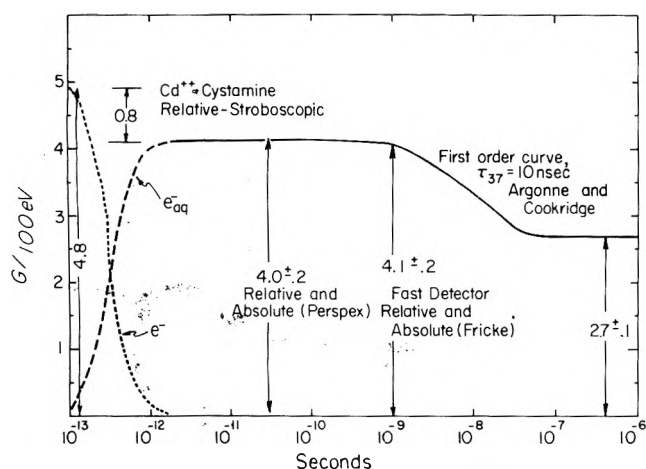


**Figure 8.** Empirical observations on electrons, indicating the initial yield of dry electrons of 4.8 obtained from this work, the initial yield of solvated electrons of  $4.0 \pm 0.2$  from previous work on this system, and the yield of  $4.1 \pm 0.2$  obtained by Jonah, *et al.*, at Argonne. Also indicated is lack of decay over the initial 350 psec noted in this lab and the 10-nsec decay to the steady-state value of 2.7 noted by Jonah, *et al.*,<sup>12</sup> and also Buxton<sup>9</sup> at Cookridge.

with  $t$  in seconds. These experimental facts are summarized in Figure 8.

As  $e_{aq}^-$  has this decay behavior, then if a solvated electron scavenger is present the yield of product as a function of scavenger concentration will have the following behavior. At low concentrations,  $<10^{-4}$  M, the yield will be that of  $e_{aq}^-$  in the bulk of solution, 2.7–2.8. At intermediate concentrations,  $10^{-4}$  to  $10^{-1}$  M, the scavenger will compete with spur processes and a higher yield will be observed. Above  $\sim 10^{-1}$  M the scavenger will probably react with dry electrons giving a further increase.

The form of the solvated electron decay is known and so the yield of product as a function of scavenger concentration can be calculated. In pure water,  $e_{aq}^-$  decays with an apparent rate constant of  $10^8$  sec<sup>-1</sup> to its steady-state value. It is assumed that the scavenger will compete with this process.<sup>43</sup> The resultant equation becomes

$$G(P)_{e_{aq}^-} = 2.7 + 1.3(k[S]/10^8 + k[S]) \quad (IV)$$

In this equation,  $k$  is the normal rate constant for the reaction of the scavenger [S] and  $e_{aq}^-$ . Of course, it might be argued that a homogeneous competition equation should not be applied to a spur process. However, this simple equation depicts satisfactorily the observed results from the period of 1 to 50 nsec.<sup>10,42</sup> This yield is indicated in Figure 9 as the solid line.

The line (---) is Balkas, Fendler, and Schuler's semiempirical relation

$$g(C1^-) = 2.55 + (2.23(1.3[C1^-])^{1/2}) / (1 + (1.3[C1^-])^{1/2}) \quad (V)$$

obtained from ref 4 and using  $k_{CH_3Cl + e_{aq}^-} = 9 \times 10^9$  M<sup>-1</sup> sec<sup>-1</sup>. A comparison with this relation is made because it was cited as verification of the spur diffusion theory. A Laplace transform of this relation into the time domain also gave an initial yield of solvated electrons of 4.8 with a very rapid decay over 1 nsec. Both this relation and the one above will give a universal curve for all scavengers when the yield is plotted against  $k[S]$ . Both curves agree quite well with the relationship  $k[S] = 5 \times 10^9$  sec<sup>-1</sup> or in concentra-

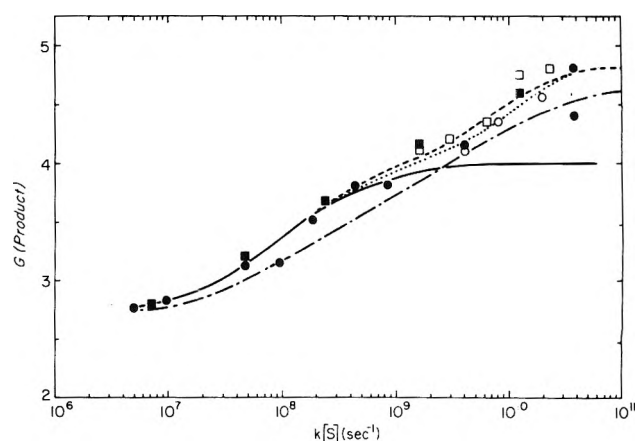
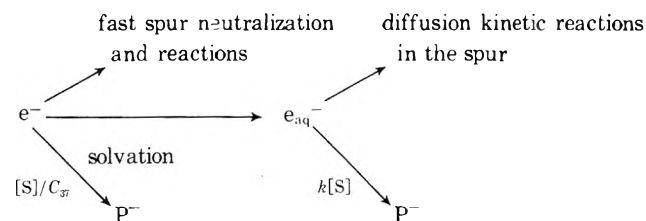


**Figure 9.** Plot of yield of electron produce vs.  $k[S]$  for  $Cd^{2+}$  (●, ○) and RSSR (■, □). The solid points were obtained by our conventional pulse radiolysis system, while the open points were obtained by the stroboscopic pulse radiolysis system. The solid line is the prediction of the spur decay, eq IV. The (---) and (····) lines are from eq VIII for  $Cd(ClO_4)_2$  and cystamine, respectively. These are extensions of the solid line in concentrated solutions including the dry electron analysis. The (-·-·) line is the semiempirical prediction of Balkas, *et al.*,<sup>4</sup> in agreement with their product yield observations.

tion solutions as high as 0.1 M for  $Cd^{2+}$  and RSSR<sup>-</sup>. Above these concentrations the observed yields deviate from the calculated curve obtained from the known  $e_{aq}^-$  decay (solid line from eq IV). It is at these concentrations that dry electron scavenging has been shown to become significant, giving rise, as stated earlier, to an increase of 20% at the highest concentrations. The concentration dependence for dry electron scavenging has earlier been shown to be exponential<sup>17,18</sup> obeying the relation  $[(e_{aq}^-)] = [(e_{aq}^-)]_0 \exp(-[S]/C_{37})$  (see eq II). The yield of electron product was found to follow the loss of  $e_{aq}^-$  but with an increase in yield as shown in Figure 6. The increase in the extra yield was found to be 20%, so that yield of the electron addition product P can be described by the reaction of the  $e_{aq}^-$  precursors, as shown by



The initial pool of electrons is at least 4.8/100 eV. In water, a fraction of the neutralization and recombination reactions occur in the radiation spur, leaving the observed value of  $g(e_{aq}^-)_{30 \text{ psec}} = 4.0 \pm 0.3$ . The yield of dry electrons which react with the scavengers occurs in times shorter than 30 psec is shown in Figure 6. The radiation product approximates the expression

$$G(P)_{e^-} = 4.8(1 - \exp(-[S]/C_{37})) \quad (VI)$$

in which there is a competition between the fast spur and solvation processes and the logarithmic dry electron scavenging process.

The remaining yield of product  $G(P)_{e_{aq}^-}$  is calculated from the  $g(e_{aq}^-)_{30 \text{ psec}}$  of 4.0, the  $10^{-8}$  sec spur decay, and the reduced yield of  $e_{aq}^-$  of  $[e_{aq}^-]/[e_{aq}^-]_0 = \exp(-[S]/C_{37})$  resulting from dry electron scavenging. This product yield

would therefore be

$$G(P)_{e_{aq}^-} = \exp(-[S]/C_{37})(2.7 + 1.3k[S]/10^8 + k[S]) \quad (\text{VII})$$

Therefore, the total yield of the electron products is then

$$G(P)_{\text{total}} = G(P)_{e^-} + G(P)_{e_{aq}^-} \quad (\text{VIII})$$

This description is not completely accurate since it assumes that the dry electron and  $e_{aq}^-$  scavenging processes are sequential, but because the dry electron rates seem to be much faster than the  $e_{aq}^-$  rates,<sup>18</sup> a reasonable approximation can be used. At present, there is no method of measuring the true dry electron rates.

Obviously a different dry electron correction must be applied for each scavenger with its own  $C_{37}$  value. Therefore, a universal curve cannot be plotted against  $k[S]$ . Each curve will be slightly different as  $C_{37}$ 's values are not directly related to dilute  $e_{aq}^-$  rate constants<sup>17</sup> in dilute solutions. However, according to results from Lam, *et al.*,<sup>41</sup> there is a general relationship between the  $C_{37}$  value and the rate constant,  $k_{\text{concn}}$ , of  $e_{aq}^-$  in concentrated solution of the scavengers. This relationship is described by

$$C_{37}k_{\text{concn}} = 1.0 \pm 0.2 \times 10^{10} \text{ sec}^{-1} \quad (\text{IX})$$

The concentrated solution rate constant,  $k_{\text{concn}}$ , is related to the dilute rate constant  $k_{\text{dil}}$  by a parameter  $\alpha$ , which must be determined for each scavenger.

$$k_{\text{concn}} = \alpha k_{\text{dil}} \quad (\text{X})$$

As shown in our lab<sup>17,18,41</sup>  $\alpha$  is usually  $\sim 0.5$  for singly positively charged scavengers,  $\sim 1$  for neutral scavengers, and  $\sim 2$  for singly negatively charged scavengers.

Therefore, formula VIII can be expressed in the form

$$G(P)_{\text{total}} = 4.8(1 - \exp(k[S]/10^{10})) + \exp(k[S]/10^{10})(2.7 + k[S]/(10^8 + k[S])) \quad (\text{XI})$$

This formula only describes the scavenging curve when the changes of  $k$  in different concentrations are accurately determined.<sup>43</sup> Yields for all electron scavengers should follow the solid line in Figure 9 until  $\sim 10^{-1} M$  shown by Balkas, *et al.*,<sup>4</sup> to be true and then they will deviate slightly according to their particular dry electron scavenging ability. The broken line and dotted line curves are reasonable approximations of the scavenging process in cadmium perchlorate and cystamine, respectively,<sup>43</sup> at high concentrations.

It can be seen that the fit of eq XI to the data is excellent. In this way the scavenging results obtained at high concentrations and early times have been used to predict the yields which are obtained over the entire concentration range using conventional pulse radiolysis and picosecond pulse radiolysis. This total curve, indicated by the solid line plus dotted line, is very similar to the curve of Balkas, *et al.*,<sup>3</sup> which agrees so well with the spur diffusion theory and other published data. Both theories predict roughly the same yield for products. Only extremely accurate yield determination would detect differences between the predictions of these two models. However, the dry electron-solvated electron theory is consistent with the observed yield of  $e_{aq}^-$  at present earliest observable time (30 psec) whereas the normal spur theory is not.

The significant point is that the yield curve calculated in this paper from observed results agrees just as well with published data on yield values as does the spur diffusion

model. More than one model can be found which can fit these yield data. However, the spur diffusion model is at variance with the observations on  $e_{aq}^-$  decay and yield at times less than 1 nsec. After  $\sim 1$  nsec the  $e_{aq}^-$  decay behaves qualitatively as predicted by spur diffusion theory, however, before this time dry electron and possibly dry hole reactions do become important. It must be noted again that the  $e^-$  designation includes the possibility that long-range interaction models (encounter pair<sup>23</sup> or electron quantum mechanical tunnelling<sup>21,22</sup>) might explain the fast reactions, but more work is still needed to determine the correct electron attachment mechanism.

*Acknowledgments.* We wish to acknowledge the continued cooperation of the staff of the linear accelerator laboratory at the University of Toronto. Mr. W.B. Taylor was invaluable for design of the electronic circuits, and the mechanical design and maintenance of the equipment was performed by Mr. Peter Nieksch. Financial support was received from the Medical Research Council of Canada, the National Research Council of Canada, and the National Cancer Institute of Canada. We also wish to acknowledge the helpful and critical comments of M.J. Bronskill and K.Y. Lam.

## References and Notes

- (1) E. M. Fielden and E. J. Hart, *Radiat. Res.*, **32**, 564 (1967).
- (2) In agreement with some investigators the "g value" is defined as the yield of the species formed by the radiation (molecule/100 eV), and the "G value" is the observed product yield. The subscript describes the observed time of the g value.
- (3) H. A. Schwarz, *J. Phys. Chem.*, **73**, 1928 (1969).
- (4) T. J. Balkas, J. H. Fendler, and R. H. Schuler, *J. Phys. Chem.*, **74**, 4497 (1970).
- (5) G. R. Freeman, *Advan. Chem. Ser.*, **No. 82**, 339 (1968).
- (6) W. H. Hamill, *J. Phys. Chem.*, **73**, 1341 (1969).
- (7) A. M. Koules-Pujo, B. D. Michael, and E. J. Hart, *Int. J. Radiat. Phys. Chem.*, **3**, 333 (1971).
- (8) J. K. Thomas and R. V. Bensasson, *J. Chem. Phys.*, **46**, 4147 (1967).
- (9) G. V. Buxton, *Proc. Roy. Soc., Ser. A*, **327**, 9 (1972).
- (10) J. W. Hunt, R. K. Wolff, M. J. Bronskill, C. D. Jonah, E. J. Hart, and M. S. Matheson, *J. Phys. Chem.*, **77**, 425 (1973).
- (11) R. K. Wolff, M. J. Bronskill, J. E. Aldrich, and J. W. Hunt, *J. Phys. Chem.*, **77**, 1350 (1973).
- (12) C. D. Jonah, E. J. Hart, and M. S. Matheson, *J. Phys. Chem.*, **77**, 1838 (1973).
- (13) A. H. Samuel and J. L. Magee, *J. Chem. Phys.*, **21**, 1080 (1953).
- (14) A. Kuppermann in "Radiation Research," Silini, Ed., North Holland Publishing Co., Amsterdam, 1967.
- (15) D. A. Flanders and H. A. Fricke, *J. Chem. Phys.*, **28**, 1126 (1958).
- (16) (a) T. Sawai and W. H. Hamill, *J. Chem. Phys.*, **52**, 3843 (1970); (b) P. L. T. Bevan and W. H. Hamill, *Trans. Faraday Soc.*, **66**, 2533 (1970).
- (17) R. K. Wolff, M. J. Bronskill, and J. W. Hunt, *J. Chem. Phys.*, **53**, 4211 (1970).
- (18) J. E. Aldrich, M. J. Bronskill, R. K. Wolff, and J. W. Hunt, *J. Chem. Phys.*, **55**, 530 (1971).
- (19) H. A. Schwarz, *J. Chem. Phys.*, **55**, 3647 (1971).
- (20) R. M. Noyes, *Progr. React. Kinet.*, **1**, 5 (1961).
- (21) J. R. Miller, *J. Chem. Phys.*, **56**, 5173 (1972).
- (22) J. R. Miller, *J. Phys. Chem.*, **76**, 2641 (1972).
- (23) G. Czapski and E. Peled, *J. Phys. Chem.*, **77**, 893 (1973).
- (24) (a) M. Anbar and E. J. Hart, *Advan. Chem. Ser.*, **No. 81**, 74 (1968); (b) E. J. Hart and M. Anbar in "The Hydrated Electron," Wiley-Interscience, New York, N.Y., 1970, pp 185-189.
- (25) M. J. Bronskill, W. B. Taylor, R. K. Wolff, and J. W. Hunt, *Rev. Sci. Instrum.*, **41**, 333 (1970).
- (26) M. J. Bronskill, R. K. Wolff, and J. W. Hunt, *J. Chem. Phys.*, **53**, 4201 (1970).
- (27) J. E. Aldrich, P. Foldvary, J. W. Hunt, W. B. Taylor, and R. K. Wolff, *Rev. Sci. Instrum.*, **43**, 991 (1972).
- (28) J. W. Hunt, C. L. Greenstock, and M. J. Bronskill, *Int. J. Radiat. Phys. Chem.*, **4**, 87 (1972).
- (29) J. H. Baxendale, E. M. Fielden, and J. P. Keene, *Proc. Roy. Soc., Ser. A*, **286**, 320 (1965).
- (30) G. E. Adams, G. S. McNaughton, and B. D. Michael in "The Chemistry of Ionization and Excitation," G. R. A. Johnson and G. Scholes, Ed., Taylor and Francis, 1967.
- (31) H. E. Johns and J. R. Cunningham in "The Physics of Radiology," 2nd ed., M. Friedman, Ed., Charles C Thomas, Springfield, Ill., 1969, p 737.

- (32) R. Braams, *Radiat. Res.*, **27**, 319 (1966).  
 (33) T. L. Penner, J. E. Aldrich, R. K. Wolff, and J. W. Hunt, manuscript in preparation.  
 (34) E. Hayon and M. Moreau, *J. Chem. Phys.*, **62**, 391 (1965).  
 (35) R. K. Wolff, Ph.D. Thesis, Department of Medical Biophysics, University of Toronto, 1972.  
 (36) R. K. Wolff, S. Chenery, and J. W. Hunt, "Fast Processes in Radiation Chemistry and Biology," G. E. Adams, B. D. Michael, and E. M. Fielden, Ed. Wiley, New York, N.Y., in press.  
 (37) M. Anbar and E. J. Hart, *J. Phys. Chem.*, **69**, 1244 (1965).  
 (38) J. Rabani, *Advan. Chem. Ser.*, No. 50, 242 (1965).  
 (39) E. Peled, D. Meisel, and G. Czapski, *J. Phys. Chem.*, **76**, 3677 (1972).  
 (40) M. Eigen and T. DeMaeyer, *Z. Electrochem.*, **59**, 986 (1955).  
 (41) K. Y. Lam and J. W. Hunt, *Int. J. Radiat. Phys. Chem.*, in press.  
 (42) C. D. Jonah, E. J. Hart, J. R. Miller, and M. S. Matheson, Abstract presented at the Fifth International Congress of Radiation Research, Seattle, Washington, 1974, has shown that eq IV does not describe the time from 0.1 to 1 ns accurately. However, changes in this period will not alter the scavenging markedly.  
 (43) In concentrations  $>0.1$  M, the  $k_{\text{concn}}$  values were used in the fast electron attachment process, eq VII, VIII, and IX. In more dilute solutions, corrections of the  $k$  were made for the ionic strength of the solutions (summarized by Anbar and Hart,<sup>24a</sup>) and assuming large effective radius of the reactor.<sup>41</sup>

## An Infrared Study of the Photolysis of Trifluoromethyl Hypofluorite and Hypochlorite in Argon Matrices at 8°K

Richard R. Smardzewski and W. B. Fox\*

Chemistry Division, U. S. Naval Research Laboratory, Washington, D. C. 20375 (Received June 10, 1974)

Publication costs assisted by the U. S. Naval Research Laboratory

Ultraviolet photolysis of trifluoromethyl hypofluorite, CF<sub>3</sub>OF, in dilute argon matrices at 8°K yielded only carbonyl fluoride, COF<sub>2</sub>; no evidence was obtained for the formation of the expected peroxide, CF<sub>3</sub>OOCF<sub>3</sub>. However, the analogous hypochlorite derivative, CF<sub>3</sub>OCl, photodissociated at wavelengths below 280 nm under similar conditions to produce both COF<sub>2</sub> and the peroxide CF<sub>3</sub>OOCF<sub>3</sub>, along with lesser amounts of CF<sub>3</sub>OF, ClF, and COFCl. The appearance of the latter is attributed to a secondary photolytic decomposition of CF<sub>3</sub>OCl induced by wavelengths below 230 nm.

### Introduction

Since its discovery,<sup>1</sup> trifluoromethyl hypofluorite, CF<sub>3</sub>OF, has been shown through extensive reaction studies to be an important reagent for introducing CF<sub>3</sub>O groups into simple molecules.<sup>2-8</sup> Similar behavior has been observed recently in the case of the corresponding hypochlorite derivative, CF<sub>3</sub>OCl.<sup>9-13</sup> As a consequence of the inherently weak nature of O-halogen bonds, in the majority of reactions involving both fluoroalkyl hypohalites, the CF<sub>3</sub>O radical is generally thought to be a primary reaction intermediate.<sup>14</sup> Because the CF<sub>3</sub>O· radical has not been directly observed in these systems, it was of interest to attempt its isolation under conditions suitable for spectroscopic examination, and we therefore undertook an investigation of the photolyses of CF<sub>3</sub>OF and CF<sub>3</sub>OCl in argon matrices at 8°K.

### Experimental Section

Gaseous trifluoromethyl hypofluorite, CF<sub>3</sub>OF (PCR Inc., 98% minimum purity) was used without further purification in a thoroughly passivated vacuum manifold fabricated from 316 stainless steel with Teflon as the gasket material. The analogous hypochlorite derivative, CF<sub>3</sub>OCl, was prepared in nearly quantitative yields from the reaction of carbonyl fluoride (Air Products and Chemicals, Inc., 98%) and chlorine monofluoride (Ozark-Mahoning Co.) in the presence of cesium fluoride (ICN-K&K Laboratories, Inc., 99%) catalyst at -20°.<sup>9</sup>

The vacuum vessel, cryogenic refrigeration system, and infrared spectrophotometer have been described else-

where.<sup>15</sup> In order to prevent reaction with the cold (8°K) CsI window, approximately 1 mmol of argon was deposited at the beginning of each experiment. Deposition rates through the stainless steel spray-on line were monitored and maintained at ca. 0.5-1.0 mmol/hr for 8-18-hr by previously calibrated thermocouple gauge readings downstream of the vernier metering valves.

A high-pressure, quartz-mercury vapor lamp (Philips HPK 125W) was used as the primary photolytic source; wavelengths were restricted to the 230-400- and 300-400-nm regions, respectively, by the judicious choice of two ultraviolet interference filters ( $\lambda_{\text{max}}$  350 and 360 nm). In certain experiments, a Pyrex filter was used to attenuate wavelengths below ca. 280 nm. Preceding the interference filters was a quartz focusing lens (2-in. diameter, 3-in. focal length), followed by a water filter (5-cm path length). In a few cases, an argon ion laser (Spectra-Physics Model 164-00) was employed as a photolysis source with its beam appropriately expanded to irradiate the entire sample area (2.83 cm<sup>2</sup>). Samples were irradiated both during and after deposition for periods of 1-16 hr.

Infrared absorption spectra were recorded over the 200-4000-cm<sup>-1</sup> spectral region, both during and after sample deposition, on a Beckman IR-12 filter-grating spectrophotometer. Survey spectra were recorded at speeds of 100 and 40 cm<sup>-1</sup>/min, while the high-resolution scans were run at 4 cm<sup>-1</sup>/min using an expanded frequency scale (10-20 cm<sup>-1</sup>/in.). Spectra slitwidths were 2.5 cm<sup>-1</sup> at 400 cm<sup>-1</sup> and 0.7-0.8 cm<sup>-1</sup> at 800, 1100, and 1800 cm<sup>-1</sup>; absolute

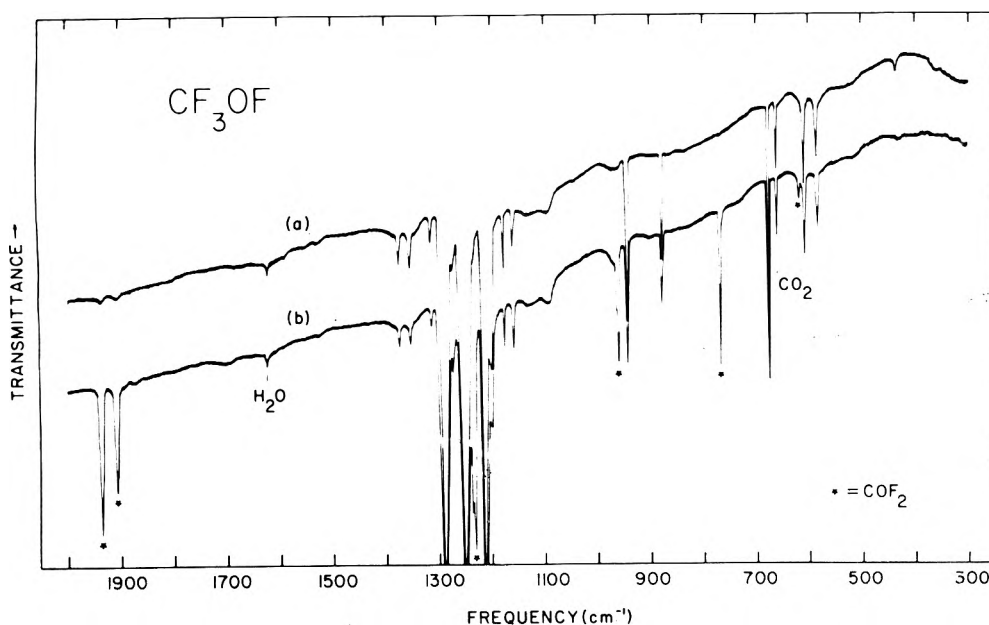


Figure 1. Matrix infrared spectrum of Ar/CF<sub>3</sub>OF = 100, 41 μmol of CF<sub>3</sub>OF: spectrum a, initial deposit; spectrum b, sample after 15-hr photolysis at 230–400 nm.

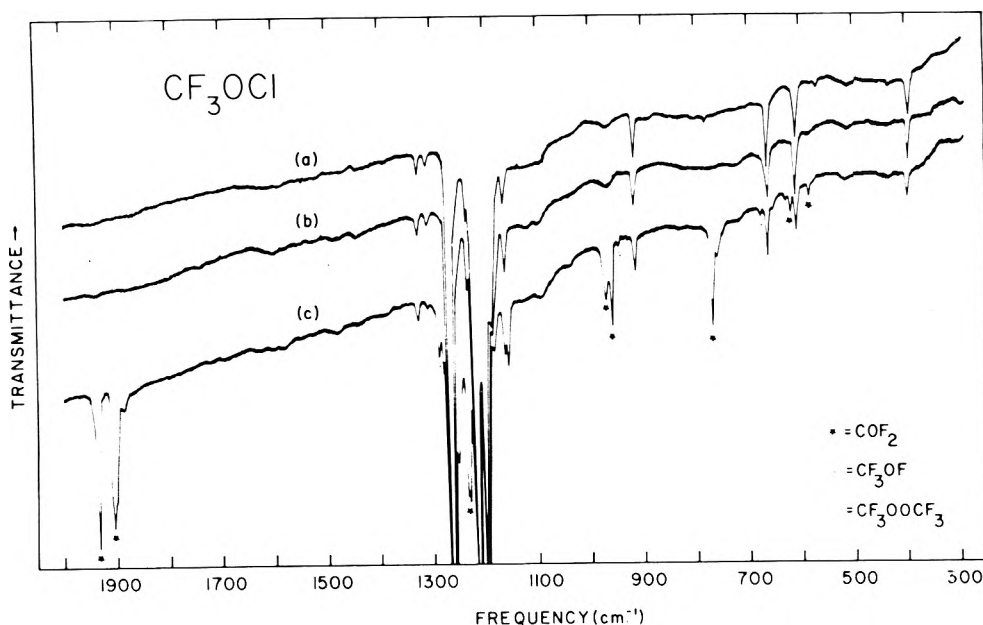


Figure 2. Infrared matrix spectrum of Ar/CF<sub>3</sub>OCl = 100, 26 μmol of CF<sub>3</sub>OCl: (a) initial matrix deposit; (b) sample after 1-hr photolysis at 280–900 nm; (c) sample after 1-hr photolysis at 220–900 nm.

frequencies were read to an accuracy of  $\pm 0.5 \text{ cm}^{-1}$ . The estimated accuracy of absorbance measurements was  $\pm 0.005 \text{ OD}$ .

## Results

**CF<sub>3</sub>OF Photolysis.** The infrared spectrum of CF<sub>3</sub>OF in solid argon near 8°K is shown in Figure 1a for an Ar/CF<sub>3</sub>OF molar ratio of 100. The resultant absorption frequencies of monomeric CF<sub>3</sub>OF are in agreement with the values obtained in the gas phase.<sup>16–18</sup> Trace amounts of H<sub>2</sub>O and CO<sub>2</sub> were observed during most experiments, primarily as a consequence of the difficulty in achieving extremely low pressures at cryogenic temperatures.<sup>19</sup> After 15 hr of photolysis ( $\lambda < 400 \text{ nm}$ ), the more intense features of COF<sub>2</sub><sup>20</sup> had begun to appear (Figure 1b), but no other products were observed. It is noteworthy that bis(trifluoro-

romethyl) peroxide, CF<sub>3</sub>OOCF<sub>3</sub>, which is observed in minor quantities in the gas-phase photolysis<sup>6</sup> of CF<sub>3</sub>OF, was not produced in detectable amounts. This was concluded from a comparison of the argon matrix frequencies of CF<sub>3</sub>OOCF<sub>3</sub><sup>21</sup> and a careful search of those spectral regions where the peroxide is an intense absorber. The weak band at  $1160.8 \text{ cm}^{-1}$ , which was present initially, is most probably due to a trace of peroxide impurity in the CF<sub>3</sub>OF sample. Relevant frequency values are contained in Table I. Similar observations were noted in a single experiment involving a nitrogen matrix. Several additional experiments were run with an Ar/CF<sub>3</sub>OF molar ratio of 500, and although longer periods of photolysis were required, the only observable product was again carbonyl fluoride.

**CF<sub>3</sub>OCl Photolysis.** In contrast to CF<sub>3</sub>OF, the matrix photolysis of the analogous hypochlorite derivative,

**TABLE I: Infrared Absorptions (cm<sup>-1</sup>) Produced by Mercury-Arc Photolysis of CF<sub>3</sub>OF in an Argon Matrix**

Before photolysis <sup>a</sup>	After photolysis <sup>b</sup>	Assignment
	1942.3 (0.30)	COF <sub>2</sub>
	1937.8 (0.49)	COF <sub>2</sub>
	1915.1 (0.19)	COF <sub>2</sub>
	1909.8 (0.26)	COF <sub>2</sub>
1379.1 (0.05)		CF <sub>3</sub> OF
1356.0 (0.06)		CF <sub>3</sub> OF
1316.9 (0.04)		CF <sub>3</sub> OF
1290.2 (0% T) <sup>c</sup>		CF <sub>3</sub> OF
1252.1 (0% T) <sup>c</sup>		CF <sub>3</sub> OF
	1238.8 (0.69)	COF <sub>2</sub>
	1234.2 (0.78)	COF <sub>2</sub>
1214.1 (0% T) <sup>c</sup>		CF <sub>3</sub> OF
1199.5 (0.28)		CF <sub>3</sub> OF
1178.0 (0.10)		CF <sub>3</sub> OF
1160.8 (0.06) <sup>d</sup>		CF <sub>3</sub> OOCF <sub>3</sub>
	965.7 (0.11)	COF <sub>2</sub>
	961.7 (0.19)	COF <sub>2</sub>
945.2 (0.27)		CF <sub>3</sub> OF
883.1 (0.14)		CF <sub>3</sub> OF
	769.8 (0.26)	COF <sub>2</sub>
678.0 (0.46)		CF <sub>3</sub> OF
669.3 (0.02)		CO <sub>2</sub> impurity
663.5 (0.09)		CO <sub>2</sub> impurity
	619.8 (0.03)	COF <sub>2</sub>
608.5 (0.14)		CF <sub>3</sub> OF
584.7 (0.08)		CF <sub>3</sub> OF
434.7 (0.01)		CF <sub>3</sub> OF

<sup>a</sup> Optical densities given in parentheses. <sup>b</sup> Photolysis for 15 hr at 230-400 nm. <sup>c</sup> Average of four experiments. <sup>d</sup> Occurs in region of intense CF<sub>3</sub>OOCF<sub>3</sub> absorption.

CF<sub>3</sub>OCl, proved to be quite complex. In Figure 2a is illustrated the infrared spectrum, in the 300-2000-cm<sup>-1</sup> region, of an argon matrix of CF<sub>3</sub>OCl at 8°K where Ar/CF<sub>3</sub>OCl = 100. The absorption frequencies obtained for matrix-isolated CF<sub>3</sub>OCl are in agreement with the gas-phase values<sup>12</sup> and are summarized in Table II. The spectrum depicted in Figure 2b, obtained after a period of 1 hr of Pyrex-filtered photolysis (cutoff λ ~280 nm), was essentially unchanged. However, after an identical period of photolysis with the full light of the mercury arc using only the water filter (transmits 220-900 nm), the spectrum designated in Figure 2c was recorded. In addition to the appearance of the infrared features of COF<sub>2</sub>, the most intense fundamentals of CF<sub>3</sub>OOCF<sub>3</sub>,<sup>22</sup> CF<sub>3</sub>OF, and ClF were also observed. The <sup>35</sup>ClF fundamental was, in fact, coincident with an intense fundamental of COF<sub>2</sub> at 770.3 cm<sup>-1</sup>, although its <sup>37</sup>Cl isotopic counterpart (24.47% natural abundance) was present at 762.2 cm<sup>-1</sup> as a weaker feature.<sup>23</sup>

The infrared spectrum of an Ar/CF<sub>3</sub>OCl = 100 deposit after prolonged illumination for 16 hr with filtered mercury arc radiation (230-400 nm) was essentially identical with that in Figure 2c obtained after only 1 hr of water-filtered photolysis. However, after long-term (16 hr) irradiation using only the water filter (transmits 220-900 nm), three new infrared features began to appear at frequencies of 1866.5, 1098.4, and 1086.6 cm<sup>-1</sup> which are assignable to the COFCl molecule.<sup>24</sup>

Several matrix experiments were conducted with an argon ion laser as the radiation source. In all cases, how-

**TABLE II: Major Infrared Absorptions (cm<sup>-1</sup>) Produced as a Result of the Photolysis of CF<sub>3</sub>OCl in an Argon Matrix at 8°K (Ar/CF<sub>3</sub>OCl = 100)**

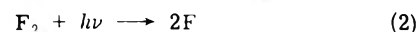
Before photolysis <sup>a</sup>	After photolysis <sup>b</sup>	Assignment
	1942.8 (0.41)	COF <sub>2</sub>
	1937.8 (0.57)	COF <sub>2</sub>
	1914.9 (0.36)	COF <sub>2</sub>
	1910.1 (0.57)	COF <sub>2</sub>
1331.1 (0.04)		CF <sub>3</sub> OCl
1315.0 (0.04)		CF <sub>3</sub> OCl
	1301.9 (0.03)	CF <sub>3</sub> OOCF <sub>3</sub>
	1290.4 (0.18)	CF <sub>3</sub> OF
	1282.5 (0.19)	CF <sub>3</sub> OOCF <sub>3</sub>
1268.1 (0% T)		CF <sub>3</sub> OCl
	1253.9 (0.44) <sup>c</sup>	CF <sub>3</sub> OOCF <sub>3</sub> + CF <sub>3</sub> OF
	1238.5 (0.41)	COF <sub>2</sub>
	1234.5 (0.60)	COF <sub>2</sub>
1219.1 (0% T)		CF <sub>3</sub> OCl
	1213.9 (0.39)	CF <sub>3</sub> OF
1200.2 (0% T)		CF <sub>3</sub> OCl
1165.1 (0.07)		CF <sub>3</sub> OCl
	1159.4 (0.17)	CF <sub>3</sub> OOCF <sub>3</sub>
	971.9 (0.09)	COF <sub>2</sub>
	961.9 (0.16)	COF <sub>2</sub>
	945.2 (0.01)	CF <sub>3</sub> OF
917.9 (0.08)		CF <sub>3</sub> OCl
781.0 (0.02)		CF <sub>3</sub> OCl
	770.3 (0.22) <sup>c</sup>	COF <sub>2</sub> + <sup>35</sup> ClF
	762.2 (0.04)	<sup>37</sup> ClF
	678.2 (0.03)	CF <sub>3</sub> OF
665.0 (0.07)		CF <sub>3</sub> OCl
	628.5 (0.02)	CF <sub>3</sub> OOCF <sub>3</sub>
	619.3 (0.05)	COF <sub>2</sub>
610.4 (0.05)		CF <sub>3</sub> OCl
	583.5 (0.04)	COF <sub>2</sub>
560.3 (0.02)		CF <sub>3</sub> OCl
396.9 (0.03)		CF <sub>3</sub> OCl

<sup>a</sup> Optical densities given in parentheses. <sup>b</sup> Photolysis for 16 hr at 230-400 nm. <sup>c</sup> Composite band.

ever, after equivalent periods of photolysis (3 hr) with the 5145- (2 W), 4880- (1.1 W), and 4579-Å (150 mW) laser lines, both during and after matrix deposition, no photodecomposition was observed.

## Discussion

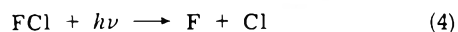
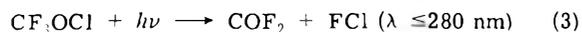
The mercury-arc photolysis of CF<sub>3</sub>OF in an argon matrix at 8°K yields COF<sub>2</sub> as the only product observable by infrared spectroscopy, and, at the low photon energies employed, it is energetically more probable that molecular rather than atomic fluorine is concomitantly eliminated in the first photochemical step (eq 1). In this manner, the



bonding energy of the F<sub>2</sub> molecule (~38 kcal/mol) can contribute to the overall energy balance. Moreover, an appreciable activation energy barrier would minimize the importance of the COF<sub>2</sub> + F<sub>2</sub> recombination reaction. Subsequent photodissociation of molecular fluorine (eq 2) would then produce F atoms, which are sufficiently mobile to escape the argon matrix cage.<sup>15</sup>

While it is possible that  $\text{CF}_3\text{OF}$  may undergo stepwise degradation to  $\text{COF}_2$  through a transient  $\text{CF}_3\text{O}\cdot$  radical, no infrared evidence was obtained for such an intermediate. Presumably the  $\text{CF}_3\text{O}\cdot$  radical, if in fact it does exist, is markedly unstable with respect to fluorine atom elimination under the experimental conditions employed. A similar occurrence was observed earlier<sup>25</sup> during the matrix photolysis of trifluoroamine oxide,  $\text{F}_3\text{NO}$ , which did not afford the intermediate  $\text{F}_2\text{NO}\cdot$  radical but photoeliminated two fluorine atoms to produce nitrosyl fluoride,  $\text{FNO}$ .

The results obtained in the  $\text{CF}_3\text{OCl}$  matrix photolysis, particularly in view of their complexity compared with the  $\text{CF}_3\text{OF}$  study, are not easily understood, although the initial events are probably similar to those of the hypofluorite photolysis. Thus the following diffusion-limited matrix processes are likely to be of primary importance:



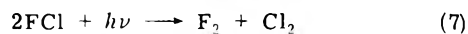
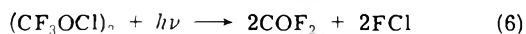
The predominance of carbonyl fluoride,  $\text{COF}_2$ , as a product of the matrix photolysis of  $\text{CF}_3\text{OCl}$  is in agreement with the observations of other workers.<sup>26</sup> The chlorine monofluoride,  $\text{ClF}$ , which is also formed can undergo additional photolysis in the matrix to produce  $\text{F}$  and  $\text{Cl}$  atoms, and a host of subsequent halogen atom reactions may then occur, although these would be considered to be of minor significance at these dilutions. Here again, as in the case of  $\text{CF}_3\text{OF}$ , no *direct* evidence was obtained for a  $\text{CF}_3\text{O}\cdot$  intermediate, although the appearance of the peroxide,  $\text{CF}_3\text{OOCF}_3$ , and the hypofluorite,  $\text{CF}_3\text{OF}$ , would seem to suggest that a  $\text{CF}_3\text{O}\cdot$  transient intermediate may be sufficiently long-lived to undergo matrix diffusion and combination with another  $\text{CF}_3\text{O}\cdot$  radical or an  $\text{F}$  atom.

However, an alternative explanation involving molecular aggregation of  $\text{CF}_3\text{OCl}$ , followed by photolysis, can account for these results. At an  $\text{Ar}/\text{CF}_3\text{OCl}$  molar ratio of 100, it is conceivable that partial molecular aggregation of a polar species such as  $\text{CF}_3\text{OCl}$  will commence upon deposition. Such molecular aggregates have been well documented in the past for a variety of fluorinated molecular species including  $\text{SF}_4$ ,<sup>27</sup>  $\text{BF}_3$ ,<sup>28</sup>  $\text{ClF}_3$ ,  $\text{BrF}_3$ ,<sup>29</sup> and  $\text{ClF}_5$ .<sup>30</sup> Under similar circumstances, the formation of the peroxide from  $\text{CF}_3\text{OCl}$  would be enhanced. For example, in the simplest case (*i.e.*, the dimer), peroxide formation is easily visualized (eq 5). This is consistent with the observation that the



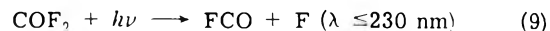
gas-phase photolysis of  $\text{CF}_3\text{OCl}$  is known to produce  $\text{CF}_3\text{OOCF}_3$  in 91% yield.<sup>12</sup>

The formation of minor amounts of  $\text{CF}_3\text{OF}$  during  $\text{CF}_3\text{OCl}$  photolysis may be a consequence of the fluorination of  $\text{COF}_2$ , since it is known that gas-phase photolysis of molecular fluorine and  $\text{COF}_2$  yields  $\text{CF}_3\text{OF}$  as a product.<sup>6</sup> While the mechanism of  $\text{CF}_3\text{OF}$  formation in the matrix is not known with certainty, a reasonable postulate for reactions in the matrix cage would be



Naturally, molecular  $\text{F}_2$  and  $\text{Cl}_2$  would escape detection as infrared observable products.

The appearance of the infrared features of  $\text{COFCl}$  only after prolonged photolysis of  $\text{CF}_3\text{OCl}$  at the shorter wavelengths can be accounted for by the secondary photolysis of  $\text{COF}_2$  (eq 9) to produce the  $\text{FCO}$  radical which can then proceed to react with a  $\text{Cl}$  atom in the same matrix cage (eq 10). Results obtained from the filtered photolysis study in-



indicate that this process is favored at wavelengths below *ca.* 230 nm. Such a mechanism is consistent with the observation of earlier workers<sup>20</sup> that the infrared features assigned to the  $\text{FCO}$  radical will indeed appear, although weakly, after extended periods of mercury-arc photolysis of  $\text{COF}_2$  in argon matrices. Unfortunately, in our study, because the concentration of  $\text{COF}_2$  was minimal at any given time, the absorption features of the  $\text{FCO}$  radical remained undetected.

*Acknowledgment.* One of us (R.R.S.) wishes to extend his gratitude to the National Research Council for support of this research under the auspices of an NRC-NRL Resident Research Associateship. In addition, special thanks are accorded to Dr. Ronald A. De Marco for many helpful and stimulating discussions.

## References and Notes

- (1) K. B. Kellogg and G. H. Cady, *J. Amer. Chem. Soc.*, **70**, 3986 (1948).
- (2) R. S. Porter and G. H. Cady, *J. Amer. Chem. Soc.*, **79**, 5625 (1957).
- (3) R. S. Porter and G. H. Cady, *J. Amer. Chem. Soc.*, **79**, 5628 (1957).
- (4) J. A. C. Allison and G. H. Cady, *J. Amer. Chem. Soc.*, **81**, 1089 (1959).
- (5) G. Pass and H. L. Roberts, *Inorg. Chem.*, **2**, 1016 (1963).
- (6) P. J. Aymonino, *Proc. Chem. Soc.*, 341 (1964).
- (7) C. J. Hoffman, *Chem. Rev.*, **64**, 91 (1964).
- (8) M. Lustig and J. M. Shreeve, *Advan. Fluorine Chem.*, **7**, 175 (1973).
- (9) D. E. Gould, L. R. Anderson, D. E. Young, and W. B. Fox, *Chem. Commun.*, 1564 (1968).
- (10) D. E. Gould, L. R. Anderson, D. E. Young, and W. B. Fox, *J. Amer. Chem. Soc.*, **91**, 1310 (1969).
- (11) D. E. Young, L. R. Anderson, D. E. Gould, and W. B. Fox, *J. Amer. Chem. Soc.*, **92**, 2313 (1970).
- (12) C. J. Schack and W. Maya, *J. Amer. Chem. Soc.*, **91**, 2902 (1969).
- (13) C. J. Schack, R. D. Wilson, J. S. Muirhead, and S. N. Cohn, *J. Amer. Chem. Soc.*, **91**, 2907 (1969).
- (14) W. A. Sheppard and C. M. Sharts, "Organic Fluorine Chemistry," W. A. Benjamin, New York, N.Y., 1969, p 230.
- (15) R. R. Smardzewski and W. B. Fox, *J. Chem. Phys.*, **60**, 2980 (1974).
- (16) P. M. Wilt and E. A. Jones, *J. Inorg. Nucl. Chem.*, **30**, 2933 (1968).
- (17) P. M. Wilt and E. A. Jones, *J. Inorg. Nucl. Chem.*, **29**, 2108 (1967).
- (18) P. J. Aymonino, *J. Inorg. Nucl. Chem.*, **27**, 2675 (1965).
- (19) H. Dubost and L. Aboual-Marguin, *Chem. Phys. Lett.*, **17**, 269 (1972).
- (20) D. E. Milligan, M. E. Jacox, A. M. Bass, J. J. Comford, and D. E. Mann, *J. Chem. Phys.*, **42**, 3187 (1965).
- (21) R. R. Smardzewski and W. B. Fox, unpublished results.
- (22) J. R. Durig and D. W. Wertz, *J. Mol. Spectrosc.*, **25**, 467 (1968).
- (23) L. Andrews, F. K. Chi, and A. Arkell, *J. Amer. Chem. Soc.*, **96**, 1997 (1974).
- (24) A. H. Nielsen, T. G. Burke, P. J. H. Woltz and E. A. Jones, *J. Chem. Phys.*, **20**, 596 (1952).
- (25) R. R. Smardzewski and W. B. Fox, *J. Chem. Phys.*, **60**, 2193 (1974).
- (26) K. O. Christe and D. Pilipovich, *J. Amer. Chem. Soc.*, **93**, 51 (1971).
- (27) R. L. Redington and C. V. Berney, *J. Chem. Phys.*, **43**, 2020 (1965).
- (28) J. M. Bassler, P. L. Timms, and J. L. Margrave, *J. Chem. Phys.*, **45**, 2704 (1966).
- (29) R. A. Frey, R. L. Redington, and A. L. Khidir-Aljibury, *J. Chem. Phys.*, **54**, 344 (1971).
- (30) K. O. Christe, *Spectrochim. Acta, Sect. A*, **27**, 631 (1971).

## The Lippmann Equation and the Ideally Polarizable Electrode

Jean-Pierre Badiali and Jerry Goodisman\*

*"Physique des Liquides et Electrochimie," Groupe de Recherches du CNRS, Associé à la Faculté des Sciences, 75230 Paris, Cedex 05, France (Received June 4, 1974)*

*Publications costs assisted by Syracuse University*

The Lippmann equation for the ideally polarizable interface is normally derived by thermodynamics, using the Gibbs dividing surface. Therefore, the quantities appearing in the Lippmann equation can have no reference to the actual charge distribution in the interfacial region. For example, the quantity referred to as surface charge is actually a sum of surface excesses, rather than the integral of a true charge density. In this article we derive, by statistical mechanical methods, the Lippmann equation for a model at the molecular level, thus giving a precise physical definition to all quantities which appear. First, we derive the conditions for mechanical equilibrium for a system (the interface between metal and solution) in which an electric field is present, and whose properties are inhomogeneous and anisotropic. From the balance of forces, we obtain equations for the surface tension in terms of the pressure, electric field, electric charge density, and electric polarization at each point within the system. Considering a spherically symmetric system (mercury drop), we then proceed to a direct calculation of the change in the surface tension produced by a change in the potential drop across the interface, maintaining thermal equilibrium, constant temperature, and the pressure and chemical composition in homogeneous regions (on the boundaries of the interfacial region). Since an ideally polarizable interface does not permit charge transport across it, we introduce a surface within the interface on which the charge density is always zero. This surface serves to divide the interfacial region into two parts, thus allowing the surface charge to be defined as the integral of the charge density over the metal side of the interface. Only the solution side is treated by statistical mechanics. Boltzmann distributions for charged and polarizable species (solute and solvent) are used to guarantee thermal equilibrium. The Lippmann equation is obtained (a) considering only ions and supposing a dielectric constant equal to that of vacuum and (b) considering ions and molecules in thermal equilibrium, and a dielectric constant varying from point to point and changing with field. Finally, the response of our system to an imposed alternating potential is considered. A direct calculation of the impedance shows that it behaves, in the low-frequency limit, as a pure capacitance, and that the value of this capacitance is the derivative of the previously defined surface charge density with respect to the potential drop across the interface.

### I. Introduction

The Lippmann equation and the concept of the capacity of the double layer have long been of fundamental importance in electrochemistry, and continue to play an important role in modern developments.<sup>1,2</sup> Nevertheless, there are a certain number of ambiguities connected with these concepts which do not seem to have been adequately clarified in the literature.

The Lippmann equation is concerned with the surface tension of the interface between an ideally polarizable electrode and an ionic solution. (Recently, an extension of the equation to a reversible electrode has been given.<sup>1</sup>) According to this equation, the change in surface tension, divided by the change in the potential drop across the interface, gives the negative of the surface charge density (charge per unit area) of the electrode, if certain parameters are held constant. Keeping the Helmholtz (parallel-plate condenser) model of the double layer in mind, this permits the identification of (a) the second derivative of the surface tension with potential and (b) the capacity of the double layer obtained from impedance measurements. Thus a connection is made between the two principal methods for obtaining information on double layer structure.

A number of proofs of the Lippmann equation have been given, all by thermodynamic methods.<sup>3</sup> The use of thermodynamics gives the equation great generality, but at the same time means that the actual forces and interactions which determine the surface tension and its variation with potential are not considered. Correspondingly, the exact interpretation of the quantities appearing in the equation is not specified, but must await the use of a model. This can lead to problems in the interpretation of experimental results; for example, it is sometimes necessary<sup>1,4</sup> to distinguish between the "free" surface charge and the "thermodynamic" surface charge—it is the latter which enters the Lippmann equation.

When the Gibbs dividing surface is used for the derivation of the Lippmann equation, one can say nothing about the location of the charge or the distribution of the potential in the interface, since there is no interfacial region in the Gibbs picture. In particular, the charge of the double layer is not defined geometrically; the total charge is zero, so that each position of the Gibbs dividing surface leads to a different geometrically defined charge  $+Q$  on one side and a charge  $-Q$  on the other. The charge appearing in the Lippmann equation is actually a combination of Gibbs surface excesses. Of course, thermodynamically derived results constitute necessary conditions which must be obeyed by any particular model, and are useful in discussion<sup>1,5</sup> of such models.

\* Address correspondence to this author at the Department of Chemistry, Syracuse University, Syracuse, New York 13210.

In this article, we consider several models for the ideally polarizable electrode and derive the Lippmann equation from statistical mechanical considerations, without recourse to thermodynamics. This allows the unambiguous definition, in terms of microscopic properties, of all the quantities which appear. Surprisingly, no derivation of this kind seems to have been presented in the literature, in spite of the long history of the Lippmann equation. Thermodynamic reasoning is universally used, followed by interpretation in terms of models.

We consider two descriptions of the "solution:" ions located in a region of dielectric constant  $\epsilon_0$  (corresponding to a gas, a fused salt, or a plasma), and ions located in a region of dielectric constant  $\epsilon$ , which may vary from point to point. The electrode (metal side of the double layer) is taken as an external source of potential; a variation in its charge leads to variations in the potential drop across the "solution" and in the surface tension. Further discussion of the models is given in section II. For each model of the solution, we derive the laws of mechanical equilibrium from purely microscopic considerations, employing Newton's laws for the coulombic interactions between the particles of which the atoms and molecules are composed. From the equilibrium conditions an equation for the surface tension is deduced. This is done for the case of dielectric constant  $\epsilon_0$  (only ions present) in section III, and for the case of dielectric constant  $\epsilon$  (ions and polarizable species present) in section V. The change in the surface tension and its ratio to the change in potential drop are computed directly. Then the Lippmann equation is derived in the two cases (sections IV and VI).

It is universal to refer<sup>2,6</sup> to the derivative of the surface charge density with respect to the potential drop across the double layer as the differential capacity of the double layer. In the case of the simple Helmholtz (parallel-plate condenser) model,<sup>2</sup> this quantity is evidently the capacity, in the sense of the impedance. However, it does not seem to have been shown in the literature that the ideally polarizable electrode actually behaves, to an alternating imposed voltage, as a capacitive circuit element.

In section VII, we show in general that, for sufficiently low frequency  $\omega$  of the alternating voltage, the ideally polarizable electrode presents an impedance of  $(i\omega C)^{-1}$ , where the capacitance  $C$  is the derivative of the electrode charge with respect to the potential drop across the interface. In conjunction with the results of the preceding sections, this means that the second derivative of the surface tension with respect to the potential drop is indeed identical with the capacity obtained from impedance measurements. This fact is well established experimentally by the work of Frumkin,<sup>7</sup> Cachet,<sup>8</sup> and others.

Section VIII contains a summary of our results and some discussion. We believe that the work presented here can be important in giving significance at the microscopic (*i.e.*, molecular) level to some of the macroscopic (*i.e.*, thermodynamic) laws of electrochemistry.

## II. Models Employed

A number of previous workers<sup>9</sup> have discussed electrocapillary phenomena in statistical mechanical terms. The review of Ono and Kondo<sup>10</sup> contains particularly valuable discussions of such work. In summary, it may be said that these authors attempt a more rigorous and general treatment than we present here, and consequently arrive at more complicated and mathematical results. We attempt to

emphasize physical concepts and thus work with simplified models.

We do not attempt, for example, to *treat the entire* system of solvated ions, metal ions, electrons, solvent molecules, etc., but define at the outset the separation of the system into two phases. The existence of a surface of separation is fundamental to our definition of the ideally polarizable electrode: for there to be no charge transfer across the interface, it suffices that there be a surface on which the charge density always vanishes. We identify this surface as the surface which separates the phases.

The system is taken as spherically symmetric, since the experimental measurements of electrocapillarity, to which our theoretical results are always implicitly referred, involve the mercury drop. Thus, the metal phase is found in the region  $r < r_\Sigma$  and the solution phase in the region  $r > r_\Sigma$ . The interface region extends from the surface  $r = r_i$  to the surface  $r = r_e$ , where  $r_i < r_\Sigma < r_e$  and all properties are homogeneous for  $r < r_i$  and  $r > r_e$ .

The interactions within the metal phase are never considered. This does not imply the region  $r < r_\Sigma$  does not contribute to the surface tension or to the potential drop across the interface. We are not interested in the calculation of the surface tension itself, but in the calculation of the change in the surface tension which accompanies a change in the potential drop, with the aim of indicating the physical effects which must be taken into consideration to produce the Lippmann equation. Thus, we assume that the contributions of the region  $r < r_\Sigma$  to the surface tension and to the potential drop are independent of the potential drop. The potential difference between  $r_\Sigma$  and  $r_i$  will be independent of the overall potential drop if the charge distribution within the metal phase remains unchanged. This is the case, for example, if the charge of the metal is on the surface (in which case the potential difference between  $r_\Sigma$  and  $r_i$  vanishes).

We consider explicitly the ions and atoms of the solution, interacting with each other and with the electrode or metal phase. The distribution of these ions and atoms is supposed to be determined by a Boltzmann-like distribution function. We suppose that the potential of the metal acting on an atom or ion of the solution is the sum of an electrostatic part of a "chemical" part. The former is the interaction of a charged or polarizable particle with a charged sphere; it depends on the total charge of the sphere but not on how this charge is distributed.

The second contribution is a potential  $W_i(r)$  ( $r > r_\Sigma$ ) which may be different for each species, thus taking into account specific chemical effects. Since  $r_\Sigma$  divides the metal phase from the solution phase,  $W_i$  for charged species should approach infinity as  $r$  approaches  $r_\Sigma$ . It is reasonable to suppose that the chemical force due to the electrode dies off rapidly with  $r$ , so that  $W_i$  has become constant for  $r > r_e$ . We make no other assumption as to the behavior of  $W_i$  between  $r_\Sigma$  and  $r_e$  (it may be totally repulsive or contain an attractive part, corresponding to adsorption). However, we assume that  $W_i$  is independent of the charge of the electrode. This assumption has been commonly accepted as a realistic one by physical chemists;<sup>3a,c,11</sup> it is at the root of the division of the electrochemical potential into electrical and chemical parts.

When the charge of the electrode is changed, we assume that the atoms and ions of the solution rearrange themselves to form a new state of equilibrium, *i.e.*, a canonical distribution obtains before and after the change. However,

since overall electroneutrality must be maintained, the systems before and after the change are different, containing different numbers of particles. In conformity with the role of the electrode as an external source of potential, all its properties, including the value of  $r_\Sigma$ , are supposed to be unchanged.

Within this general framework, two models for the solution phase are considered. First, in sections III and IV, we consider ions in a medium of dielectric constant  $\epsilon_0$  (vacuum). There is no polarization of the medium. This is appropriate to ions in the gas phase (plasma) or a molten salt. The only electrostatic interactions are the attractions and repulsions between point charges. Short-range interionic interactions may be considered to be included in the pressure. It will be assumed that the change in the pressure which accompanies a change in the potential drop across the interface may be approximated by the change in kinetic pressure,  $\Sigma n_i kT$ . This means that the contribution of the short-range interactions to the pressure change is supposed to be relatively unimportant. This assumption is parallel to the assumption that the potentials of chemical force  $W_i(r)$  are independent of potential drop.

In sections V and VI we include the effect of polarizable atoms, which give a dielectric constant  $\epsilon$  different from  $\epsilon_0$ . These atoms represent the solvent. It should be noted that we use the word "atom" in a general way, to include molecules, ions, etc. The polarization at each point is given by  $(\epsilon - \epsilon_0)E$ , where  $E$  is the electric field at this point. The value of  $\epsilon$  may differ from point to point, because the number of polarizable atoms differs (electrostriction) or because the polarizability per atom differs (saturation). The latter effect may be less important than the former.<sup>12</sup> Interactions between ions and solvent atoms which are not electrostatic in character may be included in the model, provided that their effects on the change of pressure are unimportant compared to the change of kinetic pressure.

### III. Balance of Forces for Interacting Ions

In this section, we calculate conditions for mechanical equilibrium between molecular entities composed of charged particles which interact according to Coulomb's law. Each molecular entity is charged but nonpolarizable. Of course, it is necessary to imagine additional short-range interactions to ensure stability of the system. From the laws of mechanical equilibrium we derive an expression for the surface tension.

The formalism we employed was used by Mazur<sup>13</sup> in a discussion of the electromagnetic properties of matter from a statistical mechanical point of view. The "atoms," numbered by an index  $k$ , are composed of point particles of masses  $m_{ki}$  and charges  $e_{ki}$ , located at positions  $\mathbf{R}_{ki}$ . The position of the constituent particle, numbered by  $ki$ , relative to the center of gravity  $\mathbf{R}_k$  of the atom  $k$ , is denoted by  $\mathbf{r}_{ki}$ , where

$$\mathbf{r}_{ki} = \mathbf{R}_{ki} - \mathbf{R}_k = \mathbf{R}_{ki} - \sum_i^{(k)} m_{ki} \mathbf{R}_{ki} / m_k \quad (1)$$

and  $m_k = \Sigma_i m_{ki}$ . Let  $f$  represent the statistical distribution function in phase space, so that the average value of a dynamical quantity  $\alpha$  is given by  $\langle \alpha f \rangle$ , the fences indicating integration over the phase space. In particular, the probability per unit volume of finding the center of gravity of the  $k$ th atom at point  $\mathbf{R}$  at time  $t$  is given by  $\langle \delta(\mathbf{R}_k - \mathbf{R}) f \rangle$ , where  $\delta$  is the Dirac delta function. Thus the number density of atoms at point  $\mathbf{R}$  at time  $t$  is

$$\rho_n(\mathbf{R}, t) = \sum_k \langle \delta(\mathbf{R}_k - \mathbf{R}) f \rangle \quad (2)$$

and the charge density at point  $\mathbf{R}$  at time  $t$  is

$$\rho(\mathbf{R}, t) = \langle \sum_{ki} e_{ki} \delta(\mathbf{R}_k - \mathbf{R}) f \rangle = \langle \sum_k e_k \delta(\mathbf{R}_k - \mathbf{R}) f \rangle \quad (3)$$

where  $e_k = \Sigma_i e_{ki}$ .

Following Mazur, we derive the equilibrium of forces by calculating the time rate of change of the translational momentum density  $\rho_m \mathbf{v}$ , where the mass density is

$$\rho_m(\mathbf{R}, t) = \langle \sum_{ki} m_{ki} \delta(\mathbf{R}_k - \mathbf{R}) f \rangle = \langle \sum_k m_k \delta(\mathbf{R}_k - \mathbf{R}) f \rangle \quad (4)$$

and the mean velocity is

$$\mathbf{v} = \langle \sum_k m_k \dot{\mathbf{R}}_k \delta(\mathbf{R}_k - \mathbf{R}) f \rangle / \langle \sum_k m_k \delta(\mathbf{R}_k - \mathbf{R}) f \rangle \quad (5)$$

We obtain

$$\partial(\rho_m \mathbf{v}) / \partial t = -\nabla_{\mathbf{R}} \cdot (\rho_m \mathbf{v} \mathbf{v} + \mathbf{p}_K) + \sum_k \langle m_k \ddot{\mathbf{R}}_k \delta(\mathbf{R}_k - \mathbf{R}) f \rangle \quad (6)$$

where

$$\mathbf{p}_K = \langle \sum_k m_k (\dot{\mathbf{R}}_k - \mathbf{v})(\dot{\mathbf{R}}_k - \mathbf{v}) \delta(\mathbf{R}_k - \mathbf{R}) f \rangle$$

is the kinetic pressure tensor. At thermal equilibrium,  $\mathbf{p}_K = nkT$  times the unit tensor, where  $n$  is the number of atoms per unit volume. We consider a system in static equilibrium, so that  $\mathbf{v} = 0$ , and  $\partial(\rho_m \mathbf{v}) / \partial t = 0$ . Our treatment is purely classical, and considers explicitly only the coulombic interactions between the particles of which the atoms are composed. We thus introduce *ad hoc* a contribution to the pressure tensor which is due to exchange forces, van der Waals forces, and other interactions which cannot be explained by classical electrostatics. Denoting it by  $\mathbf{p}_S$ , and setting eq 6 equal to zero, we have

$$0 = -\nabla_{\mathbf{R}} \cdot (\mathbf{p}_K + \mathbf{p}_S) + \langle \sum_k m_k \ddot{\mathbf{R}}_k \delta(\mathbf{R}_k - \mathbf{R}) f \rangle \quad (7)$$

The electrostatic force  $\mathbf{F}_k = m_k \ddot{\mathbf{R}}_k$  may be considered as including a contribution of an external electric field  $\mathbf{E}^{\text{ext}}$  and a contribution of the other particles. In general

$$m_k \ddot{\mathbf{R}}_k = \sum_i m_{ki} \ddot{\mathbf{R}}_{ki} = \sum_i e_{ki} \mathbf{E}^{\text{ext}}(\mathbf{R}_{ki}) - \sum_i \nabla_{\mathbf{R}_{ki}} \sum_{l, j}^{(i \neq k)} (4\pi\epsilon_0)^{-1} e_{ki} e_{lj} |\mathbf{R}_{ki} - \mathbf{R}_{lj}|^{-1} \quad (8)$$

The quantities  $\mathbf{R}_{li}$  may be expanded in a Taylor series in  $\mathbf{r}_{ki}$ . In this section, we consider only zero-order terms, which corresponds to taking into account only the interactions between the total charges of the atoms. Then

$$m_k \ddot{\mathbf{R}}_k = e_k \mathbf{E}^{\text{ext}}(\mathbf{R}_k) - (4\pi\epsilon_0)^{-1} \nabla_{\mathbf{R}_k} \sum_l^{(l \neq k)} e_k e_l |\mathbf{R}_k - \mathbf{R}_l|^{-1}$$

where  $e_k = \Sigma_i e_{ki}$  and (see eq 3)

$$\begin{aligned} \nabla_{\mathbf{R}} \cdot (\mathbf{p}_K + \mathbf{p}_S) &= \sum_k \mathbf{E}^{\text{ext}}(\mathbf{R}_k) e_k \delta(\mathbf{R}_k - \mathbf{R}) f + \\ &(4\pi\epsilon_0)^{-1} \int \langle \sum_{k, l} e_k e_l (-\nabla_{\mathbf{R}_k} |\mathbf{R}_k - \mathbf{R}_l|^{-1}) \delta(\mathbf{R}_k - \mathbf{R}) \times \\ &\delta(\mathbf{R}_l - \mathbf{R}') f \rangle d\mathbf{R}' = \mathbf{E}^{\text{ext}}(\mathbf{R}) \rho(\mathbf{R}) - (4\pi\epsilon_0)^{-1} \times \\ &\int \nabla_{\mathbf{R}} |\mathbf{R} - \mathbf{R}'| \langle \sum_k e_k \delta(\mathbf{R}_k - \mathbf{R}) \sum_l e_l \delta(\mathbf{R}_l - \mathbf{R}') f \rangle d\mathbf{R}' \quad (9) \end{aligned}$$

The last quantity in fences is a sum of two-particle distribution functions. We write the two-particle distribution function for particles  $k$  and  $l$  as a product of one-particle distribution functions multiplied by a correlation factor

$$\langle \delta(\mathbf{R}_k - \mathbf{R}) \delta(\mathbf{R}_l - \mathbf{R}') f \rangle = \langle \delta(\mathbf{R}_k - \mathbf{R}) f \rangle \langle \delta(\mathbf{R}_l - \mathbf{R}') f \rangle (1 + h_{kl}(\mathbf{R}, \mathbf{R}')) \quad (10)$$

The correlation function  $h_{kl}(\mathbf{R}, \mathbf{R}')$  depends on  $\mathbf{R}'$  and on  $\mathbf{R} - \mathbf{R}'$ , approaching zero as  $|\mathbf{R} - \mathbf{R}'|$  approaches infinity. Thus the last term in (9) is

$$-(4\pi\epsilon_0)^{-1} \sum_{k,l} \int \nabla_{\mathbf{R}} |\mathbf{R} - \mathbf{R}'|^{-1} e_k e_l \langle \delta(\mathbf{R}_k - \mathbf{R}) f \rangle \times \langle \delta(\mathbf{R}_l - \mathbf{R}') f \rangle (1 + h_{kl}(\mathbf{R}, \mathbf{R}')) d\mathbf{R}' = \sum_k e_k \rho^{(k)}(\mathbf{R}) \times \int \mathbf{E}_l(\mathbf{R}, \mathbf{R}') d\mathbf{R}' - (4\pi\epsilon_0)^{-1} \int \nabla_{\mathbf{R}} |\mathbf{R} - \mathbf{R}'|^{-1} \times \sum_k e_k \rho^{(k)}(\mathbf{R}) \sum_l e_l \rho^{(l)}(\mathbf{R}') h_{kl}(\mathbf{R}, \mathbf{R}') d\mathbf{R}'$$

where  $\mathbf{E}_l(\mathbf{R}, \mathbf{R}')$  is the average electric field at  $\mathbf{R}$  due to particles  $l$  at  $\mathbf{R}'$ . Since this quantity, summed over  $l$  and integrated over  $\mathbf{R}'$ , is the average electric field at  $\mathbf{R}$  due to particles in the system, we may combine it with  $\mathbf{E}^{\text{ext}}(\mathbf{R})$  to obtain the total electric field at  $\mathbf{R}$ ,  $\mathbf{E}(\mathbf{R})$ . Now eq 9 becomes

$$\nabla_{\mathbf{R}}(\mathbf{p}_K + \mathbf{p}_S) = \mathbf{E}(\mathbf{R}) - (4\pi\epsilon_0)^{-1} \times \int \nabla_{\mathbf{R}} |\mathbf{R} - \mathbf{R}'|^{-1} \sum_{k,l} e_k e_l \rho^{(k)}(\mathbf{R}) \rho^{(l)}(\mathbf{R}') h_{kl}(\mathbf{R}, \mathbf{R}') d\mathbf{R}'$$

The last term may be written as

$$-(4\pi\epsilon_0)^{-1} \nabla_{\mathbf{R}} \int |\mathbf{R} - \mathbf{R}'|^{-1} \sum_{k,l} e_k e_l \rho^{(k)}(\mathbf{R}) \rho^{(l)}(\mathbf{R}') \times h_{kl}(\mathbf{R}, \mathbf{R}') d\mathbf{R}' + (4\pi\epsilon_0)^{-1} \int |\mathbf{R} - \mathbf{R}'|^{-1} \sum_l e_l \rho^{(l)}(\mathbf{R}') \times \nabla_{\mathbf{R}} \left[ \sum_k e_k \rho^{(k)}(\mathbf{R}) h_{kl}(\mathbf{R}, \mathbf{R}') \right] d\mathbf{R}' \equiv -\nabla_{\mathbf{R}} \mathbf{p}_U + \mathbf{F}^*(\mathbf{R})$$

Finally

$$\nabla_{\mathbf{R}} \cdot (\mathbf{p}_K + \mathbf{p}_U + \mathbf{p}_S) = \mathbf{E}(\mathbf{R}) \rho(\mathbf{R}) + \mathbf{F}^*(\mathbf{R}) \quad (11)$$

Of the three contributions to the pressure tensor,  $\mathbf{p}_K$  and  $\mathbf{p}_U$  are isotropic. The contribution due to short-range forces is anisotropic, even if the forces themselves are central, because it involves the two-particle distribution function. If the forces are extremely short range (hard spheres, in the limit) the anisotropy disappears. The force  $\mathbf{F}^*(\mathbf{R})$  is also anisotropic; in fact, it has only one nonvanishing component, in the radial direction, in the case of spherical symmetry. In a homogeneous medium,  $\mathbf{F}^*$  and  $\mathbf{p}_U$  vanish. We note that  $\mathbf{F}^*$  is intrinsically due to interparticle correlations and cannot be expressed in general as the gradient of a pressure since  $\nabla \times \mathbf{F}^*$  is not zero.

In what follows, we shall neglect  $\mathbf{F}^*$  (however see Appendix, eq A6). This is apparently done by other authors who write the equations for mechanical equilibrium in terms of macroscopic or average quantities. We use the remaining expression

$$\nabla \cdot \mathbf{p} = \mathbf{E}(\mathbf{R}) \rho(\mathbf{R}) \quad (12)$$

to express the condition of mechanical equilibrium in the presence of an electric field. We consider the spherically symmetric region between a sphere of radius  $r_i$  and a sphere of radius  $r_e$ .  $\mathbf{E}$  is necessarily in the radial direction, while  $\mathbf{p}$  has at each point two independent components,  $p_N$  along the radial direction and  $p_T$  in all perpendicular directions. The properties of the system are homogeneous for

$r < r_i$  and  $r > r_e$ , and vary continuously from  $r_i$  to  $r_e$ . Our first goal is to derive a convenient expression for the surface tension in terms of the pressure and electric field at each point in the system.

We have first the experimental definition of the surface tension (Laplace equation):

$$p_i - p_e = 2\sigma/r_\sigma \quad (13)$$

Here,  $p_i$  and  $p_e$  are the (isotropic) pressures for  $r_i$  and  $r_e$ ,  $\sigma$  is the surface tension, and  $r_\sigma$  the radius of the surface of tension. Another expression for  $\sigma$  and  $r_\sigma$  is obtained by noting that the three-dimensional interfacial region is supposed to behave as a geometric surface of radius  $r_\sigma$ ,  $r_i < r_\sigma < r_e$ , on which the surface tension acts. This means that, instead of taking into account the actual values of  $p_N$  and  $p_T$  at each point in the interface, we may consider that our system consists of a homogeneous bulk phase with pressure  $p_i$  and corresponding values of other properties for  $r < r_\sigma$ , a homogeneous bulk phase with pressure  $p_e$  and corresponding values of other properties for  $r > r_\sigma$ , and a tension  $\sigma$  acting at  $r_\sigma$ .

In the Appendix we show that the volume force  $\mathbf{E}\rho$  is equivalent, in the case of spherical symmetry, to a surface force, i.e., the integral of  $\mathbf{E}\rho$  over any volume is equal to the integral of the normal component of a fictitious pressure over the surface bounding the volume. In particular, one can use the force laws which obtain in the absence of field, provided one replaces  $p_T$  by  $p_T + \frac{1}{2}\epsilon_0 E^2$  and  $p_N$ , the radial component of the pressure, by  $p_N - \frac{1}{2}\epsilon_0 E^2$  (see eq A4). Now we consider the part of the interfacial region contained between the half-plane  $\phi = 0$  and the half-plane  $\phi = \alpha$ , where  $\phi$  is the polar angle. In calculating the work done in increasing  $\alpha$  by  $d\alpha$ , a virtual displacement which maintains the symmetry of the system, we may use the exact description of the forces in terms of  $p_N$  and  $p_T$  or the description in terms of  $\sigma$  and  $r_\sigma$ . Equating the two, we obtain the desired equation for  $\sigma$  and  $r_\sigma$ .

The normal force acting on the area between the circles  $r$  and  $r + dr$  and between the rays  $\theta$  and  $\theta + d\theta$  ( $\theta =$  azimuthal angle) is  $p_T(r)r = dr d\theta$  and the distance moved by these points during the displacement is  $r \sin \theta d\alpha$ . Thus, replacing  $p_T$  by  $p_T + \frac{1}{2}\epsilon_0 E^2$ , as indicated above, the work done in increasing  $\alpha$  by  $d\alpha$ , including the effect of the electric field, is

$$W = \int_0^\pi d\theta \int_{r_i}^{r_e} dr (p_T(r) + \frac{1}{2}\epsilon_0 E^2) r^2 \sin \theta d\alpha \quad (14)$$

If we consider the system as having a pressure  $p_i$  for  $r < r_\sigma$ , a pressure  $p_e$  for  $r > r_\sigma$ , and a tension  $\sigma$  at  $r = r_\sigma$ , the work is

$$W = \int_0^\pi d\theta \left[ \int_{r_i}^{r_\sigma} dr p_i r^2 \sin \theta + \int_{r_\sigma}^{r_e} dr p_e r^2 \sin \theta - \sigma r_\sigma^2 \sin \theta \right] d\alpha \quad (15)$$

since  $\sigma$  is a tension. Equating the expressions for  $W$  and rearranging, we find

$$\sigma r_\sigma^2 = \int_{r_i}^{r_\sigma} (p_i - p_T - \frac{1}{2}\epsilon_0 E^2) r^2 dr + \int_{r_\sigma}^{r_e} (p_e - p_T - \frac{1}{2}\epsilon_0 E^2) r^2 dr \quad (16)$$

This equation has also been derived by Sanfeld and others<sup>14</sup> using other arguments.

Other equations are possible, but (16) has several advan-

tages for our purposes. We are interested in calculating the change in  $\sigma$  which accompanies a change in potential, keeping interior and exterior pressures, temperature, and other parameters constant. The explicit appearance of  $p_i$  and  $p_e$  in (16) makes it easy to ensure that they are held constant when  $\sigma$  is changed. A second advantage is the way in which  $r_\sigma$  enters (16). When  $\sigma$  changes,  $r_\sigma$  will certainly change as well, and the calculation of  $\Delta r_\sigma$  would be troublesome. As we will see below, use of (16) makes such a calculation unnecessary.

We now proceed to the calculation of  $\Delta\sigma$  and the change in  $U$ , the potential drop across the double layer, leading to the Lippmann equation. In the Lippmann equation, as derived thermodynamically, pressure, temperature, and chemical potentials of bulk phases are held constant in calculation of  $\Delta\sigma/\Delta U$ . Our derivation will give a precise sense to these conditions.

#### IV. Lippmann Equation for Phase of Dielectric Constant $\epsilon_0$

We start from eq 16 and 13, which define  $\sigma$  and  $r_\sigma$ . For a change in the interface which maintains  $p_i$  and  $p_e$  constant, we have

$$\Delta\sigma r_\sigma^2 + 2\sigma r_\sigma \Delta r_\sigma = - \int_{r_i}^{r_e} \Delta(p_T + \frac{1}{2}\epsilon_0 E^2) r^2 dr + p_i r_\sigma^2 \Delta r_\sigma - p_e r_\sigma^2 \Delta r_\sigma$$

By virtue of (13), the terms in  $\Delta r_\sigma$  disappear, leaving

$$\Delta\sigma r_\sigma^2 = - \int_{r_i}^{r_e} \Delta p_T r^2 dr - \frac{1}{2}\epsilon_0 \Delta \int_{r_i}^{r_e} E^2 r^2 dr \quad (17)$$

The second integral may be written in terms of the electrostatic potential  $\psi$ :

$$-(4\pi)^{-1} \int \mathbf{E} \cdot \nabla \psi d\tau = -(4\pi)^{-1} \int \psi \mathbf{E} \cdot d\mathbf{S} + (4\pi)^{-1} \int \psi (\nabla \cdot \mathbf{E}) d\tau$$

Since  $\mathbf{E} = 0$  on the boundary surface (the spheres of radii  $r_i$  and  $r_e$ ), the surface integral vanishes. Using the Poisson equation, we have

$$\Delta\sigma r_\sigma^2 = - \int_{r_i}^{r_e} \Delta p_T r^2 dr - \frac{1}{2} \int_{r_i}^{r_e} \Delta(\psi \rho) r^2 dr \quad (18)$$

for a change maintaining  $p_i$  and  $p_e$  constant. By the definition of the ideally polarizable electrode (see section II), there is a surface, corresponding to  $r = r_\Sigma$ , on which the charge density vanishes:  $\rho(r_\Sigma) = 0$ . This surface also serves to divide the electrode or metal phase from the solution phase. Thus the electrode charge is obtained by integrating the charge density from  $r_i$  to  $r_\Sigma$  and the electrode surface charge density  $Q$  is obtained by dividing the electrode charge by  $4\pi r_\Sigma^2$ . Similarly the charge of the solution is obtained by integration of  $\rho$  from  $r_\Sigma$  to  $r_e$ . The charge density  $\rho$  is supposed to vanish for  $r \leq r_i$  and  $r \geq r_e$ . Since the electric field is zero at  $r = r_i$  and at  $r = r_e$ , we must have the electroneutrality condition

$$\int_{r_\Sigma}^{r_e} r^2 \rho dr = -Q r_\Sigma^2 \quad (19)$$

As discussed in section II, our model permits us, in calculating  $\Delta\sigma$  and  $\Delta U$ , to consider only the solution part. The change in  $U$  is produced by addition of charge to the metal phase, which produces a rearrangement of charge density in the solution, whose total charge must change to maintain electroneutrality. In summary, the electrode is considered

as a system of fixed properties, whose charge may be varied without changing its other properties.

We now have

$$\Delta\sigma r_\sigma^2 = - \int_{r_\Sigma}^{r_e} \Delta p_T r^2 dr - \frac{1}{2} \int_{r_\Sigma}^{r_e} (\Delta\psi \rho + \psi \Delta\rho) r^2 dr \quad (20)$$

If we take, as we may without loss of generality, the potential at  $r = r_\Sigma$  as zero, the potential at a point  $r > r_\Sigma$  is given by

$$\psi(r) = \frac{1}{\epsilon_0 r} \int_{r_\Sigma}^r \rho r' dr - \frac{1}{\epsilon_0} \int_{r_\Sigma}^r r \rho dr - \frac{Q}{\epsilon_0} r_\Sigma + \frac{1}{\epsilon_0 r} Q r_\Sigma^2 \quad (21)$$

Since  $U$  is supposed to be the potential drop in going from the electrode to the homogeneous region of the solution

$$U = \int_{r_\Sigma}^{r_e} \frac{1}{\epsilon_0} \rho r dr + \frac{Q}{\epsilon_0} r_\Sigma \quad (22)$$

where (19) has been used. Now suppose that  $Q$  is changed to  $Q + \Delta Q$ , so that, at each point between  $r_\Sigma$  and  $r_e$ ,  $\rho$  changes to  $\rho + \Delta\rho$  and  $\psi$  changes to  $\psi + \Delta\psi$ . A direct calculation using eq 19, 21, and 22 yields

$$\int_{r_\Sigma}^{r_e} \psi \Delta\rho r^2 dr = U \Delta Q r_\Sigma^2 - \epsilon_0^{-1} \int_{r_\Sigma}^{r_e} dr \int_{r_\Sigma}^r dr' \Delta\rho(r') \rho(r) (r' r^2 - r r'^2)$$

and

$$\int_{r_\Sigma}^{r_e} \Delta\psi \rho r^2 dr = \int_{r_\Sigma}^{r_e} \psi \Delta\rho r^2 dr$$

In the calculation of  $\Delta p_T$ , we consider only the kinetic pressure contribution,  $nkT$ , assuming that the other contributions do not change appreciably with  $\Delta Q$ . Since the temperature is to be held constant during the change

$$\Delta p_T = kT \Delta n = kT \sum_i \Delta n_i(r)$$

where  $n_i(r)$  is the concentration of ion  $i$ . Thus we have

$$\Delta\sigma r_\sigma^2 = -kT \sum_i \int_{r_\Sigma}^{r_e} \Delta n_i r^2 dr - \int_{r_\Sigma}^{r_e} (\Delta\psi \rho) r^2 dr \quad (23)$$

In changing  $Q$  we are supposed to go from one equilibrium state to another, and to maintain the properties of the solution where it is homogeneous, corresponding to holding chemical potential constant. The equilibrium condition will be imposed by assuming Boltzmann distributions before and after the change in  $Q$ , with  $n_i(r_e)$  constant. Thus

$$n_i(r) = n_i(r_e) \exp(-[V_i(r) - V_i(r_e)]/kT) \quad (24)$$

The potential energy  $V_i(r)$  contains an electrostatic part  $q_i \psi(r)$  and a chemical part  $W_i(r)$  due to the electrode (see section II). Therefore, since  $n_i(r_e)$  is constant

$$\Delta n_i(r) = n_i(r_e) \exp(-[V_i(r) - V_i(r_e)]/kT) (-q_i/kT) (\Delta\psi(r) - \psi(r_e)) = n_i(r) (-q_i/kT) (\Delta\psi(r) + \Delta U)$$

We have used the fact that  $\psi(r_e) = -U$ . Substituting into (23)

$$\Delta\sigma r_\sigma^2 = \sum_i \int_{r_\Sigma}^{r_e} n_i q_i (\Delta\psi + \Delta U) r^2 dr - \int_{r_\Sigma}^{r_e} \Delta\psi \rho r^2 dr \quad (25)$$

Now  $\rho = \sum n_i q_i$ , so the first part of the "pressure" term cancels out the "electrostatic" term. The similarity of "kinetic pressure" and electrostatic terms has been discussed by Frenkel,<sup>9b</sup> who emphasized the dangers of neglecting one while changing the other.

Equation 25 may now be written

$$\Delta \sigma r_\sigma^2 = \int_{r_\Sigma}^{r_e} \rho \Delta U r^2 dr = \Delta U (-Q r_\Sigma^2)$$

Now the effective thickness of the interfacial region is, in reality, always very small compared to its radius. For experiments with a mercury drop, the radius of the interface is of the order of 500  $\mu$ , while the thickness of the interfacial region is about 100  $\text{\AA}$ . Since  $r_\sigma$  and  $r_\Sigma$  both lie within the interfacial region, their values are essentially equal. Thus  $\Delta \sigma = -Q \Delta U$ ; the Lippmann result is proved:

### V. Balance of Forces in the Presence of a Polarizable Medium

In this section we consider the possibility of having net dipole moments on some molecules. Returning to eq 7 and 8, we retain terms through second order in the  $r_{ki}$  in the Taylor series expansions, and, following Mazur, neglect quadrupole moments. The electric dipole moment of molecule  $k$  is defined as

$$\mu_k = \sum_i e_{ki} r_{ki} \quad (26)$$

We now have

$$m_k \ddot{\mathbf{R}}_k = e_k \mathbf{E}^{\text{ext}}(\mathbf{R}_k) + \mu_k \cdot \nabla_k \mathbf{E}^{\text{ext}}(\mathbf{R}_k) - \nabla_k \times \sum_{i \neq k} (e_k e_i \dot{\mathbf{V}}_{ki} + e_i \mu_k \cdot \mathbf{U}_{ki} + e_k \mu_i \mathbf{U}_{ik} + \mu_k \mu_i \cdot \mathbf{T}_{ki}) \quad (27)$$

where we have introduced the following abbreviations:

$$\mathbf{V}_{ki} \equiv (4\pi\epsilon_0)^{-1} |\mathbf{R}_k - \mathbf{R}_i|^{-1}$$

$$\mathbf{U}_{ki} \equiv (4\pi\epsilon_0)^{-1} \nabla_k |\mathbf{R}_k - \mathbf{R}_i|^{-1}$$

$$\mathbf{T}_{ki} \equiv (4\pi\epsilon_0)^{-1} \nabla_k \nabla_i |\mathbf{R}_k - \mathbf{R}_i|^{-1}$$

We must now calculate, for insertion in eq 7

$$\langle m_k \mathbf{R}_k \delta(\mathbf{R}_k - \mathbf{R}) f \rangle = \mathbf{E}^{\text{ext}}(\mathbf{R}) + \mathbf{P} \cdot \nabla_R \mathbf{E}^{\text{ext}}(\mathbf{R}) - \sum_{k, l} \int d\mathbf{R}' [e_k e_l \langle \nabla_R \mathbf{V}_{kl} \delta(\mathbf{R} - \mathbf{R}_k) \delta(\mathbf{R}' - \mathbf{R}_l) f \rangle + e_l \langle \nabla_R \mu_k \cdot \mathbf{U}_{kl} \delta(\mathbf{R} - \mathbf{R}_k) \delta(\mathbf{R}' - \mathbf{R}_l) f \rangle + e_k \langle \nabla_R \mu_l \cdot \mathbf{U}_{lk} \delta(\mathbf{R} - \mathbf{R}_k) \delta(\mathbf{R}' - \mathbf{R}_l) f \rangle + \langle \nabla_R \mu_k \mu_l \cdot \mathbf{T}_{kl} \delta(\mathbf{R} - \mathbf{R}_k) \delta(\mathbf{R}' - \mathbf{R}_l) f \rangle] \quad (28)$$

Here  $\mathbf{P}$  is the electric dipole moment per unit volume,

$$\mathbf{P} = \left\langle \sum_k \mu_k \delta(\mathbf{R} - \mathbf{R}_k) \right\rangle$$

i.e., the polarization.

As in section III, we may separate terms corresponding to local properties from terms corresponding to correlations. For example, the dipole moment of molecule  $k$  at point  $\mathbf{R}$ , for a given configuration of charges of other particles, is equal to its average value plus a fluctuation or correlation term. Similarly, the two-particle distribution functions are written as products of one-particle distribution functions and a correlation factor  $1 + h_{kl}(\mathbf{R}, \mathbf{R}')$  (eq 10). Some of the terms reflecting the correlations may be written as divergences of local pressure tensors as shown by Mazur<sup>13</sup> and interpreted as representing short-range forces. There remain terms which cannot be so written, as in

section II. Assuming that these can be ignored we have from (2)

$$\nabla_R \cdot \mathbf{p}' = \rho \mathbf{E}^{\text{ext}}(\mathbf{R}) + \mathbf{P} \cdot \nabla_R \mathbf{E}^{\text{ext}}(\mathbf{R}) + \rho \mathbf{E}^{(1)}(\mathbf{R}) + \mathbf{P} \cdot \nabla_R \mathbf{E}^{(1)}(\mathbf{R}) + \rho \mathbf{E}^{(2)}(\mathbf{R}) + \mathbf{P} \cdot \nabla_R \mathbf{E}^{(2)}(\mathbf{R}) \quad (29)$$

Here  $\nabla_R \mathbf{p}'$  includes all short-range terms which can be written as divergences, and

$$\mathbf{E}^{(1)}(\mathbf{R}) = -(4\pi\epsilon_0)^{-1} \nabla_R \int d\mathbf{R}' \rho(\mathbf{R}') |\mathbf{R} - \mathbf{R}'|^{-1}$$

$$\mathbf{E}^{(2)}(\mathbf{R}) = -(4\pi\epsilon_0)^{-1} \nabla_R \int d\mathbf{R}' P(\mathbf{R}') \cdot \nabla_{R'} |\mathbf{R} - \mathbf{R}'|^{-1}$$

representing, respectively, the field at  $\mathbf{R}$  due to the ionic charges and the field at  $\mathbf{R}$  due to molecular dipoles.

Equation 29 may now be written

$$\nabla_R \cdot \mathbf{p} = \rho \mathbf{E}(\mathbf{R}) + \mathbf{P} \cdot \nabla_R \mathbf{E}(\mathbf{R}) \quad (30)$$

where  $\mathbf{E}(\mathbf{R}) = \mathbf{E}^{\text{ext}} + \mathbf{E}^{(1)} + \mathbf{E}^{(2)}$  is the total field at point  $\mathbf{R}$ . It must be remembered that certain contributions which are undeniably of electrostatic origin, but include the effect of correlations, have been included in the "pressure" term and others have been ignored. There is thus some arbitrariness in writing the electrical force as the right member of eq 30. Mazur<sup>13</sup> and Sanfeld<sup>14</sup> have discussed this point in detail, and emphasized that the balance of forces may be written in a number of apparently different ways; in each case the meaning of pressure is different.

If we use (30) in the place of (12) to calculate the equilibrium condition for a volume of our system, we obtain

$$\int \mathbf{p} \cdot d\mathbf{S} = \int \rho \mathbf{E} d\tau + \int \mathbf{P} \cdot \nabla \mathbf{E} d\tau \quad (31)$$

Although the right side of (30) is not the gradient of a tensor, so that the volume integrals in (31) cannot in general be written as surface integrals, simplification is possible in the case of spherical symmetry. The vectors  $\mathbf{E}$  and  $\mathbf{P}$  are necessarily in the radial direction at each point in our system. Then, as shown in the Appendix (eq 7), the right side of (31) may be replaced by the integral over the surface of the normal component of a fictitious pressure. This means that we may calculate forces by ignoring the electric field terms and replacing  $\rho_T$  by  $\rho_T + \frac{1}{2}\epsilon_0 E_r^2$  and  $\rho_N$  by  $\rho_N + (\frac{1}{2}\epsilon_0 - \epsilon) E_r^2$ .

Again, we consider the volume and the fictitious displacement of section III. Equation 14 is unchanged, since only the tangential pressure enters. Therefore, eq 16 is unchanged. As previously, we now have to consider a change in  $U$  and the corresponding change in surface tension  $\sigma$ , while assuring that we pass from one state of equilibrium to another, maintaining constant the internal and external pressure, the temperature, and the composition of the two phases in homogeneous regions.

### VI. Lippmann Equation in the Presence of Polarization

We take as our point of departure eq 17. We assume no contributions from the region  $r < r_\Sigma$  so that our basic equation for the change in surface tension is

$$\Delta \sigma r_\sigma^2 = - \int_{r_\Sigma}^{r_e} \Delta \rho_T r^2 dr - \frac{1}{2} \epsilon_0 \int_{r_\Sigma}^{r_e} \Delta (E^2) r^2 dr \quad (32)$$

Now, the Poisson equation is

$$\nabla \cdot \mathbf{D} = \rho$$

where  $\mathbf{D} = \epsilon \mathbf{E}$  and the dielectric constant  $\epsilon$  at each point may depend on the electric field and on the position. The polarization is related to the field and the dielectric constant by

$$P = (\epsilon - \epsilon_0)E$$

The electric polarization at each point is proportional to the number of molecules per unit volume. The nature of these "molecules" is not specified, and their properties may be considered as depending on the chemical environment, in particular on the distance from the electrode. We have in mind, of course, induced polarization due to orientation of permanent dipole moments by an electric field.

As before, we take into account, in the calculation of  $\Delta p_T$ , only the change in the kinetic pressure. At constant temperature, this is  $\Delta n kT$ . Now, however, the total concentration  $n$  includes a contribution from solvent molecules, as well as from the ions. For simplicity, we assume that we may separate the two kinds of particles: the ions are nonpolarizable and the solvent molecules are not charged.

Thus

$$\Delta p_T = kT \left( \sum_i \Delta n_i + \Delta n_0 \right) \quad (33)$$

where the subscript 0 refers to the solvent. We assume, for all species, a Boltzmann distribution. For the ions we have eq 24, which led to

$$\Delta n_i(r) = n_i(r) (-q_i/kT) (\Delta\psi(r) + \Delta U) \quad (34)$$

The electrostatic energy of an orientable or polarizable molecule is given by

$$- \int_0^E \alpha E' dE'$$

where  $\alpha$  is the molecular electric polarizability and  $E$  the electric field. The molecules may of course be rotating species possessing permanent dipole moments. The value of  $\alpha$  may differ from point to point and may also depend on  $E'$  (dielectric saturation effect): it is well known that a strong enough electric field can essentially totally orient the solvent molecules, reducing their response to an additional imposed field and hence decreasing  $\alpha$ . The variation of  $\alpha$  with position is the electrostrictive effect: because the energy of a molecule decreases with field, such molecules tend to concentrate in regions of higher electric field. This means that the dielectric constant varies from point to point because the number of molecules changes. Thus in the equation

$$\epsilon - \epsilon_0 = n_0 \alpha \quad (35)$$

we assume that  $n_0$  follows a Boltzmann distribution

$$n_0/n_{0e} = \exp \left( - \left[ - \int_0^E \alpha E' dE' + W_0(r) \right] / kT \right)$$

Here  $n_{0e}$  is the concentration of solvent at  $r = r_e$  (where  $E = 0$ ), which is supposed to remain constant. The potential  $W_0$  is due to the electrode, and may include an attraction leading to adsorption, as well as a repulsive potential for  $r \cong r_\Sigma$ . However, we suppose  $W_0$  is independent of  $U$ , as in the case of the corresponding potential for the ions. This corresponds to a separation of "electrostatic" and "chemical" effects.

Now we may write

$$\Delta n_0 = n_{0e} \exp \left[ \left( \int_0^E \alpha E' dE' - W_0(r) \right) / kT \right] \times \Delta \left( \int_0^E \alpha E' dE' \right) / kT = n_0 (\alpha / kT) E \Delta E \quad (36)$$

Substituting into eq 33, we have

$$\Delta p_T = - \sum_i q_i n_i \Delta\psi + \Delta U + \frac{1}{2} n_0 \alpha \Delta(E^2) = -\rho(\Delta\psi + \Delta U) + \frac{1}{2}(\epsilon - \epsilon_0)\Delta(E^2)$$

This in turn is used in eq 32, giving

$$\Delta \sigma r_\sigma^2 = \int_{r_\Sigma}^{r_e} \rho \Delta\psi r^2 dr + \Delta U \int_{r_\Sigma}^{r_e} \rho r^2 dr - \frac{1}{2} \int_{r_\Sigma}^{r_e} (\epsilon - \epsilon_0) \Delta(E^2) r^2 dr - \frac{\epsilon_0}{2} \int_{r_\Sigma}^{r_e} \Delta(E^2) r^2 dr$$

The terms in  $\epsilon_0$  vanish, and

$$\Delta \sigma r_\sigma^2 = \int_{r_\Sigma}^{r_e} \rho \Delta\psi r^2 dr - \Delta U Q r_\Sigma^2 - \int_{r_\Sigma}^{r_e} \epsilon E \cdot \Delta E r^2 dr \quad (37)$$

The first integral in this equation may be treated by using Poisson's equation and integrating by parts

$$\int_{r_\Sigma}^{r_e} \rho \Delta\psi r^2 dr = (4\pi)^{-1} \int_{r_\Sigma}^{r_e} (\nabla \cdot \mathbf{D}) \Delta\psi d\tau = (4\pi)^{-1} \times \left[ \int_{r_\Sigma}^{r_e} d\mathbf{S} \cdot (\mathbf{D} \Delta\psi) - \int_{r_\Sigma}^{r_e} d\tau \nabla \cdot (\Delta\psi) \cdot \mathbf{D} \right] = - \int_{r_\Sigma}^{r_e} \Delta(-\mathbf{E}) \cdot \mathbf{D} r^2 dr$$

We have used the fact that  $\mathbf{D}$  vanishes at  $r = r_e$  while  $\psi$  and  $\Delta\psi$  vanish at  $r = r_\Sigma$ . Note that  $\Delta$  here signifies "the change in" and not the Laplacian.

Finally, eq 37 becomes

$$\Delta \sigma r_\sigma^2 = \int_{r_\Sigma}^{r_e} \Delta \mathbf{E} \cdot \mathbf{D} r^2 dr - \int_{r_\Sigma}^{r_e} \epsilon \mathbf{E} \cdot \Delta \mathbf{E} r^2 dr - \Delta U Q r_\Sigma^2$$

which may be rewritten

$$\Delta \sigma r_\sigma^2 \Delta U = -Q r_\Sigma^2 / r_\sigma^2 \cong -Q \quad (38)$$

Thus we again have the Lippmann equation.

We emphasize that in the present case, where  $\epsilon$  differs from  $\epsilon_0$ , it was necessary to consider the distribution of solvent molecules and how it changes with  $U$ . As before, the anisotropy in the pressure tensor does not enter; indeed, we assume that the change in the kinetic pressure with  $U$  is more important than the change in the other contributions to pressure. By starting from a microscopic picture and using statistical mechanics, we were able to enumerate the changes contributing to the satisfaction of the Lippmann equation. The statistical mechanical treatment, in contrast to the thermodynamic one, allows explicit definition of the quantities entering the equations.

## VII. Capacity of the Ideally Polarizable Electrode

In this section, we consider the response of an ideally polarizable electrode to an imposed alternating potential, with a view to a direct calculation of the impedance. We recall that, as part of our definition of the ideally polarizable electrode, we used the existence of a surface on which  $\rho = 0$  (section II). We also wish to recall that the changes in  $\Delta\sigma$  and  $\Delta Q$  were supposed to be carried out in such a way that the system passes from one equilibrium state to another.

Let the potential  $U$  across the electrode be the steady potential  $U_s$  plus the alternating potential  $U_0 e^{i\omega t}$ . The effect of the alternating potential is to induce an alternating current, which, divided into  $U_0 e^{i\omega t}$ , yields the impedance. No continuous current is possible because no charge can pass the surface  $r = r_\Sigma$ . The current may be calculated at any point in the circuit, provided that one considers the total current, which is conserved. This current is

$$\mathbf{J} = \rho \mathbf{v} + \partial \mathbf{D} / \partial t \quad (39)$$

The term  $\rho \mathbf{v}$  represents the transport of charge with velocity  $\mathbf{v}$ ; the second term is the displacement current. On the surface  $r = r_\Sigma$ , only the displacement current is present.

We thus have to calculate  $\partial \mathbf{D}_\Sigma / \partial t$ . If the frequency  $\omega$  of the applied voltage is sufficiently small, we may invoke the adiabatic theorem,<sup>16</sup> which states that while the Hamiltonian is being changed, the system remains in a state of equilibrium at each instant. In a state of equilibrium, all properties of the system are determined by the external, macroscopic parameters. Therefore the value of  $\mathbf{D}_\Sigma$  at any time depends only on the value of the external parameters at that time, so that  $\mathbf{D}_\Sigma$  varies only by virtue of the variation of these parameters. If the pressure, temperature, composition at  $r_e$ , etc. are kept constant, there is only one parameter which varies, namely, the potential across the system.

The fact that  $\mathbf{D}_\Sigma$  varies with time only through the variation of  $U$  is expressed mathematically as

$$\frac{\partial \mathbf{D}_\Sigma}{\partial t} = \frac{\partial \mathbf{D}_\Sigma}{\partial U} \frac{dU}{dt} = \frac{\partial \mathbf{D}_\Sigma}{\partial U} U_0 i \omega e^{i \omega t}$$

Thus we have for the impedance

$$Z = \frac{U_0 e^{i \omega t}}{i \omega U_0 e^{i \omega t} (\partial \mathbf{D}_\Sigma / \partial U)} = \left( i \omega \frac{\partial \mathbf{D}_\Sigma}{\partial U} \right)^{-1} \quad (40)$$

The impedance is clearly that of a capacitance, the capacity being

$$C = \partial \mathbf{D}_\Sigma / \partial U$$

It will be remembered that this partial derivative is to be calculated by changing  $U$  in such a way that the system is always in a state of equilibrium.

Equation 40 establishes that, as  $\omega$  approaches zero, the ideally polarizable electrode behaves as a true capacity toward the perturbation of the voltage across it by an alternating potential. If there is no matter on the surface  $r = r_\Sigma$ ,  $\mathbf{D}_\Sigma = E_\Sigma$ . In any case, Gauss's theorem permits us to show that  $\mathbf{D}_\Sigma = Q$ , where  $-Qr_\Sigma^{-2}$  is the total charge of the solution.

Combining this result with that obtained previously, we have

$$C = \partial Q / \partial U = -\partial^2 \sigma / \partial U^2 \quad (41)$$

This result is familiar in electrochemistry but a general demonstration of the existence of the capacity of the ideally polarizable electrode seems not to have been presented.

### VIII. Conclusions

We have derived the Lippmann equation by a nonthermodynamic method, in terms of a specific physical model. We attempted in our model and in our derivation to simulate the actual experimental conditions for which the validity of the Lippmann equation is demonstrated (spherical electrode, solution of constant composition, etc). This does not seem to have been done previously.

Our proof is quite different from the usual thermodynamic one, and it gives an explicit physical meaning to all quantities entering the equation. This is not true when the equation is derived thermodynamically. For example, the charge per unit area of the electrode  $Q$  appears<sup>3</sup> as a combination of Gibbs surface excesses, which are invariant to the position of the Gibbs dividing surface. Clearly, this surface can play no role in separating the solution from the metal phase. One has to invoke a specific model which as-

signs charged species to one side of the interface or the other. No spatial separation between the components of the solution and metal phases is implied by the thermodynamic treatment.

Furthermore, the thermodynamic treatment can say nothing about how the charged species are actually distributed in the interfacial region or about how they interact. By introducing a model we come to grips directly with the structure of the interfacial region. Correspondingly, we are forced to consider the existence of a physical surface which divides the solution phase from the metal phase. However a natural way of introducing such a surface is given by the model itself. An ideally polarizable electrode does not allow the passage of a steady-state current between the region outside the interface and the region inside. This can be assured if  $\rho$  vanishes at some point in the circuit, *i.e.*, on a surface  $r = r_\Sigma$ . The surface on which the charge density vanishes is a natural one for dividing up the charge of the system. The charge density for  $r < r_\Sigma$  is assigned to the metal and that for  $r > r_\Sigma$  to the solution.

In addition to the surface  $r = r_\Sigma$  on which  $\rho$  vanishes, our models involve charged and polar entities (ions and molecules). It is clear that these entities may be relatively complex. We require simply that the charge density at any point be expressible in terms of densities of ions at that point and that the polarization of the medium be expressible in terms of the densities of molecules and the electric field at that point. We have furthermore introduced, for the density of each chemical species, a Boltzmann distribution with a potential energy consisting of independent electrical and chemical parts, the electrical part depending on the total electrical potential or field at a point. Actually, the assumption of a Boltzmann distribution is not necessary, since we have used only the equation for the relative change of concentration with a change in electric potential or electric field. Our assumption, strictly speaking, is that the change in concentration at a given point depends essentially on the change of the electrical condition (eq 34 and 36). The Boltzmann distribution with independent chemical and electrical parts is sufficient, but not necessary, for this purpose.

This brings us to an important point; because we are interested in calculating the change in the surface tension rather than the surface tension itself, we were able to arrive at a concrete and explicit result. A number of physical quantities, which are difficult to calculate in a reasonable way, do not enter, since they may be reasonably supposed to be unimportant to the change of surface tension. That our model is insufficient for calculation of the surface tension itself becomes evident in the following example.

Using eq 13 to eliminate  $p_i$  from eq 16 we have

$$\frac{\sigma}{3} \left( r_\sigma^{-2} + \frac{2r_i^3}{r_\sigma} \right) = \int_{r_i}^{r_e} (p_e - p_T - \frac{1}{2} \epsilon_0 E^2) r^2 dr \quad (42)$$

If we neglect (a) the contribution of the region  $r_i < r_\Sigma$ , (b) the contribution to the pressure other than the kinetic pressure, and (c) the chemical force potential  $W_i$ , we have

$$p_e - p_T = kT \sum_i n_{ie} (1 - \exp[q_i(\psi + U)/kT])$$

where  $n_{ie}$  is the concentration of species  $i$  at  $r_e$ . In the expansion of the exponential, the leading term cancels out the "1" and the next term vanishes because  $\sum_i q_i n_{ie} = \rho(r_e) = 0$ . The following term in the expansion gives a negative contribution to  $p_e - p_T$ . Since  $-\frac{1}{2} \epsilon_0 E^2$  is necessarily negative, (42) predicts  $\sigma$  to be *negative*. This is because we have

ignored the contribution of the metal phase and of the short-range repulsion in  $W_i$ . In our model, both of these are assumed independent of potential, so that they give a positive but constant contribution to  $\sigma$  as a function of potential. At the potential of zero charge the electric field and the concentration gradients vanish. At other potentials, these give a negative contribution to  $\sigma$ , as shown above. That  $\sigma$  goes through a maximum at the point of zero charge is well known.

The example above emphasizes one of the important points that emerge from calculations of the kind carried out in this article. In the computation of the change of  $\sigma$ , we observe cancellation between contributions arising from electric field terms and contributions arising from pressure terms. This is simply because the pressure depends on the concentration and the concentrations of charged and polar species are partly determined by electrical forces. This sort of compensation is necessary in a demonstration of the Lippmann equation from a molecular point of view. One can show this more explicitly by deducing the Lippmann equation from the well-known Guoy-Chapman model. A discussion of the Lippmann equation in this context has recently been given,<sup>17</sup> some previous work on the subject was early done by Herzfeld and by Frumkin.<sup>18</sup>

### Appendix

Although the volume force  $\mathbf{E}\rho$  cannot in general be shown equivalent to a surface force (it is not the gradient of a tensor), the symmetry of the present problem permits a simplification of this kind. Consider the basic infinitesimal volume element, formed by the surfaces

$$r = r_0, \quad r = r_0 + dr, \quad \theta = \theta_0, \quad \theta = \theta_0 + d\theta, \\ \phi = \phi_0, \quad \phi = \phi_0 + d\phi$$

Here  $\theta$  is the azimuthal angle and  $\phi$  the polar angle. The bounding surfaces may be taken as plane in the present discussion. The electric force on this volume is

$$\mathbf{F} = \mathbf{K} \int dV \epsilon_0 E_r r_0^{-2} d(r_0^2 E_r) / dr \quad (\text{A1})$$

where  $\mathbf{K}$  is a unit vector in the radial direction and the volume of the element is

$$dV = r_0^2 \sin \theta_0 dr d\theta d\phi$$

Poisson's equation has been used in (A1). It will be shown that  $\mathbf{F}$  may be written as an integral over the bounding surface of  $d\mathbf{S} \cdot \mathbf{p}'$  where  $\mathbf{p}'$  is a fictitious pressure tensor with components  $p_{N'}$  and  $p_{T'}$  in the radial and tangential directions and  $d\mathbf{S}$  is the normal element of surface.

It is clear that the integral of  $d\mathbf{S} \cdot \mathbf{p}'$  will be in the  $\mathbf{K}$  direction so that we need calculate only the component in this direction to show equivalence to  $\mathbf{F}$ . The integral of  $d\mathbf{S} \cdot \mathbf{p}'$  over the face defined by  $r = r_0 + dr$  is

$$-p_{N'}(r_0 + dr)(r_0 + dr)^2 \sin \theta_0 d\theta d\phi$$

and the corresponding quantity for the face  $r = r_0$  is

$$p_{N'}(r_0)(r_0)^2 \sin \theta_0 d\theta d\phi$$

Expanding  $p_{N'}(r_0 + dr)$  in a power series in  $dr$  and keeping the term first order in  $dr$ , we have a net contribution to  $\mathbf{K} \cdot \mathbf{p} \cdot d\mathbf{S}$  of

$$-(2r_0 p_{N'} + r_0^2 dp_{N'} / dr) dr d\theta d\phi \sin \theta_0$$

The total force on the faces  $\phi = \phi_0$  or  $\phi = \phi_0 + d\phi$  is  $p_{T'}(r_0)r_0 dr d\theta$ ; to obtain the component of the force in the  $\mathbf{K}$  direction, we must multiply by a direction cosine. In Fig-

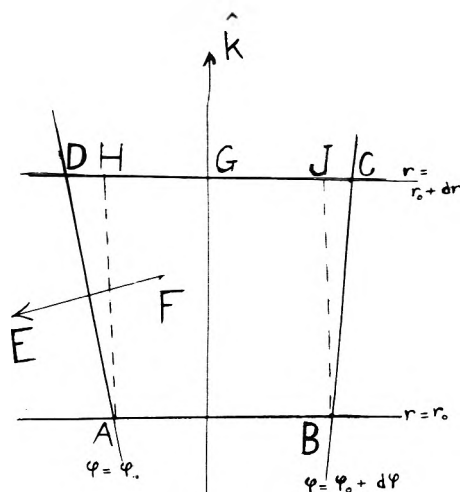


Figure 1. Face of the infinitesimal volume element corresponding to  $\theta = \text{constant}$ . The faces corresponding to  $r = \text{constant}$  and to  $\phi = \text{constant}$  are viewed end-on.  $\mathbf{EF}$  is normal to the face  $AD$  and  $\mathbf{k}$  represents the radial direction, so is normal to the faces  $CD$  and  $AB$ .

ure 1, we show the faces  $\phi = \phi_0$  and  $\phi = \phi_0 + d\phi$ , viewed in a direction perpendicular to a surface  $ABCD$  on which  $\theta$  is constant. The direction cosine is  $\cos(\angle EFG)$ ; since  $\mathbf{EF}$  is normal to  $AD$ ,  $\cos(\angle EFG) = \sin(\angle DAH)$ . Now  $\overline{AB} = r_0 \sin \theta_0 d\phi = \overline{HJ}$  and  $\overline{DC} = (r_0 + dr) \sin \theta_0 d\phi$ , so that  $\sin(\angle DAH) = (\frac{1}{2} dr \sin \theta_0 d\phi) / (\overline{AD})$ . Since  $\overline{AD} = dr$  (to the order of our calculations),  $\cos(\angle EFG) = \frac{1}{2} \sin \theta_0 d\phi$  and the net contribution of the faces considered is, in the  $\mathbf{K}$  direction

$$2(p_{T'}(r_0)r_0 dr d\theta)(\frac{1}{2} \sin \theta_0 d\phi).$$

In a similar manner, we show that the net contribution of the faces  $\theta = \theta_0$  and  $\theta = \theta_0 + d\theta$  is

$$r_0 p_{T'}(r_0) \sin \theta_0 dr d\theta d\phi$$

Thus the total force calculated in terms of  $\mathbf{p}'$  on the six faces is

$$\mathbf{F}' = \mathbf{K} \left[ 2p_{T'} r_0 \sin \theta_0 dr d\theta d\phi - \frac{d}{dr} (r_0^2 p_{N'}) \sin \theta_0 dr d\theta d\phi \right] \quad (\text{A2})$$

Setting this quantity equal to  $\mathbf{F}$  we obtain

$$\epsilon_0 E_r \frac{d}{dr} (r_0^2 E_r)_0 = 2p_{T'} r_0 - \frac{d}{dr} (r_0^2 p_{N'})_0 \quad (\text{A3})$$

as a condition on  $p_{T'}$  and  $p_{N'}$ . Equation A3 is satisfied if we take

$$p_{T'} = \frac{1}{2} \epsilon_0 E_r^2 \quad p_{N'} = -\frac{1}{2} \epsilon_0 E_r^2 \quad (\text{A4})$$

Then the volume force due to the electric field is equal to the integral of the normal component of  $\mathbf{p}'$  over the surface. Since this holds for the basic infinitesimal volume element, it holds for an arbitrary volume which may be built from the infinitesimal elements; the contribution of the volume force is additive over the elements while, for the contribution of the surface force, only that of the exterior surface remains. Stated another way, the force on an arbitrary volume may be calculated by ignoring the electric field but replacing the ordinary pressure tensor  $\mathbf{p}$  by  $\mathbf{p} + \mathbf{p}'$ .

Now we consider the volume defined by

$$r_0 < r < r_0 + dr; \quad 0 < \theta < \alpha; \quad 0 < \phi < 2\pi$$

Applying our rule and demanding that the total force vanish, we have

$$2(p_T + p_T')r_0 = d(r^2 p_N' + r^2 p_N)/dr$$

or

$$(2p_T + \epsilon_0 E_r^2)r_0 = d[r^2(p_N - \frac{1}{2}\epsilon_0 E_r^2)] \quad (\text{A5})$$

This condition for mechanical equilibrium has been derived by Sanfeld and others.<sup>14</sup>

The force  $\mathbf{F}^*$  of section III is, like the electric field, also in the radial direction at each point. It is not the gradient of a pressure-like term ( $\nabla \times \mathbf{F}^* \neq 0$ ), but its effect can also be taken into account by a fictitious pressure. Since  $\mathbf{F}^*$  is a short-range force by virtue of  $h_{kl}$ , we may suppose it to be included in  $\mathbf{p}$ .

In the presence of electric polarization, the volume force (see eq 31) may again be replaced by a surface force. In this case, the force on the basic infinitesimal volume element includes a term due to electric polarization  $P_r$ . Equation A1 is replaced by

$$\mathbf{F} = K dV \left( E_r r_0^2 \frac{d(r^2 \epsilon E_r)_0}{dr} + P_r \frac{dE_r}{dr} \right) \quad (\text{A6})$$

where  $P_r = (\epsilon - \epsilon_0)E_r$ . In this case we have, similarly to (A3)

$$E_r \frac{d}{dr} (r^2 \epsilon E_r)_0 + \frac{1}{2}(\epsilon - \epsilon_0)r_0^2 \frac{d(E_r^2)}{dr} = 2p_T' r_0 - \frac{d}{dr} (r^2 p_N')$$

This is satisfied if we take

$$p_T' = \frac{1}{2}\epsilon_0 E_r^2 \quad p_N' = \frac{1}{2}(\epsilon_0 - 2\epsilon)E_r^2 \quad (\text{A7})$$

Thus, in the case of spherical symmetry, one can use the force laws valid in the absence of electric field, provided that the tangential pressure is replaced by  $p_T + \frac{1}{2}\epsilon_0 E_r^2$  and the radial pressure is replaced by  $p_N + \frac{1}{2}(\epsilon_0 - 2\epsilon)E_r^2$ . Of course, the previous rule, in the absence of polarization, is a special case of this one.

## References and Notes

- (1) A. Frumkin, O. Petry, and B. Damaskin, *J. Electroanal. Chem.*, **27**, 81 (1970).
- (2) B. B. Damaskin, *Elektrokhimiya*, **5**, 771 (1969) [English translation: *Sov. Electrochem.*, **5**, 717 (1969)]. G. Morand and J. Hladik, "Electrochimie des Sels Fondus," Masson, Paris, 1969; J. O'M. Bockris and D. M. Dražić, "Electrochemical Science," Taylor and Francis, London, 1972.
- (3) (a) J. O'M. Bockris and A. K. N. Reddy, "Modern Electrochemistry," Plenum Press, New York, N.Y., 1970, Chapter 7; (b) A. Sanfeld, "An Introduction to the Thermodynamics of Charged and Polarized Layers," Wiley-Interscience, London, 1968, Chapter 14; (c) M. J. Spaarnay, "The Electrical Double Layer," Pergamon Press, Oxford, 1972, Chapter 2 ["International Encyclopedia of Physical Chemistry and Chemical Physics," Vol. 14-4].
- (4) W. Lorenz, *Z. Phys. Chem. (Leipzig)*, **219**, 421 (1962); **224**, 145 (1963); **232**, 176 (1966).
- (5) B. B. Damaskin, *Elektrokhimiya*, **5**, 771 (1969) [English translation: *Sov. Electrochem.*, **5**, 717 (1969)].
- (6) P. Delahay, "Double Layer and Electrode Kinetics," Wiley-Interscience, New York, N.Y., 1965, Chapter 2.
- (7) M. A. Proskurnin and A. N. Frumkin, *Trans. Faraday Soc.*, **31**, 110 (1935).
- (8) D. Schuhmann, C. Cachet, I. Epelboin, and L. Viet, *J. Chim. Phys.*, **62**, 1214 (1965); C. Cachet, I. Epelboin, J. C. Lestrade, and P. Ravel, *C. R. Acad. Sci.*, **264**, 1524 (1967); C. Cachet, I. Epelboin, J. C. Lestrade, and K. C. Narasimhan, *Bull. Soc. Chim. Fr.*, **5**, 1452 (1969); C. Cachet, Thesis, University of Paris, 1971.
- (9) (a) F. H. Stillinger and J. G. Kirkwood, *J. Chem. Phys.*, **33**, 1282 (1960); (b) J. Frenkel, "Kinetic Theory of Liquids," Dover Publications, New York, N.Y., 1946, p 361; (c) S. Levine, G. M. Bell, and D. Calvert, *Can. J. Chem.*, **40**, 518 (1962); (d) F. H. Stillinger, *J. Chem. Phys.*, **35**, 1584 (1961); (e) F. P. Buff and F. H. Stillinger, *J. Chem. Phys.*, **39**, 1911 (1963); (f) V. S. Krylov, *Electrochim. Acta*, **9**, 1247 (1964); (g) F. P. Buff, *J. Chem. Phys.*, **23**, 419 (1955).
- (10) S. Ono and S. Kondo, "Molecular Theory of Surface Tension in Liquids: Handbuch der Physik X," 1960, p 134.
- (11) (a) S. Levine, J. Mingsins, and G. M. Bell, *J. Electroanal. Chem.* **13**, 280 (1967); (b) Reference 6, Chapter 5.
- (12) Reference 6, Section 4-5.
- (13) P. Mazur, *Advan. Chem. Phys.*, **1**, 309 (1958).
- (14) A. Sanfeld, "Introduction to the Thermodynamics of Charged and Polarized Layers," Wiley-Interscience, London, 1968, Chapter 17.
- (15) Reference 9b, Chapters 6 and 7.
- (16) L. Landau and E. Lifschitz, "Physique Statistique," Mir, Moscow, 1967, Section 11.
- (17) J. Goodisman, *J. Chim. Phys.*, accepted for publication.
- (18) K. Herzfeld, *Phys. Zeit.*, **21**, 28, 61 (1920); A. Frumkin, *Acta Physicochim. URSS*, **18**, 473 (1943).

## Conductivities and Thermodynamics of Dissociation of Fluorenyl Salts and Their Complexes with Dimethyldibenzo-18-crown-6

T. E. Hogen-Esch and J. Smid\*<sup>1</sup>

Chemistry Department, State University of New York, College of Environmental Science and Forestry, Syracuse, New York 13210  
(Received July 29, 1974)

Publication costs assisted by the National Science Foundation and the Petroleum Research Fund

Dissociation constants of fluorenylsodium, difluorenylstrontium, and difluorenylbarium as well as their complexes with 4,4'-dimethyldibenzo-18-crown-6 were measured in tetrahydrofuran (THF) and tetrahydropyran (THP) over a temperature range from 25 to  $-70^{\circ}$  ( $-40^{\circ}$  for THP). Fluorenylsodium in THP and difluorenylbarium in THF are tight ion pairs over the entire temperature range, the respective  $\Delta H_d^{\circ}$  values being  $-5.0$  and  $-4.8$  kcal/mol, while  $\Delta S_d^{\circ}$  is  $-60.5$  and  $-54.4$  eu. Addition of the crown compound to fluorenylsodium results in the formation of a crown separated ion pair, identified by its optical absorption maximum of 373 nm. In both THF and THP the dissociation of this complex is essentially thermoneutral. Difluorenylstrontium in THF forms on cooling the mixed tight-loose ion pair  $\text{FlSr}||\text{Fl}$ , the enthalpy change as determined from spectrophotometric measurements being  $-12.3$  kcal/mol. The dissociation of the tight ion pair of this salt has a  $\Delta H_d^{\circ} = -14.4$  kcal/mol,  $\Delta S_d^{\circ}$  being  $-76$  eu. Crown ether converts the tight ion pair of difluorenylstrontium and -barium into the asymmetrically complexed mixed ion pair  $\text{Fl}^{-}\text{M}^{2+}\text{CrownFl}^{-}$  as shown from the optical spectrum. The dissociation of both complexes into the free ions  $\text{Fl}^{-}$  and  $\text{FlM}^{+}$ , Crown is thermoneutral. The complex with strontium changes on cooling to the fully separated ion pair  $\text{Fl}^{-}||\text{Sr}^{2+},\text{Crown},\text{Fl}^{-}$  which dissociates endothermically into  $\text{Fl}^{-}$  and  $\text{FlSr}^{+},\text{Crown}$ . The dissociation constants of the crown separated ion pair complexes are significantly smaller than those of the corresponding THF separated ion pairs, probably due to shorter interionic distances in the former species.

Previously reported conductance studies on solutions of fluorenyl carbanion salts in tetrahydrofuran (THF) and 1,2-dimethoxyethane (DME) have demonstrated the profound effect of changes in ion pair structure on the thermodynamics of dissociation of these salts.<sup>2,3</sup> The fluorenyl carbanion is well suited as a probe for studying ion pair structures as its optical spectrum is sensitive to the interionic ion pair distance. Spectrophotometric measurements, therefore, provide a simple technique for the quantitative study of ion pair equilibria such as the conversion of tight into loose ion pairs.<sup>4</sup> Changes in ion pair structure can be induced by varying the temperature, counterion, solvent, or pressure, or by addition of cation chelating agents.<sup>4-7</sup>

The ability of macrocyclic polyethers or crown ethers to form stable complexes with alkali and alkaline earth cations has stimulated considerable interest in these compounds.<sup>8</sup> Solubilization of inorganic reagents by crown ethers in nonpolar media or the addition of crown ethers to organometallics can produce a strong enhancement in the reactivity of the anion,<sup>9</sup> although a decrease in reactivity can also occur,<sup>10</sup> depending on the cation's role in the reaction mechanism. The change in reactivity and stereochemical behavior of the ionic species in the presence of crown compounds is often caused by the formation of ion pair complexes of different structures or may be the result of increased formation of reactive free ions.<sup>11</sup> For a deeper understanding of these phenomena it is essential to have data available on the thermodynamics of dissociation of ion pairs and their crown complexes in low polarity media.

In this study the conductance behavior of the 1:1 complex of 4,4'-dimethyldibenzo-18-crown-6 with difluorenylbarium and -strontium in THF and that of the same crown with fluorenylsodium in THF and THP (tetrahydropyran) is discussed. The enthalpies and entropies of dissociation of

these complexes are compared with those of the uncomplexed salts, and the differences interpreted in terms of their ion pair structure. The data reveal that the dissociation of the crown complexes is nearly thermoneutral, and that the dissociation constants of the crown separated ion pairs are often considerably lower than those of the THF separated ion pairs.

### Experimental Section

Purification of tetrahydrofuran and tetrahydropyran as well as the preparation of fluorenylsodium,<sup>3</sup> difluorenylbarium,<sup>12</sup> and difluorenylstrontium<sup>13</sup> has been described previously. The respective salts were recrystallized under vacuum from a concentrated THF solution, and the filtered crystals redissolved in pure THF or THP.

Complexes of 4,4'-dimethyldibenzo-18-crown-6<sup>14</sup> with the three salts were prepared under vacuum by adding the solid crown compound to the carbanion solution. The addition was monitored spectrophotometrically at 373 nm, the absorption maximum of the crown separated fluorenyl ion pair, and was completed when the optical spectrum did not change further.

The all-glass apparatus and the experimental procedures for measuring the conductances of the air and moisture sensitive solutions has been fully described elsewhere.<sup>2,3</sup> Conductances were measured at 1000 Hz with a 1673 General Radio Corp. automatic capacitance bridge coupled with a 1672 digital control unit. Salt concentrations were varied from  $10^{-4}$  to  $5 \times 10^{-6}$  M, the temperature at each concentration being varied in about  $10^{\circ}$  intervals from 20 to  $-70^{\circ}$  ( $-40^{\circ}$  for THP solutions). The temperature dependence of the density, viscosity, and dielectric constant of THF and THP were taken from the literature.<sup>2,15</sup> Salt concentrations were obtained spectrophotometrically by

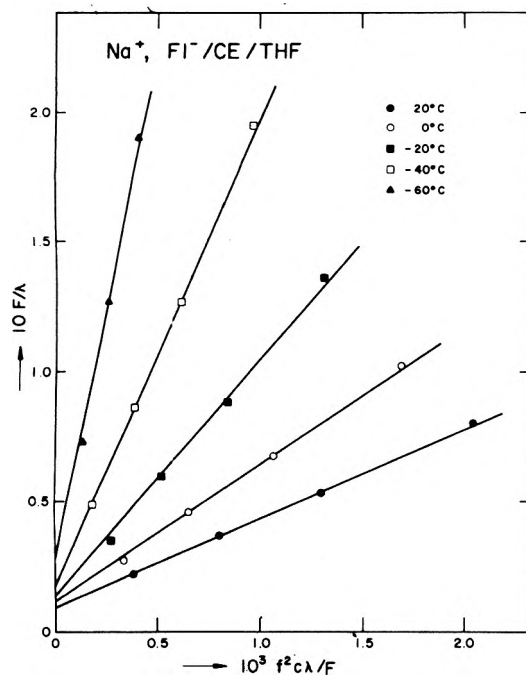


Figure 1. Fuoss conductivity plots for the dimethyldibenzo-18-crown-6 complex of fluorenylsodium in THF.

means of a Cary 14 spectrophotometer, employing cells of different pathlengths attached to the conductance apparatus. Absorption coefficients,  $\epsilon_m$ , for the fluorenyl salts were derived from spectral measurements using a titration procedure described elsewhere.<sup>16</sup> The following values for the main absorption band were found at 20°C: fluorenylsodium (THF)  $\epsilon_m$  10,800 at 356 nm; fluorenylsodium (THP)  $\epsilon_m$  12,000 at 354 nm; 1:1 complex of fluorenylsodium with dibenzo-18-crown-6 in THF and THP,  $\epsilon_m$  14,400 at 373 nm; difluorenylbarium (THF)  $\epsilon_m$  7300 at 347 nm,<sup>12</sup> and its crown complex  $\epsilon_m$  7200 at 373 nm; difluorenylstrontium  $\epsilon_m$  7500 at 343 nm (the estimated  $\epsilon_m$  value given in ref 13 was too high) and its crown complex  $\epsilon_m$  7850 at 373 nm. The  $\epsilon_m$  values given for the divalent salts are based on the fluorenyl carbanion, and the concentrations calculated from them must, therefore, be divided by two to arrive at the molar salt concentration. The 1:1 complex of difluorenylstrontium and  $N-(CH_2CH_2OCH_2CH_2OCH_2CH_2)_3-N$  (the latter compound was kindly supplied to us by Dr. Lehn) was also used in a few experiments. The  $\epsilon_m$  of this "cryptate"<sup>17</sup> at 373 nm is 14,400, based on the value of 7500 found for the uncomplexed strontium salt.

## Results

Interpolated conductance values at 20, 10, 0°, etc. from plots of conductance *vs.* temperature at five or six different salt concentrations were used to obtain the equivalent conductances as a function of concentration. The low degree of dissociation of the salts makes it impossible to estimate the respective  $\Lambda_0$  values from plots of  $\Lambda$  *vs.*  $c^{1/2}$ . These values are needed to apply the Fuoss conductance equation  $F/\Lambda = 1/\Lambda_0 + f^2 C \Lambda / K_d \Lambda_0^2$ . In a previous publication<sup>3</sup> we estimated the  $\Lambda_0$  of  $F\text{INa}$  in THF at 20° to be 95  $\text{cm}^2 \text{ohm}^{-1} \text{equiv}^{-1}$ , making use of the known  $\Lambda_0^+$  value of Na. It was also shown that  $\Lambda_0$  at other temperatures could be obtained by applying Walden's rule. The same rule is used to approximate  $\Lambda_0$  in THP,<sup>18</sup> a solvent with a considerably higher viscosity than THF. The THP solvated  $\text{Na}^+$  ion is not

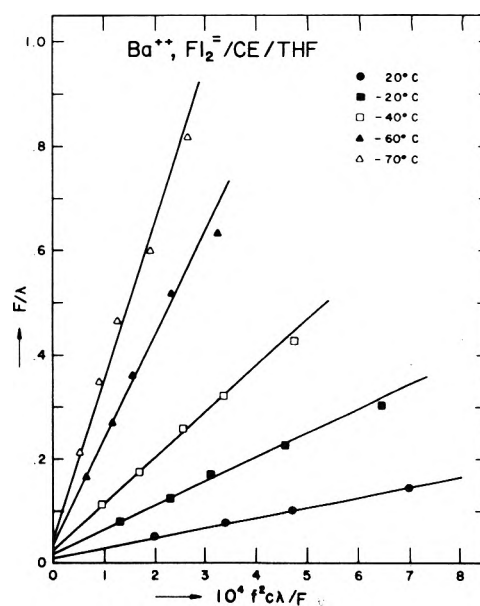


Figure 2. Fuoss conductivity plots for the dimethyldibenzo-18-crown-6 complex of difluorenylbarium in THF.

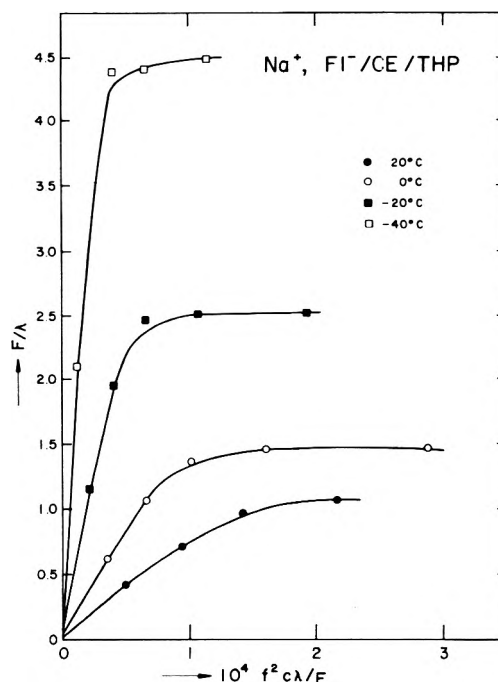


Figure 3. Fuoss conductivity plots for the dimethyldibenzo-18-crown-6 complex of fluorenylsodium in THP.

expected to be much different in size than the THF solvated ion. On the other hand, replacing the solvation shell by a crown compound significantly increases the radius of the solvated cation as observed from the lower  $\Lambda_0$  values found recently for crown-sodium salt complexes in acetonitrile<sup>19</sup> and dimethoxyethane.<sup>20</sup> We therefore determined the  $\Lambda_0$  of the crown complex of  $\text{NaBPh}_4$  in THF and found its value at 25° to be 78.7  $\text{cm}^2 \text{ohm}^{-1} \text{equiv}^{-1}$ ,  $K_d$  being  $6.23 \times 10^{-5} M$ . Since  $\Lambda_0^- = 41$ ,<sup>21</sup> one finds  $\Lambda_0^+$  for the  $\text{Na}^+$ -crown cation equal to 37.7 as compared to 45.2 for the THF solvated cation. The value of 37.7 was used as a basis for calculating the  $\Lambda_0$  values of the fluorenylsodium crown complex in

**TABLE I: Ion Pair Dissociation Constants of Fluorenylsodium and of Its Dimethyldibenzo-18-crown-6 Complex in THF and THP**

T, °C	THF				THP			
	Fl <sup>-</sup> , Na <sup>+</sup>		Fl <sup>-</sup> , Crown, Na <sup>+</sup>		Fl <sup>-</sup> , Na <sup>+</sup>		Fl <sup>-</sup> , Crown, Na <sup>+</sup>	
	$\Lambda_0$	$10^6 K_d, M$	$\Lambda_0$	$10^6 K_d, M$	$\Lambda_0$	$10^9 K_d, M$	$\Lambda_0$	$10^9 K_d, M$
20	95	0.75	88.0	3.75	55.8	0.356	51.5	38.2
10	84.2	1.3	78.0	3.83	47.4	0.476	43.7	41.4
0	75.0	2.1	69.4	3.86	39.7	0.660	36.6	41.4
-10	66.5	3.7	61.5	3.87	32.8	0.955	30.3	38.2
-20	58.0	6.6	53.7	3.83	26.8	1.38	24.8	31.3
-30	50.3	11.5	46.5	3.69	21.5	2.10	19.8	27.8
-40	42.8	20.6	39.6	3.62	16.9	3.38	15.6	25.0
-50	36.6	30.0	33.9	3.35				
-60	29.7	40.5	27.5	3.27				
-70	23.9	48.0	22.1					

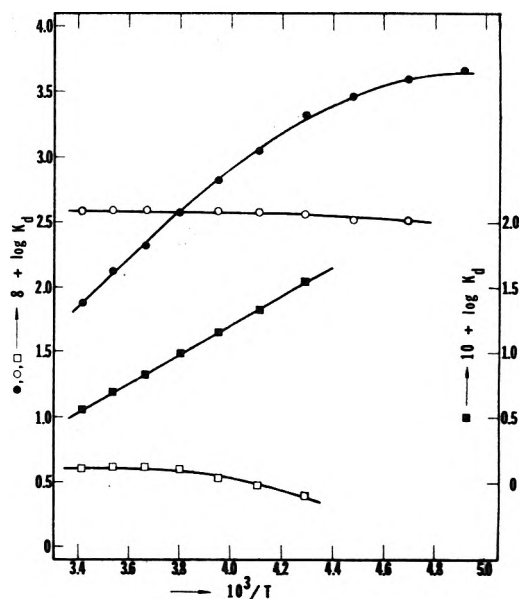
**TABLE II: Ion Pair Dissociation Constants of Difluorenylbarium and -strontium and of Their Complexes with Dimethyldibenzo-18-crown-6 in THF**

T, °C	FlSr-Crown-		FlBa-Crown-	
	SrFl <sub>2</sub> 10 <sup>7</sup> K <sub>d</sub> , M	Fl <sup>-</sup>   Sr <sup>2+</sup>    10 <sup>7</sup> K <sub>d</sub> , M	Ba- Fl <sub>2</sub> 10 <sup>8</sup> - K <sub>d</sub> , M	FlBa- Crown- Fl 10 <sup>8</sup> - K <sub>d</sub> , M
20	1.73	7.40	0.530	65.3
10	3.90	7.70	0.752	71.5
0	7.35	7.68	1.09	72.0
-10	13.3	7.68	1.55	71.0
-20	19.4	7.32	2.27	73.8
-30	23.6	7.00	3.26	74.5
-40	26.0	6.23	4.81	72.5
-50	26.4	4.85	7.14	67.0
-60	26.8	3.87	11.7	66.5
-70	25.6	2.72	22.0	67.5

<sup>a</sup> Complex of difluorenylstrontium with N-(CH<sub>2</sub>CH<sub>2</sub>OCH<sub>2</sub>CH<sub>2</sub>-OCH<sub>2</sub>CH<sub>2</sub>)<sub>3</sub>-N, the spectrum of which is identical with that of a fully separated fluorenyl ion pair.

THF and THP, again using Walden rule. The  $\Lambda_0^+$  value of the FlM<sup>+</sup> crown species and those of the FlM<sup>+</sup>(THF)<sub>n</sub> species resulting from the dissociation of the divalent salts cannot be obtained due to low degrees of dissociation. We have used the same  $\Lambda_0$  in THF for these salts as for fluorenylsodium, assuming that the replacement of part of the THF molecules by a fluorenyl moiety or of that of nearly all solvent molecules by one fluorenyl and one crown molecule will not drastically affect the size of the cation. Due to this assumption the error in  $\Lambda_0^+$  may be as high as 20% or that in  $\Lambda$  as high as 10%, but the error in the relative  $K_d$  values (*i.e.*, as a function of temperature) is little affected by this assumption.

Some of the Fuoss plots are depicted in Figures 1-3, and for the sake of clarity only five of the ten temperatures are shown on each plot. Good straight lines are found in all cases except for the fluorenylsodium-crown complex in THP (see Figure 3). It is known that crown complexes of fluorenylsodium have a strong tendency to aggregate, especially the crown separated ion pairs.<sup>22</sup> This aggregation depends on the dielectric constant and polarity of the solvent

**Figure 4.** Temperature dependence of the dissociation constant of fluorenylsodium and of its crown complex in THF and THP: (●) FlNa-THF; (○) FlNa-Crown-THF; (■) FlNa-THP; (□) FlNa-Crown-THP.

and was found to be more pronounced in THP than in THF. Although ion pair aggregation to quadrupoles would decrease the observed  $\Lambda$  values at higher salt concentrations, the planarity of the fluorenyl anion and that of the crown separated ion pair would also favor triple ion formation, and this in turn results in an enhanced conductance as found experimentally. However, the behavior is probably more complex as the drop in  $1/\Lambda$  at higher salt concentration is more abrupt than expected from triple ion formation only. No triple ions were found for fluorenylsodium itself over the investigated concentration range, but the potassium and cesium salts in THP yield a significant fraction of triple ions.<sup>23</sup>

The dissociation constants computed from the slopes of the Fuoss plots as well as the  $\Lambda_0$  values used in the calculations are compiled in Table I for the sodium salts in THF and THP, and in Table II for the divalent salts. Because of the approximations used in estimating the  $\Lambda_0$  values the uncertainties in the  $K_d$  values in some cases may be as high as 25%. Table II also includes  $K_d$  values for the difluo-

**TABLE III: Enthalpies and Entropies of Dissociation of Fluorenyl Salts and Their Complexes with Dimethyldibenzo-18-crown-6**

Cation	Solvent	$\Delta H_d^\circ$ , kcal/mol		$\Delta S_d^\circ$ , eu	
		20°	-70°	20°	-70°
Na	THF	-8.3	-1.4	-56	-27
Na-Crown	THF	0	0	-25.0	-25.0
Na	THP	-5.0	-5.0 (-40°)	-60.5	-60.8 (-40°)
Na-Crown	THP	0	+1.7 (-40°)	-35	-27.5 (-40°)
Sr	THF	-13.3	0	-76	-25
Sr-Crown	THF	0	+2.6	-28	-17
Sr-Cryptate	THF	-0.7	0	-31	-28
Ba	THF	0	0	-54.4	-54.4
Ba-Crown	THF	0	0	-28.5	-28.5

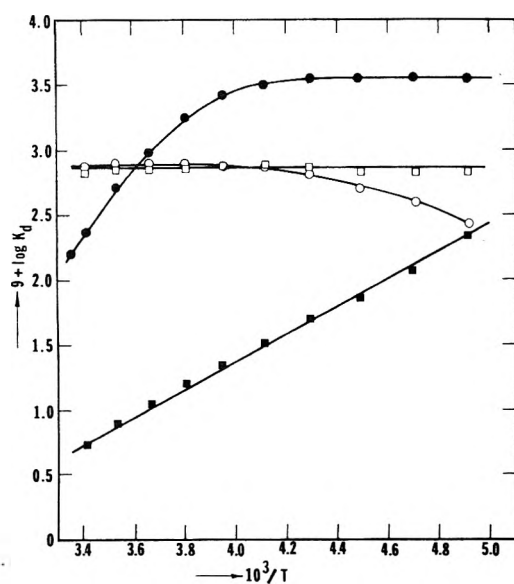


**Figure 5.** Temperature dependence of the dissociation constants of difluorenylstrontium and -barium and their crown complexes in THF: (●) SrFl<sub>2</sub>-THF; (○) SrFl<sub>2</sub>-Crown-THF; (■) BaFl<sub>2</sub>-THF; (□) BaFl<sub>2</sub>-Crown-THF.

renylstrontium cryptate complex, but the measurements were carried out at one concentration only ( $3 \times 10^{-5} M$ ).

Plots of  $\log K_d$  vs.  $1/T$ , including that of fluorenylsodium in THF which was published earlier,<sup>2,3</sup> are depicted in Figures 4 and 5. The enthalpies,  $\Delta H_d^\circ$ , were calculated from the tangent of the plots at 20 and at -70° (-40° for THP), while  $\Delta S_d^\circ$  was obtained from the relationship  $\Delta S_d^\circ = \Delta H_d^\circ/T + R \ln K_d$ . The data are collected in Table III.

## Discussion

*Fluorenylsodium and Its Crown Complex in THF and THP.* The conductance behavior of fluorenylsodium in THF has previously been discussed in detail.<sup>2,3</sup> At room temperature the salt exists predominantly as a tight ion pair, but changes into a solvent separated ion pair at lower temperatures:



The temperature dependence of the apparent dissociation constant,  $K_d$ , is described by the relationship  $\Delta H_d^\circ =$

$\Delta H_s^\circ + \Delta H_i^\circ(1 + K_i)$ , where  $K_i$  and  $\Delta H_i^\circ$  refer to the equilibrium constant and change in enthalpy, respectively, of the ion pair equilibrium, while  $\Delta H_s^\circ$  denotes the enthalpy change on dissociation of the separated ion pair.<sup>2</sup> Spectral measurements yield a  $\Delta H_i^\circ$  of -7.6 kcal/mol over the entire temperature range, while  $\Delta H_d^\circ$  changes from -8.3 kcal/mol at 20° to -1.4 kcal/mol at -70°.<sup>2,3</sup>

In tetrahydropyran the absorption maximum of the main spectral band of fluorenylsodium at 20° is at 354 nm. No evidence of any loose ion pair formation is found down to -40°, and as a result a nearly perfect van't Hoff relationship (see Figure 4) is found with a very low entropy of dissociation. The  $\Delta S_d^\circ$  of -60.5 eu in THP (Table III) is nearly identical with that found for the contact ion pair in THF ( $\Delta S_c^\circ = -60$  eu, see ref 2; the value -55 eu for  $\Delta S_d^\circ$  in Table III is that of Fl<sup>-</sup>Na<sup>+</sup> in THF at 20°, which contains about 5% loose ion pairs). Apparently the number of solvent molecules immobilized in the dissociation process is similar in the two solvents. The interaction between cation and solvent is expected to be weaker in THP as reflected in the enthalpy change of only -5.0 kcal/mol as compared to -9.5 kcal/mol for the tight ion pair in THF.<sup>2</sup> The ion pair in THP is also tighter than in THF, judging from the 2 nm lower  $\lambda_m$  value of the fluorenyl absorption band. Nearly identical values for the thermodynamic parameters in THP were found by Boileau and Sigwalt,  $\Delta H_d^\circ = -5.3$  kcal/mol and  $\Delta S_d^\circ = -62$  eu.<sup>23</sup>

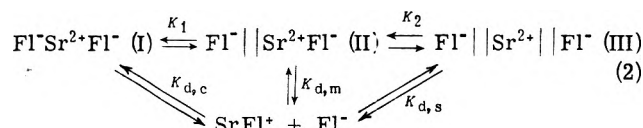
Dimethyldibenzo-18-crown-6 converts the tight fluorenylsodium ion pair to a separated ion pair crown complex, the absorption maximum in both solvents being 373 nm. The complex formation constant is high, and the crown remains bound to the sodium ion even at the low concentrations used in our conductance experiments.<sup>24</sup>

We have demonstrated<sup>2,3</sup> that the sphere in continuum model provides a reasonable approximation of the dissociation of solvated loose ion pairs of fluorenyl salts. For such a model  $K_d$  is proportional to  $\exp(-e^2/aDkT)$ .<sup>25</sup> Assuming the same interionic distance  $a$  in THF and THP, one can calculate the  $K_d$  for the ion pair complex in THP from its value in THF and the respective dielectric constants of the two solvents, since  $\log K_d(\text{THP}) = \log K_d(\text{THF})D(\text{THF})/D(\text{THP})$ . This yields  $K_d(\text{THP}) = 2.3 \times 10^{-8} M$  at -40°, very close to the experimental value (Table I). However, the calculated  $K_d$  at 20° is  $5 \times 10^{-8} M$ , considerably higher than the experimental value ( $3.56 \times 10^{-8} M$ ). This indicates a shorter interionic ion pair distance in THP at 20° than in THF. It is known<sup>11</sup> that a crown separated ion pair can convert to a crown complexed tight ion pair when present in a solvent of lower polarity. For example, the reaction  $Fl^-, Na^+, 15C5 \rightleftharpoons Fl^-, 15C5, Na^+$  (15C5 refers to monobenzo-15-crown-5) which is exothermic has an equilibrium constant of 1.8 in THF but only 0.5 in THP.<sup>11</sup> While the dimethyldibenzo-18-crown-6 complex with fluorenylsodium in THP has its absorption maximum at 373 nm, this  $\lambda_m$  is not very sensitive to the ion pair distance above 4 Å. A closer approach of Na<sup>+</sup> to Fl<sup>-</sup> is, therefore, not excluded, and becomes more likely at elevated temperatures. Note also the lower  $K_d$  values of the crown complex in THF at lower temperatures relative to that of the THF separated ion pair (almost a factor 15 at -60°). This again may be due in part to a smaller interionic distance in the complex which is facilitated by the planar structure of both the fluorenyl anion and the crown-cation complex.

Over most of the temperature range the dissociation of

the complex is thermoneutral in both solvents. The Denison-Ramsey equation  $\Delta H_d^\circ = (Ne^2/aD)(1 + d \ln D/d \ln T)$  which was found to be applicable for separated ion pairs<sup>2,3</sup> predicts thermoneutrality when  $d \ln D/d \ln T = -1$ . The value found in THF is  $-1.16$  and in THP  $-0.97$ ,<sup>15</sup> resulting in a  $\Delta H_d^\circ$  value close to zero when  $a$  is  $\approx 5-7$  Å. Note also that the decrease in the  $K_d$  of the complex by a factor  $10^2$  when THF is replaced by THP is entirely due to the lower entropy in THP.

*Difluorenylstrontium and -barium and Their Respective Crown Complexes.* The change in the solvation state of the difluorenylstrontium ion pair was shown to follow a stepwise process involving the formation of a mixed tight-loose ion pair.<sup>13</sup> The dissociation can be represented by the following equilibria:



where the subscripts *c*, *m*, and *s* in the  $K_d$ 's refer to the contact (I), mixed (II), and completely solvent separated (III) ion pair, respectively. The tight ion pair I is the predominant species ( $\lambda_m$  343 nm) at room temperature, but it rapidly converts into II at lower temperatures,  $\Delta H_1$  being  $-12.3$  kcal/mol.<sup>13</sup> Above  $-50^\circ$ , where  $K_2 < 0.1$ <sup>13</sup> the apparent dissociation constant  $K_d$  can be approximated by

$$K_d = K_1 K_{d,m} (1 + K_1) \quad (3)$$

and the apparent enthalpy of dissociation  $\Delta H_d^\circ$  by

$$\Delta H_d^\circ = \Delta H_{d,m}^\circ + \Delta H_1^\circ / (1 + K_1) \quad (4)$$

The enthalpy of dissociation  $\Delta H_{d,c}^\circ$  of species I is equal to  $\Delta H_1^\circ + \Delta H_{d,m}^\circ$ . The quantity  $\Delta H_{d,m}^\circ$  is found by first calculating  $K_1$  from  $\Delta H_1^\circ = -12.3$  kcal/mol and  $\Delta S_1^\circ = -47$  eu,<sup>13</sup> yielding  $K_1 = 0.095$  at  $20^\circ$  and  $K_1 = 88$  at  $-50^\circ$ . Substituting these values in (4) one obtains  $\Delta H_{d,m}^\circ = -2.1$  kcal/mol at  $20^\circ$  and  $\Delta H_{d,m}^\circ = 0$  kcal/mol at  $-50^\circ$ . Hence at  $20^\circ$   $\Delta H_{d,c}^\circ = -14.4$  kcal/mol, which is nearly 5 kcal/mol more exothermic than the dissociation of a fluorenylsodium tight ion pair. This difference can be entirely attributed to the high exothermicity of formation of the mixed ion pair II from I, since the value  $-2.1$  kcal/mol for  $\Delta H_{d,m}^\circ$  is about what one would expect for a solvated ion pair in which the solvation shell around the cation does not significantly change on dissociation. Although the coulomb interaction between  $\text{SrFl}^+$  and  $\text{Fl}^-$  is considerably stronger than between  $\text{Fl}^-$  and  $\text{Na}^+$  (as is also reflected in the  $\lambda_m$  of 343 nm), the high field strength of  $\text{Sr}^{2+}$  provides a strong binding force for THF molecules. Also, more solvent molecules are immobilized on formation of II than on separation of a fluorenylsodium ion pair. In the sandwich type  $\text{Fl}^-\text{Sr}^{2+}\text{Fl}^-$  structure the cation is not very accessible to THF, while the fluorenylsodium contact ion pair is already externally solvated by a few THF molecules. The values found for the entropy changes appear to confirm this, with  $\Delta S_1^\circ$  being  $-47$  eu for the strontium salt<sup>13</sup> and  $-33$  eu for the sodium salt.<sup>2</sup>

Reasonably accurate thermodynamic data can be obtained by determining the conductance as a function of temperature at one concentration only. It was shown<sup>3</sup> that at a salt concentration  $\gg K_d$  one may write

$$R d \ln \Lambda / d(1/T) = -E_{vis} - \frac{1}{2} \Delta H_d^\circ \quad (5)$$

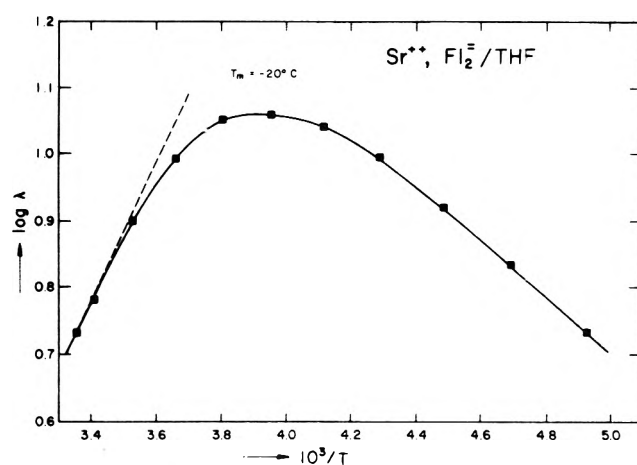


Figure 6. Plot of  $\log \Lambda$  vs.  $1/T$  for difluorenylstrontium in THF. Concentration of  $\text{SrFl}_2 = 1.6 \times 10^{-4}$  M.

where  $E_{vis}$  denotes the activation energy of viscous flow which is  $-2$  kcal/mol for THF. A plot of  $\log \Lambda$  vs.  $1/T$  is depicted in Figure 6 and shows a maximum at  $-20^\circ$  where  $\Delta H_d^\circ = -2E_{vis} = -4$  kcal/mol. From the tangent of this plot one finds  $\Delta H_d^\circ = -13.7$  kcal/mol at  $20^\circ$  and  $\Delta H_d^\circ = -0.1$  kcal/mol at  $-50^\circ$ , both values being very close to those derived from the actual  $K_d$  values.

Below  $-50^\circ$  the completely separated ion pair III is present in significant amounts, but  $\Delta H_2^\circ$  is only  $-2.8$  kcal/mol, and  $\Delta S_2^\circ = -17$  eu.<sup>13</sup> Separation of the second anion requires, of course, a considerable amount of energy, and judging from the differences in  $\Delta S_1^\circ$  and  $\Delta S_2^\circ$ , the number of additional THF molecules bound to the  $\text{Sr}^{2+}$  appears to be less than in the conversion of I to II.

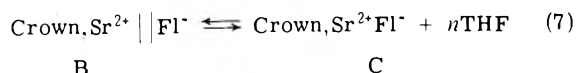
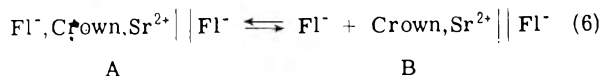
Dibenzo-18-crown-6 and  $\text{SrFl}_2$  form a 1:1 complex with absorption maxima at 348 and 373 nm, clearly a mixed ion pair of the type  $\text{Fl}^-\text{Sr}^{2+}\text{Crown}\text{Fl}^-$ . Although the  $\text{Sr}^{2+}$  should fit neatly in to the cavity of this crown ether (ratio of the respective diameters is about 0.8), the asymmetrically complexed ion pair is electrostatically more stable. The complex formation constant in THF is very high and could not be determined spectrophotometrically.

The dissociation of this complex into free ions is thermoneutral in the temperature range from  $-30$  to  $20^\circ$  (Table III), similar as found for the crown complexes of fluorenylsodium. Note again that the  $K_d$  of the crown complexed mixed ion pair is much smaller than that of the THF separated mixed ion pair II. In fact, the dissociation constant is not much higher than that found for a  $\text{SrFl}_2$  solution containing predominantly tight ion pairs (*i.e.*, between  $20$  and  $-10^\circ$ ). The explanation may be similar as suggested for the crown complex of the sodium salt, *viz.*, a shorter interionic distance as compared to the THF separated pair. Also, the dissociation of the mixed ion pair yields the  $\text{FlSr}^+\text{Crown}$  complex in which the  $\text{Sr}^{2+}$  is sandwiched in between the fluorenyl carbanion and the crown compound (species C of eq 7). This species is not expected to pick up any additional solvent molecules, in contrast to the sodium salt which dissociates into a crown complexed free alkali ion that can be solvated by THF molecules perpendicular to the crown ring.

The dissociation of the difluorenylstrontium-crown complex appears to be endothermic at low temperature, and the entropy change is also considerably less negative than found in other systems (Table III). The reason for this becomes clear when the spectrum of the complex is measured

as a function of temperature. In THF, the spectrum does not change except for the usual dependence of the "pure" ion pair spectra on temperature which were found from spectra of  $\text{SrFl}_2$  in THF and  $\text{Fl}^-, \text{Crown}, \text{Na}^+$  in THF. However, in THF the species  $\text{Fl}^-, \text{Sr}^{2+}, \text{Crown}, \text{Fl}^-$  rapidly changes to a completely separated ion pair  $\text{Fl}^- \parallel \text{Sr}^{2+}, \text{Crown}, \text{Fl}^-$ , the  $\Delta H$  of this process being  $-5.7$  kcal/mol and  $\Delta S = -25$  eu. The same transition for the THF mixed ion pair II into III (see eq 2) is much more difficult ( $\Delta H_2^\circ = -2.8$  kcal/mol,  $\Delta S_2^\circ = -17$  eu) with  $K_2$  being only 0.17 at  $-70^\circ$ , as compared to  $K_2 = 4.3$  for the crown complex. This is not surprising if we remember that the conductance data suggested a shorter interionic distance between  $\text{Fl}^-$  and  $\text{Sr}^{2+}$  when separated by the crown ether. Greater coulomb repulsion between the two anions in the crown complex means that the second  $\text{Fl}^-$  anion will separate more easily from the  $(\text{Fl crown Sr})^+$  cation than is the case in the THF mixed ion pair II.

Our spectroscopic data indicate, therefore, that at  $-70^\circ$  we measure the dissociation of the fully separated crown complex. This can be represented by



where the notation  $\parallel$  denotes  $n$  or more THF molecules. Strong electrostatic interaction between  $\text{Sr}^{2+}$  and  $\text{Fl}^-$  makes it likely that the externally complexed  $\text{SrFl}^+$  cation denoted by C is more stable than species B. The first equilibrium is that of the dissociation of a solvent separated ion pair without a significant change in the solvation shell of the cation, and it closely resembles that of the dissociation of the cryptate complex (Table III), with  $\Delta H_d^\circ = 0$  kcal/mol and  $\Delta S_d^\circ = -28$  eu at  $-70^\circ$ . Since the overall  $\Delta H_d$  for the crown complex at  $-70^\circ$  is  $+2.6$  kcal/mol and  $\Delta S_d^\circ = -17$  eu (Table III), one finds for the conversion of B  $\rightarrow$  C an enthalpy change of  $+2.6$  kcal/mol and  $\Delta S = +11$  eu. The reaction should indeed be endothermic and exotropic since THF molecules are released, and it is interesting to note that nearly identical values are found for the conversion of a crown separated fluorenyl potassium ion pair into a crown complexed tight ion pair.<sup>11</sup>

Difluorenylbarium is a tight ion pair over nearly the entire temperature range. The weaker interaction between the  $\text{BaFl}^+$  cation and THF is the reason for the nearly two orders of magnitude lower  $K_d$  values of the barium salt as compared to the strontium compound, in spite of the higher coulomb interaction in the tight ion pair of the latter

salt. As a result, both the  $\Delta H_d^\circ$  and  $\Delta S_d^\circ$  are considerably less negative for difluorenylbarium.

Addition of crown ether forms the 1:1 asymmetrically coordinated crown complex<sup>12,26</sup> which, contrary to the strontium complex, does not convert into a fully separated ion pair on lowering the temperature. The thermodynamic parameters are consistent with those found for the other crown complexes.

*Acknowledgment.* The authors gratefully acknowledge the financial support of the National Science Foundation (PO-37799) and of the Donors of the Petroleum Research Fund administered by the American Chemical Society. They also wish to thank Dr. K. H. Wong, W. Ellenberg, and F. Davidowsky for their assistance in some of the spectral and conductance measurements.

## References and Notes

- (1) Author to whom correspondence should be addressed.
- (2) T. E. Hogen Esch and J. Smid, *J. Amer. Chem. Soc.*, **88**, 318 (1966).
- (3) T. Ellingsen and J. Smid, *J. Phys. Chem.*, **73**, 2712 (1969).
- (4) J. Smid, *Angew. Chem., Int. Ed. Engl.*, **11**, 112 (1972).
- (5) T. E. Hogen Esch and J. Smid, *J. Amer. Chem. Soc.*, **88**, 307 (1966).
- (6) L. L. Chan and J. Smid, *J. Amer. Chem. Soc.*, **90**, 4654 (1968).
- (7) (a) S. Claesson, B. Lundgren, and M. Szwarc, *Trans. Faraday Soc.*, **66**, 3053 (1970); (b) W. J. LeNoble and A. R. Das, *J. Phys. Chem.*, **74**, 3429 (1970).
- (8) For a general discussion of these compounds, see (a) C. J. Pedersen and H. K. Frensdorff, *Angew. Chem., Int. Ed. Engl.*, **11**, 16 (1972); (b) J. Christensen, J. O. Hill, and R. M. Izatt, *Science*, **174**, 459 (1971); (c) D. J. Cram and J. M. Cram, *ibid.*, **183**, 803 (1974).
- (9) (a) R. D. Guthrie, D. A. Jaeger, W. Meister, and D. J. Cram, *J. Amer. Chem. Soc.*, **93**, 5137 (1971); (b) L. M. Thomassen, T. Ellingsen, and J. Ugelstad, *Acta Chem. Scand.*, **25**, 3024 (1971); (c) D. J. Sam and H. E. Simmons, *J. Amer. Chem. Soc.*, **94**, 4024 (1972); (d) C. L. Liotta and H. P. Harris, *ibid.*, **96**, 2230 (1974).
- (10) (a) J. P. Collman, J. N. Cawse, and J. I. Brauman, *J. Amer. Chem. Soc.*, **94**, 5906 (1972); (b) C. J. Chang, R. F. Kiesel, and T. E. Hogen Esch, *ibid.*, **95**, 8446 (1973); (c) E. R. Minnich, L. D. Long, J. M. Ceraso, and J. L. Dye, *ibid.*, **95**, 1061 (1973).
- (11) U. Takaki, T. E. Hogen-Esch, and J. Smid, *J. Amer. Chem. Soc.*, **93**, 6760 (1971).
- (12) U. Takaki and J. Smid, *J. Amer. Chem. Soc.*, **96**, 2588 (1974).
- (13) T. E. Hogen-Esch and J. Smid, *J. Amer. Chem. Soc.*, **94**, 9240 (1972).
- (14) C. J. Pedersen, *J. Amer. Chem. Soc.*, **89**, 7017 (1967).
- (15) D. Nicholls, C. Sutphen, and M. Szwarc, *J. Phys. Chem.*, **72**, 1021 (1968).
- (16) L. Ambroz, K. H. Wong, and J. Smid, *Anal. Chem.*, **44**, 872 (1972).
- (17) J. M. Lehn, *Structure Bonding*, **16**, 1 (1973).
- (18) M. Shinohara, Ph.D. Thesis, State University of New York, College of Environmental Science and Forestry, Syracuse, N.Y., 1969.
- (19) D. F. Evans, S. L. Wellington, J. A. Nadis, and E. L. Cussler, *J. Solution Chem.*, **1**, 602 (1972).
- (20) E. Shchori and J. Jagur-Grodzinski, *Isr. J. Chem.*, **11**, 243 (1973).
- (21) C. Carvajal, K. J. Toelle, J. Smid, and M. Szwarc, *J. Amer. Chem. Soc.*, **87**, 5548 (1965).
- (22) U. Takaki and J. Smid, *J. Phys. Chem.*, **76**, 2152 (1972).
- (23) S. Boileau and P. Sigwalt, *Electrochim. Acta*, in press.
- (24) K. H. Wong, T. E. Hogen Esch, and J. Smid, *J. Amer. Chem. Soc.*, **92**, 666 (1970).
- (25) F. Accascina and R. M. Fuoss, "Electrolytic Conductance," Wiley, New York, N.Y., 1959.
- (26) T. E. Hogen Esch and J. Smid, *J. Amer. Chem. Soc.*, **91**, 4580 (1969).

## Thermodynamics of Aggregation of Long Chain Carboxylic Acids in Benzene

O. Levy,\* G. Y. Markovits, and I. Perry

Department of Chemistry, University of the Negev, Beer-Sheva and Practical Engineering College, Beer-Sheva, Israel (Received June 21, 1974)

Publication costs assisted by the Practical Engineering College

Vapor pressure osmometric measurements on benzene solutions of  $\gamma$ -hexanoic,  $n$ -nonanoic, and  $n$ -dodecanoic acids were performed at 31°. The osmometric data in the concentration range  $0.5\text{--}9.0 \times 10^{-2} M$  were interpreted in terms of dimer and trimer equilibria and oligomerization constants were calculated. The aggregation tendency increases with increasing chain length and the same trend was observed in the calculated activity coefficients. Enthalpies of aggregation, estimated from the heats of dilution and the distribution of the oligomers, were found to be  $-7.6$  to  $-9.2$  kJ per mole monomer units for the dimer and from  $-9.2$  to  $-10.9$  kJ per mole of monomer units for the trimer, for the three acids studied. The heats of dilution for concentrations up to  $0.04 M$  were the same for the three acids studied and the differences in the free energy were attributed to an entropy contribution. The activity of the solute, calculated from osmometric measurements, was combined with the integral heat of dilution data to calculate the entropy change for the aggregation process.

The aggregation behavior of long-chain carboxylic acids in organic solvents has been studied extensively by several methods. These include ebullioscopy and cryoscopy,<sup>1,2</sup> dielectric measurements,<sup>3,4</sup> ir spectroscopy,<sup>5,6</sup> and distribution measurements.<sup>7</sup> However, the results obtained from these techniques differ and various factors have been invoked to explain the discrepancies. For example, the presence of water in the organic phase has been used to explain the discrepancies in results obtained from distribution studies from other techniques.<sup>7</sup>

The self aggregation of the carboxylic acids is usually studied by means of colligative, nmr, and spectroscopic methods and the free energy change of the aggregation process is obtained. Enthalpy changes for the process are consequently deduced from the temperature dependence of equilibrium constants by means of van't Hoff plots. However, this method has been criticized and two major limitations can be pointed out: (I) the assumption that  $\Delta H$  is independent of temperature severely limits the temperature range, and (II) experimental uncertainty in the equilibrium constants as a function of temperature leads to large uncertainties in the derived enthalpy values. For example, a reasonable value for the enthalpy change is ca. 17 kJ/mol, which leads to an expected 20% change in the value of the equilibrium constant for a 10° change. However, the experimental error in the equilibrium constant often reaches 10%. Furthermore it has been pointed out<sup>8</sup> that the entropy titration method is not applicable for systems yielding stepwise complex (or aggregate) formation if the differences between the stability constants is under a certain limit ( $\sim 10^4$ ).

From the above discussion it is obvious that a rigorous study of the thermodynamic parameters involved in molecular association processes requires the combination of free-energy data (colligative measurements) with enthalpy data (calorimetric measurements).

In the present work we chose to study three carboxylic acids ( $n$ -hexanoic (HC6),  $n$ -nonanoic (HC9), and  $n$ -dode-

canoic (HC12)) in benzene in order to evaluate the thermodynamic parameters for the aggregation process, by combining osmometric (vapor pressure lowering) with calorimetric measurements.

### Experimental Section

Osmometric measurements were performed using a Hewlett-Packard vapor pressure osmometer Model 302 B by a technique described elsewhere.<sup>9</sup> Calorimetric heats of dilution were measured with a LKB titration calorimetric system Model 8700. A 100-ml glass vessel equipped with thermistors and heater and containing 75 ml of pure benzene was allowed to reach thermal equilibrium in a thermostat ( $\pm 0.001^\circ$ ). Different volumes ranging between 0.5 and 3.0 ml of titrant,  $0.2 M$  acid in benzene, were added from a calibrated buret ( $\pm 0.1\%$ ) (Metrom 274E) and the heat effect was measured. After each addition of the titrant, electrical energy calibrations were performed. Since the process of mixing is endothermic, the calibration runs following the addition are adjusted so as to heat up the system to the initial temperature. In this way the measurements are performed in the same temperature range, close to the temperature of the thermostat, as checked by means of calibrated thermistors and a Hewlett-Packard quartz thermometer Model 2801A. This procedure ensures that no temperature differences exist between the vessel and the added solution. For each system triplicate runs were made, the reproducibility being better than  $\pm 1\%$ . The same accuracy was obtained for the calibration runs.

The acids used were BDH products, while the benzene was a Mallinckrodt product. All solutions were prepared by weight.

### Results and Discussion

**Osmometric Data.** The results of the osmometric measurements for the three acids in benzene are given in Table I, where  $B$  is the analytical salt concentration and  $S$  the measured osmometric concentration. From these data the mean aggregation number,  $\bar{n} = B/S$ , can be calculated.

Assuming that the dissociation of the acids in the nonpo-

\* Address correspondence to this author at the Practical Engineering College, Beer-Sheva, P.O. Box 45, Beer-Sheva, Israel.

**TABLE I: Osmometric Data for the Three Acids in Benzene at 31°**

<i>n</i> -Hexanoic acid		<i>n</i> -Nonanoic acid		<i>n</i> -Dodecanoic acid	
<i>B</i> , <i>M</i> × 10 <sup>2</sup>	<i>S</i> , <i>M</i> × 10 <sup>2</sup>	<i>B</i> , <i>M</i> × 10 <sup>2</sup>	<i>S</i> , <i>M</i> × 10 <sup>2</sup>	<i>B</i> , <i>M</i> × 10 <sup>2</sup>	<i>S</i> , <i>M</i> × 10 <sup>2</sup>
0.46	0.38	0.40	0.32	0.50	0.38
0.69	0.54	0.72	0.54	0.87	0.62
0.97	0.72	0.95	0.70	1.36	0.92
1.38	0.98	1.12	0.81	1.64	1.08
1.90	1.28	1.89	1.27	2.50	1.57
3.20	2.00	2.19	1.43	4.30	2.54
4.67	2.77	2.57	1.65	5.20	3.00
6.33	3.65	3.66	2.25	6.08	3.45
7.60	4.25	5.20	3.00	7.17	4.00
8.70	4.82	6.70	3.80	9.00	4.89
		7.50	4.17		
		8.75	4.78		

**TABLE II: Dimerization and Trimerization Constants of Carboxylic Acids in Benzene at 31°**

Acid	Log β <sub>2</sub>	Log β <sub>3</sub>
<i>n</i> -Hexanoic	1.90 ± 0.03	3.29 ± 0.08
<i>n</i> -Nonanoic	1.96 ± 0.02	3.30 ± 0.03
<i>n</i> -Dodecanoic	2.15 ± 0.04	3.33 ± 0.11

lar and low dielectric constant benzene is negligible, and that the extent of nonspecific nonidealities due to solute-solvent interactions is equally insignificant, the deviation from an ideal behavior ( $\bar{n} = 1$ ) is then due to specific solute-solute interactions leading to the formation of aggregates. Thus, the total concentration of the solute, *B*, is given by

$$B = b + nb^n\beta_n + pb^p\beta_p + \dots \quad (1)$$

where *b* is the concentration of the monomeric species in mole/liter and  $n < p < \dots$  are the number of monomers in the *n* and *p* aggregates formed, and β's are the overall stability constants of these aggregates, defined as  $\beta_n = [b]^n/[b_n]$  and  $\beta_p = [b]^p/[b_p]$ . The concentration of the solute, as determined osmotically, *S*, is given by

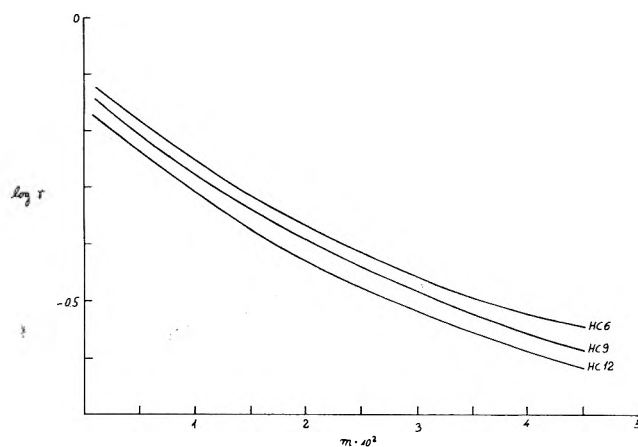
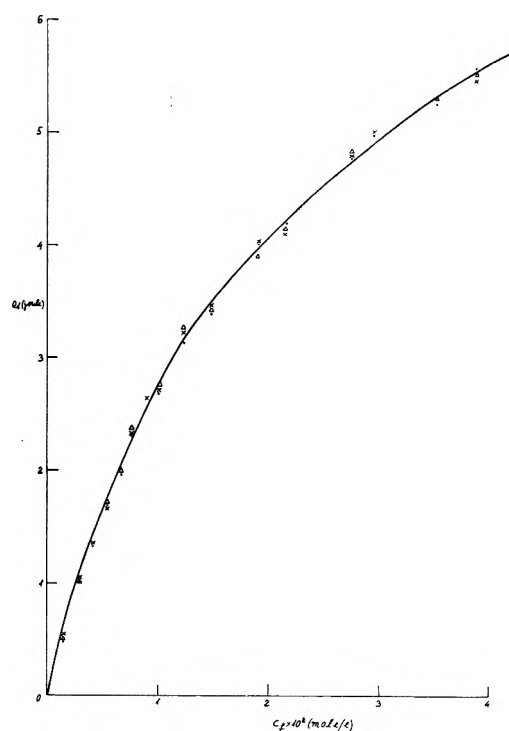
$$S = b + b^n\beta_n + b^p\beta_p + \dots \quad (2)$$

Following the calculation model described elsewhere<sup>9</sup> and using a least-squares computer program, the best fit of experimental data is obtained for an oligomerization model describing the process of aggregation in terms of a monomer-dimer-trimer equilibrium ( $n = 2, p = 3$ ). The calculated overall aggregation constants are compiled in Table II.

Using these formation constants, the fraction of monomer in the form of a particular aggregate as a function of the total concentration of the solute can be calculated<sup>10</sup> from the relationship

$$\alpha_n = n\beta_n[B]^n / \sum_1^n n\beta_n[B]^n \quad (3)$$

Figure 1 shows a typical plot of the oligomer distribution as a function of total solute concentration for *n*-nonanoic acid in benzene at 31°.


**Figure 1.** Activity coefficients of the acids in benzene as function of concentration at 31°.

**Figure 2.** Heat of dilution of the acids in benzene as function of final concentration at 31°: (●) HC6, (Δ) HC9, (X) HC12.

An alternative approach is to interpret the deviation from ideality through the calculation of activity coefficients of the solutes using the Gibbs-Duhem relationship.<sup>11</sup> Figure 2 shows the plot of the activity coefficients, log γ, as a function of the solute concentration. Table III presents the polynomial expansion of log γ as a function of solute molality. Though the possibility of higher aggregation has not been excluded in the past,<sup>12</sup> it has generally been thought<sup>1,2,7</sup> that fatty acids form only dimers in nonionizing media. We have of course attempted to interpret the present experimental data in terms of the simple monomer-dimer equilibrium, but the fit obtained was significantly worse than that for the model suggested above. We are thus inclined to believe that an aggregation beyond the dimer is indeed possible, though the fraction of the trimer formed is low, as shown in Figure 2.

The tendency toward aggregation increases with increas-

TABLE III: Polynomial Expansion of Log  $\gamma$  as a Function of Solute Molality ( $m$ )

HC6	$\log \gamma = -0.1075 - 16.49m + 182m^2 - 800m^3$	Std dev = 0.0086
HC9	$\log \gamma = -0.1312 - 16.61m + 182m^2 - 800m^3$	Std dev = 0.0099
HC12	$\log \gamma = -0.1564 - 17.41m + 196m^2 - 860m^3$	Std dev = 0.0109

TABLE IV: Heats of Dilution as a Function of Final Solute Concentration

$C_f, M \times 10^3$	$Q_d, J$		
	HC6	HC9	HC12
1.32	0.510	0.531	0.527
2.63	1.025	1.025	1.033
3.92	1.347	1.359	
5.20	1.715	1.732	1.711
6.45	1.975	1.987	
7.70	2.293	2.326	2.297
8.91			2.627
10.1	2.698	2.749	2.757
12.5	3.150	3.226	3.188
14.8	3.422	3.464	3.477
19.3	4.004	3.891	4.008
21.4	4.226	4.217	4.196
27.6	4.765	4.820	4.800
29.5	4.983		5.000
35.2	5.247	5.314	
38.7	5.556	5.481	5.439

TABLE V: Enthalpy of Formation of the Dimer and Trimer for the Three Acids in Benzene at 31°

Acid	$\Delta H_2, \text{kJ/mol of monomer}$	$\Delta H_3, \text{kJ/mol of monomer}$
HC6	$7.61 \pm 0.33$	$9.20 \pm 0.04$
HC9	$8.28 \pm 0.37$	$9.08 \pm 0.04$
HC12	$9.12 \pm 0.50$	$10.92 \pm 0.03$

however, has been found from ebullioscopic and cryoscopic measurements<sup>1,2</sup> and ir spectral data.<sup>5</sup> Since the differences toward aggregation in the homologous series of fatty acids are rather small (Table II) only precise data through careful experimentation and the use of especially sensitive physicochemical measurements can be expected to reveal these differences. The osmometric data reported here are believed to meet these criteria.

*Calorimetric Data.* The heats of dilution ( $Q_d$ ) as a function of the final solute concentration ( $c_f$ ) for the three acids are presented in Table IV and Figure 3. The thermal effects for the three acids in benzene are trendless and almost within the experimental error and can be combined into the polynomial

$$Q_d = 96.85C_f - 5971C_f^2 + 9.81 \times 10^4 C_f^3 - 9.67 \times 10^5 C_f^4 \quad \text{standard deviation} = 0.014 \quad (4)$$

where  $C_f$  represents the final solute molarity.

*Enthalpy, Entropy, and Free Energy of Aggregation.* Calculating the initial oligomer distribution in the 0.2 M starting solution and the oligomer distribution in the various final solutions after each addition, and from the knowledge of the moles added in order to reach a given concentration, the change in the concentration of the various oligomers can be calculated. If  $\alpha_1^i, \alpha_2^i,$  and  $\alpha_3^i$  are the initial fractions of monomer as monomer, dimer, and trimer, respectively, and  $\alpha_1^f, \alpha_2^f,$  and  $\alpha_3^f$  are the final fractions of monomer in the same oligomers, and  $m$  is the number of moles of solute added to reach the final concentration  $C_f$ ; the initial and final concentrations of the oligomers (expressed in terms of monomer) are  $m\alpha_1^i, m\alpha_2^i, m\alpha_3^i,$  and  $m\alpha_1^f, m\alpha_2^f, m\alpha_3^f,$  respectively.

Assuming that the measured heat effect is due to the change in the concentration of oligomer (dimer and trimer) we obtain

$$(m\alpha_2^f - m\alpha_2^i)\Delta H_2 + (m\alpha_3^f - m\alpha_3^i)\Delta H_3 = Q_d \quad (5)$$

where  $\Delta H_2$  and  $\Delta H_3$  are the enthalpy change when a monomer enters a dimer or trimer, respectively.

In this manner a set of equations was obtained for each acid studied and  $\Delta H_2$  and  $\Delta H_3$  were calculated using a least-squares computer program. Table V gives the results of the above calculation.

The aggregation energy, expressed in terms of monomer, seems to be constant for the three acids studied and almost independent on the oligomer (dimer or trimer). The enthalpy of formation of dimer is  $\sim 16.7 \text{ kJ/mol}$  ( $\Delta H_2 \times 2$ ) and

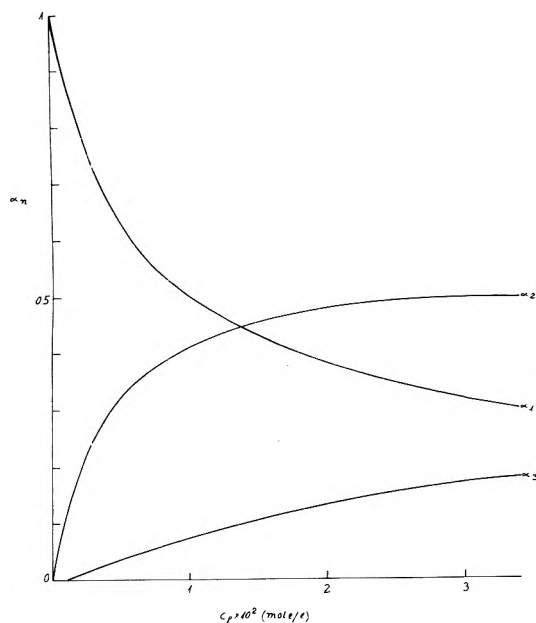


Figure 3. Degree of formation of oligomers ( $\alpha_n$ ) of nonanoic acid (HC9) in benzene as function of total concentration at 31°.

ing chain length of the acid, as reflected by the values in Table I, and the  $\beta_2$  and  $\beta_3$  values in Table II. An increasing deviation from ideal behavior with increasing chain length, as expressed through the activity coefficients shown in Figure 2 and Table III, is in line with an increasing tendency toward aggregation. A similar trend has been observed previously for the lower homologs of carboxylic acid in benzene,<sup>13</sup> and for a number of fatty acids ranging from octanoic to tetradecanoic acids in heptane.<sup>14</sup> A reverse trend,

TABLE VI: Thermodynamic Functions of the Aggregation Process of Carboxylic Acid in Benzene at 304 K

$10^3m$	$-\Delta H_i,$ kJ/mol	HC6		HC9		HC12	
		$-\Delta G,$ kJ/mol	$-\Delta S,$ eu	$-\Delta G,$ kJ/mol	$-\Delta S,$ eu	$-\Delta G,$ kJ/mol	$-\Delta S,$ eu
1.53	5.23						
3.06	10.36						
4.55	14.52						
6.03	17.98	14.17	3.00	14.31	2.89	14.48	2.75
7.49	21.11	13.74	5.79	13.89	5.68	14.07	5.54
8.95	24.03	13.41	8.35	13.55	8.24	13.74	8.10
11.8	26.46	12.92	10.64	13.08	10.52	13.26	10.38
14.5	28.64	12.58	12.62	12.74	12.50	12.93	12.35
17.2	30.46	12.33	14.25	12.48	14.23	12.69	13.97
22.4	32.01	11.97	15.76	12.13	15.64	12.34	15.47
24.9	33.32	11.84	16.89	12.00	16.77	12.21	16.60
32.0	34.29	11.53	17.89	11.70	17.76	11.92	17.59
40.9	34.90	11.25	18.59	11.41	18.46	11.63	18.30
45.0	35.45	11.12	19.13	11.30	19.00	11.52	18.81

for the trimer  $\sim 29.2$  kJ/mol ( $\Delta H_3 \times 3$ ). Keeping in mind that a molecule of dimer contains two hydrogen bonds due to its particular structure<sup>15</sup> it turns out that the trimer has a cyclic structure with three equivalent bonds. The energies obtained are of the order of magnitude expected for this kind of hydrogen bonds.<sup>16</sup> In order to calculate the entropy change for the aggregation process we have calculated the integral heat of dilution ( $\Delta H_i$ ) from the calorimetric data and combined them with the free energy ( $\Delta G$ ) calculated from activity data. The thermodynamic parameters of the aggregation process obtained are given in Table VI as a function of solute molal concentration

The changes in entropy of aggregation are in line with the trends obtained in activity coefficients calculated and aggregation behavior of the three acids as found osmometrically.

#### References and Notes

- (1) A. W. Ralston, "Fatty Acids and Their Derivatives," Wiley, New York, N.Y., 1948, p 376.
- (2) W. S. Singleton in "Fatty Acids," K. S. Markeley, Ed., Wiley, New York, N.Y., 1960, p 609.
- (3) H. A. Pohl, M. E. Hobbs, and P. M. Gross, *Ann. N.Y. Acad. Sci.*, **40**, 389 (1940); *J. Chem. Phys.*, **9**, 408 (1941).
- (4) A. A. Maryott, M. E. Hobbs, and P. M. Gross, *J. Amer. Chem. Soc.*, **71**, 1671 (1949).
- (5) S. S. Singh, *Indian J. Chem.*, **6**, 393 (1968).
- (6) D. Hadzi and H. Sheppard, *Proc. Roy. Soc., Ser. A*, **216**, 247 (1953).
- (7) D. S. Flett and M. J. Jaycock in "Ion Exchange and Solvent Extraction," Vol. III, J. A. Marinsky and Y. Marcus, Ed., Marcel Dekker, New York, N.Y., 1973.
- (8) J. J. Christensen, R. N. Izatt, L. D. Hansen, and J. A. Partridge, *J. Phys. Chem.*, **70**, 2003 (1966).
- (9) A. S. Kertes and G. Markovits, *J. Phys. Chem.*, **72**, 4202 (1968); A. S. Kertes, O. Levy, and G. Markovits, *ibid.*, **74**, 3568 (1970).
- (10) A. S. Kertes, H. Gutman, O. Levy, and G. Y. Markovits, Proceedings of the Vth International Conference on Surface Activity, Zurich 1972; G. Y. Markovits, O. Levy, and A. S. Kertes, *J. Colloid Interface Sci.*, **42**, 4247 (1974).
- (11) A. S. Kertes and G. Markovits in "Thermodynamics of Nuclear Materials, 1967," IAEA, Vienna, 1968, p 227.
- (12) G. Loveluck, *J. Phys. Chem.*, **64**, 385 (1960).
- (13) I. Kojima, M. Yoshida, and M. Tanaka, *J. Inorg. Nucl. Chem.*, **32**, 987 (1970).
- (14) D. S. Goodman, *J. Amer. Chem. Soc.*, **80**, 3887 (1958).
- (15) L. Pauling and L. O. Brockway, *Proc. Nat. Acad. Sci. U. S.*, **755** (1938).
- (16) G. C. Pimental and A. L. McClellan, "The Hydrogen Bond," W. A. Freeman, New York, N.Y., 1960.

# Effect of Zinc, Gallium, and Germanium Ions on the Structural and Magnetic Properties of Nickel Ions Supported on Alumina

A. Cimino, M. Lo Jacono, and M. Schiavello\*

*Istituto di Chimica Generale ed Inorganica, Università di Roma, and Centro di Studio su "Struttura ed Attività Catalitica di Sistemi di Ossidi," del Consiglio Nazionale delle Ricerche, Roma, Italy (Received June 3, 1974)*

\* Publication costs assisted by Consiglio Nazionale delle Ricerche

The influence of a small addition of  $Zn^{2+}$ ,  $Ga^{3+}$ , and  $Ge^{4+}$  ions on the structural properties of nickel ions supported on  $\gamma$ - and  $\eta$ - $Al_2O_3$  has been studied. The presence of the above ions, all having preference for tetrahedral sites, favors a normal cation distribution in the "surface spinel,"  $NiAl_2O_4$ , as revealed by means of X-ray, magnetic, uv, and visible reflectance spectra measurements. The observed behavior is explained by polarization of the anion toward the tetrahedral sites. The reducibility of nickel ions of some  $Ga^{3+}$  containing specimens was also studied and was shown to be smaller than the reducibility of  $Ga^{3+}$  free specimens. The same effect of  $Ga^{3+}$  on reducibility is indicated by a lower catalytic cracking of 2,2-dimethylbutane at 400° and 20 atm of  $H_2$ . The results are in agreement with the difficulty of reducing nickel ions in tetrahedral sites.

## 1. Introduction

In a preceding study of the supported oxide system nickel oxide on alumina<sup>1a</sup> it was shown that a surface spinel (nickel aluminate), only a few layers thick, was formed. As in  $NiAl_2O_4$ , nickel ions occupy tetrahedral (A) sites and octahedral (B) sites in the lattice, but unlike the situation in bulk  $NiAl_2O_4$ , the relative  $[Ni_{oct}^{2+}]/[Ni_{tet}^{2+}]$  ratio is not fixed by the temperature only, it depends on the nature of the supporting alumina ( $\gamma$  or  $\eta$ ), and on the atmosphere (damp or dry). Furthermore, a catalytic study of  $N_2O$  decomposition suggested that the external layer of the supported  $Ni^{2+}/Al_2O_3$  system is richer in tetrahedral  $Ni^{2+}$  than the average content.<sup>1b,2</sup>

The type of symmetry adopted by nickel ions influences directly their reactivity; thus, for example, a supported oxide rich in  $Ni_{tet}^{2+}$  is much more difficult to reduce by hydrogen than a supported oxide rich in  $Ni_{oct}^{2+}$ . It was of interest therefore to investigate what other parameters could influence the  $[Ni_{oct}^{2+}]/[Ni_{tet}^{2+}]$  ratio, in addition to the above mentioned parameters (atmosphere, type of alumina). It was thought that small additions of ions of suitable size, and with a definite preference for a given symmetry, could have an influence on the  $[Ni_{oct}^{2+}]/[Ni_{tet}^{2+}]$  ratio. Accordingly,  $Ga^{3+}$ ,  $Zn^{2+}$ , or  $Ge^{4+}$ , all having a marked preference for tetrahedral sites, were added. Indeed a study, carried out by Krischner, Torkar, and Hornisch,<sup>3</sup> showed the influence of the above ions on the crystal field strength in the octahedral sites of the spinel structure. This paper reports the results of the effect of the above additions, studied by means of X-ray, spectroscopic (uv and visible), and magnetic methods. On Ga-added aluminas with nickel, a study of the ease of reduction of nickel ions by hydrogen was carried out. On the same Ni-containing specimens a check was made of cracking and hydrogenolysis patterns to explore the influence of gallium additions.

## 2. Experimental Section

**2.1. Catalysts Preparation and Analysis.** The majority of the specimens were prepared according to the following procedure. The  $\gamma$ - and  $\eta$ - $Al_2O_3$ , prepared according to the

method described by MacIver, Tobin, and Barth,<sup>4</sup> were impregnated with a comparable volume of gallium nitrate or zinc nitrate solutions of desired concentration. Only  $\gamma$ - $Al_2O_3$  was impregnated with germanium dioxide solution. In all cases, the soaked mass was dried at 120° then ground and heated at 500° for 15 hr. The  $Ga_2O_3$ - $Al_2O_3$ ,  $ZnO$ - $Al_2O_3$ , and  $GeO_2$ - $Al_2O_3$  supports so obtained were impregnated with a solution of nickel nitrate of known concentration. The material was then dried at 120°, ground, and fired at 600° for 24 hr in air. The sequence of additions is important, since it controls the final properties of the specimens. Thus, the simultaneous addition of gallium and nickel salts to the aluminas gives rise to less reproducible results.

A  $NiGa_2O_4$  specimen was also prepared by impregnating gallium oxide with the stoichiometric amount of nickel nitrate solution, drying at 120°, firing at 700°, grinding, and finally firing at 900° for 70 hr, and at 1100° for 40 hr. The X-ray analysis showed no phases different from  $NiGa_2O_4$ .

The  $\gamma$ - and  $\eta$ - $Al_2O_3$  based specimens are designated respectively by the symbols  $A_\gamma GaN$ ,  $A_\eta GaN$ ,  $A_\gamma Zn$ ,  $A_\eta Zn$  and  $A_\gamma GeN$ , followed by two numbers: the first indicates the gallium or zinc or germanium and the second the nickel concentration, expressed in atomic per cent.

The analysis of the nickel content was made by atomic absorption spectroscopy (Model 303 Perkin-Elmer for Ga- and Zn-containing specimens and AA5 Pechtron for Ge-containing specimens). The dissolution of the specimens was performed by addition of a few drops of concentrated  $H_2SO_4$  to the specimen (50–100 mg) and after digestion, boiling until complete dissolution. Standard solutions were prepared with an aluminum ion concentration similar to that present in the samples to be analyzed.

Lists of the specimens together with their main features are reported in Tables I–III.

**2.2. Magnetic, Reflectance, and X-Ray Measurements.** Magnetic susceptibility determination were performed by the Gouy method in the temperature range 100–300°K in an atmosphere of helium.

X-Ray measurements were made with a Debye-Scherrer camera using the  $Cu K\alpha$  (Ni-filtered) radiation at room

TABLE I: Gallium-Containing Specimens and Their Properties

Samples	Ni content, <sup>a</sup> wt %	Curie		Magnetic moment, BM	Weiss temp, $-\theta$ , °K	Ni <sub>tet</sub> <sup>2+</sup> , %
		constant, C, erg G <sup>-2</sup> mol <sup>-1</sup> °K				
A <sub>γ</sub> GaN 0.6:1	1.22	1.15		3.04	2	5
A <sub>γ</sub> GaN 0.6:3	3.03	1.61		3.59	52	51
A <sub>γ</sub> GaN 0.6:6	5.84	1.66		3.64	77	56
A <sub>γ</sub> GaN 4:1	1.26	1.20		3.08	0	10
A <sub>γ</sub> GaN 4:3	3.55	1.40		3.34	27	30
A <sub>γ</sub> GaN 4:6	5.91	1.38		3.33	20	28
A <sub>γ</sub> GaN 0.3:6	5.75	1.42		3.38	12	32
A <sub>γ</sub> GaN 0.6:6	5.61	1.53		3.51	40	43
A <sub>γ</sub> GaN 2.5:6	6.09	1.46		3.43	28	36
A <sub>γ</sub> GaN 4:6	5.81	1.37		3.32	10	27
A <sub>γ</sub> GaN 5:6	5.73	1.31		3.26	5	21
A <sub>γ</sub> GaN 0.6:1	1.12	1.25		3.16	0	15
A <sub>η</sub> GaN 0.6:3	3.19	1.41		3.36	30	31
A <sub>η</sub> GaN 0.6:6	5.89	1.47		3.43	31	37
A <sub>η</sub> GaN 4:1	1.28	1.16		3.05	18	7
A <sub>η</sub> GaN 4:3	3.40	1.36		3.30	30	26
A <sub>η</sub> GaN 4:6	6.43	1.28		3.21	22	18
NiGa <sub>2</sub> O <sub>4</sub>	22.3	1.36		3.30	7	0

<sup>a</sup> Analytical, see text.

TABLE II: Zinc-Containing Specimens and Their Properties

Samples	Ni content, <sup>a</sup> wt %	Curie		Weiss temp, $-\theta$ , °K
		constant, C, erg G <sup>-2</sup> mol <sup>-1</sup> °K	Magnetic moment, BM	
A <sub>γ</sub> Zn 0.6:3	3.15	1.27	3.19	2
A <sub>γ</sub> Zn 0.6:6	6.29	1.25	3.17	3
A <sub>γ</sub> Zn 4:3	3.70	1.30	3.24	6
A <sub>γ</sub> Zn 4:6	6.99	1.23	3.14	2
A <sub>η</sub> Zn 0.6:3	3.24	1.31	3.23	20
A <sub>η</sub> Zn 0.6:6	6.40	1.19	3.09	10
A <sub>η</sub> Zn 4:3	3.32	1.40	3.35	15
A <sub>η</sub> Zn 4:6	6.51	1.22	3.12	1

<sup>a</sup> Analytical, see text.

TABLE III: Germanium-Containing Specimens and Their Properties

Samples	Ni content, <sup>a</sup> wt %	Curie constant, C, erg G <sup>-2</sup> mol <sup>-1</sup> °K		Weiss temp, $-\theta$ , °K	Magnetic moment, BM
A <sub>γ</sub> GeN 0.3:3	3.20	1.36	14	3.31	
A <sub>γ</sub> GeN 0.3:6	5.82	1.35	11	3.30	
A <sub>γ</sub> GeN 0.6:1	1.19	1.39	24	3.34	
A <sub>γ</sub> GeN 0.6:3	3.20	1.43	17	3.39	
A <sub>γ</sub> GeN 0.6:6	6.09	1.39	15	3.34	
A <sub>γ</sub> GeN 1.5:3	3.19	1.43	20	3.39	
A <sub>γ</sub> GeN 1.5:6	6.12	1.44	23	3.40	
A <sub>γ</sub> GeN 3:1	1.14	1.85	57	3.90	
A <sub>γ</sub> GeN 3:3	3.28	1.35	17	3.30	
A <sub>γ</sub> GeN 3:6	6.00	1.40	23	3.35	
A <sub>γ</sub> GeN 5:3	3.17	1.33	11	3.28	
A <sub>γ</sub> GeN 5:6	6.06	1.34	14	3.29	

<sup>a</sup> Analytical, see text.

temperature (exposure time 8 hr). Details of the procedures used for magnetic and X-ray determinations were given elsewhere.<sup>5</sup>

The reflectance spectra, carried out for AGaN and AZN specimens, were recorded by a Beckman DK1 A spectrophotometer using as reference  $\gamma$ - or  $\eta$ -Al<sub>2</sub>O<sub>3</sub> which contained Ga<sub>2</sub>O<sub>3</sub> or ZnO. The measurements were carried out in the wavelength range 2500–270 nm at room temperature.

**2.3. Reduction Experiments.** Reduction of hydrogen was performed for a few Ga-containing representative specimens. The amount of nickel reduced was measured by hydrogen adsorption.<sup>6</sup> An all glass flow system was employed. The catalyst (~0.200 g) was placed in a Pyrex reduction cell (~6 cm<sup>3</sup>) limited by two fritted disks. The procedure was as follows. (a) The specimen was outgassed for 4 hr at 480° at  $P \approx 10^{-5}$  Torr. The amount of H<sub>2</sub> adsorbed at  $P = 0.8$  Torr at 20° was determined by a McLeod gauge. This amount was found to be negligible. (b) The specimen was reduced for 2 hr at increasing temperature steps in a flow of H<sub>2</sub> (120 cm<sup>3</sup>/min) at 200, 300, 400, 450, and 520°. After each reduction step the sample was outgassed at the same reduction temperature and then cooled under dynamic vacuum. The amount of H<sub>2</sub> adsorbed was determined as in a. (c) Following the determination of the H<sub>2</sub> adsorbed after the 2-hr reduction at 520°, a further reduction at 520° for 10 hr was performed and the new volume of adsorbed H<sub>2</sub> was measured.

### 3. Experimental Results

**3.1. Reflectance Spectra.** The reflectance spectra were recorded for AGaN and AZN specimens. The pattern of their spectra is essentially the same, therefore only one is reported. In Figure 1 the reflectance spectrum of A<sub>γ</sub>GaN 0.6:6 is shown together with those of a Ni<sup>2+</sup>/γ-Al<sub>2</sub>O<sub>3</sub> (Ni 6% atomic) specimen and a NiGa<sub>2</sub>O<sub>4</sub> specimen. The spectrum of NiGa<sub>2</sub>O<sub>4</sub> has been recorded using a specimen which had been ground for 20 hr in a mechanical mortar. The mean diameter of the particles was 370 Å, calculated according to the method of Scherrer, as described by Klug and Alexan-

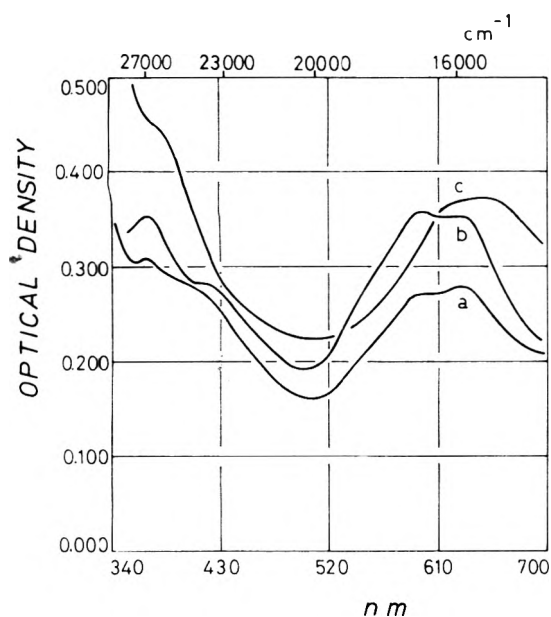


Figure 1. Reflectance spectra of (a)  $\text{Ni}^{2+}/\gamma\text{-Al}_2\text{O}_3$  (6 at % Ni); (b)  $\text{A}\gamma\text{GaN}$  0.6:6; (c)  $\text{NiGa}_2\text{O}_4$ .

der.<sup>7</sup> The same spectrum was obtained for an unground specimen of  $\text{NiGa}_2\text{O}_4$  and for another one ground for 5 hr (mean diameter of the particle = 520 Å). From an inspection of Figure 1 the following points emerge.

(i) The general pattern of the  $\text{A}\gamma\text{GaN}$  0.6:6 is qualitatively similar to that of the spinel  $\text{NiAl}_2\text{O}_4$  and of the specimens  $\text{Ni}^{2+}/\text{Al}_2\text{O}_3$ .<sup>1</sup> Thus a surface spinel,  $\text{NiAl}_2\text{O}_4$ , as in the  $\text{Ni}^{2+}/\text{Al}_2\text{O}_3$  specimens, is formed also on the  $\text{Ga}^{3+}$  impregnated specimens.

(ii) The intensity ratio of the bands at 370 and 590–630 nm for the  $\text{Ni}^{2+}/\gamma\text{-Al}_2\text{O}_3$  sample is higher than unity whereas for  $\text{A}\gamma\text{GaN}$  0.6:6 it is about unity. Recalling that the band at 370 nm is the most intense band for  $\text{Ni}_{\text{oct}}^{2+}$  and the bands at 590–630 nm are the most intense for  $\text{Ni}_{\text{tet}}^{2+}$  one is led to the conclusion that the amount of  $\text{Ni}_{\text{tet}}^{2+}$  is higher on the  $\text{Ni}^{2+}/\text{Ga}_2\text{O}_3\text{-Al}_2\text{O}_3$  than on the  $\text{Ni}^{2+}/\text{Al}_2\text{O}_3$  specimens. This conclusion applies to the  $\text{Ni}^{2+}/\text{ZnO-Al}_2\text{O}_3$  specimens as well.

(iii) The shift of adsorption band 590–630 nm of curve c ( $\text{NiGa}_2\text{O}_4$ ) to higher values is due to the weaker field present in  $\text{NiGa}_2\text{O}_4$  compared to  $\text{NiAl}_2\text{O}_4$ , caused by the longer cation-anion distance (lattice parameter  $a = 8.258$  Å in  $\text{NiGa}_2\text{O}_4$ , 8.046 Å in  $\text{NiAl}_2\text{O}_4$ ).

**3.2. X-Ray Measurements.** The analysis of the results can be made along lines similar to those discussed in ref 1. In particular, the variation of reflection intensities points to the incipient formation of a surface spinel. It was noted that the lines were sharper than in the case of the  $\text{Ni}^{2+}/\text{Al}_2\text{O}_3$  specimens.

**3.3. Magnetic Measurements.** The values of the Curie constant  $C$ , of the Weiss temperature  $\theta$ , derived from the Curie-Weiss law [(molar susceptibility)  $\chi = C/(T - \theta)$ ], as well the magnetic moment  $\mu$  (Bohr magneton units) are reported in Tables I-III. In Figure 2 the values of  $C$  vs.  $[\text{Ni}^{2+}]$  are reported for the specimens  $\text{A}\gamma\text{GaN}$  0.6: $x$ ,  $\text{A}\eta\text{GaN}$  0.6: $x$ , and  $\text{A}\gamma\text{GaN}$  4: $x$ ,  $\text{A}\eta\text{GaN}$  4: $x$ . For comparison the  $C$  values for  $\text{Ni}^{2+}/\gamma\text{-Al}_2\text{O}_3$  and  $\text{Ni}^{2+}/\eta\text{-Al}_2\text{O}_3$  are also reported.<sup>1</sup> Figure 3 reports the values of  $C$  vs.  $[\text{Ga}^{3+}]$  for the specimens having a variable gallium content and a constant nickel content (6 or 3% atomic - specimens  $\text{AGaN}$

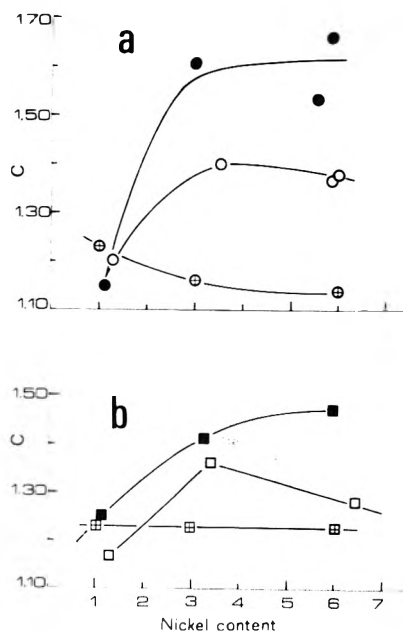


Figure 2. Curie constant,  $C$ , vs. nickel content (atomic per cent): (a) ●,  $\text{A}\gamma\text{GaN}$  0.6: $x$ ; ○,  $\text{A}\gamma\text{GaN}$  4: $x$ ; ⊕,  $\text{Ni}^{2+}/\gamma\text{-Al}_2\text{O}_3$ ; (b) ■,  $\text{A}\eta\text{GaN}$  0.6: $x$ ; □,  $\text{A}\eta\text{GaN}$  4: $x$ ; ⊕,  $\text{Ni}^{2+}/\eta\text{-Al}_2\text{O}_3$ .

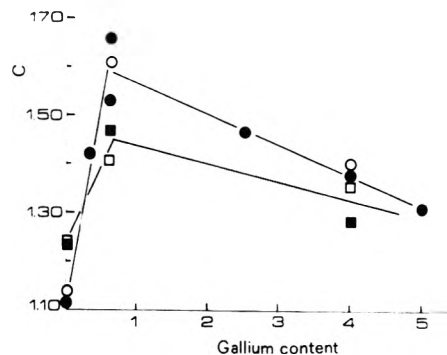


Figure 3. Curie constant,  $C$ , vs. gallium content (atomic per cent): ●,  $\text{A}\gamma\text{GaN}$   $x:6$ ; ■,  $\text{A}\eta\text{GaN}$   $x:6$ ; ○,  $\text{A}\gamma\text{GaN}$   $x:3$ ; □,  $\text{A}\eta\text{GaN}$   $x:3$ .

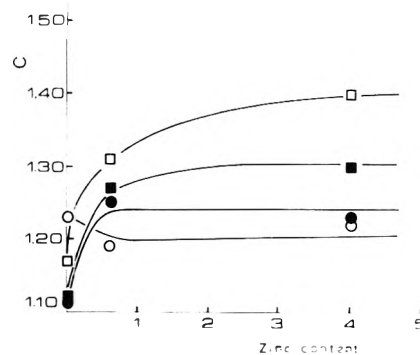


Figure 4. Curie constant,  $C$ , vs. zinc content (atomic per cent): ■,  $\text{A}\gamma\text{Zn}$   $x:3$ ; □,  $\text{A}\eta\text{Zn}$   $x:3$ ; ●,  $\text{A}\gamma\text{Zn}$   $x:6$ ; ○,  $\text{A}\eta\text{Zn}$   $x:6$ .

$x:3$  and  $\text{AGaN}$   $x:6$ ). Figure 4 reports the values of  $C$  vs.  $[\text{Zn}^{2+}]$  and Figure 5 the values of  $C$  vs.  $[\text{Ge}^{4+}]$ .

From the inspection of these figures it can be inferred that (i) catalysts containing gallium, zinc, and germanium

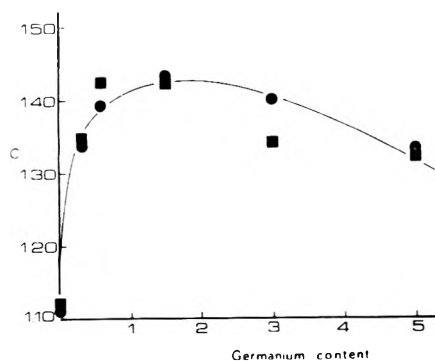


Figure 5. Curie constant,  $C$ , vs. germanium content (atomic per cent): ■,  $A_7\text{GeN } x:3$ ; ●,  $A_7\text{GeN } x:6$ .

ions have higher  $C$  values compared to those of the  $\text{Ni}^{2+}/\text{Al}_2\text{O}_3$  catalysts; (ii) for a given content (3 or 6% atomic) the highest  $C$  values are found at gallium content equal to 0.6% and a germanium content between 0.6 and 1.5% atomic. For the zinc containing specimens there is not a definite trend, and constancy can be assumed within experimental error, after an initial and significant increase of  $C$  caused by after an initial and significant increase of  $C$  caused by small  $\text{Zn}^{2+}$  additions. Thus small additions of  $\text{Ga}^{3+}$ ,  $\text{Ge}^{4+}$ , and  $\text{Zn}^{2+}$  are most effective in influencing the  $C$  value.

In principle, the  $C$  value is sensitive to the distribution of nickel ions among A and B sites, a higher  $C$  value corresponding to a higher  $[\text{Ni}_{\text{tet}}^{2+}]/[\text{Ni}_{\text{oct}}^{2+}]$  ratio. It is then appropriate to discuss the magnetic results in order to establish whether the increase of  $C$  corresponds to a real increase of the tetrahedral nickel ion concentration.

Figure 6 reports the values of  $C$  vs.  $-\theta$  for the specimens  $A_7\text{GaN } x:6$  and for  $\text{NiGa}_2\text{O}_4$ <sup>8</sup> as reference and it can be seen that an increase of  $C$  is accompanied by an increase of  $\theta$ . It is recalled that the values of  $\theta$  are dependent on the magnetic interactions between the paramagnetic ions. High values of  $\theta$  indicate a high degree of interaction. In a spinel structure having the formula  $A[\text{B}_2]\text{O}_4$  (where A and B are the cations in tetrahedral and octahedral sites, respectively) two types of interactions take place: cation-cation and cation-anion-cation.<sup>9</sup> So the following interactions must be taken into account: B-B, B-O-B, B-O-A. According to Goodenough,<sup>9</sup> the B-O-A antiferromagnetic interactions are important, when the  $e$  orbitals of the B cations and the  $t_2$  orbitals of the A cations are incomplete. This is the case for  $\text{Ni}^{2+}$  since the electronic configuration in the octahedral B site is  $t_{2g}^6-e_g^2$  and the tetrahedral A site is  $e^4-t_2^4$ . Moreover the B-B ( $90^\circ$ ) antiferromagnetic interaction is important when the B cations have the  $t_{2g}$  orbitals half-filled. In the present case, shown above, the  $t_{2g}$  orbitals for  $\text{Ni}_{\text{oct}}^{2+}$  are completely filled and consequently the B-B ( $90^\circ$ ) antiferromagnetic interactions are negligible. It can be concluded that the antiferromagnetic interaction in  $\text{NiGa}_2\text{O}_4$  is low because they are of the B-B and B-O-B ( $90^\circ$ ) type (remember that the cation configuration is  $\text{Ga}[\text{NiGa}]\text{O}_4$ <sup>8</sup>). By the same argument, the small  $C$  value found for  $A\text{GaN}$  specimens with high gallium content points to a large occupancy of B sites by  $\text{Ni}^{2+}$  ions. By contrast, in specimens which have relatively high  $\text{Ni}_{\text{tet}}^{2+}$  content, strong B-O-A interactions at  $125^\circ$  occur and high  $\theta$  values are then observed (see Figure 6). This phenomenon is less visible in the zinc and germanium containing specimens because of the relatively small variation of  $C$ . In conclusion the high  $C$  values at high added ion concentration is a confirmation of

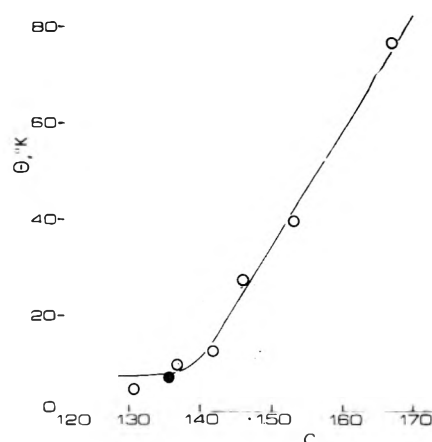


Figure 6. Weiss temperature,  $-\theta$ , vs. Curie constant,  $C$ : O,  $A_7\text{GaN } x:6$ ; ●,  $\text{NiGa}_2\text{O}_4$  from ref 8.

the presence of a high concentration of nickel in tetrahedral sites.

An estimate of the  $\text{Ni}^{2+}$  distributed in octahedral and tetrahedral sites can be now made. Using the experimental values of the Curie constant,  $C$ , and assuming the  $\text{Ni}^{2+}$  to be present completely as surface spinel,  $\text{NiAl}_2\text{O}_4$ , it is possible to use the law of additivity for  $C$ :

$$C_{\text{expt}} = x_{\text{oct}}^{\text{Ni}} C_{\text{oct}} + x_{\text{tet}}^{\text{Ni}} C_{\text{tet}} \quad (\text{I})$$

where  $x_{\text{oct}}^{\text{Ni}}$  and  $x_{\text{tet}}^{\text{Ni}}$  are the molar fractions for nickel in octahedral and tetrahedral sites in the spinel and  $C_{\text{oct}}$  and  $C_{\text{tet}}$  are the Curie constants for  $\text{Ni}^{2+}$  in octahedral and tetrahedral sites. Taking  $C_{\text{oct}} = 1.10$  and  $C_{\text{tet}} = 2.10$ ,<sup>1</sup> it is possible to derive the values of  $x_{\text{oct}}^{\text{Ni}}$  and  $x_{\text{tet}}^{\text{Ni}}$  from eq I. In Table I the per cent of  $\text{Ni}^{2+}$  in tetrahedral sites is reported for the gallium-containing specimens. It can be said that the values of  $[\text{Ni}_{\text{tet}}^{2+}]$  given are approximate and they depend on the choice of  $C_{\text{oct}}$  and  $C_{\text{tet}}$ . On the other hand, if the  $C_{\text{oct}}$  and  $C_{\text{tet}}$  values are changed, the absolute values of  $[\text{Ni}_{\text{tet}}^{2+}]$  are affected, but not their relative values. For example, a change of the  $C_{\text{oct}}$  value from 1.10 to 1.23, intermediate between 1.10 and 1.36, which is the value found for bulk  $\text{NiGa}_2\text{O}_4$ , is reflected in a variation from 56 to 49% in the tetrahedral nickel concentration for the specimens  $A_7\text{GaN } 0.6:6$ .

**3.4. Reduction Experiments.** The specimens used were  $A_7\text{GaN } 0.6:6$  ( $[\text{Ni}_{\text{tet}}^{2+}] = 43\%$ ),  $A_7\text{GaN } 0.3:6$  ( $[\text{Ni}_{\text{tet}}^{2+}] = 32\%$ ),  $A_7\text{GaN } 5:6$  ( $[\text{Ni}_{\text{tet}}^{2+}] = 21\%$ ), and the specimen without Ga,  $\text{Ni}^{2+}/\gamma\text{-Al}_2\text{O}_3$  (Ni 6% atomic and  $[\text{Ni}_{\text{tet}}^{2+}] = 2\%$ ). The results are shown in Figure 7, where the volume ( $\text{cm}^3$ , STP) of  $\text{H}_2$  adsorbed per gram of nickel, designated as  $V$  of  $\text{H}_2/\text{g}$  of Ni, is reported as function of the reduction temperature. The surface areas of the specimens range from 123 to 136  $\text{m}^2 \text{g}^{-1}$ . It is immediately evident that the  $\text{Ni}^{2+}/\gamma\text{-Al}_2\text{O}_3$  specimen is more reducible than the  $A_7\text{GaN}$  specimens. Thus the previous finding that the  $\text{Ni}_{\text{tet}}^{2+}$  is less reducible than the  $\text{Ni}_{\text{oct}}^{2+}$ <sup>1b</sup> is confirmed. An important point must be noted. It has been found that a specimen  $\text{Ni}^{2+}/\eta\text{-Al}_2\text{O}_3$  (6 at % Ni, fired at  $600^\circ$  for 24 hr in dry nitrogen), having  $[\text{Ni}_{\text{tet}}^{2+}] = 22\%$ , was not reduced at all even at  $520^\circ$ .<sup>1b</sup> The AGN specimens having  $[\text{Ni}_{\text{tet}}^{2+}]$  in an amount higher than in the specimen  $\text{Ni}^{2+}/\eta\text{-Al}_2\text{O}_3$  are all more reducible although with difficulty. This result can be explained by taking into account the fact that the outer layers of  $\text{Ni}^{2+}/\text{Al}_2\text{O}_3$  are richer in tetrahedral nickel in comparison to the amount deducible from the magnetic

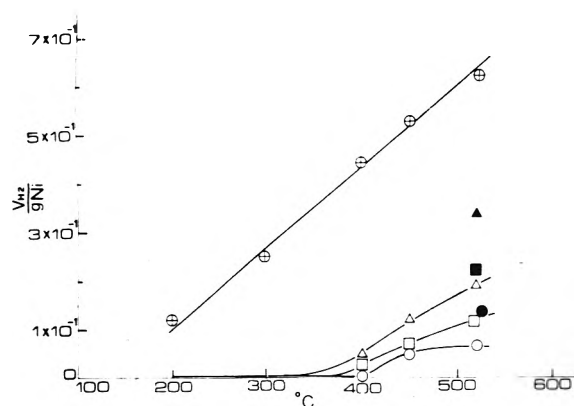


**Figure 7.** H<sub>2</sub> uptake (cm<sup>3</sup> at STP/g of Ni) due to the reduction treatment vs. temperature of reduction: O, A $\gamma$ GaN 0.6:6; □, A $\gamma$ GaN 0.3:6;  $\Delta$ , A $\gamma$ GaN 5:6;  $\oplus$ , Ni<sup>2+</sup>/ $\gamma$ -Al<sub>2</sub>O<sub>3</sub> (6 at % Ni); ●,  $\blacktriangle$ ,  $\blacksquare$ , points taken after 10-hr reduction at 520°.

measurements,<sup>1b</sup> and that the difference between surface layers and bulk is especially amplified by specimens treated in a dry atmosphere.<sup>1b</sup> The outer layers are thus more resistant to reduction, and the whole process is kinetically hindered. In addition to this effect, a possible specific role of the support ( $\gamma$  vs.  $\eta$ ) cannot be excluded, if the nucleation and growth of reduced nickel is affected by the surface environment.

**3.5. Cracking and Hydrogenolysis Pattern.** An apparatus designed for the high pressure flow method was used. The experiments were carried out in the laboratories of Snam Progetti (S. Donato, Milano). The hydrocarbon was 2,2-dimethylbutane (DMB), in the 1:5 ratio with hydrogen. The total pressure was 20 atm and the test temperatures were 400 and 420°. The products were collected at -80°, and analyzed by gas chromatography. The amount of unreacted DMB is especially relevant to the present report, since when metallic nickel is formed, it readily catalyzes hydrocracking reactions. It was found that at 400°, the Ni<sup>2+</sup>/ $\gamma$ -Al<sub>2</sub>O<sub>3</sub> (Ni 6 at %) catalyst left 77.5% of DMB unaltered, while the A $\gamma$ GN 0.6:6 left 96.9% unaltered. At 420° the figures were 49.8 and 83.8, respectively. The greater stability against reduction of specimens based on Ga-containing aluminas is thus confirmed even at high hydrogen pressures, and in the presence of hydrocarbons.

## Discussion

The experimental results have shown that the distribution of Ni<sup>2+</sup> ions among A (tetrahedral) and B (octahedral) sites, in the surface spinel formed when nickel oxide is supported on alumina, is affected by the presence of small additions of Ga<sup>3+</sup>, Zn<sup>2+</sup>, or Ge<sup>4+</sup> ions to the alumina. It was shown, in fact, that if the quantities of the ions seeking tetrahedral sites, namely, Ga<sup>3+</sup>, Zn<sup>2+</sup>, and Ge<sup>4+</sup>, are small, initial additions of Ni<sup>2+</sup> ions will be accommodated in B sites, but subsequent to that, accommodation of Ni<sup>2+</sup> in A sites is favored, in comparison to the situation of pure alumina.

A discussion, aimed at a rational explanation for these findings, is given below.

**Influence of Gallium Ions on the Nickel Ion Distribution.** In order to rationalize the influence of gallium ions on the nickel ion distribution between A and B sites, it is useful to recall a few details of the crystal chemistry of the spinel structure.

The transition alumina  $\gamma$  or  $\eta$  can be described in terms of the anion packing, which is practically that of a spinel

structure, and of cation distribution among tetrahedral and octahedral voids. The cation distribution, however, must respect the stoichiometry Al<sub>2</sub>O<sub>3</sub>. If  $\frac{1}{3}$ Al<sub>2</sub>O<sub>3</sub> is considered (in order to deal with four oxygen atoms as in the spinel formula M''M'''O<sub>4</sub>), the alumina can be written as Al<sub>8/3</sub>O<sub>4</sub>. Therefore, one-third of cation are missing in Al<sub>2</sub>O<sub>3</sub>, compared to a spinel which has a total of 3 cations per four oxygen ions. The cation vacancies can be distributed in different ways among cationic sites, normally occupied in a spinel. The formula



with  $0 \leq x \leq \frac{1}{3}$  describes the possibilities that the vacancies are distributed among tetrahedral and octahedral sites in such a way as to exclude complete absence of Al<sup>3+</sup> cations in either A or B sites. For the present discussion we can disregard differences between  $\gamma$ - and  $\eta$ -Al<sub>2</sub>O<sub>3</sub>. The data of Leonard, *et al.*,<sup>10</sup> indicate that the fraction of Al<sup>3+</sup> in tetrahedral sites is about  $\frac{1}{3}$ , which would pose  $x = \frac{2}{9}$ . Hence in practice the cation vacancies are distributed among octahedral and tetrahedral sites with the same (2:1) ratio adopted by the cations.

This equilibrium distribution is strongly altered when Ga<sup>3+</sup> ions are incorporated. The Ga<sup>3+</sup> ions have a strong preference for tetrahedral sites, and therefore Ga containing alumina will show more trivalent ions in tetrahedral sites (hence a higher  $x$  value) and more cation vacancies in octahedral sites compared to Ga-free alumina. The high concentration of vacancies in octahedral sites has two distinct effects: (a) it leaves more B sites empty; (b) it lowers the average charge of B sites, and it increases the average charge of A sites. The effect a will result in a statically higher availability for incoming divalent ions. The effect b will strongly polarize the anion toward A sites, thus decreasing the crystal field around B sites.

The addition of nickel ions to gallium-containing alumina can now be examined. Qualitatively one can expect two effects: (I) because of point a above the nickel ions will be accommodated into B site vacancies is favored; (II) because of point b above, the crystal field stabilization energy (CFSE) of the nickel ions is smaller than in the absence of Ga<sup>3+</sup> ions. The CFSE decrease occurs for both sites, but to a larger extent in the octahedral sites, thus resulting in a net decrease of the octahedral site preference (OSP). The nickel ions therefore can interchange with the Al<sup>3+</sup> ions, present as a major constituent in Ga-poor specimens, more easily than when a large CFSE is present.

The experimental observations match this picture fully. The magnetic data of Figure 3 show that the first nickel ions added go into octahedral sites (low  $C$  value). However, as their concentration increases, the  $[\text{Ni}_{\text{tet}}^{2+}]$  increases (high  $C$  value), thus showing that the surface spinel which is being formed is characterized by a lower octahedral site preference of Ni<sup>2+</sup> ions if compared to a pure nickel aluminate spinel. In this way one can explain the apparent contradiction that Ga-containing aluminas, with more A sites occupied (by Ga<sup>3+</sup> ions) than in pure alumina, also favor the occupation of the A sites by Ni<sup>2+</sup>. When the concentration of Ga<sup>3+</sup> is increased (see specimens with  $[\text{Ga}^{3+}] > 0.6$ ) the probability that Ni<sup>2+</sup> can interchange with Al<sup>3+</sup> ions will decrease, and therefore the tendency by Ni<sup>2+</sup> ions to go into A sites will also decrease. The presence of a maximum in the  $C$  vs. Ga<sup>3+</sup> plot (Figure 3) can therefore be rationalized. In different words, one could also note that as the

$\text{Ga}^{3+}$  values increases, domains are formed which effectively tend toward nickel gallate, which is inverse:  $\text{Ga}[\text{Ni-Ga}]\text{O}_4$ .<sup>8</sup>

The considerations expressed above are in practice emphasizing the role of the anion polarization, a problem which has been discussed by Blasse<sup>11</sup> among the factors which affect the cation distribution. He showed indeed that the normal distribution is favored by anion polarization.

It is interesting to note that in addition to the polarization caused by the vacancy concentration in B sites, discussed before, the effect of the surface also acts in the same direction. Indeed, the presence of a surface, and hence of coordinatively unsaturated sites, will favor occupation by cations of tetrahedral sites, which can make use of the limited number of anions in the best way to shield the positive charge. Once again, therefore, in the outer layer the vacancy concentration in the B sites will be higher than in the bulk, thus assisting the process described before.

*Influence of Zinc Addition.* Upon addition of  $\text{Zn}^{2+}$  ions, the cation vacancies in eq 1 are gradually filled, but because of the tetrahedral site preference of  $\text{Zn}^{2+}$  ions, the distribution of the remaining vacancies will differ appreciably from that present at the beginning. Namely, more vacancies will be left in the octahedral sites. It is true that concomitantly with the introduction of  $\text{Zn}^{2+}$  ions, some  $\text{Al}^{3+}$  ions will be able to move into octahedral positions, but this process will only be complete when a stoichiometric zinc aluminate is formed,  $\text{Zn}[\text{Al}_2]\text{O}_4$ . Before that, the defective structure of the surface zinc aluminate-alumina solid solution will leave more vacancies in B sites than in A sites. Thus, the situation will be qualitatively similar (even though not to the same extent) to that encountered with  $\text{Ga}^{3+}$  addition, where vacancies concentrated in B sites. As a consequence, anion polarization will occur toward cations in A sites. While  $\text{Ni}^{2+}$  ions will initially go into B sites which are statistically more available, their OSP is decreased, thus favoring for subsequent additions, an interchange with  $\text{Al}^{3+}$  ions, and an increase of  $[\text{Ni}_{\text{tet}}^{2+}]$ .

Finally, the specific influence of the zinc ions should be considered with respect to the appreciably covalent character of the  $\text{Zn}^{2+}-\text{O}^{2-}$  bond. The covalent character is effectively decreasing the charge on the anions, again acting toward a decrease of the OSP of the  $\text{Ni}^{2+}$  ions.

It is interesting to compare the situation here encountered with that found in bulk  $\text{Ni}_x\text{Zn}_{1-x}\text{Al}_2\text{O}_4$ , studied by Porta, *et al.*<sup>12</sup> In the solid solutions, the very first addition of  $\text{Ni}^{2+}$  (therefore  $x \approx 0$ ) results in a higher concentration of  $\text{Ni}^{2+}$  in B sites,  $\beta$ . As the nickel ion concentration increases, their occupancy of B sites steeply decreases percentage-wise, until  $x \approx 0.2$ . After this value,  $\beta$  increases again. One can see that there is a parallelism with the supported system  $\text{Ni}^{2+}/\text{ZnO}-\text{Al}_2\text{O}_3$ , where initially  $\text{Ni}^{2+}$  goes into B sites, but afterward the occupation of A sites is favored. Furthermore (in solid solution work), the increase of the value as  $x \rightarrow 1$  (high percentage of  $\text{Ni}^{2+}$ ) is not steep. This is in agreement with the observation that in the supported system, when the  $\text{Ni}^{2+}$  value is large and  $\text{Zn}^{2+}$  is small, there is little variation of the distribution among A and B sites.

*Influence of Germanium Addition.* The influence of  $\text{Ge}^{4+}$  ions can be discussed along lines similar to those outlined above, keeping in mind that no spinel is formed with the  $\text{Al}_2\text{O}_3$  support (in contrast to  $\text{Zn}^{2+}$  additions) and that no simple interchange with the  $\text{Al}^{3+}$  ions can take place, because of the difference of charge. However, some  $\text{Ge}^{4+}$

can be accommodated into the alumina structure if some defects are created. This is especially plausible at the surface where an excess of anions can be introduced, during the preparation.

If some  $\text{Ge}^{4+}$  ions occupy tetrahedral positions, their influence on the polarization term will be large and once more the  $\text{Ni}^{2+}$  ions will at first be accommodated in B sites because of their statistically greater availability, but successive additions, as the  $\text{Ni}^{2+}$  builds up, will interchange more easily with  $\text{Al}^{3+}$  in A sites, because of the reduced OSP of  $\text{Ni}^{2+}$ , caused by the anion polarization. This is reflected in the step ascending part of the curve of Figure 5. If the  $[\text{Ni}^{2+}]$  is large, however, the tendency to form the spinel  $\text{Ni}_2\text{GeO}_4$  will be large, and a new phase will tend to segregate, since the nickel germanate is not soluble in  $\text{NiAl}_2\text{O}_4$ .<sup>13</sup> The same tendency to segregation takes place when the  $[\text{Ge}^{4+}]$  is large.

### Concluding Remarks

The above discussion gives a consistent picture of the action of ions seeking tetrahedral sites on the physicochemical properties of  $\text{Ni}^{2+}/\text{Al}_2\text{O}_3$  systems. It emphasizes the role of polarization effects and this is in line with the finding on supported  $\text{Ni}^{2+}$  over pure aluminas and on nickel aluminate, where the surface constituted a major alteration in the energy parameters normally considered for a bulk spinel. It can be noted that explanations based on purely statistical grounds would fail, because more octahedral sites are available than tetrahedral ones, and yet the magnetic and optical data show that while initial additions of  $\text{Ni}^{2+}$  ions go into octahedral sites, further additions prefer the tetrahedral sites. Also any reasoning based solely on charge/radius ratio would fail, because the same qualitative effect is shown by a fairly large, low charge ion ( $\text{Zn}^{2+}$ ) and by a small, high charge ion ( $\text{Ge}^{4+}$ ). A strict parallelism exists with the observation by Krischner, Torkar, and Hornisch<sup>3</sup> who studied the influence of  $\text{Zn}^{2+}$ ,  $\text{Ga}^{3+}$ , and  $\text{Ge}^{4+}$  additions to  $\text{Al}_2\text{O}_3$  by measuring the shift of the optical absorption of  $\text{Cr}^{3+}$  ions. Convincing evidence was obtained that the crystal field around the  $\text{Cr}^{3+}$  ions was weakened upon addition of those ions.

The influence of small additions to the supporting oxide can be of great significance in the overall properties of the supported oxide systems. A change in the distribution of  $\text{Ni}^{2+}$  ions among A and B sites can indeed be reflected in several chemical properties of the supported system. One such property, reducibility by hydrogen, has been tested in the present work, and while it consistently points to a larger occupation of tetrahedral sites it also suggests means of affecting the reducibility of  $\text{Ni}^{2+}$  ions in supported systems. Other properties, such as catalytic activity, can also be affected, either as a direct result of influencing the relative concentration of ions endowed with different properties because of dependence on the site symmetry, or as an indirect result, by affecting side reactions brought about by reduction of the transition ion to the metallic state. An exploratory test, described in section 3.5, confirms this hypothesis. Further work along these lines is in progress, also with a view to clarify the role of different aluminas.

*Acknowledgments.* The catalytic experiments were carried out in the Research Laboratories of Snam Progetti (San Donato, Milano) to whom we express our thanks. Thanks are also due to Dr. B. Notari and Dr. L. Forlani (Snam Progetti) for their help in the catalytic experiments,

and to Mr. G. Minelli for the help given in the experimental work.

### References and Notes

- (1) (a) M. Lo Jacono, M. Schiavello, and A. Cimino, *J. Phys. Chem.*, **75**, 1044 (1971); (b) M. Schiavello, M. Lo Jacono, and A. Cimino, *ibid.*, **75**, 1051 (1971).
- (2) A. Cimino and M. Schiavello, *J. Catal.*, **20**, 202 (1971).
- (3) H. Krischner, K. Torkar, and P. Hornisch, *Monatsh. Chem.*, **99**, 1733 (1968).
- (4) D. S. MacIver, H. H. Tobin, and R. T. Barth, *J. Catal.*, **2**, 485 (1963).
- (5) A. Cimino, M. Lo Jacono, P. Porta, and M. Valigi, *Z. Phys. Chem. (Frankfurt am Main)*, **51**, 301 (1966).
- (6) J. C. Yates, W. F. Taylor, and J. H. Sinfelt, *J. Amer. Chem. Soc.*, **86**, 2996 (1964).
- (7) H. P. Klug and L. E. Alexander, "X-Ray Diffraction Procedures," Wiley, New York, N.Y., 1954, p. 491.
- (8) S. Greenwald, S. Y. Pickart, and F. H. Grannis, *J. Chem. Phys.*, **22**, 1957 (1954).
- (9) J. B. Goodenough, "Magnetism and the Chemical Bond," Interscience, New York, N.Y., 1963, p. 165.
- (10) A. J. Leonard, P. N. Semaille, J. J. Fripiat, *Proc. Brit. Ceram. Soc.*, 103 (1969).
- (11) G. Blasse, *Philips Res. Rep. Suppl.*, **3**, 18 (1964).
- (12) V. Bucciarelli, A. Cimino, and P. Porta, to be submitted for publication.
- (13) F. C. Romeijn, *Philips Res. Rep.*, **8**, 321 (1953).

## Crystal Structures of Three Solid Solution Phases of Ammonium Nitrate and Potassium Nitrate

James R. Holden\* and Charles W. Dickinson

Naval Surface Weapons Center, White Oak, Maryland 20910 (Received May 13, 1974)

Publication costs assisted by the Naval Surface Weapons Center

The crystal structures of ammonium nitrate (AN)-potassium nitrate (KN) solid solutions of eight different compositions in three different polymorphic forms have been determined by X-ray diffraction. The crystal structures of AN-IV and KN-II have been refined from X-ray diffraction data. The unit cell of AN-IV is orthorhombic, space group  $Pm\bar{m}n$  containing two formula units. The cell dimensions are  $a = 5.724$ ,  $b = 5.455$ ,  $c = 4.945$  Å for AN-IV and  $a = 5.758$ ,  $b = 5.456$ ,  $c = 4.942$  Å for a solid solution containing 3.2 at. % potassium ion at the cation sites. Solid solutions of KN in AN-III are orthorhombic, space group  $Pnma$  with four formula units per cell. The cell dimensions range from  $a = 7.694$ ,  $b = 5.827$ ,  $c = 7.158$  Å for 5.0 at. % potassium to  $a = 7.635$ ,  $b = 5.739$ ,  $c = 7.026$  Å for 36.6 at. % potassium. The unit cell of KN-II is orthorhombic, space group  $Pnma$  with four formula units. The cell dimensions are  $a = 6.436$ ,  $b = 5.430$ ,  $c = 9.192$  Å for KN-II and  $a = 6.458$ ,  $b = 5.444$ ,  $c = 9.211$  Å for a solid solution containing 4.8 at. % ammonium ion. The cation coordination "sphere" in the AN-III type structures consists of 11 oxygen atoms from 7 nitrate ions. The potassium ions are randomly distributed through the cation sites, and the effective ionic radius appears to be a linear function of the potassium content.

### Introduction

The crystal structures of potassium nitrate-ammonium nitrate solid solutions of eight different compositions have been determined by single-crystal X-ray diffraction techniques. Our object was to determine which forces control the stability limits of the three solid solution polymorphs with ranges of room temperature stability. The crystal structures of ammonium nitrate (AN) and potassium nitrate (KN), previously determined by neutron diffraction, have also been refined from X-ray data for direct comparison.

There are five known polymorphic forms of AN. The two which pertain to this study are AN-IV, stable between  $-17$  and  $32.23^\circ$ , and AN-III, stable between  $32.23$  and  $84.10^\circ$ .<sup>1</sup> There are three known polymorphs of KN. KN-II is stable from below room temperature to about  $128^\circ$  where it transforms to KN-I.<sup>2</sup> On cooling, KN-I transforms at about  $124^\circ$  to metastable KN-III which in turn transforms back to KN-II at about  $110^\circ$ .<sup>2</sup>

At least four different solid solution phases have been re-

ported; KN dissolved in AN-IV (KN-AN-IV), KN dissolved in AN-III (KN-AN-III), AN dissolved in KN-III (AN-KN-III), and AN dissolved in KN-II (AN-KN-II). As increasing amounts of KN are dissolved in solid AN, the IV-III transition temperature falls from  $32.23^\circ$  for pure AN to below room temperature and KN-AN-III becomes the stable phase.<sup>3,4</sup> The presence of ammonium ion in KN-III stabilizes this phase to the extent that it can be cooled to room temperature. However, it has been reported that in the presence of water it transforms to a mixture of KN-AN-III and AN-KN-II indicating that it is not thermodynamically stable at room temperature.<sup>5</sup> Therefore, as the potassium ion content increases, the three room temperature stable solid solution polymorphs are KN-AN-IV, KN-AN-III then AN-KN-II.

The crystal structure of AN-IV was reported by both West<sup>6</sup> and Hendricks, Posnjak, and Kracek<sup>7</sup> in 1932. It has been redetermined more accurately by Choi, Mapes, and Prince<sup>8</sup> by neutron diffraction. The crystal structure of KN-II was reported by Edwards<sup>9</sup> in 1931 and redetermined

TABLE I: Preliminary Crystal Data

	Weight % KN in salt mix	Crystal size, mm	Cell dimensions, Å			Crystal volume per formula unit, Å <sup>3</sup>
			<i>a</i>	<i>b</i>	<i>c</i>	
AN-IV (C, M, and P) <sup>b</sup>			5.745	5.438	4.942	77.20
AN-IV	0	0.40 × 0.22 × 0.20	5.724(5)	5.455(4)	4.945(3)	77.20
KN-AN-IV	3	0.41 × 0.19 × 0.19	5.758(2)	5.456(3)	4.942(2)	77.61
AN-III (G and W) <sup>c</sup>			7.65	5.83	7.14	79.61
KN-AN-III-a	4	0.40 × 0.28 × 0.19	7.694(4)	5.827(3)	7.158(3)	80.22
KN-AN-III-b	10 <sup>a</sup>	0.33 × 0.16 × 0.15	7.669(2)	5.821(2)	7.120(2)	79.46
KN-AN-III-c	10	0.47 × 0.16 × 0.13	7.660(4)	5.800(4)	7.112(4)	78.99
KN-AN-III-d	20	0.34 × 0.18 × 0.12	7.656(1)	5.777(1)	7.083(1)	78.32
KN-AN-III-e	40 <sup>a</sup>	0.50 × 0.24 × 0.20	7.662(3)	5.764(3)	7.062(3)	77.97
KN-AN-III-f	30	0.39 × 0.12 × 0.11	7.635(1)	5.739(1)	7.026(1)	76.97
AN-KN-II	40	0.32 × 0.16 × 0.12	6.458(5)	5.444(5)	9.211(6)	80.96
KN-II (N and L) <sup>d</sup>			6.4309	5.4142	9.1659	79.78
KN-II	100	0.34 × 0.14 × 0.09	6.436(1)	5.430(1)	9.192(2)	80.31

<sup>a</sup> Second crop by evaporation. <sup>b</sup> Reference 8. <sup>c</sup> Reference 11. <sup>d</sup> Reference 10.

by Nimmo and Lucas<sup>10</sup> also by neutron diffraction. The crystal structure of AN-III was reported by Hendricks, Posnjak and Kracek<sup>7</sup> in 1932 and redetermined by Goodwin and Whetstone<sup>11</sup> in 1947. It has been reported from the results of X-ray powder diffraction that the unit cell dimensions of KN-AN-III decrease with increasing KN content, because the ionic radius of potassium, 1.33 Å, is smaller than the effective radius of the ammonium ion, 1.48 Å.<sup>12</sup> The same cause is cited for the increase of the cell dimensions of AN-KN-III with increasing AN content.<sup>9</sup>

### Experimental Section

Table I lists the preliminary data from the crystals used in this study in order of increasing KN content. Also included for comparison are the cell dimensions used in the most recent reports of the structures of AN-IV,<sup>8</sup> AN-III,<sup>11</sup> and KN-II.<sup>10</sup> All crystals were grown by slow cooling or subsequent vaporation at room temperature of saturated water solutions. The weight per cent KN in the dissolved salt mixture is listed followed by the dimensions of the sample crystal. Crystals AN-KN-II and KN-AN-III-e were selected from subsequent crops of crystals grown from the same solution. All crystals grew as long thin needles and the specimens used for diffraction measurements were sections broken from longer needles. The needle axes coincide with the *a* axes of the AN-IV type crystals, the *b* axes of the AN-III type crystals, and the *a* axes of the KN-II type crystals as reported in this paper. All crystals were first aligned and examined with a precession camera then transferred to a Picker FACS-1 computer-controlled automatic diffractometer equipped with a graphite (HOG) monochromator. The unit cell dimensions were obtained from a least-squares fit of the diffraction angles of 12 strong reflections using 0.71069 Å as the wavelength of Mo K $\alpha$  radiation. All crystals are orthorhombic. The numbers in parentheses are standard deviations estimated by the least-squares procedure. The crystal volumes per formula unit are included for comparison of the packing densities in the three polymorphic forms.

The periodic absences in the observed X-ray reflections confirm the previously reported space groups for all three

structure types. However, for this report, the parameters for AN-III and KN-II have been converted to refer to "standard settings" listed in the "International Tables for X-ray Crystallography."<sup>13</sup> Thus, the space group of AN-IV and KN-AN-IV is *Pmmn* (No. 59); that of AN-III, KN-AN-III, AN-KN-II, and KN-II is *Pnma* (No. 62). AN-IV and KN-AN-IV contain two formula units per cell; the others contain four formula units per cell.

### Refinement of Structures

Reflection intensities were measured by "standard" diffractometer procedures. Data treatment, least-squares structure refinements, and subsequent evaluations were carried out by "standard" calculation methods using a CDC 6400 and the "XRAY System of Crystallographic Programs."<sup>14</sup> Details are given in the microfilm edition of this journal.<sup>15</sup> The starting atomic positions for least-squares refinement were obtained from previously reported structures of AN-IV, AN-III, and KN-II. Hydrogen atom positions were not well defined by the data. The positions reported from the neutron diffraction determination of AN-IV<sup>8</sup> were used in the refinement of the structure of KN-AN-IV (see Table II). The hydrogen positions given in Table III for the AN-III type structures were estimated from an electron density calculation (Fourier summation) but not entered into the least-squares refinement. Note that the large values of the temperature factors (*U* values) produced by the least-squares procedure mean that these atoms make only a small contribution to the calculated structure factors.

The potassium content of each solid solution crystal listed in Tables II-IV was obtained by including a cation site occupancy factor with the other parameters of the least-squares refinement. Even though the correlation factors were as high as 0.5 between the site occupancy factor and the thermal parameters of the ammonium nitrogen atom in the KN-AN-III structures and 0.66 between the site occupancy factor and scale factor in AN-KN-II, good convergence was obtained because all final shift/error ratios were below 0.5.<sup>15</sup>

TABLE II: Atomic Parameters for AN-IV Type Structures<sup>a</sup>

	AN-IV (C, M, and P) <sup>b</sup>	AN-IV This work	KN-AN-IV
At. fraction K <sup>+</sup>	0	0	0.032(4)
N/K <sup>+</sup>			
<i>x</i>	7500	7500	7500
<i>y</i>	2500	2500	2500
<i>z</i>	-836(4)	-839(5)	-830(5)
<i>U</i> <sub>11</sub>	268(11)	222(12)	243(13)
<i>U</i> <sub>22</sub>	441(13)	469(16)	488(17)
<i>U</i> <sub>33</sub>	285(11)	310(13)	324(14)
N(2)			
<i>x</i>	2500	2500	2500
<i>y</i>	2500	2500	2500
<i>z</i>	5067(3)	5074(5)	5080(4)
<i>U</i> <sub>11</sub>	325(10)	296(13)	317(12)
<i>U</i> <sub>22</sub>	312(09)	314(13)	314(11)
<i>U</i> <sub>33</sub>	191(10)	247(12)	193(10)
O(1)			
<i>x</i>	2500	2500	2500
<i>y</i>	2500	2500	2500
<i>z</i>	7629(6)	7639(4)	7645(3)
<i>U</i> <sub>11</sub>	355(14)	312(12)	316(10)
<i>U</i> <sub>22</sub>	470(18)	499(14)	488(12)
<i>U</i> <sub>33</sub>	199(13)	220(10)	190(10)
O(2)			
<i>x</i>	4342(5)	4364(4)	4364(3)
<i>y</i>	2500	2500	2500
<i>z</i>	3832(5)	3835(4)	3836(3)
<i>U</i> <sub>11</sub>	521(15)	453(11)	459(11)
<i>U</i> <sub>22</sub>	742(19)	824(15)	793(15)
<i>U</i> <sub>33</sub>	375(13)	453(11)	421(10)
<i>U</i> <sub>13</sub>	210(10)	220(10)	224(08)
H(1)			
<i>x</i>	6045(12)		
<i>y</i>	2500		
<i>z</i>	-1898(17)		
<i>U</i> <sub>11</sub>	870(41)		
<i>U</i> <sub>22</sub>	750(38)		
<i>U</i> <sub>33</sub>	1106(48)		
<i>U</i> <sub>13</sub>	-604(41)		
H(2)			
<i>x</i>	7500		
<i>y</i>	1011(16)		
<i>z</i>	324(16)		
<i>U</i> <sub>11</sub>	784(35)		
<i>U</i> <sub>22</sub>	1055(47)		
<i>U</i> <sub>33</sub>	922(43)		
<i>U</i> <sub>23</sub>	461(39)		

<sup>a</sup> Fractional translations and temperature factors  $\times 10^4$ . <sup>b</sup> Reference 8.

## Discussion

The bond lengths and angles found for the nitrate ions in potassium nitrate (KN), ammonium nitrate (AN), and their solid solutions are listed in Table V. Note that in the AN-III type structures N(2)-O(1) covers a range of 0.014 Å, and N(2)-O(2) a range of 0.012 Å but that there are no trends as the potassium content of the cell increases. Since these ranges are four to six times the standard deviations estimated for individual determinations by the usual least-squares procedure, one might attach some significance to

the large differences. However, because the structures differ only in potassium content and there is no apparent correlation between the individual bond distances and the potassium content, it is doubtful that the differences are real. Therefore, these results would indicate that the true limit of error for an individual determination is two to three times that estimated by least squares.

However, the differences between the N(2)-O(1) and N(2)-O(2) bond lengths found for the AN-IV type structures range between 30 and 40 times the estimated standard deviations and are certainly significant. Choi, Mapes, and Prince<sup>8</sup> attribute this difference to the fact that O(1) is involved in four strong hydrogen bonds whereas O(2) is not. This explanation is consistent with the greater symmetry found for the nitrate ion in KN-II. It should be noted that there is also no significant difference in the bond lengths found in the nitrate ions of the AN-III type structures.

None of the solid solution crystals reported in this paper produced any X-ray reflections not accounted for by the reported unit cell or any detectable intensities at the positions of space group extinctions. Therefore, there is no evidence for a nonrandom distribution of potassium ions at the ammonium sites of the AN-IV or AN-III type structures or for a nonrandom distribution of ammonium ions at the potassium sites in AN-KN-II.

Figures 1-3 show the arrangement of the ions and the coordination of the cations in the three structure types covered in this paper: AN-IV, AN-III, and KN-II. The cation positions, shown as the major component, actually contain a random distribution of ammonium and potassium ions such that the probability of finding a potassium ion at one particular site is equal to the atomic fraction of potassium in the crystal. The positions of the surrounding atoms are probably slightly different when a site is occupied by a potassium ion than when it is occupied by an ammonium ion so the nitrate ion positions found by the diffraction procedure would also be a weighted average of their positions throughout the crystal.

The projection directions of Figures 1-3 were chosen such that the ions lie on mirror planes parallel to the paper at  $\frac{1}{4}$  or  $\frac{3}{4}$  of the cell translation interval perpendicular to the paper. The oxygen and hydrogen atom positions listed in Tables II-IV are identified in the figures. In all cases O(1) lies on the mirror plane with N(2) while O(2) and its symmetrically related mate (the third oxygen atom of the nitrate ion) lie above and below the mirror plane. In KN-AN-IV, the ions also lie on mirror planes perpendicular to the *b* axis. The interionic distances labeled A through F refer to the corresponding columns in Table VI; G through J refer to Table VII.

The determining factor in most ionic crystal structures is the cation coordination. In the AN-IV type structures, (Figure 1), each cation is surrounded by 12 oxygen atoms from 8 nitrate ions (4 on the same mirror plane, 2 above, and 2 below). Four of the 12 oxygen atoms form hydrogen bonds with the four hydrogen atoms of the ammonium ion. These bonds, shown as B and C in Figure 1, have H-O distances of 2.050(7) and 2.161(7) Å and N-H-O angles of 154.4(8) and 172.6(9)° in AN-IV as reported by Choi, Mapes, and Prince.<sup>8</sup> Using the hydrogen positions from their neutron diffraction determination, our corresponding distances would be 2.042 and 2.164 Å for AN-IV and 2.054 and 2.162 Å for KN-AN-IV. The closest approach to the center of the cation, A, is not a hydrogen bond. The other

TABLE III: Atomic Parameters for AN-III Type Structures<sup>a</sup>

	AN-III		KN-AN-III				
	(G and W) <sup>b</sup>	<i>a</i>	<i>b</i>	<i>c</i>	<i>d</i>	<i>e</i>	<i>f</i>
At. fraction K <sup>+</sup>	0	0.050(3)	0.093(3)	0.120(4)	0.250(5)	0.333(4)	0.366(4)
N/K <sup>+</sup>							
<i>x</i>	-200	-106(3)	-110(3)	-114(4)	-118(5)	-113(2)	-125(2)
<i>y</i>	7500	7500	7500	7500	7500	7500	7500
<i>z</i>	3200	3169(3)	3168(4)	3168(4)	3167(5)	3166(2)	3162(2)
<i>U</i> <sub>11</sub>		396(11)	366(14)	382(15)	266(21)	357(9)	356(9)
<i>U</i> <sub>22</sub>		296(10)	291(13)	314(14)	320(20)	272(9)	265(8)
<i>U</i> <sub>33</sub>		356(11)	357(13)	357(15)	373(21)	342(9)	354(8)
<i>U</i> <sub>13</sub>		-19(8)	-24(10)	-11(1)	4(13)	-5(5)	-2(5)
N(2)							
<i>x</i>	1450	1550(2)	1550(3)	1554(3)	1557(3)	1557(2)	1555(3)
<i>y</i>	2500	2500	2500	2500	2500	2500	2500
<i>z</i>	1400	1257(2)	1268(3)	1264(3)	1268(3)	1280(3)	1293(3)
<i>U</i> <sub>11</sub>		302(8)	289(10)	285(10)	264(11)	270(9)	269(9)
<i>U</i> <sub>22</sub>		288(8)	306(11)	300(10)	332(12)	320(10)	306(9)
<i>U</i> <sub>33</sub>		319(9)	318(10)	323(10)	306(11)	300(9)	314(9)
<i>U</i> <sub>13</sub>		-22(6)	-5(7)	-11(7)	-29(8)	-34(7)	-15(7)
O(1)							
<i>x</i>	850	598(3)	600(3)	598(3)	602(4)	603(3)	602(3)
<i>y</i>	2500	2500	2500	2500	2500	2500	2500
<i>z</i>	3000	2663(3)	2678(3)	2679(3)	2694(4)	2717(3)	2717(3)
<i>U</i> <sub>11</sub>		614(12)	609(14)	609(14)	585(15)	543(12)	560(13)
<i>U</i> <sub>22</sub>		428(9)	437(12)	432(12)	399(13)	393(10)	381(11)
<i>U</i> <sub>33</sub>		413(10)	404(11)	387(11)	370(12)	363(10)	374(10)
<i>U</i> <sub>13</sub>		193(8)	184(10)	179(10)	153(11)	136(9)	141(9)
O(2)							
<i>x</i>	1750	2011(2)	2012(2)	2015(2)	2022(2)	2023(2)	2019(2)
<i>y</i>	600	640(2)	638(3)	640(3)	643(3)	632(3)	618(3)
<i>z</i>	600	534(2)	537(2)	540(2)	543(2)	545(2)	551(2)
<i>U</i> <sub>11</sub>		492(8)	489(9)	495(9)	487(10)	471(8)	468(8)
<i>U</i> <sub>22</sub>		351(7)	380(9)	379(9)	384(11)	385(9)	374(9)
<i>U</i> <sub>33</sub>		539(8)	526(9)	532(10)	515(11)	516(9)	539(9)
<i>U</i> <sub>12</sub>		77(5)	67(6)	79(6)	60(7)	59(6)	73(6)
<i>U</i> <sub>13</sub>		49(5)	43(7)	43(7)	49(8)	51(6)	51(6)
<i>U</i> <sub>23</sub>		-93(5)	-99(6)	-111(7)	-115(7)	-130(6)	-128(7)
H(1)							
<i>x</i>		-1118	-1125	-1130	-1135	-1139	-1145
<i>y</i>		7500	7500	7500	7500	7500	7500
<i>z</i>		4024	4027	4028	4031	4032	4033
<i>U</i>		1769(348)	963(203)	2945(830)	6851(4324)	7359(4574)	4517(2169)
H(2)							
<i>x</i>		981	980	978	974	969	970
<i>y</i>		7500	7500	7500	7500	7500	7500
<i>z</i>		3910	3913	3913	3916	3916	3916
<i>U</i>		1217(212)	1397(301)	867(186)	2002(646)	1712(491)	1218(356)
H(3)							
<i>x</i>		-144	-148	-151	-156	-161	-163
<i>y</i>		8887	8889	8894	8899	8902	8909
<i>z</i>		2372	2366	2365	2361	2357	2350
<i>U</i>		1751(198)	1754(222)	1685(256)	2357(487)	2227(457)	2784(662)

<sup>a</sup> Fractional translations and temperature factors  $\times 10^4$ . <sup>b</sup> Reference 11.

approaches D (the distance from the central cation to the O(2) atom labeled D), and E make a broad range of coordination distances, 0.36 Å. The O-O distance shown as G is the only short interanion contact in any of the structure types.

In the AN-III type structures, each cation is surrounded by 11 oxygen atoms from 7 nitrate ions (3 on the same mir-

ror plane, 2 above, and 2 below). The hydrogen positions shown in Figure 2 were estimated from electron density calculations.<sup>15</sup> If correct, these positions would indicate no strong hydrogen bonding. The only possibility would be a pair of bifurcated bonds accompanying the distances designated as E. The H-O distances would be 2.22 Å in KN-AN-III-a and the N-H-O angles would be 150°. The dis-

**TABLE IV: Atomic Parameters for KN-II Type Structures<sup>a</sup>**

	KN-II			
	(E) <sup>b</sup>	(N and L) <sup>c</sup>	This work	AN-KN-II
At. fraction K <sup>+</sup>	1.000	1.000	1.000	0.952(6)
N/K <sup>+</sup>				
x	2500	2568(2)	2551(1)	2553(8)
y	2500	2500	2500	2500
z	4160	4166(1)	4164(1)	4164(1)
U <sub>11</sub>		378(8)	311(5)	336(4)
U <sub>22</sub>		275(7)	238(4)	255(4)
U <sub>33</sub>		261(4)	248(4)	261(4)
U <sub>13</sub>		15(6)	11(2)	14(1)
N(2)				
x	4170	4152(1)	4156(3)	4155(3)
y	2500	2500	2500	2500
z	7500	7548(1)	7551(3)	7548(2)
U <sub>11</sub>		233(4)	192(9)	208(8)
U <sub>22</sub>		275(3)	250(11)	271(9)
U <sub>33</sub>		303(4)	297(11)	315(9)
U <sub>13</sub>		3(3)	16(8)	14(6)
O(1)				
x	4170	4107(2)	4098(4)	4109(3)
y	2500	2500	2500	2500
z	8830	8902(1)	8907(3)	8908(2)
U <sub>11</sub>		522(6)	500(15)	529(12)
U <sub>22</sub>		408(6)	407(14)	437(13)
U <sub>33</sub>		282(4)	272(11)	288(9)
U <sub>13</sub>		-72(3)	-80(9)	-87(8)
O(2)				
x	4170	4151(1)	4129(3)	4133(2)
y	4440	4492(1)	4501(3)	4493(3)
z	6860	6866(1)	6864(2)	6865(2)
U <sub>11</sub>		495(4)	493(10)	541(9)
U <sub>22</sub>		258(4)	268(9)	290(7)
U <sub>33</sub>		415(4)	392(9)	417(8)
U <sub>12</sub>		-48(2)	-38(7)	-45(6)
U <sub>13</sub>		48(3)	52(7)	54(6)
U <sub>23</sub>		48(3)	64(7)	65(5)

<sup>a</sup> Fractional translations and temperature factors  $\times 10^4$ . <sup>b</sup> Reference 9. <sup>c</sup> Reference 10.

tances between the center of the cation and the 11 oxygen atoms which make up its coordination "sphere" (A through F in Figure 2) cover a narrower range than in AN-IV, 0.23 Å.

In the KN-II type structures, each cation is surrounded by 9 oxygen atoms from 6 nitrate ions (2 on the same mirror plane, 2 above, and 2 below). The distance range in the coordination "sphere" is quite narrow, 0.09 Å. (See Figure 3.)

The monovalent cations which can partially replace ammonium ion in AN to form solid solutions are those with ionic radii close to the effective ionic radius of ammonium ion.<sup>12</sup> Thus, using the values listed by Pauling,<sup>16</sup> potassium (1.33 Å), tellurium (1.44 Å), rubidium (1.48 Å), and cesium (1.69 Å) will replace ammonium (1.48 Å), but sodium (0.95 Å) will not. As might be expected, the way in which a dissolved ion changes the polymorphic transition temperatures of AN depends upon its ionic radius relative to that of ammonium.<sup>12</sup> Figure 4 shows the change in crystal volume per formula unit at room temperature as the potassium content increases. The size of the rectangle around each

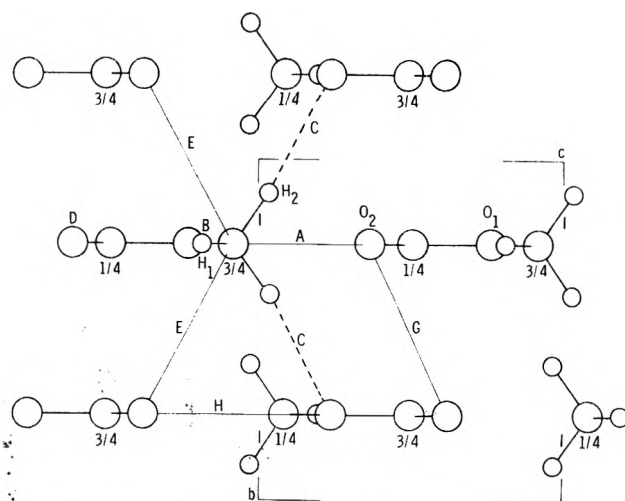


Figure 1. Cation coordination in AN-IV type structures.

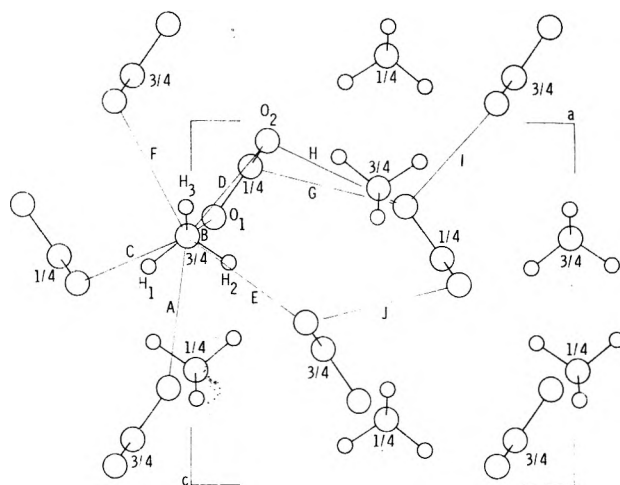


Figure 2. Cation coordination in AN-III type structures.

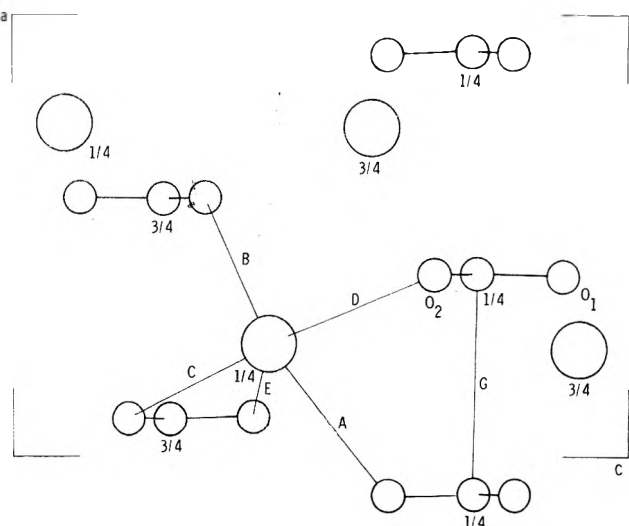


Figure 3. Cation coordination in KN-II type structures.

point represents two estimated standard deviations on either side as calculated from cell dimensions listed in Table I and the atomic fractions listed in Tables II-IV. Among the AN-III type structures, the formula volume definitely

TABLE V: Nitrate Ion Bond Lengths and Angles

	N(2)-O(1), Å	N(2)-O(2), Å	O(1)-N(2)-O(2), deg	O(2)-N(2)-O(2'), deg
AN-IV (C, M, and P) <sup>a</sup>	1.266(4)	1.222(3)	120.0(3)	120.0(3)
AN-IV This work	1.268(3)	1.230(3)	119.9(1)	120.3(2)
KN-AN-IV	1.268(3)	1.237(2)	119.8(1)	120.4(2)
KN-AN-III-a	1.245(3)	1.252(2)	120.1(1)	119.8(2)
KN-AN-III-b	1.240(3)	1.254(2)	120.2(1)	119.6(2)
KN-AN-III-c	1.245(3)	1.247(2)	120.1(1)	119.9(2)
KN-AN-III-d	1.247(4)	1.242(2)	120.2(1)	119.6(2)
KN-AN-III-e	1.251(3)	1.247(2)	120.3(1)	119.4(2)
KN-AN-III-f	1.237(3)	1.251(2)	120.3(1)	119.4(2)
AN-KN-II	1.254(3)	1.254(2)	120.1(1)	119.8(2)
KN-II (N and L) <sup>b</sup>	1.241(2)	1.246(1)	120.1(1)	119.9(2)
KN-II This work	1.247(4)	1.257(2)	120.1(1)	119.7(2)

<sup>a</sup> Reference 8. <sup>b</sup> Reference 10.

TABLE VI: Coordination Distances to Listed Cation (Å)

	A	B	C	D	E	F
No. to each cation	2	2	2	2	4	
AN-IV (C, M, and P) <sup>a</sup>	2.935(4)	2.971(3)	3.147(3)	3.200(4)	3.272(3)	
AN-IV	2.926(3)	2.959(3)	3.153(2)	3.187(3)	3.282(3)	
KN-AN-IV	2.929(3)	2.976(1)	3.149(2)	3.195(2)	3.286(3)	
No. to each cation	1	2	2	2	2	2
KN-AN-III-a	3.007(3)	2.986(2)	3.022(2)	3.092(2)	3.116(3)	3.217(3)
KN-AN-III-b	2.982(4)	2.982(1)	3.009(3)	3.082(3)	3.109(3)	3.203(3)
KN-AN-III-c	2.977(4)	2.971(2)	3.000(3)	3.077(3)	3.105(3)	3.200(3)
KN-AN-III-d	2.955(5)	2.960(1)	2.987(3)	3.072(4)	3.099(4)	3.191(4)
KN-AN-III-e	2.930(2)	2.953(1)	2.978(2)	3.064(2)	3.103(2)	3.185(2)
KN-AN-III-f	2.918(3)	2.939(1)	2.962(2)	3.041(2)	3.100(2)	3.172(2)
No. to each cation	1	2	2	2	2	
AN-KN-II	2.847(3)	2.856(2)	2.890(2)	2.900(2)	2.935(3)	
KN-II (N and L) <sup>b</sup>	2.828(2)	2.845(4)	2.885(3)	2.884(3)	2.925(1)	
KN-II	2.843(3)	2.848(2)	2.879(2)	2.893(2)	2.925(1)	

For AN-IV type structures

A O(2) at  $x, y, z$  and  $1\frac{1}{2} - x, y, z$

B O(1) at  $x, y, -1 + z$  and  $1 + x, y, -1 + z$

C O(1) at  $1 - x, -y, 1 - z$  and  $1 - x, 1 - y, 1 - z$

D O(2) at  $x, y, -1 + z$  and  $1\frac{1}{2} - x, y, -1 + z$

E O(2) at  $1 - x, -y, -z; 1 - x, 1 - y, -z$

$1\frac{1}{2} - x, -y, -z,$  and  $1\frac{1}{2} - x, 1 - y, -z$

For AN-III type structures

A O(1) at  $-x, 1 - y, 1 - z$

B O(1) at  $x, y, z$  and  $x, 1 + y, z$

C O(2) at  $-\frac{1}{2} + x, 1 + y, \frac{1}{2} - z; -\frac{1}{2} + x, \frac{1}{2} - y, \frac{1}{2} - z$

D O(2) at  $x, 1 + y, z$  and  $x, \frac{1}{2} - y, z$

E O(2) at  $\frac{1}{2} - x, \frac{1}{2} + y, \frac{1}{2} + z; \frac{1}{2} - x, -y, \frac{1}{2} + z$

F O(2) at  $-x, 1 - y, -z; -x, -\frac{1}{2} + y, -z$

For KN-II type structures

A O(1) at  $-\frac{1}{2} + x, y, 1\frac{1}{2} - z$

B O(2) at  $1 - x, 1 - y, 1 - z; 1 - x, \frac{1}{2} - y, 1 - z$

C O(2) at  $\frac{1}{2} - x, -\frac{1}{2} + y, -\frac{1}{2} + z; \frac{1}{2} - x, -y, -\frac{1}{2} + z$

D O(2) at  $x, y, z; x, \frac{1}{2} - y, z$

E O(1) at  $\frac{1}{2} - x, -\frac{1}{2} + y, -\frac{1}{2} + z; \frac{1}{2} - x, \frac{1}{2} + y, -\frac{1}{2} + z$

<sup>a</sup> Reference 8. <sup>b</sup> Reference 10.

decreases as the proportion of cation positions occupied by the smaller potassium ions increases. As expected, ammonium ions appear to increase the formula volume in KN-II; however, contrary to expectation, potassium ions appear to increase the formula volume in AN-IV. Also, note that the

relative size of the formula volumes in the three structure types is the reverse of what would be predicted based solely on the volume of the cations present. That is, AN-IV structures with the most ammonium ions have smaller formula volumes than AN-III structures with more potassium ions,

TABLE VII: Anion-Anion Distances Less Than 3.3 Å

	G	H	I	J
No. to each nitrate	4	2		
AN-IV (C, M, and P) <sup>a</sup>	3.049(4)	3.243		
AN-IV	3.049(4)	3.244(4)		
KN-AN-IV	3.050(3)	3.242(3)		
No. to each nitrate	2	2	2	2
KN-AN-III-a	3.209(3)	3.233(3)	(3.310)	3.274(2)
KN-AN-III-b	3.196(4)	3.219(3)	3.291(3)	3.265(5)
KN-AN-III-c	3.187(4)	3.209(3)	3.286(3)	3.266(4)
KN-AN-III-d	3.184(4)	3.198(3)	3.267(3)	3.275(5)
KN-AN-III-e	3.180(3)	3.192(3)	3.249(3)	3.275(4)
KN-AN-III-f	3.168(3)	3.183(3)	3.235(3)	3.257(4)
No. to each nitrate	2	2		
AN-KN-II	3.230(3)	3.274(3)		
KN-II (N and L) <sup>b</sup>	3.217	3.257		
KN-II	3.219(3)	3.257(3)		
For AN-IV type structures				
G O(2) to O(2) at $1-x, -y, 1-z$ , and at $1-x, 1-y, 1-z$				
H O(1) to O(2) at $x, y, 1+z$ , and at $1/2-x, y, 1+z$				
For AN-III type structures				
G O(1) to N(2) at $-1/2+x, y, 1/2-z$				
H O(1) to O(2) at $-1/2+x, 1/2-y, 1/2-z$ and at $-1/2+x, y, 1/2-z$				
I O(1) to O(2) at $1/2-x, 1/2+y, 1/2+z$ and at $1/2-x, -y, 1/2+z$				
J O(2) to O(2) at $-x, -y, -z$				
For KN-II type structures				
G N(2) to N(2) at $-1/2+x, y, 1/2-z$ and at $1/2+x, y, 1/2-z$				
H O(2) to O(2) at $x, 1/2-y, z$				

<sup>a</sup> Reference 8. <sup>b</sup> Reference 10.

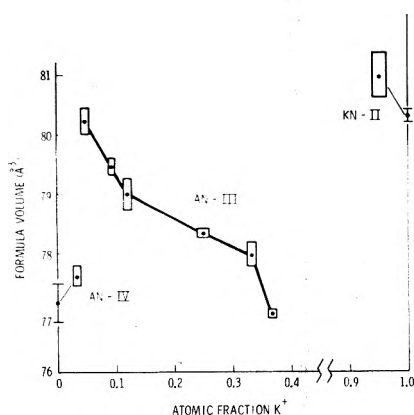


Figure 4. Crystal volume per formula unit vs. fraction of cation sites occupied by potassium ion.

which in turn have smaller volumes than KN-II with nearly all potassium ions.

The volumes of the first five AN-III type solid solutions form a logical trend with increasing potassium content; that is, decreasing at a decreasing rate (see Table I and Figure 4). However, the last point, KN-AN-III-f, does not follow this trend. A possible explanation is that this composition is not thermodynamically stable at room temperature, but that this crystal formed at a higher temperature and then supercooled. The evidence to support this postulate is that crystals AN-KN-II and KN-AN-III-e were selected from successive crops produced by evaporation of the same solution at room temperature. Therefore, the composition of KN-AN-III-e might be expected to be near the limit of solubility of KN in AN-III at room temperature. On the other hand, KN-AN-III-f was selected from a batch of

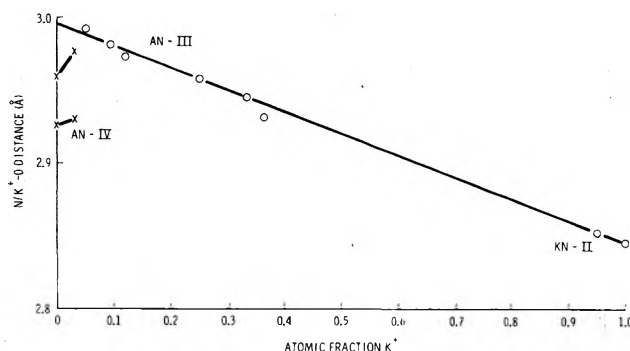


Figure 5. Shortest cation-oxygen distances vs. fraction of cation sites occupied by potassium ion.

crystals which grew either during or after cooling of a solution of a 30/70 wt % mixture of KN and AN heated to about 80°.

If these structures are controlled primarily by electrostatic forces, the oxygen atoms should form coordination spheres around the cations such that the cation-oxygen distances are equal to the sum of the effective ionic radii. The observed range of cation-oxygen distances would be explained by the fact that the oxygen atoms are parts of rather bulky nitrate ions and not separate spherical ions. In this case, the shortest distances should be the best measure of the contact distance. The circles in Figure 5 are a plot of the average of the three shortest cation-oxygen distances (columns A and B in Table VI) in the AN-III and KN-II type structures vs. the atomic fraction potassium ion at the cation sites. Excluding KN-AN-III-f for the reasons cited above, a least-squares fit of these points to a straight line gives the following:

$$D = 2.996 - 0.1501F$$

where  $D$  is the interionic distance and  $F$  is the atomic fraction potassium. This line is shown in Figure 5.

This relation gives 2.846 Å as the interionic contact distance between a potassium ion and a nitrate oxygen atom ( $F = 1.000$ ). Using the value given by Pauling<sup>16</sup> for the ionic radius of potassium, 1.331 Å, one obtains 1.515 Å for the effective ionic radius of a nitrate oxygen atom. The extrapolated value for the ionic contact distance between an ammonium ion and a nitrate oxygen atom is 2.996 Å ( $F = 0.000$ ). Subtracting 1.515 Å gives 1.481 Å as the effective ionic radius of the ammonium ion, which is exactly the value given by Pauling.<sup>16</sup> In view of the accuracy of the distances and atomic compositions used to make this correlation, the precision of this agreement is fortuitous. However, it indicates that the unit cell dimensions and atomic positions of the AN-III type solid solution structures can be explained by assuming that the ammonium-potassium cation behaves as a single entity whose effective radius is a linear function of the potassium content.

An indication that 1.515 Å is a reasonable value for the ionic radius of the oxygen atom is the fact that twice this value, 3.030 Å, is slightly smaller than the shortest distance between oxygen atoms in any of the structures, 3.050 Å (see Table VII):

The  $\times$  points in Figure 5 mark the shortest distances between cation centers and oxygen atoms in the AN-IV type structures (A and B in Table VII). These distances are shorter than would be predicted by the relation given above which correlates the distances found in the AN-III and KN-II type structures. However, distance B involves hydrogen bonding<sup>9</sup> and, if the hydrogen atom positions are stabilized by hydrogen bonding, A is a contact distance between an oxygen atom and the ammonium nitrogen atom instead of the ammonium ion acting as a unit.

Because the atomic positions in the AN-III type solid solutions do not change significantly with potassium content, the positions listed for KN-AN-III-a at room temperature ( $22 \pm 2^\circ$ ) are probably a better approximation of the values for AN-III above the transition temperature ( $32.23^\circ$ ) than those reported in 1947<sup>11</sup> based on less accurate X-ray data. The positional parameters found for KN-II at  $100^\circ$  are not grossly different from those found at  $25^\circ$ .<sup>10</sup> In any case, the transition at  $32.23^\circ$  appears to be from a polymorph (AN-IV) in which hydrogen bonding is an important factor to one in which it is not (AN-III). The extra stabilization energy provided by hydrogen bond formation in AN-IV must be partially offset by the greater electrostatic repulsion due to shorter distances between oxygen atoms carrying partial

negative charges (those designated G in Table VII). When the hydrogen bond energy is sufficiently lowered due to increased thermal motion of the hydrogen atoms, AN-III becomes the lower energy (stable) form. As potassium replaces ammonium ion in a KN-AN-IV solid solution, the hydrogen bonding energy is "diluted" and the temperature at which KN-AN-III becomes the lower energy form is lowered. At an atomic fraction of between 0.032 and 0.050 (if crystals KN-AN-IV and KN-AN-III-a from this study were both thermodynamically stable), KN-AN-III becomes the stable polymorph at room temperature.

*Acknowledgment.* The authors gratefully acknowledge financial support from the Army Materiel Command, Picatinny Arsenal, Dover, N.J. and the Naval Ordnance Systems Command, Washington, D.C.

*Supplementary Material Available.* A listing of structure factor amplitudes will appear following these pages in the microfilm edition of this volume of the journal. Photocopies of the supplementary material from this paper only or microfiche (105 × 148 mm, 24× reduction, negatives) containing all of the supplementary material for the papers in this issue may be obtained from the Journals Department, American Chemical Society, 1155 16th St., N.W., Washington, D. C. 20036. Remit check or money order for \$8.00 for photocopy or \$2.00 for microfiche, referring to code number JPC-75-249.

## References and Notes

- (1) T. Seiyama and N. Yamazoe, *J. Crystal Growth*, **2**, 255 (1968).
- (2) F. Jona and G. Shirane, "Ferroelectric Crystals," Pergamon Press, Oxford, 1962.
- (3) J. Whetstone, *Can. J. Res.*, **26B**, 499 (1948).
- (4) E. Jancke, H. Hamacher, and E. Rahlfs, *Z. Anorg. Allg. Chem.*, **206**, 357 (1932).
- (5) R. V. Coates and J. M. Crewe, *Nature (London)*, **190**, 1190 (1961).
- (6) C. D. West, *J. Amer. Chem. Soc.*, **54**, 2256 (1932).
- (7) S. B. Hendricks, E. Pösnjak, and F. C. Kracek, *J. Amer. Chem. Soc.*, **54**, 2766 (1932).
- (8) C. S. Choi, J. E. Mapes, and E. Prince, *Acta Crystallogr., Sect. B*, **28**, 1357 (1972).
- (9) D. A. Edwards, *Z. Kristallogr. Kristallgeom.*, **80**, 154 (1931).
- (10) J. K. Nimmo and B. W. Lucas, *J. Phys. C: Solid State Phys.*, **6**, 201 (1973).
- (11) T. H. Goodwin and J. Whetstone, *J. Chem. Soc.*, 1455 (1947).
- (12) J. Morand, *Ann. Chem. (Paris)*, **10**, 1018 (1955).
- (13) "International Tables for X-ray Crystallography," Vol. III, Kynoch Press, Birmingham, England, 1962.
- (14) J. M. Stewart, G. J. Kruger, H. L. Ammon, C. Dickinson, and S. R. Hall, Technical Report No. TR-192, Computer Science Center of the University of Maryland, 1972.
- (15) See paragraph at end of text regarding supplementary material.
- (16) L. Pauling, "Nature of the Chemical Bond," 3rd ed, Cornell University Press, Ithaca, N.Y. 1960.

# Electrical Conductances of Some Aqueous Rare Earth Electrolyte Solutions at 25°. III. The Rare Earth Nitrates<sup>1</sup>

J. A. Rard and F. H. Spedding\*

Ames Laboratory—USAEC and Department of Chemistry, Iowa State University, Ames, Iowa 50010 (Received August 9, 1974)

Publication costs assisted by the U.S. Atomic Energy Commission

The electrical conductances of the aqueous trinitrates of La, Pr, Nd, Sm, Gd, Tb, Dy, Ho, Er, Yb, and Lu were measured over the concentration range of approximately 0.004 *m* to saturation at 25°. Below 0.9 *m* the equivalent conductances, at constant molality, decrease from La to Sm and then rise to Lu. Above 0.9 *m*, the equivalent conductances increase from La to Lu. These results imply that in dilute solutions the amount of complex formation increases from La to Sm and then decreases to Lu while, at higher concentrations, the amount of complex formation decreases from La to Lu. The trends in the aqueous rare earth nitrate series are discussed in terms of changes in inner- and outer-sphere coordination across the rare earth series.

## Introduction

The major differences between the rare earth nitrate and the rare earth chloride and perchlorate systems arise from the larger amount of complex formation present for the nitrates and the greater strength of the ionic interactions involved. In dilute nitrate solutions, many workers believe that a mixture of inner- and outer-sphere complexes occurs with the predominant species being outer sphere while rare earth chloride and perchlorate solutions are believed to form only outer-sphere complexes. Evidence for outer-sphere rare earth nitrate complexes includes Nd<sup>3+</sup> absorption spectra<sup>2,3</sup> and Eu<sup>3+</sup> thermodynamic data.<sup>4</sup> Ultrasonic absorption data<sup>5,6</sup> have been interpreted as showing a much larger fraction of inner-sphere coordination. Electrical conductance results for dilute rare earth nitrate solutions<sup>7,8</sup> indicate that complex formation is beginning to play a major role even at very low concentrations.

In more concentrated nitrate solutions nmr,<sup>9-11</sup> optical absorbance,<sup>9</sup> and Raman data<sup>12-14</sup> indicate that the predominant complex is inner sphere with binding probably occurring through the oxygens of the nitrates.<sup>13,14</sup> In concentrated solutions it has been suggested that two nitrates may be in the rare earth inner coordination sphere.<sup>14</sup> Neutral<sup>13</sup> and even negative charged species<sup>15</sup> have been suggested when a considerable excess of nitrate ions are present. Three doubly coordinated nitrates and four water molecules have been found adjacent to the rare earth ion in the hydrated Pr and Nd crystals.<sup>16</sup>

The first formation constants for the rare earth nitrate complexes have been measured at an ionic strength of one using liquid extraction techniques.<sup>17</sup> A maximum in complex formation was found in the vicinity of Sm, with the heavy rare earths complexed less than the light ones. At an ionic strength of four, visible spectra measurements seem to show a similar trend in the first formation constants.<sup>18,19</sup>

The electrical conductance of a salt solution is a sensitive function of the amount and nature of anion-cation complexes present. In an earlier paper, the extensively complexed rare earth sulfate systems were studied<sup>20</sup> but the limited solubilities of the sulfates allow little flexibility for studying inner-sphere complex formation in solutions of the stoichiometric salts. A pressure study of the Eu sulfate

complexes indicates that these complexes are probably predominantly inner sphere.<sup>21</sup> In this present paper, conductance data are presented for the aqueous rare earth nitrates in which both outer- and inner-sphere complexes are believed to occur by moderate concentrations.

## Experimental Section

The equipment, techniques, and procedures are the same as described in the perchlorate paper.<sup>22</sup> Solutions of the stoichiometric salts were prepared by the method of Spedding, Pikal, and Ayers.<sup>23</sup> Each specific conductivity was calculated from the average resistance of three or four measurements. These average resistances are reliable to  $\pm 0.02\%$  for concentrations above 0.01 *m*. Below 0.01 *m*, the cell resistances were measured in parallel with several of the bridge resistors and the conductivities are reliable only to  $\pm 0.2\%$ . The oil bath temperature was controlled to  $24.99 \pm 0.01^\circ$ . Each concentrated stock and saturated solution was analyzed by both EDTA<sup>24</sup> and sulfate<sup>23</sup> methods and is reliable to  $\pm 0.1\%$  or better. When sulfate analyses were performed, the rare earth nitrate samples were first predecomposed with HCl, followed by evaporation to dryness, before the H<sub>2</sub>SO<sub>4</sub> additions were made. This treatment eliminated the possibility of nitrate ion coprecipitation. All dilutions were prepared by weight from samples of the appropriate stock solution and conductivity water. The conductance data for each salt, except for the saturated solution, are therefore self consistent to a greater degree than the absolute error in the stock concentration indicates.

Above 5.5 *m*, the viscosities of the rare earth nitrate solutions are quite large so the filling and rinsing of the capillary cells becomes more difficult. By 6.0 *m*, filling and rinsing becomes so difficult that only three place accuracy was obtainable in the resistance measurements. This situation obviously only occurs for the concentrated Yb(NO<sub>3</sub>)<sub>3</sub> and Lu(NO<sub>3</sub>)<sub>3</sub> solutions.

## Errors and Data Treatment

The calculations and error treatments were done in the same manner as for the perchlorates<sup>22</sup> and errors of similar size were obtained. The density data of Spedding and co-workers<sup>25</sup> were fitted to polynomial equations of the form

TABLE III: Conductance Polynomial Coefficients for Nitrates

Salt	$B_0/B_4$	$B_1/B_5$	$B_2/B_6$	$B_3/B_7$
La(NO <sub>3</sub> ) <sub>3</sub>	115.952716	-175.225859	279.429544	-390.538087
	314.552366	-139.465816	32.3516152	-3.09424485
Pr(NO <sub>3</sub> ) <sub>3</sub>	113.840235	-170.310674	251.818908	-319.065783
	234.099819	-94.4325869	19.8816906	-1.72486870
Nd(NO <sub>3</sub> ) <sub>3</sub>	113.626725	-177.045110	266.598683	-327.541711
	232.686311	-91.3287088	18.7648090	-1.59022150
Sm(NO <sub>3</sub> ) <sub>3</sub>	112.585469	-180.137332	273.924249	-332.450421
	238.721067	-98.0212982	21.8637691	-2.08358289
Gd(NO <sub>3</sub> ) <sub>3</sub>	113.154322	-173.936802	268.594652	-342.006532
	256.769865	-109.871081	25.4419662	-2.50193664
Tb(NO <sub>3</sub> ) <sub>3</sub>	113.040173	-163.627147	252.776985	-330.248694
	247.421721	-103.055855	22.7969831	-2.11472803
Dy(NO <sub>3</sub> ) <sub>3</sub>	113.806350	-164.065631	267.431681	-361.512638
	274.438686	-114.956755	25.4972522	-2.36944647
Ho(NO <sub>3</sub> ) <sub>3</sub>	113.768854	-159.363170	255.234721	-333.206061
	237.125233	-90.3121540	17.6349871	-1.39602299
Er(NO <sub>3</sub> ) <sub>3</sub>	113.920368	-157.910509	254.067972	-326.107978
	224.113480	-81.1431465	14.7733427	-1.06139279
Yb(NO <sub>3</sub> ) <sub>3</sub>	113.571797	-152.986021	242.129516	-304.408444
	203.662033	-71.7685022	12.7891347	-0.911881200
Lu(NO <sub>3</sub> ) <sub>3</sub>	113.029556	-148.800824	226.898044	-277.832674
	180.229400	-60.8685888	10.2220201	-0.669968973

$$d = \sum_{i=0}^5 A_i m^i \quad (1)$$

where  $m$  is the molality. The resulting coefficients are listed in Table I.<sup>26</sup> The densities obtained from eq 1 were used in calculating the equivalent conductances of the solutions studied.

The conductance data are reported in Table II.<sup>26</sup> For each salt 33–36 concentrations were run. The units of the specific conductivity,  $L$ , are (absolute ohm)<sup>-1</sup> cm<sup>-1</sup> and the units of the equivalent conductance,  $\Lambda$ , are (absolute ohm)<sup>-1</sup> cm<sup>2</sup> equiv<sup>-1</sup>. Seventh-order polynomial equations of the form

$$\Lambda = \sum_{i=0}^7 B_i m^{i/2} \quad (2)$$

were used to fit the equivalent conductance data above 0.1  $m$ . These coefficients are listed in Table III and the saturated solution molalities, to be used with eq 1 and 2, are given in Table IV. The inverse square of the probable error in the equivalent conductance was used as the weighting factor for each value. The probable errors in the equivalent conductance were calculated to range from 0.04 ohm<sup>-1</sup> cm<sup>2</sup> equiv<sup>-1</sup> at 0.05  $m$  to less than 0.01 near saturation. Equation 2 represents the equivalent conductances within the experimental error of the measurements.

Relative per cent differences were calculated from the equation

$$\frac{\Lambda_{\text{RE}(\text{NO}_3)_3} - \Lambda_{\text{Lu}(\text{NO}_3)_3}}{\Lambda_{\text{Lu}(\text{NO}_3)_3}} \times 100 \quad (3)$$

where RE represents the rare earth of interest. These differences allow the data to be presented in convenient graphical form. The full accuracy of the conductance data cannot be seen on a direct plot of the data but the real differences between the various rare earth nitrates can be clearly seen on graphs of these per cent differences.

TABLE IV: Aqueous Rare Earth Nitrate Molal Solubilities at 25°

Rare earth	Molality	Rare earth	Molality
La	4.6100	Dy	4.7382
Pr	5.0166	Ho	5.0183
Nd	4.6184	Er	5.4348
Sm	4.2811	Tm	5.9483
Gd	4.3766	Yb	6.6500
Tb	4.5395	Lu	6.8219

The dilute solution conductances of seven of the rare earth nitrates studied in this research have been previously reported.<sup>7,8,27</sup> The very dilute solution resistances reported here were measured in parallel with some of the bridge resistors and their conductances are only reliable to 0.2%. The conductances reported in the literature should be reliable to about 0.1% so the two sets of dilute data should all agree to within 0.3% in the region of overlap. This was found to be the case.

## Results

Figure 1 is a plot of the equivalent conductances of lutetium perchlorate,<sup>22</sup> chloride,<sup>28</sup> and nitrate as a function of the molality. The order in which these curves occur as a function of the anion is the same for each of the other rare earths.

Figure 2 is a plot of the relative per cent differences from La to Sm and Figure 3 gives the corresponding curves from Sm to Lu. It should be noted that the curves from La to Sm cross at the same concentration, within experimental error. From Sm on, except for Yb–Lu, the per cent differences are cleanly separate. Dilute solution conductance data<sup>27</sup> indicate that other crossovers are beginning to occur by 0.005  $m$  and most of the conductances, at concentrations studied in this research, occur in different order from that observed at infinite dilution.

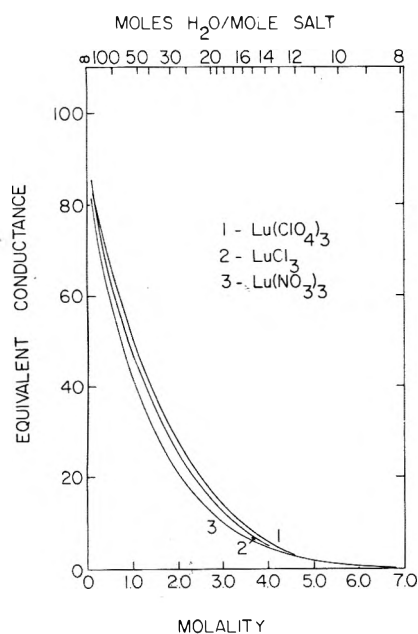


Figure 1. Equivalent conductances of three aqueous lutetium electrolytes.

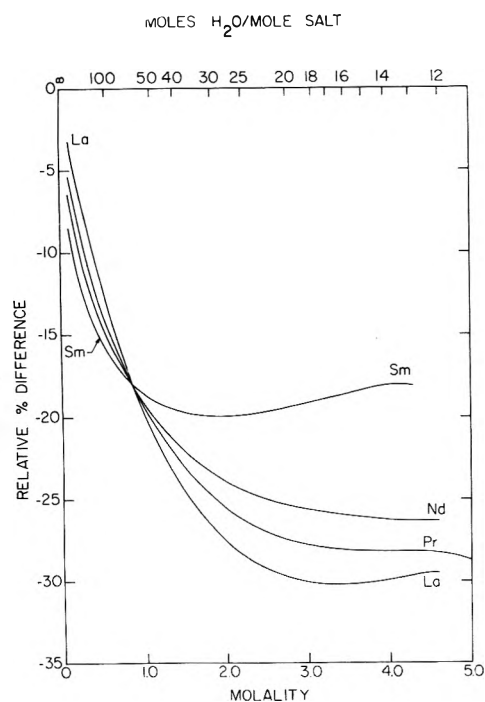


Figure 2. Per cent differences in equivalent conductances relative to  $\text{Lu}(\text{NO}_3)_3$  for some light rare earth nitrates.

The relative per cent differences are given at several molalities in Figures 4 and 5. At 0.5 *m* the nitrate conductances decrease from La to Sm (and probably Eu) and then rise to Lu (the rare earth sulfate conductances<sup>20</sup> also fall in this order). At 0.9 *m* the nitrate conductances are essentially constant from La to Sm and then rise to Lu. At higher molalities the conductances increase monotonically from La to Lu. By 4.0 *m* the conductances "bulge upward" in the middle of the rare earth series. The nitrate solution viscosity data<sup>29</sup> also exhibit a "bulge upward" in the middle of the series at high concentrations, indicating that this slight modification in shape is real.

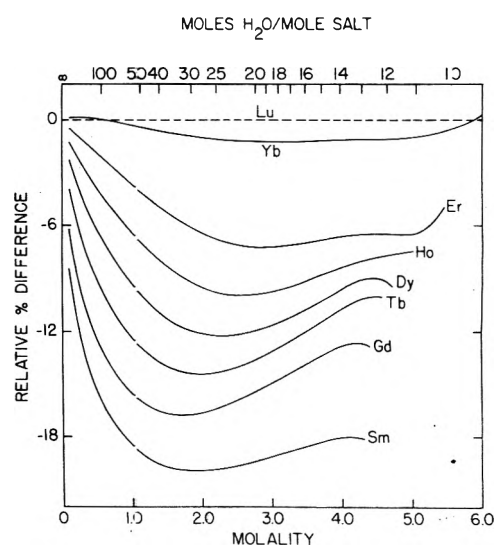


Figure 3. Per cent differences in equivalent conductances relative to  $\text{Lu}(\text{NO}_3)_3$  for some middle and heavy rare earth nitrates.

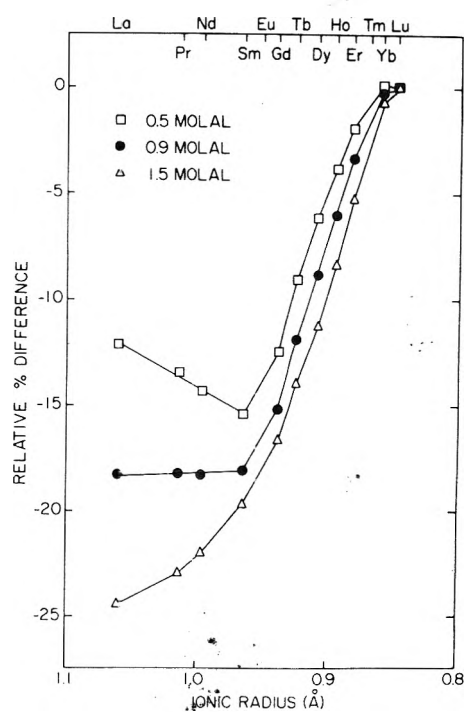


Figure 4. Relative per cent differences in equivalent conductances at constant molality for the rare earth nitrates.

In order to emphasize the differences in the nitrate transport data from that of the chlorides and perchlorates, series plots of the equivalent conductances and relative viscosities<sup>22,28-32</sup> are given at 1.2 and 4.2 *m* in Figures 6 and 7. From dilute solution to over 2.0 *m*, the chloride and perchlorate conductance and viscosity series plots have a distinct S shape. The overall decrease in conductance and increase in viscosity were interpreted as being due to an increase in the net hydration of the rare earth ions across the rare earth series as the lanthanide contraction occurs. The possibility of an inner-sphere hydration decrease between Nd and Tb<sup>23</sup> has been suggested from apparent molal volume data. An inner-sphere hydration change of this type would also modify the total hydration and would cause the

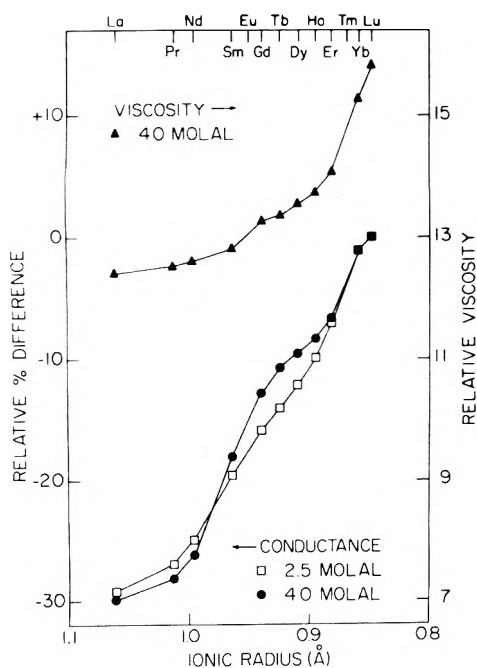


Figure 5. Relative per cent differences in equivalent conductances and relative viscosities at constant molality for the rare earth nitrates.

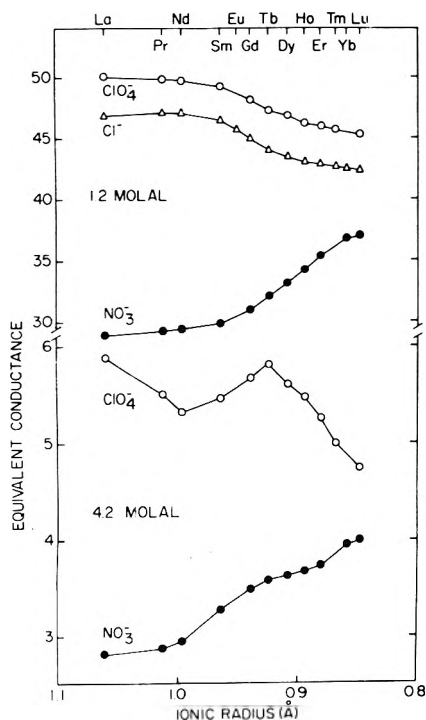


Figure 6. Equivalent conductances of rare earth chlorides, perchlorates, and nitrates at constant molality.

conductance to change more rapidly with ionic radius, giving rise to the S shape.

As seen in Figures 6 and 7, the perchlorate conductances and viscosities show a distinct two-series trend at 4.2 *m*. This two-series trend is present in its complete form in the perchlorate conductances by 3.5 *m* and in the viscosities by 3.7 *m* and persists to saturation for both properties. By 3.0 *m* these two properties are already showing intermediate behavior between the low concentration S shape and the high concentration two-series shape. The high concentra-

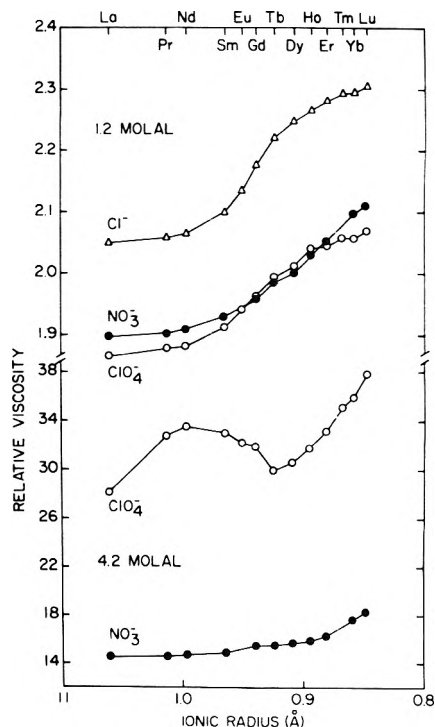


Figure 7. Relative viscosities of rare earth chlorides, perchlorates, and nitrates at constant molality.

tion modification in behavior is less well developed in the chlorides<sup>28,31</sup> but would presumably appear in its complete form if the chlorides were more soluble.

At high concentrations, water sharing between ions becomes extensive and the overall hydration increase across the rare earth chloride and perchlorate series can no longer occur. However, the increase in the rare earth ion's surface charge density across the series will cause the strength of outer-sphere ion pairs, formed at these high concentrations, to increase across the series. Transport in these solutions should involve the breaking and re-forming of these ion pairs. The increasing strength of these ion pairs gives rise to the trends from La to Nd and Tb to Lu in the perchlorate solutions. In these concentrated solutions the gradual release of the inner-sphere water between Nd and Tb helps to reduce the extent of ion-pair formation and acts to reduce the viscosity. The net result is the reversal in trends between Nd and Tb observed in the perchlorate data.

In Figure 8 the pH values of five of the rare earth nitrate solutions of the stoichiometric salts are shown as a function of the molality. These pH values indicate that the nitrate solutions hydrolyze less than the corresponding chloride and perchlorate solutions at equal molalities.<sup>22,28</sup> This is to be expected if the nitrate ions penetrate the inner sphere of the rare earth ions since the lower cation charge should result in less hydrolysis.

As seen above, the rare earth nitrate series trends are considerably different than the chlorides and perchlorates. The model used to explain the rare earth chloride and perchlorate transport property series trends involved the retention of the rare earth inner hydration sphere water molecules up to saturation and this has been confirmed by X-ray diffraction studies.<sup>33,34</sup> Penetration of the rare earth inner sphere by nitrate ions would displace water molecules and give rise to markedly different transport property behavior.

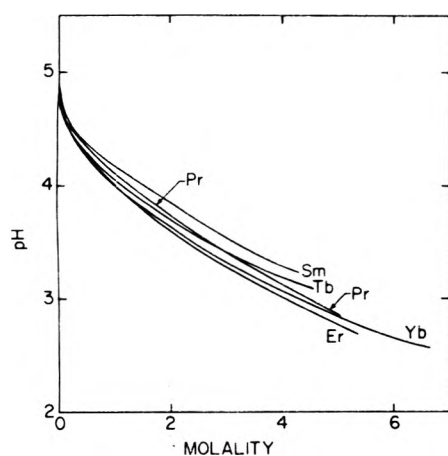


Figure 8. The pH values of some rare earth nitrates as a function of the molality.

The electrical conductance of a salt depends on the charge, mobility, and concentration of each ionic species present in solution. The mobility of a hydrated nitrate or hydrogen ion should be similar for each rare earth nitrate solution, at constant molality, with a possible gradual decrease across the series as the viscosity increases from La to Lu. From the chloride and perchlorate solution data we saw that the conductance decreases across the series for the hydrated rare earth ions. For complexes having the same inner-sphere stoichiometry (and net charge), we would expect the same consideration to apply since the surface charge density on similar species should still increase across the series. Consequently, the decrease in conductance at low concentrations, from La to Sm, and the increase from Sm to Lu can only be due to an increase in the amount of complex formation from La to Sm and a decrease from Sm to Lu. That is, the average nitrate ligand number increases from La to Sm and then decreases to Lu. At higher concentrations the conductance data indicate that the amount of complex formation decreases from La to Lu.

The correctness of this interpretation at lower concentrations is indicated by the presence of a maximum in the stability constants for the first rare earth nitrate complex at ionic strengths of one<sup>4,17</sup> and four.<sup>18,19</sup> The maximum, in each case, occurred in the vicinity of Sm and the heavy rare earths were less complexed than the light ones. The stability constants at an ionic strength of one have been interpreted as being due to predominantly outer-sphere ion pairing with possibly a few per cent of inner-sphere complexes.<sup>3</sup>

When inner-sphere complex formation becomes important, the same trend can hardly be expected to persist. Abrahamer and Marcus<sup>9</sup> suggested the possibility that both the total ligand number and the inner-sphere ligand number decrease across the rare earth series, from nmr, spectral, and electromigration data for concentrated solutions containing an excess of nitrate ions. From the data reported here it is clear that the maximum in complex formation disappears by 0.9 *m* for solutions of the stoichiometric salts and *the average ligand number does indeed decrease from La to Lu at higher concentrations.* It is interesting to note that some nonaqueous rare earth nitrate solutions resemble the concentrated aqueous rare earth nitrates in having the amount of complex formation decrease across the rare earth series.<sup>35,36</sup>

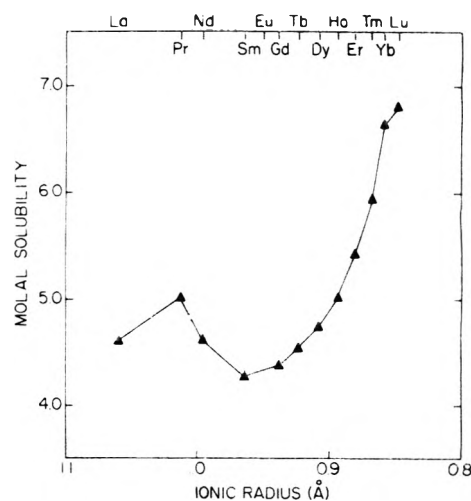


Figure 9. Solubilities of the aqueous rare earth nitrates at 25°.

Since the amount of complex formation decreases across the rare earth nitrate series, at high concentrations, one would expect that the number of water molecules bound by the heavy rare earths to be greater than the number bound by the light rare earths at equal molalities. A similar, but smaller effect, is the increase in the strength of the ion-water interaction across the series, for species with the same inner-sphere coordination, due to the decreasing ionic radius. From these elementary considerations one might expect the viscosities of the rare earth nitrates to increase monotonically across the rare earth series since the number of water molecules associated with the cation increases from La to Lu. As seen in Figures 5 and 7, this does occur. By a similar argument, the activity of water in rare earth nitrate solutions, at constant molalities, should decrease across the series. Results for three rare earth nitrates<sup>37</sup> indicate that this is the case. In addition, the partial molal volume of water in rare earth nitrate solutions, at high concentrations, indicate that the amount of electrostriction increases across the rare earth series.<sup>25</sup>

After appreciable amounts of inner-sphere nitrate complexes form, the effect of the lanthanide contraction will now possibly be exerted mainly on the inner-sphere nitrates, rather than the water molecules, and result in a "squeezing out" of the inner-sphere nitrates across the rare earth series. Obviously, any change in the position of nitrate ions may involve replacement by water molecules.

At high concentrations polymeric species have been suggested.<sup>14</sup> The very low conductances observed for the highly concentrated  $\text{Yb}(\text{NO}_3)_3$  and  $\text{Lu}(\text{NO}_3)_3$  solutions indicate that appreciable amounts of neutral hydrated species may form at these high concentrations.

From Figure 3 it appears that the  $\text{Yb}(\text{NO}_3)_3$  conductance crosses the  $\text{Lu}(\text{NO}_3)_3$  conductance curve at high and low concentrations. At 6.0 *m* the conductances are quite low and are reliable to three significant figures so the high concentration crossover could well be real since similar reversals are observed for other properties.

Figure 9 is a plot of the molal solubilities of the rare earth nitrates at 25°. It is interesting to note that the solubility variation across the rare earth series is qualitatively similar to the rare earth chloride<sup>28</sup> and sulfate<sup>38</sup> solubilities but not to the rare earth perchlorate solubilities.<sup>22</sup>

*Acknowledgments.* The authors thank Dr. A. Habenschuss for helpful suggestions concerning this manuscript.

The rare earth oxides were purified by ion-exchange methods by Dr. J. E. Powell's group.

*Supplementary Material Available.* Tables I and II, listings of the density coefficients and conductance data, will appear immediately following this article in the microfilm edition of the journal. Photocopies of the supplementary material from this paper only or microfiche (105 × 148 mm, 24× reduction, negatives) containing all of the supplementary material for the papers in this issue may be obtained from the Journals Department, American Chemical Society, 1155 16th St., N.W., Washington, D.C., 20036. Remit check or money order for \$4.00 for photocopy or \$2.00 for microfiche, referring to code number JPC-75-257.

## References and Notes

- (1) This work was performed at the Ames Laboratory of the U. S. Atomic Energy Commission. This paper is based, in part, on the Ph.D. dissertation of J. A. Rard, Iowa State University, Ames, Iowa, Feb 1973.
- (2) G. R. Choppin, D. E. Henrie, and K. Buijs, *Inorg. Chem.*, **5**, 1743 (1966).
- (3) K. Bukietynska and G. R. Choppin, *J. Chem. Phys.*, **52**, 2875 (1970).
- (4) G. R. Choppin and W. F. Strazik, *Inorg. Chem.*, **4**, 1250 (1965).
- (5) R. Garnsey and D. W. Ebdon, *J. Amer. Chem. Soc.*, **91**, 50 (1969).
- (6) H. B. Silber, N. Scheinin, G. A. Atkinson, and J. J. Grecsek, *J. Chem. Soc., Faraday Trans. 1*, **68**, 1200 (1972).
- (7) F. H. Spedding and S. Jaffe, *J. Amer. Chem. Soc.*, **76**, 884 (1954).
- (8) D. J. Heiser, Ph.D. Thesis, Iowa State University, Ames, Iowa, 1957.
- (9) I. Abrahamer and Y. Marcus, *Inorg. Chem.*, **6**, 2103 (1967).
- (10) J. Reuben and D. Fiat, *J. Chem. Phys.*, **51**, 4909 (1969).
- (11) K. Nakamura and K. Kawamura, *Bull. Chem. Soc. Jap.*, **44**, 330 (1971).
- (12) R. E. Hester and R. A. Plane, *Inorg. Chem.*, **3**, 769 (1964).
- (13) J. Knoeck, *Anal. Chem.*, **41**, 2069 (1969).
- (14) D. L. Nelson and D. E. Irish, *J. Chem. Phys.*, **54**, 4479 (1971).
- (15) Y. Marcus and I. Abrahamer, *J. Inorg. Nucl. Chem.*, **22**, 141 (1961).
- (16) I. M. Rumanova, G. F. Voldina, and N. V. Belov, *Kristallografiya*, **9**, 624, 642 (1964); translated in *Crystallography*, **9**, 545 (1965).
- (17) D. F. Peppard, G. W. Mason, and I. Hucher, *J. Inorg. Nucl. Chem.*, **24**, 881 (1962).
- (18) N. A. Coward and R. W. Kiser, *J. Phys. Chem.*, **70**, 213 (1966).
- (19) A. Anagnostopoulos and P. O. Sakellaris, *J. Inorg. Nucl. Chem.*, **32**, 1740 (1970).
- (20) F. H. Spedding and S. Jaffe, *J. Amer. Chem. Soc.*, **76**, 882 (1954).
- (21) C. F. Hale and F. H. Spedding, *J. Phys. Chem.*, **76**, 2925 (1972).
- (22) F. H. Spedding and J. A. Rard, *J. Phys. Chem.*, **78**, 1435 (1974).
- (23) F. H. Spedding, M. J. Pikal, and B. O. Ayers, *J. Phys. Chem.*, **70**, 2440 (1966).
- (24) F. H. Spedding, P. F. Cullen, and A. Habenschuss, *J. Phys. Chem.*, **78**, 1106 (1974).
- (25) F. H. Spedding, L. E. Shiers, M. A. Brown, J. L. Baker, L. Gutierrez, and A. Habenschuss, to be submitted to *J. Phys. Chem.*
- (26) See paragraph at end of text regarding supplementary material.
- (27) F. H. Spedding and G. Atkinson in "The Structure of Electrolytic Solutions," W. J. Hamer, Ed., Wiley, New York, N.Y., 1959, Chapter 22.
- (28) F. H. Spedding, J. A. Rard, and V. W. Saeger, *J. Chem. Eng. Data*, **19**, 373 (1974).
- (29) F. H. Spedding, L. E. Shiers, and J. A. Rard, accepted for publication by *J. Chem. Eng. Data*.
- (30) F. H. Spedding and M. J. Pikal, *J. Phys. Chem.*, **70**, 2430 (1966).
- (31) F. H. Spedding, D. L. Witte, L. E. Shiers, and J. A. Rard, *J. Chem. Eng. Data*, **19**, 369 (1974).
- (32) F. H. Spedding, L. E. Shiers, and J. A. Rard, accepted for publication by *J. Chem. Eng. Data*.
- (33) L. L. Martin and F. H. Spedding, submitted to *J. Chem. Phys.*
- (34) L. L. Martin and F. H. Spedding, unpublished results.
- (35) D. G. Karraker, *J. Chem. Educ.*, **47**, 424 (1970).
- (36) J. A. Sylvanovich Jr., and S. K. Madan, *J. Inorg. Nucl. Chem.*, **34**, 1675 (1972).
- (37) F. H. Spedding, L. E. Shiers, and J. A. Rard, unpublished results.
- (38) The sulfate solubility curve in ref 20 was inadvertently misplotted and all points should be displaced to the next lowest rare earth.

## A Limiting Law for the Conductance of the Rod Model of a Salt-Free Polyelectrolyte Solution

Gerald S. Manning

School of Chemistry, Rutgers University, New Brunswick, New Jersey 08903 (Received July 9, 1974)

The polyion conductance is calculated for the rod model at low concentration. The electrophoretic effect is taken from Henry's results, while the relaxation effect is computed from the effective field, previously calculated, which retards the motion of the counterions. Taken together with a previous calculation of counterion motion, the present result leads to a complete theoretical equation for the equivalent conductance  $\Lambda$  of salt-free polyelectrolyte solutions with counterions of arbitrary valence. Since the expression contains the radius of the cylinder which represents the polyion, an alternate form is obtained, which depends only on the concentration and charge density of the cylinder, and which predicts that a certain function of  $\Lambda$  is linearly dependent on  $\log c$  at low concentration.

### Introduction

The following equation has been used for many years<sup>1-3</sup> to describe the conductance of solutions of a polyelectrolyte salt with no added simple salt:

$$\Lambda = f(\lambda_c^0 + \lambda_p) \quad (1)$$

where  $\Lambda$  is the equivalent conductance of the salt in solution,  $\lambda_c^0$  is the equivalent conductance of the counterion in pure solvent,  $\lambda_p$  is the equivalent conductance of the po-

lyion species in the solution, and  $f$  is a parameter which in general is equal to  $(\lambda_c + \lambda_p)/(\lambda_c^0 + \lambda_p)$ , since the numerator, where  $\lambda_c$  is the equivalent conductance of the counterion in solution, is a generally valid expression for  $\Lambda$ .

From standard electrochemical definitions it is easy to see that eq 1 follows from the assumption<sup>1,4</sup> that the structure of the solution is such that the fraction  $(1 - f)$  of the counterions is bound to the polyion while the fraction  $f$  is free (uninfluenced by interactions with the polyion). How-

ever, modern polyelectrolyte theory indicates that this description of the structure is certainly incorrect, since even if a fraction of the counterions is bound, the remaining fraction must interact with the uncompensated charge on the polyion and hence cannot be "free." Equation 1 may also be derived by a phenomenological approach<sup>5</sup> which makes no *a priori* assumption about counterion binding; the phenomenological theory indicates that

$$f = D_c/D_c^0 \quad (2)$$

where  $D_c$  is the self-diffusion coefficient of the counterion in solution and  $D_c^0$  is the corresponding value in pure solvent. Finally, eq 1 has been derived by a molecular theory<sup>6,7</sup> which also indicates that eq 2 is satisfied and, moreover, provides an expression for  $f$  in terms of molecular properties.

The key parameter of the molecular theory is

$$\xi = e^2/\epsilon k T b \quad (3)$$

where  $e$  is the protonic charge,  $\epsilon$  the bulk dielectric constant,  $k$  Boltzmann's constant,  $T$  the absolute temperature, and  $b$  the spacing between charged groups taken along the axis of the polyion chain. The theory indicates that for  $\xi < |z_d|^{-1}$ , where  $z_c$  is the valence of the counterion, polyion-counterion interactions are governed entirely by Debye-Hückel atmosphere effects, while if  $\xi > |z_d|^{-1}$ , counterions condense on the polyion until  $\xi_{\text{net}} = |z_d|^{-1}$ , the remaining counterions again being in a Debye-Hückel atmosphere. Then

$$f = 0.866 |z_c|^{-1} \xi^{-1} \quad \xi > |z_c|^{-1} \quad (4)$$

a more complicated expression,<sup>6</sup> not reproduced here, obtaining for  $\xi < |z_d|^{-1}$ . Equation 4 has been tested for univalent counterions against tracer diffusion data, with use of eq 2, and against conductance-transference measurements, by using measured values of both  $\Lambda$  and  $\lambda_p$  in eq 1, and found to give close agreement with an *a priori* choice of  $\xi$  based on structural knowledge of the chain.<sup>6,7</sup>

A full theoretical expression for the right-hand side of eq 1, then, reduces to a theory for  $\lambda_p$ . The purpose of this paper is to give a plausible calculation of  $\lambda_p$  which takes into account both electrophoretic and relaxation effects.

### Calculation

The basis of the calculation of  $\lambda_p$  is the assumption that the polyion chain may be modeled by an infinitely long cylinder, a choice which is discussed in the next section. It is then possible to make use of Henry's calculation,<sup>8</sup> as developed by Gorin,<sup>9</sup> of the electrophoresis of long cylinders. This approach has also been used, for excess added salt, by Ross<sup>10</sup> and by Takahashi, Noda, and Nagasawa.<sup>11,12a</sup> For a long cylinder oriented parallel to an external electric field, Gorin obtains

$$u_{\parallel}^* = \epsilon \psi(a)/4\pi\eta \quad (5)$$

where  $u_{\parallel}^*$  is the electrophoretic mobility of the parallel cylinder,  $\epsilon$  is the bulk dielectric constant,  $\eta$  the bulk viscosity, and  $\psi(a)$  the electrostatic potential at the surface of the cylinder of radius  $a$ . For a cylinder oriented perpendicular to the electric field, Gorin's result is

$$u_{\perp}^* = \epsilon \psi(a)/8\pi\eta \quad (6)$$

Actually eq 6, unlike eq 5, is valid only at infinite dilution (see eq 62 and Table 8 in chapter 5 of ref 9); however, it is precisely this limit which concerns us here. If one now as-

sumes that the electrophoretic mobility  $u_p^*$  of randomly oriented cylinders is adequately represented by weighting  $u_{\parallel}^*$  by  $1/3$  and  $u_{\perp}^*$  by  $2/3$  (which would appear to be a more straightforward averaging procedure than that used by Gorin)

$$u_p^* = \epsilon \psi(a)/6\pi\eta \quad (7)$$

Asterisks have been used on the mobilities because Gorin's expressions, like Henry's, do not take into account the relaxation effect; eq 7 for the polyion mobility includes only the intrinsic frictional drag of the solvent on the cylinder combined with the additional drag (electrophoretic effect) imparted to the solvent, and hence to the cylinder, by the directed velocity of the counterions due to the external field.

The relaxation effect may be calculated indirectly from the flux  $j_c$  of uncondensed counterions

$$j_c = 0.866 |z_c| e E n_c (\zeta_c^0)^{-1} - 0.134 u_p E n_c \quad (8)$$

where  $E$  is the external field,  $\zeta_c^0$  the friction coefficient of the counterion in pure solvent,  $n_c$  the concentration of uncondensed counterions (equal to  $|z_d|^{-2} \xi^{-1}$  times the total equivalent polyion concentration), and  $u_p$  the actual electrophoretic mobility of the polyion (written without an asterisk because it includes the relaxation effect). This equation is given for the practically important case  $\xi > |z_d|^{-1}$ , and may be obtained from eq 2 of ref 6 if the latter is written for the uncondensed counterions only. The numerical factor 0.866 is merely the value of  $f$  from eq 4 when  $\xi$  is set equal to its net value  $|z_d|^{-1}$  after condensation, it being this value which governs the motion of the uncondensed counterions. The physical meaning of eq 8 is as follows. If the polyions were immobile ( $u_p = 0$ ), application of an external field  $E$  would perturb the cylindrical symmetry of the counterion atmosphere, and a restoring force would be set up which impedes the motion of the counterions in the direction of the field; hence the numerical factor in the first term of eq 8 is less than unity. The finite mobility of the polyion increases the asymmetry of the counterion atmosphere (since the directed motion of the polyion is opposite to that of the counterions) and the second term of eq 8 accounts for the resulting increment of restoring force on the counterions. The "polarizable atmosphere" is also the origin of the relaxation effect in classical ionic solution theory.<sup>12b</sup>

Now eq 8 may also be written as

$$j_c = |z_c| e (\zeta_c^0)^{-1} n_c E^* \quad (9)$$

where

$$E^*/E = 0.866 - 0.134 u_p (\zeta_c^0 / |z_c| e) \quad (10)$$

In this form it is recognized that the motion of the counterions is governed, not by the external field  $E$ , but by an effective field  $E^*$  which is diminished relative to  $E$  by electrostatic interaction with the polyion. By Newton's third law it must be the same field  $E^*$  which drives the directed motion of the polyion; that is

$$u_p j_c = u_p^* E^* \quad (11)$$

where the left-hand side by definition equals the drift velocity of the polyion. Thus,  $u_p$  equals  $u_p^*$  reduced by the relaxation effect measured by  $E^*/E$  (which in turn, according to eq 10, depends on  $u_p$ ). Combination of eq 10 and 11 then yields the following result for  $u_p$ :

$$u_p = 0.866u_p^*/[1 + 0.134(\zeta_c^0/|z_c|e)u_p^*] \quad (12)$$

where  $u_p^*$  is given by eq 7.

It remains to obtain an expression for  $\psi(a)$  in eq 7. To retain consistency with the dilute solution approximation used for the validity of eq 4 and 6,  $\psi(a)$  must be a limiting form for dilute solutions. Moreover, since the kinetic unit referred to above as the polyion was assumed to include the condensed counterions,  $\psi(a)$  is the dilute solution form of the electrostatic potential at the surface of a cylinder of radius  $a$  and surface charge density corresponding to  $\xi_{\text{net}} = |z_d|^{-1}$ . That is, it is simply the limiting form of the Debye-Hückel potential<sup>13,14</sup>

$$\psi(a) = 2|z_c|^{-1}(kT/e) \ln \kappa a \quad (13)$$

where  $\kappa$  is the Debye screening constant

$$\kappa^2 = (4\pi e^2/\epsilon kT)\xi^{-1}n_e \quad (14)$$

and  $n_e$  is the stoichiometric equivalent polyion concentration (monovalent charged groups per  $\text{cm}^{-3}$ ).

Finally, since  $\lambda_p = (F/300)u_p$ , where  $F$  is Faraday's constant, and  $\zeta_c^0 = (1.55 \times 10^{-7})|z_d|(\lambda_c^0)^{-1} \text{ dyn sec cm}^{-1}$

$$\lambda_p = \frac{279A|z_c|^{-1}|\ln \kappa a|}{1 + 43.2A(|z_c|\lambda_c^0)^{-1}|\ln \kappa a|} \quad (15)$$

where

$$A = \epsilon kT/3\pi\eta c \quad (16)$$

and  $\kappa$  is given by eq 13. Equations 1, 4, and 15 then give a complete theoretical expression for  $\Lambda$  for salt-free polyelectrolyte solutions for the case  $\xi > |z_d|^{-1}$ .

An alternate form may be given which does not contain the cylinder radius  $a$ , which for most polyion chains is a physically uncertain quantity. Equation 1, with eq 4 and 15, may be solved for  $|\ln \kappa a|$ ; then, since  $|\ln \kappa a| = -\ln \kappa a = \text{constant} - 1.15 \log c$ , where  $c$  is the polyelectrolyte salt concentration (equivalents liter<sup>-1</sup>)

$$\bar{\Lambda} = -|z_c|^{-1} \log c + \text{constant} \quad (17)$$

where

$$\bar{\Lambda} = \frac{(3.12 \times 10^{-3})A^{-1}(f^{-1}\bar{\Lambda} - \lambda_c^0)}{1 - 0.155(\lambda_c^0)^{-1}(f^{-1}\bar{\Lambda} - \lambda_c^0)} \quad (18)$$

In this form a certain function  $\bar{\Lambda}$  of  $\Lambda$  is predicted to be a linear function of  $\log c$  (base ten) with slope  $-|z_d|^{-1}$ . It cannot be used to predict absolute values of  $\Lambda$ , but, on the other hand, is independent of  $a$  and hence resembles the classical limiting laws of electrochemistry.

### Discussion

Several assumptions were made in the preceding calculation which require more extensive discussion. For the purposes of calculating  $\lambda_p$ , for example, the model of a long cylinder is not equivalent to use of the same model to calculate  $f$ .<sup>6</sup> The latter quantity measures local interactions between counterions and polyion, and because of appreciable electrostatic screening even at low concentrations, relatively short segments of the real polyion chain are involved, segments which may reasonably be expected to be rod-like due to electrostatic repulsion of charged groups. On the other hand, the global friction coefficient of the polyion chain may well not be determined only by such short segments (the chain may not be completely "free draining"), so that a degree of coiling which may not influence the value of  $f$  may have a significant effect on  $\lambda_p$  which does not appear in eq 15. In practice, therefore, it may be found that eq 1, 4, and 15, or eq 17 and 18, deviate from measurements in a concentration region for which the predicted

value of  $f$  remains accurate (when compared with conductance-transference or tracer diffusion data).

Henry's calculations<sup>8</sup> of electrophoresing cylinders contain some subtleties. The expressions for  $u_{||}^*$  and  $u_{\perp}^*$  assume that the cylinders are nonconducting. For the present theory the implication would be that the mobility of the condensed counterions along the chain is negligible. In fact, that assumption was also made to obtain eq 4 for  $f$ , and the demonstrated success<sup>6,7,15,16</sup> of the latter suggests the validity of the assumptions. Much discussion in the literature on electrophoresis and ion transport has been devoted to the location of the "surface of shear;" in this case, of the cylindrical surface of radius  $a$ . It has been assumed here that the cylindrical surface should contain the condensed counterions, so that  $u_p$  is determined by the net value of  $\xi$  after condensation. Indeed, given the nature of the condensation theory, it is difficult to envisage any other approach within its framework. Schmitt and Varoqui<sup>5</sup> have recently given a very convincing argument to justify this assumption. They show by a phenomenological derivation that negative counterion transport numbers imply that a fraction of the counterions must be considered as part of the same kinetic unit as the polyion. Negative transport numbers are indeed observed experimentally<sup>1,12a</sup> and are predicted by the condensation theory<sup>5,17</sup> by assuming that the condensed counterions have the same mobility as the polyion. Theories based on solutions of the Poisson-Boltzmann equation, on the other hand, in which all polyion-counterion interaction is an atmospheric effect, fail to predict negative counterion transport.<sup>5</sup>

It should be mentioned that negative values of  $\lambda_c$  have been frequently obtained, albeit indirectly, so that observations of this phenomenon are not restricted to the polyacrylate systems used in ref 1 and 12a. It follows from eq 1 and  $\Lambda = \lambda_c + \lambda_p$  that  $\lambda_c = f\lambda_c^0 - (1-f)\lambda_p$ . It is  $\lambda_p$  and  $f$  (the latter from measured values of  $\lambda_p$  and  $\Lambda$  in eq 1) which have frequently been measured<sup>3,6,7</sup> and yield negative values for  $\lambda_c$ . Systems for which  $\lambda_c < 0$  has been thereby confirmed include polystyrene sulfonates, which possess minimal penetration of counterion and polyion hydration layers.<sup>18</sup>

Equation 15 for  $\lambda_p$  possesses some interesting features. If its validity as a limiting law is strictly interpreted, then, in the limit  $c \rightarrow 0$  ( $\kappa \rightarrow 0$ ), it collapses to  $\lambda_p = 6.46\lambda_c^0$ . Although this result is of interest from the point of view of pure theory, since it shows that the internal retarding field due to the relaxation effect diverges in such a way as to compensate the divergence in  $u_p^*$  at zero concentration, it is doubtful if it has any practical significance. For  $c \approx 10^{-4} M$ , the second term in the denominator of the right-hand side of eq 15 is only about 20% of unity. What is of interest, however, is that  $\lambda_p$  is predicted to depend on the counterion species through  $\lambda_c^0$ , although the effect may not be large.

Detailed comparison of the theoretical expressions derived here with measurements on polystyrenesulfonates may be found in the papers of Kwak and Hayes<sup>19</sup> and Szymczak, Holyk, and Ander.<sup>20</sup>

While this paper was in preparation, a theory of polyelectrolyte conductance was published by Imai and Iwasa;<sup>21</sup> the relation between these two theories is not clear at the present time.

### References and Notes

- (1) J. R. Huizenga, P. F. Grieger, and F. T. Wall, *J. Amer. Chem. Soc.*, **72**, 2676 (1950).
- (2) H. Eisenberg, *J. Polym. Sci.*, **30**, 47 (1958).

- (3) T. Kurucsev and B. J. Steel, *Rev. Pure Appl. Chem.*, **17**, 149 (1967).  
 (4) A. Katchalsky, Z. Alexandrowicz, and O. Kedem in "Chemical Physics of Ionic Solution," B. E. Conway and R. G. Barradas, Ed., Wiley, New York, N.Y., 1966.  
 (5) A. Schmitt and R. Varoqui, *J. Chem. Soc., Faraday Trans. 2*, **69**, 1087 (1973).  
 (6) G. S. Manning, *Biopolymers*, **9**, 1543 (1970).  
 (7) G. S. Manning, *Annu. Rev. Phys. Chem.*, **23**, 117 (1972).  
 (8) D. C. Henry, *Proc. Roy. Soc., Ser. A*, **133**, 106 (1931).  
 (9) H. A. Abramson, L. S. Moyer, and M. H. Gorin, "Electrophoresis of Proteins," Reinhold, New York, N.Y., 1942, Chapter 5.  
 (10) P. D. Ross, *Biopolymers*, **2**, 9 (1964).  
 (11) T. Takahashi, I. Noda, and M. Nagasawa, *J. Phys. Chem.*, **74**, 1280 (1970).  
 (12) (a) M. Nagasawa, I. Noda, T. Takahashi, and N. Shimamoto, *J. Phys. Chem.*, **76**, 2286 (1972); (b) R. M. Fuoss and F. Accascina, "Electrolytic Conductance," Interscience, New York, N.Y., 1959.  
 (13) G. S. Manning, *J. Chem. Phys.*, **51**, 924 (1969).  
 (14) A. D. MacGillivray, *J. Chem. Phys.*, **56**, 80, 83 (1972).  
 (15) D. S. Dixler and P. Ander, *J. Phys. Chem.*, **77**, 2684 (1973).  
 (16) H. Magdelenat, P. Turq, and M. Chemla, *Biopolymers*, **13**, 1535 (1974).  
 (17) D. I. Devore and G. S. Manning, *J. Phys. Chem.*, **78**, 1242 (1974).  
 (18) U. P. Strauss and Y. P. Leung, *J. Amer. Chem. Soc.*, **87**, 1476 (1965).  
 (19) J. C. T. Kwak and R. C. Hayes, following paper.  
 (20) J. Szymczak, P. Holyk, and P. Ander, second following paper.  
 (21) N. Imai and K. Iwasa, *Isr. J. Chem.*, **11**, 223 (1973).

## Electrical Conductivity of Aqueous Solutions of Salts of Polystyrenesulfonic Acid with Univalent and Divalent Counterions

Jan C. T. Kwak\* and R. C. Hayes

Department of Chemistry, Dalhousie University, Halifax, Nova Scotia, Canada (Received July 9, 1974)

Publication costs assisted by the National Research Council of Canada

Equivalent conductivities are reported for lithium, sodium, potassium, cesium, magnesium, calcium, and strontium salts of polystyrenesulfonic acid at 25°. Concentrations for salts with univalent counterions range from  $2 \times 10^{-4}$  to 0.11 M and for salts with divalent counterions from  $4 \times 10^{-4}$  to 0.12 M. The equivalent conductivity of the salts with univalent counterions decreases with increasing concentration at the lowest concentrations, but reaches a distinct minimum between  $7 \times 10^{-3}$  and  $1 \times 10^{-2}$  M. The decrease in the low concentration range is lower than the decrease predicted by a "limiting law" for conductivity derived by Manning, but the counterion dependence of  $\Lambda$  is in reasonable agreement with theoretical calculations. Salts with divalent counterions also exhibit a minimum in  $\Lambda$ . The equivalent conductivity of these salts is well below  $\Lambda$  of salts with univalent counterions, as predicted by counterion condensation theory and the limiting law. Deviations from the limiting law depend on the type of divalent counterion present.

### Introduction

Limiting laws have been developed to describe equilibrium and transport properties of polyelectrolyte solutions.<sup>1-5</sup> Although these limiting laws apply in the limit of infinite dilution for a system consisting of infinitely long line charges and point-counterions in a dielectric continuum, experimental evidence especially for equilibrium properties of pure polyelectrolyte solutions and of mixtures of polyelectrolytes and simple electrolytes support the contention that the model applies at finite concentrations.<sup>4</sup> For polyelectrolytes the state of infinite dilution implies that interactions between different segments on the same polymer chain and between different polymer chains can be neglected. Both conditions may well be satisfied at finite concentrations even for slightly coiled polyions if the counterions effectively screen the segments from each other. Deviations from the limiting law for the activity of added simple electrolyte, due to Debye-Hückel type interactions between the small ions can be accounted for with a semiempirical method.<sup>6,7</sup>

The limiting law for the equivalent conductivity of pure polyelectrolytes can be written as:<sup>2,3,5</sup>

$$\Lambda = f(\lambda_c^0) + \lambda_p \quad (1)$$

where  $f = 0.87|z^{-1}|\xi^{-1}$ ,  $\xi$  is a charge density parameter,  $\lambda_c^0$  the limiting equivalent conductivity of the counterion,  $z$  the valency of the counterion, and  $\lambda_p$  the equivalent conductivity of the polyion at finite concentration. The complete expression for  $\lambda_p$  is given by Manning,<sup>5</sup> for our purposes it is sufficient to state that  $\lambda_p$  depends on  $z$  and  $\lambda_c^0$ , and thus on the type of counterion present, and on the concentration. This expression predicts that both  $\lambda_p$  and  $\Lambda$  decreases with increasing concentration.

Measurements of the conductivity of many polyelectrolytes have been reported, but only a few detailed studies of the concentration dependence over an extended concentration range exist.<sup>8-16</sup> The results of these investigations show a wide diversity in the concentration dependence of the equivalent conductivity of the polyelectrolyte. In most cases  $\Lambda$  decreases with increasing concentration (polyacrylates and polymethacrylates,<sup>9,12</sup> polyvinylsulfonates,<sup>13</sup> sodium carboxymethylcellulose,<sup>17</sup> salts of  $\kappa$ -carrageenan<sup>15</sup>). Jordan, *et al.*,<sup>14</sup> report  $\Lambda$  to be practically concentration independent for sodium polystyrenesulfonate, and in some cases a minimum in  $\Lambda$  is observed (lithium, sodium and potassium arabate,<sup>8,15</sup> polyvinylsulfonic acid,<sup>13</sup> sodium polystyrenesulfonate<sup>31</sup>).

In this paper the results are reported of conductivity measurements of aqueous solutions of Li, Na, K, Cs, Mg,

TABLE I: Comparison of Literature Data for Equivalent Conductivity of NaPSA Samples

Ref	NaPSA sample mol wt	Purification procedure	Degree of sulfonation	C	$\Lambda$
10	529,000	Recrystallized from ethanol	1	$6.3 \times 10^{-4}$	87
29	680,000	Dialysis		$4 \times 10^{-2}$	76
				$1 \times 10^{-4}$	52
				$4 \times 10^{-4}$	48
27	130,000	Ion exchange	0.91	$2.96 \times 10^{-4}$	38
				$7.35 \times 10^{-4}$	37
28	760,000	Ion exchange	1	$1 \times 10^{-3}$	38.5
14	520,000 <sup>a</sup>	Ion exchange	1.1	$1 \times 10^{-4}$	37
				$1.2 \times 10^{-3}$	36
30	200,000	Ion exchange	1	$5 \times 10^{-3}$	37.4
				$2.6 \times 10^{-2}$	36.9
16	70,000	Ion exchange	1	$1.8 \times 10^{-3}$	44.0
				$1.7 \times 10^{-2}$	39.3
31	500,000	Dialysis	1	$2.5 \times 10^{-3}$	37.7
				$8 \times 10^{-2}$	40.1
This work	70,000	Dialysis + ion exchange	1	$3.5 \times 10^{-4}$	43.0
				$1.2 \times 10^{-2}$	37.0
This work	500,000	Dialysis + ion exchange	1	$2.7 \times 10^{-4}$	38.9
				$1.1 \times 10^{-2}$	36.1

<sup>a</sup> Mol wt of 267,000 given for polystyrene before sulfonation.

Ca, and Sr salts of polystyrenesulfonic acid (PSA), with concentrations ranging from  $2 \times 10^{-4}$  to  $1.2 \times 10^{-1}$  M. Colligative properties of salts of this well characterized polyelectrolyte have been studied extensively, including osmotic coefficients<sup>18-21</sup> and counterion activity.<sup>22,23</sup> In an earlier publication one of the authors showed that the activity of NaCl in NaCl-NaPSA mixtures can be described over a wide concentration range with Manning's limiting law.<sup>7</sup> Polystyrenesulfonic acid can be fully converted to the desired counterion form without hydrolysis problems, and solutions of the salts are stable over long periods of time. Results of previous investigations of the conductivity of NaPSA salts are presented in Table I. The values obtained for  $\Lambda$  show large differences between different investigators with regards to the magnitude of  $\Lambda$  as well as its concentration dependence, and in all cases the measurements cover only a limited concentration range. It is possible that some of these variations were caused by problems of sample purity. In this work carefully purified samples of NaPSA from two different manufacturers, with a different molecular weight, were used and converted to other counterion forms as needed.

### Experimental Section

Sodium polystyrenesulfonate was kindly supplied by the Dow Chemical Co., Midland, Mich. (designation SC-1585, average mol wt 500,000), and by the National Starch and Chemical Corp., New York, N.Y. (designation VERSA-TL 70, average mol wt 70,000). Except where indicated, the measurements reported are for the higher molecular weight Dow Chemical Co. polymer. The original samples were purified by dialyzing an approximately 0.2 monomolar solution against 0.02 M NaCl for 1 week, followed by repeated cation and anion exchange using Dowex 50W-X8 cation exchange resin and Dowex ANGA 542 anion exchange resin. The HPSA is titrated with NaOH to pH 7 (external endpoint detection) and freeze dried. The resulting stock solution was used to prepare other cationic forms by ion ex-

changing the NaPSA to HPSA and titration with the appropriate hydroxide solution (Li, K, and Cs salts), or by adding the insoluble hydroxide (Mg salt) or carbonate (Ca and Sr salts) and filtering off the unreacted hydroxide or carbonate. Concentrations of the alkali metal salt stock solutions were determined by ion exchanging a weighed sample to HPSA and subsequent titration with standard base. Repeatability of this procedure is  $\pm 0.7\%$ . Mg, Ca, and Sr(PSA)<sub>2</sub> stock solutions were analyzed by complexometric titration, with a repeatability of  $\pm 0.3\%$ . Monoequivalent weight of NaPSA was determined as  $210 \pm 2$  for the Dow Chemical polymer and  $209 \pm 2$  for the National Starch polymer, by drying a preweighed sample to constant weight at 120° under vacuum. The final stock solution of the National Starch polymer still had a light yellow color, the stock solution of the Dow polymer was colorless. Solutions of each salt were prepared from the stock solution by dilution by weight. Double distilled equilibrium water ( $\kappa = 1.0-1.2 \times 10^{-6}$  ohm<sup>-1</sup> cm<sup>-1</sup> at 25°) was used. Densities of the more concentrated solutions (generally above 0.008 M) were determined to about  $\pm 0.05\%$  with a simple pycnometer and compared well with available published data.<sup>24,25</sup> The conductivity of the double distilled water was measured before and after the conductivity of each series was measured; the difference between these two measurements was generally less than 5%. In the case of the lowest solution concentrations used the water contributed not more than 10% of the total conductivity, resulting in an uncertainty in the polyelectrolyte conductivity of less than 1%. For higher concentrations this uncertainty diminishes rapidly.

The conductivity bridge was built using a Leeds and Northrup No. 1553 Campbell-Shackleton ratio box, following the design of Eisenberg and Fuoss.<sup>26</sup> A General Radio 1310-B oscillator and 1232-A tuned amplifier are used with a Hewlett-Packard 120B oscilloscope as null detector. All measurements were performed at 25.0°; temperature variations in the oil bath (Tamson, Neslab Instruments Inc., Portsmouth, N.H.) were  $\pm 0.005^\circ$ . Conductivity

cells with cell constants of  $0.14850 \pm 0.00008$  and  $1.4384 \pm 0.0003 \text{ cm}^{-1}$  were used. The electrodes were lightly platinized. Cell constants were determined with standard KCl solutions and checked with standard NaCl solutions. Ultra-pure KCl and NaCl (Ventron Corp., Beverly, Mass.) were dried under vacuum at  $500^\circ$  before use. All conductivities reported were measured at a frequency of 2000 Hz. The frequency dependence was determined for a few NaPSA solutions. The measured conductivity increased less than 0.1% between 1000 and 10,000 Hz.

Except for the lowest concentration points, the uncertainty in the equivalent conductivity reported is due entirely to the uncertainty in the concentration ( $\pm 0.7\%$  for the alkali metal salts,  $\pm 0.3\%$  for the Mg, Ca, and Sr salts). Because of the dilution method used the relation between the concentration of each stock solution and the dilutions made from it is accurate to  $\pm 0.1\%$ .

## Results and Discussion

The equivalent conductivities of Li, Na, K, Cs, Mg, Ca, and Sr PSA (Dow Chemical Co., SC 1585) as a function of the square root of the concentration (equivalents/liter) are shown in Figures 1 and 2. Our values for  $\Lambda$  of NaPSA are in the same range as the values obtained by most other investigators (Table I).<sup>14,16,27,28,30,31</sup> Results of two investigations<sup>10,29</sup> are considerably higher. In order to compare the equivalent conductivity of different NaPSA samples purified with the same method, values obtained with the SC 1585 sample (Dow Chemical Co., mol wt 500,000) and with the VERSA-TL 70 sample (National Starch Corp., mol wt 70,000) are compared in Figure 3. The values obtained are only 3% apart except at the lowest concentrations.

Our results for the salts with univalent counterions show the expected decrease in  $\Lambda$  with increasing concentration in the low concentration region. In all four cases a distinct minimum is reached between  $7 \times 10^{-3}$  (CsPSA) and  $10^{-2} M$  (LiPSA). The decrease in  $\Lambda$  in the low concentration region is less than the decrease predicted by eq 1, using values for  $\lambda_c^0$  given by Robinson and Stokes.<sup>32</sup> In accordance with the results of Ander, *et al.*,<sup>16</sup> the lower molecular weight (70,000) National Starch polymer shows a decrease in  $\Lambda$  which is slightly larger than the decrease predicted by eq 1. By rearranging eq 1, Manning derived the following expression (for univalent counterions):

$$\bar{\Lambda} = -\log C + \text{constant} \quad (2)$$

where  $\bar{\Lambda}$  is a function of  $\xi$ ,  $\Lambda$ ,  $\lambda_c^0$  and the polyelectrolyte concentration.<sup>5</sup> This form of the limiting law avoids the assignment and use of a cylindrical radius to the polyelectrolyte backbone. Figure 4 shows that for all four SC 1585 polystyrenesulfonates the decrease in  $\Lambda$  is lower than what is expected from the limiting law represented in the form of eq 2. Although in all four cases  $\bar{\Lambda}$  varies linearly with  $\log C$ , the average slope for the four salts is about 0.36 as opposed to a theoretical slope of 1. Table II shows that the limiting law (eq 1) provides a relatively accurate method to correlate the counterion dependence of the equivalent conductivity of the four polyelectrolyte salts studied. In this table  $\Lambda_{\text{calcd}}$  at 0.0004 M is calculated from eq 1 using a cylindrical radius for the polyelectrolyte of  $8 \times 10^{-8} \text{ cm}$ .<sup>23</sup> At higher concentrations the difference between  $\Lambda_{\text{expt}}$  and  $\Lambda_{\text{calcd}}$  is larger, but the variation,  $\Delta$ , from one salt to another is very similar. It should be noted that the parameter  $\gamma$ , defined by Eisenberg<sup>12</sup> as  $\gamma = (\Lambda_{\text{MP}} - \Lambda_{\text{NP}})/(\lambda_{\text{M}^+}^0 - \lambda_{\text{N}^+}^0)$ , where  $\Lambda$  is the measured equivalent conductivity at finite concentra-

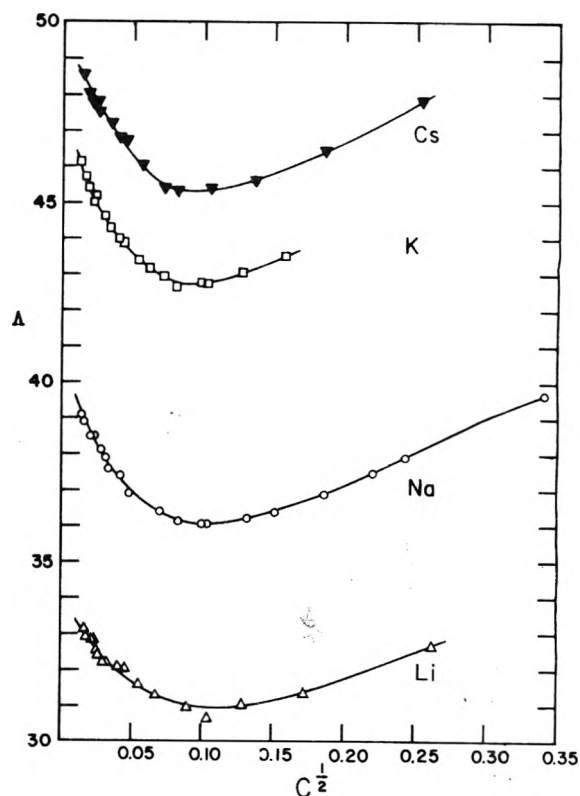


Figure 1. Equivalent conductivity  $\Lambda$  ( $\text{cm}^2 \text{equiv}^{-1} \text{ohm}^{-1}$ ) vs.  $C^{1/2}$  ( $\text{equiv}^{1/2} \text{l}^{-1/2}$ ) for LiPSA ( $\Delta$ ), NaPSA ( $\circ$ ), KPSA ( $\square$ ), and CsPSA ( $\blacktriangledown$ ).

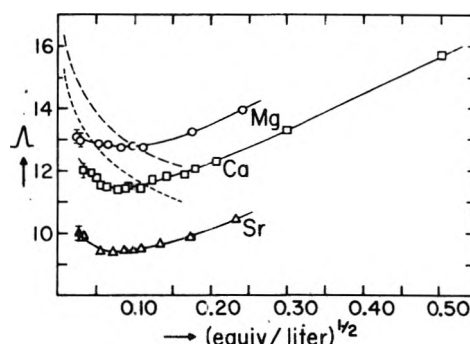


Figure 2. Equivalent conductivity  $\Lambda$  ( $\text{cm}^2 \text{equiv}^{-1} \text{ohm}^{-1}$ ) vs.  $C^{1/2}$  ( $\text{equiv}^{1/2} \text{l}^{-1/2}$ ) for  $\text{Mg}(\text{PSA})_2$  ( $\circ$ ),  $\text{Ca}(\text{PSA})_2$  ( $\square$ ), and  $\text{Sr}(\text{PSA})_2$  ( $\Delta$ ): (---) eq 1 for  $\text{Ca}(\text{PSA})_2$  and  $\text{Sr}(\text{PSA})_2$ ; (- - - -) eq 1 for  $\text{Mg}(\text{PSA})_2$ .

tion, and  $\lambda^0$  the limiting ionic conductivity averages about 0.41 at 0.01 M for the six pairs of univalent counterions, but does depend on the type of counterion. The same counterion dependence was found by Ander, *et al.*, for lower molecular weight polystyrenesulfonates,<sup>16</sup> and by Eisenberg and Mohan Ram for polyvinylsulfonates.<sup>13</sup> This could mean that the polyion mobility is indeed dependent on the type of counterion, as predicted by Manning. Jordan, *et al.*, report a difference in polyion mobility between HPSA and NaPSA solutions.<sup>14</sup> Shavit<sup>33</sup> found a difference in polyion mobility between the Na and K salts of polyacrylic acid at higher concentrations (above 0.025 M), even though Eisenberg<sup>12</sup> had found  $\gamma$  of salts of this polyacid to be independent of the type of counterion.

The four alkali metal polystyrenesulfonates studied exhibit the monotonous decrease in  $\Lambda$ , predicted by the limiting law, at the lowest concentrations only. Positive devia-

**TABLE II: Calculated (Eq 1,  $\Lambda_{\text{calcd}}$ ) and Experimental ( $\Lambda_{\text{expt}}$ , Interpolated from Data Points) Values of  $\Lambda$  for Li, Na, K, and CsPSA<sup>a</sup>**

	LiPSA	NaPSA	KPSA	Cs-PSA
$\Lambda_{\text{calcd}}$	32.9	37.8	46.8	48.2
	$\Delta = 4.9$	$\Delta = 9.0$	$\Delta = 1.4$	
$\Lambda_{\text{expt}}$	32.9	38.6	45.2	47.6
	$\Delta = 5.7$	$\Delta = 6.6$	$\Delta = 2.4$	

<sup>a</sup> Dow SC 1585, mol wt 500,000 at  $4 \times 10^{-4} M$ , 25°.

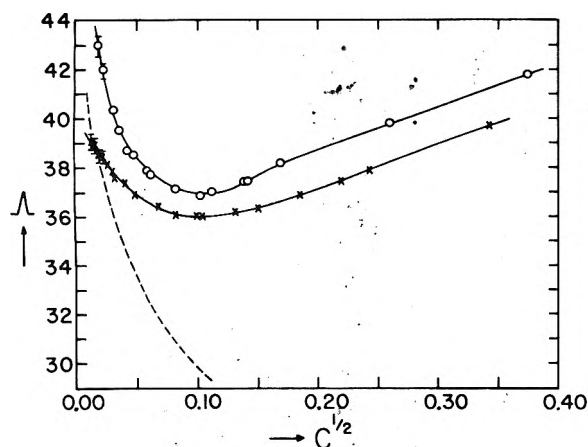


**Figure 3.** Equivalent conductivity  $\Lambda$  ( $\text{cm}^2 \text{equiv}^{-1} \text{ohm}^{-1}$ ) vs.  $C^{1/2}$  ( $\text{equiv}^{1/2} \text{l.}^{-1/2}$ ) of two NaPSA samples: (X) Dow SC 1585, mol wt 500,000 (O) National Starch Versa TL 70, mol wt 70,000; (broken line: eq 1).

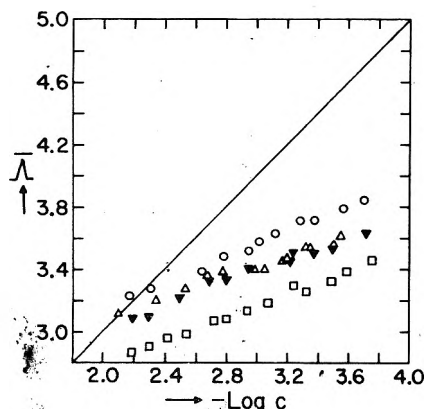


**Figure 4.**  $\bar{\Lambda}$  (defined by eq 2) of LiPSA ( $\Delta$ ), NaPSA (O), KPSA ( $\square$ ), and CsPSA ( $\blacktriangledown$ ) vs.  $-\log c$  in the low concentration region. Value of constant in eq 2 is omitted, solid line indicates theoretical slope of 1 only.

tions from the limiting law occur even at the lowest concentrations, and between 0.007 and 0.01  $M$  a distinct minimum in  $\Lambda$  is reached, followed by a continuous increase in  $\Lambda$ . Manning<sup>5</sup> noted that coiling of the polymer may influence  $\lambda_p$  more than it does the counterion mobility and equilibrium properties. Shavit<sup>33</sup> reports a 50% increase in the counterion mobility of potassium polyacrylate upon increasing the concentration from 0.025 to 0.1  $M$ . Dolar, *et al.*,<sup>31</sup> report an increase in the fraction of free counterions for NaPSA from 0.34 at 0.0025  $M$  to 0.48 at 0.075  $M$ . Considerable coiling at higher concentrations may cause the model on which the limiting laws are based to break down,

and result in a decrease in the fraction of counterions condensed on the polyion, leading to higher values for the counterion mobility and  $\Lambda$ .

Salts with divalent counterions show a similar concentration dependence of  $\Lambda$  as was found in salts with univalent counterions, but the minimum is at lower concentration and seems less pronounced, especially in the case of  $\text{Mg}(\text{PSA})_2$ . The low conductivity of these salts prevents an adequate comparison of the concentration dependence of  $\Lambda$  with eq 1 in the low concentration region. As predicted by Manning's theoretical expression, and in agreement with the general concept of counterion condensation,<sup>34</sup> the equivalent conductivity of salts with divalent counterions is appreciably less than  $\Lambda$  of salts with univalent counterions. The limiting law predicts a slightly lower equivalent conductivity for  $\text{Mg}(\text{PSA})_2$  compared to  $\text{Ca}(\text{PSA})_2$  and  $\text{Sr}(\text{PSA})_2$ , due to the lower limiting mobility of the  $\text{Mg}^{2+}$  ion. Our experiments show that  $\Lambda(\text{Mg}(\text{PSA})_2) > \Lambda(\text{Ca}(\text{PSA})_2) > \Lambda(\text{Sr}(\text{PSA})_2)$ . Osmotic coefficients are found to vary in the same way,<sup>19,35</sup> even though the limiting law does not predict a difference in the osmotic coefficients of salts with counterions of the same valency. At  $10^{-3}$  equiv/l. eq 1 predicts a value of 2.65 for the ratio  $\Lambda(\text{NaPSA})/\Lambda(\text{Mg}(\text{PSA})_2)$ , the experimental value for this ratio at  $10^{-3}$  equiv/l. is 2.91. Similarly at this concentration the theoretical value for the ratio  $\Lambda(\text{NaPSA})/\Lambda(\text{Ca}(\text{PSA})_2)$  is 2.46 and the experimental value 3.10, the theoretical value for the ratio  $\Lambda(\text{NaPSA})/\Lambda(\text{Sr}(\text{PSA})_2)$  is 2.46 and the experimental value 3.79. Similarly of course the parameter  $\gamma$  defined above is not constant for the three pairs of counterions studied. These findings show that the deviations from the limiting law in the case of salts with divalent counterions are specific for each counterion, and indicate that the larger divalent cations interact more strongly with the polymer anion.

Results of these and other transport studies of polyelectrolytes show that transport properties are more sensitive to the type of polymer backbone and possibly the polymer configuration than are equilibrium properties. Even with the same polyelectrolyte, differences in the extent of cross linkage and branching of the polyion may lead to both qualitative and quantitative differences in the equivalent conductivity and in the concentration dependence of  $\Lambda$ . Theoretical expressions for the conductivity at finite concentrations would have to take into account the local polymer structure, especially in the higher concentration ranges.

*Acknowledgment.* The authors are grateful to the Dow Chemical Co., Midland, Mich., and to the National Starch and Chemical Corp., New York, N.Y., for providing samples of NaPSA, and to Drs. P. Ander and G. S. Manning for helpful discussions and comments.

This research was supported by the National Research Council of Canada.

## References and Notes

- (1) G. S. Manning, *J. Chem. Phys.*, **51**, 924 (1969).
- (2) G. S. Manning, *J. Chem. Phys.*, **51**, 934 (1969).
- (3) G. S. Manning, *Biopolymers*, **9**, 1534 (1970).
- (4) G. S. Manning, *Annu. Rev. Phys. Chem.*, **23**, 117 (1972).
- (5) G. S. Manning, preceding paper.
- (6) J. D. Wells, *Biopolymers*, **12**, 223 (1973).
- (7) J. C. T. Kwak, *J. Phys. Chem.*, **77**, 2790 (1973).
- (8) D. R. Briggs, *J. Phys. Chem.*, **38**, 867 (1934).
- (9) A. Oth and P. Doty, *J. Phys. Chem.*, **56**, 43 (1952).

- (10) R. A. Mock, C. A. Marshall, and T. E. Slykhouse, *J. Phys. Chem.*, **58**, 498 (1954).  
 (11) H. P. Gregor and D. H. Gold, *J. Phys. Chem.*, **61**, 1347 (1957).  
 (12) H. Eisenberg, *J. Polym. Sci.*, **30**, 47 (1958).  
 (13) H. Eisenberg and G. Mohan Ram, *J. Phys. Chem.*, **63**, 671 (1959).  
 (14) D. O. Jordan, T. Kurucsev, and M. L. Martin, *Trans. Faraday Soc.*, **65**, 606 (1969).  
 (15) R. E. Nelson and P. Ander, *J. Phys. Chem.*, **75**, 1691 (1971).  
 (16) J. Szymczak, P. Holyk, and P. Ander, following paper.  
 (17) J. C. T. Kwak and A. J. Johnston, *Can. J. Chem.*, in press.  
 (18) M. Reddy and J. A. Marinsky, *J. Phys. Chem.*, **74**, 3884 (1970).  
 (19) M. Reddy, J. A. Marinsky, and A. Sarkar, *J. Phys. Chem.*, **74**, 3891 (1970).  
 (20) A. Takahashi, T. Kato, and M. Nagasawa, *J. Phys. Chem.*, **74**, 944 (1970).  
 (21) D. Kozak, J. Krištan, and A. Dolar, *Z. Phys. Chem. (Frankfurt am Main)*, **76**, 85 (1971).  
 (22) J. W. Lyons and L. Kotin, *J. Amer. Chem. Soc.*, **87**, 1670 (1965).  
 (23) S. Oman and D. Dclar, *Z. Phys. Chem. (Frankfurt am Main)*, **56**, 1 (1967).  
 (24) C. Tondre and R. Zara, *J. Phys. Chem.*, **76**, 3451 (1972).  
 (25) J. Skerjanc, *J. Phys. Chem.*, **77**, 1225 (1973).  
 (26) H. Eisenberg and R. M. Fuoss, *J. Amer. Chem. Soc.*, **75**, 2914 (1953).  
 (27) K. F. Wissbrun and A. Paterson, *J. Polym. Sci.*, **33**, 235 (1958).  
 (28) A. S. Michaels, L. Mir, and N. S. Schneider, *J. Phys. Chem.*, **69**, 1447 (1965).  
 (29) J. A. V. Butler, A. B. Robins, and K. V. Shooter, *Proc. Roy. Soc. Ser. A*, **241**, 299 (1957).  
 (30) D. Dolar, J. Špan, and A. Pretnar, *J. Polym. Sci., Part C*, **16**, 3557 (1968).  
 (31) D. Dolar, J. Špan, and S. Isaković, *Biophys. Chem.*, **1**, 312 (1974).  
 (32) R. A. Robinson and R. H. Stokes, "Electrolyte Solutions," Butterworths, London, 1959.  
 (33) N. Shavit, *Isr. J. Chem.*, **11**, 236 (1973).  
 (34) F. Oosawa, "Polyelectrolytes," Marcel Dekker, New York, N.Y., 1971.  
 (35) E. Gluckauf and G. P. Kitt, *Proc. Roy. Soc., Ser. A*, **228**, 322 (1955).

## Electrical Conductivity of Aqueous Solutions of Monovalent Salts of Polystyrenesulfonate

Janet Szymczak, Peter Holyk, and Paul Ander\*

Department of Chemistry, Seton Hall University, South Orange, New Jersey 07079 (Received July 12, 1974)

The conductivities of  $\text{Li}^+$ ,  $\text{Na}^+$ ,  $\text{K}^+$ ,  $\text{NH}_4^+$ ,  $\text{Rb}^+$ , and  $\text{Cs}^+$  salts of polystyrenesulfonic acid have been determined in salt-free aqueous solutions in the concentration range from  $1 \times 10^{-3}$  to  $2 \times 10^{-2} N$  at  $25^\circ$ . Conductivity values for each salt increase with dilution, gradually at first, followed by a rapid increase at higher dilutions. At any given concentration the conductivity values change in the order  $\text{Li}^+ < \text{Na}^+ < \text{K}^+ \approx \text{NH}_4^+ < \text{Rb}^+ \approx \text{Cs}^+$ . The conductivity parameter of Eisenberg was found to differ for different pairs of counterions. Values of the polyelectrolyte conductivities predicted from Manning's rod-like polyelectrolyte model are compared with those obtained experimentally.

### Introduction

In the absence of simple electrolyte, the electrical conductivities of dilute aqueous solutions of polyelectrolyte salts increase with decreasing polyelectrolyte concentration, slowly at first, followed by a rapid increase at higher dilutions. This behavior cannot be due to an increase in the ionization of the polyelectrolyte as dilution progresses, inasmuch as conductivity and transport experiments for several polyelectrolytes indicate that an experimentally defined charge fraction parameter, *i.e.*, the ratio of the number of counterions moving in the opposite direction in an electric field to the total number of counterions that would result from a complete dissociation of the polyelectrolyte, is independent or only slightly dependent on the concentration.<sup>1</sup> Recently, Dolar reported<sup>2</sup> that the fraction of free counterions increases with increasing polyelectrolyte concentration for aqueous solutions of sodium polystyrenesulfonate.

Empirical equations which have been employed to describe the concentration dependence of the equivalent conductance of a polyion species, which is treated as an empirical parameter, are not unique.<sup>3-5</sup>

An empirical parameter  $\phi$  defined by Eisenberg<sup>6</sup>

$$\phi = (\Lambda_{MP} - \Lambda_{NP}) / (\lambda_{M^+}^0 - \lambda_{N^+}^0) \quad (1)$$

where  $\Lambda_{MP}$  and  $\Lambda_{NP}$  are the equivalent conductances of a polyion P with counterions  $M^+$  and  $N^+$ , respectively, and

$\lambda_{M^+}^0$  and  $\lambda_{N^+}^0$  are the equivalent conductances at infinite dilution for the indicated counterions, has been found to be independent of the nature of the counterion pairs for which it was calculated and independent of polyelectrolyte concentration for a definite polyion. It has been shown<sup>7,8</sup> that the parameter  $\phi$  can be equated to the degree of ionization of a polyelectrolyte, provided it is assumed that both the degree of ionization and the mobility of the polyion are independent of the nature of the counterion. Katchalsky<sup>7</sup> has shown that  $\phi$  can also be related to the osmotic coefficient of the polyelectrolyte if the same assumptions are made. Using their data and data reported in the literature, Nelson and Ander<sup>5</sup> have interpreted  $\phi$  to be a conductometric degree of ionization, being both a measure of the unbound counterions plus a contribution to the conductivity from the bound counterions.

Recently, Manning extended his theory of polyelectrolyte solutions<sup>9-11</sup> to calculate the equivalent conductance of the polyion species by taking into account relaxation and electrophoretic effects.<sup>12</sup> Thereby, the equivalent conductance of the polyelectrolyte  $\Lambda$  could be calculated from

$$\Lambda = f(\lambda_p + \lambda_c^0) \quad (2)$$

where  $\lambda_p$  is the equivalent conductance of the polyion,  $\lambda_c^0$  is the equivalent conductance of the counterion at infinite dilution in pure solvent, and  $f$  for univalent counterions is given theoretically by

$$f = 0.866\xi^{-1} \quad \xi > 1 \quad (3)$$

where  $\xi$  is given by

$$\xi = e^2/\epsilon k T b \quad (4)$$

where  $e$  is the protonic charge,  $\epsilon$  is the dielectric constant,  $k$  is the Boltzmann constant,  $T$  is the absolute temperature, and  $b$  is the distance between charged groups in the polyelectrolyte.

In the present study we report the concentration dependence of the equivalent conductances of six salts of fully neutralized polystyrenesulfonic acid (HPSS) in aqueous solution of 25°. Thus the  $\Lambda$  values for LiPSS, NaPSS, KPSS, RbPSS, NH<sub>4</sub>PSS, and CsPSS will be compared with the values predicted from Manning's theory and the computed values of the parameter  $\phi$  will be compared for different pairs of counterions. A similar independent study for LiPSS, NaPSS, KPSS, and CsPSS in aqueous solution is reported by Kwak.<sup>13</sup>

### Experimental Section

**Preparation of Salts of Polystyrenesulfonic Acid.** The polystyrenesulfonate salts were prepared from the acid form (VERSA-TL 72), which was a gift of the National Starch and Chemical Corp., Plainfield, N.J. It is known to be of molecular weight 70,000. The manufacturer passed the sample through a cation and an anion exchange resin to remove all ionic impurities, and the sample was received as a 30% aqueous solution. A sample of the HPSS was freeze dried, and the equivalent weight was determined to be 185 ± 1 g/equiv when titrated with standard sodium hydroxide. This value is in excellent agreement with that predicted assuming 100% sulfonation.

The lithium, sodium, ammonium, potassium, rubidium, and cesium salts were prepared by titration of HPSS with the appropriate hydroxide just to the equivalence point, and isolated by freeze drying. The cesium and rubidium hydroxides were obtained from Alfa Inorganics, Ventron, Beverly, Mass. The sodium, potassium, and lithium hydroxides were obtained from Fischer Scientific Co., Fair Lawn, N.J. The sodium and potassium hydroxides were ACS certified reagent grade, and the lithium hydroxide was purified grade. The reagent grade ammonium hydroxide was a product of J. T. Baker Chemical Co., Phillipsburg, N.J.

The equivalent weight of dried NaPSS was found to be 205 ± 1 g/equiv, as determined by sulfur analysis in the Schwarzkopf Microanalytical Laboratory. This value agrees within 0.5% with the theoretical value assuming a one-to-one substitution of Na<sup>+</sup> for H<sup>+</sup>. On this basis it was assumed that there was 100% substitution of the desired counterion on the polyelectrolyte when the HPSS was titrated with the desired hydroxide.

The per cent water of each polyelectrolyte used was determined by the loss in weight when dried to constant weight *in vacuo* overnight at 65°. The per cent water was found to be 2.89 ± 0.50% for LiPSS, 3.14 ± 0.50% for NaPSS, 2.54 ± 0.15% for KPSS, 2.62 ± 0.01% for NH<sub>4</sub>PSS, 2.34 ± 0.31% for CsPSS, and 1.32 ± 0.04% for RbPSS. These results were taken into account in calculating the equivalent concentrations of the polymer solutions.

**Conductivity Measurements of Polyelectrolyte Solutions.** All the conductivity measurements were made in an oil-filled bath at 25.00 ± 0.01°. The temperature control was ± 0.005°. A Pyrex conductivity cell of a modified Shedlovsky design was employed. The electrodes were lightly

platinized with platinum black. The cell constant was determined by measuring the resistance of a 0.01 *D* KCl solution whose specific conductivity is known. The calculated cell constant was 1.1409 ± 0.0005 cm<sup>-1</sup>. This value was checked intermittently throughout the course of the study.

A Beckman laboratory conductivity bridge Model RC-18A, which utilizes a precision ac Wheatstone bridge, was used for all measurements. Resistance measurements were reproducible to within 1.5% for all polymer solutions.

All polymer solutions were prepared by weighing the polymer in 50-ml class A volumetric flasks. The flasks were filled up to the mark with deionized-distilled water, after the polymer had dissolved in a little water. Concentrations were expressed as normality. The error in calculating the equivalent concentrations is approximately 1%. The resistance of each solution was measured at 3000 Hz. It has been shown that the resistance of a polyelectrolyte solution is not frequency dependent at low frequencies.<sup>6</sup> The resistance of the conductivity water was much greater than the resistance of any polymer solution; thus, the contribution of the conductivity of the water was assumed to be negligible except for the most dilute solutions. The error in calculating the equivalent conductivity is approximated to be 3%.

### Results and Discussions

Figures 1 and 2 show  $\Lambda$  as a function of  $N^{1/2}$  for LiPSS, NaPSS, KPSS, NH<sub>4</sub>PSS, RbPSS, and CsPSS in aqueous solution at 25°. The general shapes of the curves are similar to the conductance behavior found for other polyelectrolytes in aqueous solutions for this concentration range with no simple salts present. For a given polyelectrolyte concentration, the values for  $\Lambda$  are in the order of the equivalent conductivities of the cation at infinite dilution, *i.e.*, Li<sup>+</sup> < Na<sup>+</sup> < K<sup>+</sup> ≈ NH<sub>4</sub><sup>+</sup> < Rb<sup>+</sup> ≈ Cs<sup>+</sup>. The same order has been reported for the conductivities of salt-free aqueous solutions of lithium, sodium, potassium, and ammonium polyvinylsulfonate salts.<sup>14</sup> Our results for NaPSS approximate those reported by Jordan, *et al.*,<sup>15</sup> by Dolar, *et al.*,<sup>2,16</sup> and by Tuffile.<sup>17</sup> In a recent thorough investigation of monovalent polystyrenesulfonate salts by Kwak,<sup>13</sup> values of the conductivities for LiPSS, NaPSS, KPSS, and CsPSS were in the same order with respect to the counterions as that found in the present study. However, the conductance curve for each polyelectrolyte reported by Kwak was a few per cent lower than reported here. This may be due to the different origins of our parent polymers, which also differed in molecular weight. For dilute salt-free aqueous solution of sodium polystyrenesulfonate,<sup>2</sup> of sodium polymethacrylate,<sup>16</sup> and of Graham's salt,<sup>18</sup> lower molecular weight samples resulted in slightly higher conductivities when compared to higher molecular weight analogs.

To examine eq 1 our data were used along with the literature values<sup>19</sup> for  $\lambda_{M^+}^0$  in cm<sup>2</sup> equiv<sup>-1</sup> ohm<sup>-1</sup>; 38.7 for Li<sup>+</sup>, 50.1 for Na<sup>+</sup>, 73.5 for K<sup>+</sup>, 73.4 for NH<sub>4</sub><sup>+</sup>, 77.8 for Rb<sup>+</sup>, and 77.2 for Cs<sup>+</sup>. It is obvious from eq 1, that because of experimental error meaningless values for  $\phi$  would result if the counterion pair chosen had close values for  $\lambda_{M^+}^0$  and  $\lambda_{N^+}^0$ . Plotting  $\phi$  as a function of  $N^{1/2}$  for several counterion pairs indicated that constant values of  $\phi$  are attained at the higher values of  $N$ , with  $\phi$  ranging from 0.34 to 0.48 depending on the counterion pair chosen. These results indicate that the assumption used to interpret  $\phi$  as a degree of ionization, *i.e.*, that  $\lambda_p$  is independent of the nature of the counterion, is incorrect. Jordan, *et al.*,<sup>15</sup> found from electrical

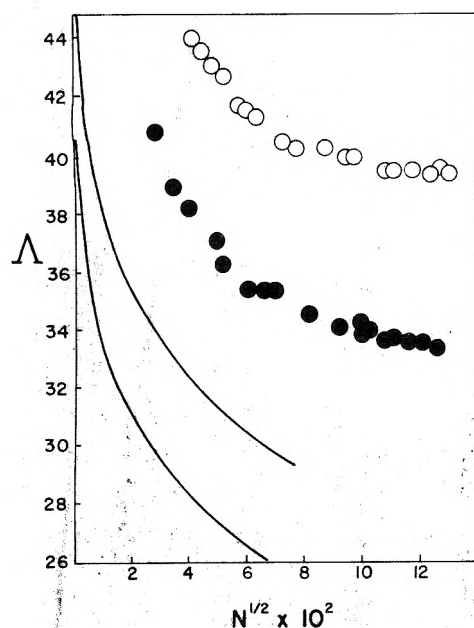


Figure 1. Equivalent conductivities as a function of the square root of the normality of polyelectrolyte for LiPSS (●) and NaPSS (○). The lines are the theoretical predictions obtained from eq 2, the upper line for NaPSS and the lower line for LiPSS.

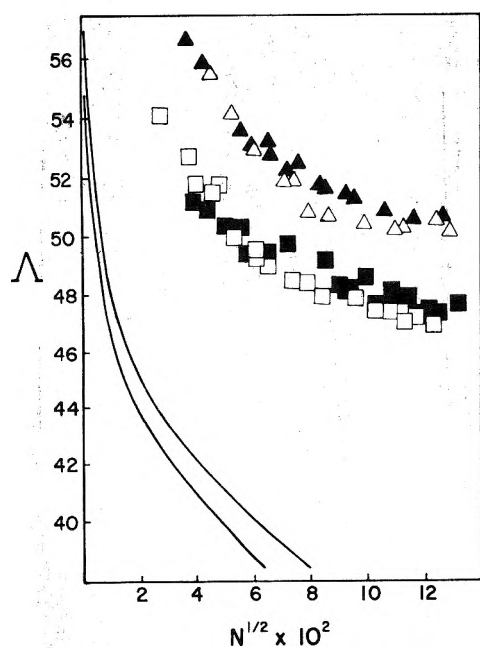


Figure 2. Equivalent conductivities as a function of the square root of the normality of polyelectrolyte for KPSS (□), NH<sub>4</sub>PSS (■), RbPSS (Δ), and CsPSS (▲). The lines are the theoretical predictions obtained from eq 2; the upper line is for KPSS and NH<sub>4</sub>PSS and the lower line for RbPSS and CsPSS.

transport and conductivity experiments that  $\lambda_p$  differed for HPSS and NaPSS.

Manning's limiting law for the conductance of the polyelectrolyte<sup>12</sup> in water at 25° is given by

$$\lambda_p = \frac{22.37 |\ln \kappa a|}{1 + 3.467(\lambda_c^0)^{-1} |\ln \kappa a|} \quad (5)$$

where  $\kappa$  is the Debye screening constant and  $a$  is the radius of the polyelectrolyte, taken here to be  $8 \times 10^{-8}$  cm.<sup>20</sup> Using  $\xi =$

TABLE II: Experimental Slopes Obtained from Figure 3

Polyelectrolyte	Slope	Correlation coefficient
LiPSS	1.8	0.97
NaPSS	1.4	0.99
KPSS	1.3	0.98
NH <sub>4</sub> PSS	0.66	0.95
RbPSS	1.7	0.98
CsPSS	1.4	0.98

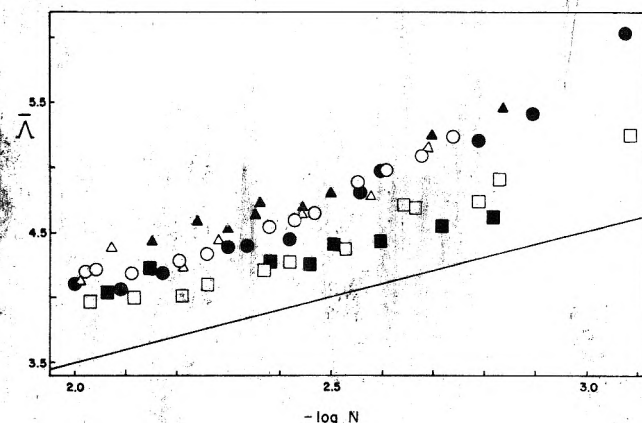


Figure 3.  $\bar{\Lambda}$  vs.  $-\log N$  for LiPSS (●), NaPSS (○), KPSS (□), NH<sub>4</sub>PSS (■), RbPSS (Δ), and CsPSS (▲). The line is a plot of the theoretical eq 6 with a slope of unity.

2.85 and eq 2, 1, and 5, theoretical curves were constructed in Figures 1 and 2. Positive deviations from the limiting law are evident even at the lowest concentration employed. Such deviations were anticipated by Manning because the degree of coiling of the polyelectrolyte may have a significant effect on  $\lambda_p$  through its influence on the frictional constant of the whole polyion. Coiling of the polyion at higher concentrations, as well as other effects, might be responsible for the increase in the counterion mobility with increasing concentration found for potassium polyacrylate.<sup>21</sup> It should be noted from eq 5 that for the same concentration, *i.e.*, the same value of  $\kappa a$ ,  $\lambda_p^{-1}$  is directly proportional to  $(\lambda_c^0)^{-1}$  and hence,  $\lambda_p$  is dependent on the nature of the counterion. Also, it should be noted that the second term in the denominator of eq 5 is not small when compared to unity; in the present study it varied from 0.071 to 0.274.

Manning was able to eliminate the parameter  $a$  in eq 5 to obtain  $\bar{\Lambda}$  as a function of  $\Lambda$  for a univalent counterion, where  $\bar{\Lambda}$  is given by

$$\bar{\Lambda} = -\log N + \text{constant} \quad (6)$$

A plot of  $\bar{\Lambda}$  vs.  $-\log N$  predicts a slope of unity. Values of  $\Lambda$ ,  $\bar{\Lambda}$ , and  $N$  are given in Table I<sup>22</sup> and plots of  $\lambda$  vs.  $-\log N$  are shown in Figure 3, the solid line indicating a slope of unity. The experimental slopes for each polyelectrolyte salt shown in Figure 3 were determined by a linear regression analysis in the concentration range of  $10^{-2} N$  and these are listed in Table II. While  $\bar{\Lambda}$  is found to be linear with  $\log N$ , the slopes obtained for each salt except NH<sub>4</sub>PSS were found to be between one and two. It is premature at the present time to attempt an explanation of the discrepancy between the experimental slopes obtained and the theoretical slope of unity. While Manning's theory appears to be most successful for predicting equilibrium properties of polyelectrolyte solutions, his theory for electrical transport

properties may require additional theoretical consideration.

*Acknowledgment.* This work was initiated by Dr. F. M. Tuffile. The authors are grateful to Drs. C. T. Kwak and G. S. Manning for their helpful comments.

*Supplementary Material Available.* Table I, containing values of the experimental and theoretical conductivities for the various salts used in this study, will appear following these pages in the microfilm edition of this volume of the journal. Photocopies of the supplementary material from this paper only or microfiche (105 × 148 mm, 24× reduction, negatives) containing all of the supplementary material for the papers in this issue may be obtained from the Journals Department, American Chemical Society, 1155 16th St., N.W., Washington, D. C. 20036. Remit check or money order for \$3.00 for photocopy or \$2.00 for microfiche, referring to code number JPC-75-269.

## References and Notes

- (1) T. Kurucsev and B. J. Steel, *Rev. Pure Appl. Chem.*, **17**, 149 (1967).
- (2) D. Dolar, J. Span, and S. Isakovic, *Biophys. Chem.*, **1**, 312 (1974).
- (3) H. P. Gregor and D. H. Gold., *J. Phys. Chem.*, **61**, 1347 (1957).
- (4) R. A. Mock, C. A. Marshall, and T. E. Slykhouse, *J. Phys. Chem.*, **58**, 498 (1954).
- (5) R. E. Nelson and P. Ander, *J. Phys. Chem.*, **75**, 1691 (1971).
- (6) H. Eisenberg, *J. Polym. Sci.*, **39**, 47 (1958).
- (7) A. Katchalsky, *Pure Appl. Chem.*, **26**, 327 (1971).
- (8) R. Varoqui and U. P. Strauss, *J. Phys. Chem.*, **72**, 2507 (1968).
- (9) G. S. Manning, *J. Chem. Phys.*, **51**, 924, 934 (1969).
- (10) G. S. Manning, *Biopolymers*, **9**, 1534 (1970).
- (11) G. S. Manning, *Annu. Rev. Phys. Chem.*, **23**, 117 (1972).
- (12) G. S. Manning, *J. Phys. Chem.*, preceding paper.
- (13) J. C. T. Kwak and R. C. Hayes, *J. Phys. Chem.*, preceding paper.
- (14) H. Eisenberg and G. Ram Mohan, *J. Phys. Chem.*, **63**, 671 (1959).
- (15) D. O. Jordan, T. Kurucsev, and M. L. Martin, *Trans. Faraday Soc.*, **65**, 606 (1969).
- (16) D. Dolar, J. Span, and A. Pretar, *J. Polym. Sci.*, **16**, 3557 (1968).
- (17) F. M. Tuffile, Ph.D. Thesis, Seton Hall University, South Orange, N.J., 1971.
- (18) A. C. Chatterji and H. H. Bhargara, *Kolloid. Z.*, **170**, 116 (1960).
- (19) R. A. Robinson and R. H. Stokes, "Electrolytic Solutions," 2nd ed, Butterworths, London, England, 1959.
- (20) S. Oman and D. Dolar, *Z. Phys. Chem. (Frankfurt Am Main)*, **56**, 1 (1967).
- (21) N. Shavit, *Isr. J. Chem.*, **11**, 235 (1973).
- (22) See paragraph at end of text regarding supplementary material.

## Absolute Viscosity of D<sub>2</sub><sup>18</sup>O between 15 and 35°

A. I. Kudish\* and D. Wolf

Isotope Department, The Weizmann Institute of Science, Rehovot, Israel (Received June 20, 1974)

Absolute viscosity values for highly enriched D<sub>2</sub><sup>18</sup>O samples have been measured at 5° intervals between 15 and 35° using a semiautomatic closed viscometer of the suspended-level type. The absolute viscosity of 100% D<sub>2</sub><sup>18</sup>O has been determined by extrapolation of the experimental data by means of Eyring's absolute rate theory of viscosity. In order to perform the above extrapolations certain assumptions had to be made concerning the nonnegligible amount of HDO present in the samples.

We undertook the present study of D<sub>2</sub><sup>18</sup>O with the original aim of completing the tabulation of viscosity data for the various isotopic species of water. In our previous<sup>1,2</sup> investigations we also tested the validity of Eyring's absolute rate theory as applied to the viscosity of mixtures of similar liquids for both binary (the H<sub>2</sub><sup>18</sup>O sample contained both H<sub>2</sub><sup>18</sup>O and H<sub>2</sub><sup>16</sup>O) and ternary (the H<sub>2</sub><sup>17</sup>O sample contained H<sub>2</sub><sup>17</sup>O, H<sub>2</sub><sup>16</sup>O, and H<sub>2</sub><sup>18</sup>O) solutions. Due to conditions at our isotope separation plant at the time our samples were collected we were presented with an even more complicated system, that of a quarternary isotope solution, *i.e.*, H, D, <sup>16</sup>O, and <sup>18</sup>O (assuming we can neglect the relatively low <sup>17</sup>O concentration in the sample as was done in the case of H<sub>2</sub><sup>18</sup>O). The presence of a nonnegligible amount of hydrogen (~4%) presents us with a major difficulty in the analysis of our experimental data. The hydrogen exists essentially (~90%) in the form of HDO in samples such as ours. In order to perform the desired extrapolations and theoretical calculations on the viscosity data one requires viscosity and density values corresponding to the pure species for all components present in solution. Pure HDO

does not exist. It exists only in solution and up to a concentration maximum of ~50%. In the discussion we will describe in detail our approach to this problem.

### Experimental Section

*Materials.* The D<sub>2</sub><sup>18</sup>O samples used in this investigation were produced at our isotope separation plant. The purification procedure was exactly as described previously.<sup>1</sup> The hydrogen isotope composition was determined by nmr analysis on a Varian A-60. The oxygen isotope analyses were made by scanning isotope exchanged CO<sub>2</sub><sup>3-5</sup> with an Atlas 150 G.D. mass spectrometer. The analyses of the D<sub>2</sub><sup>18</sup>O samples are listed in Table I. The values reported for the oxygen isotopes are the mean of four independent analyses of each sample together with their mean square deviation.

*Procedure.* The viscosity measurements were performed using a semiautomatic closed viscometer of the suspended-level type, *i.e.*, a modified semimicro Cannon-Ubbelohde viscometer. The apparatus and procedure have been described in detail previously.<sup>1</sup>

TABLE I: Isotopic Compositions of D<sub>2</sub><sup>18</sup>O Samples

Sample	% D	% H	% <sup>16</sup> O	% <sup>17</sup> O	% <sup>18</sup> O
1	95.94	4.06	4.711 ± 0.035	0.462 ± 0.009	94.827 ± 0.042
2	93.59	6.41	7.067 ± 0.017	0.377 ± 0.007	92.556 ± 0.017

TABLE II: Viscosity of Water at Various Temperatures

<i>t</i> , °C	H <sub>2</sub> <sup>16</sup> O			D <sub>2</sub> <sup>18</sup> O			
	$\eta_{\text{ext}}^a$ , cP	$\eta_{\text{lit}}^b$ , cP	$\Delta\%$	$\eta^a(1)$ , cP	$\eta^a(2)$ , cP	$\eta_{\text{calcd}}(2)$ , cP	$\Delta\%$
15	1.138 <sub>6</sub>	1.139	-0.04	1.4764	1.4732	1.4595	-0.92
20	1.0024	1.0020	+0.04	1.2898	1.2797	1.2754	-0.34
25	0.8907	0.8904	+0.03	1.1245	1.1250	1.1132	-1.04
30	0.7975	0.7975	0.00	0.9974	0.9945	0.9879	-0.66
35	0.7191	0.7194	-0.04	0.8929	0.8897	0.8846	-0.57

<sup>a</sup> The error is estimated to be ±0.0006 cP for column 2 and as high as ±0.0020 cP for columns 5 and 6 as determined by a total error analysis of all factor entering into eq 2. <sup>b</sup> Reference 6.

TABLE III: Density of D<sub>2</sub><sup>18</sup>O at Various Temperatures

<i>t</i> , °C	$\rho$ , g cm <sup>-3</sup>		
	(Sample 1)	(Sample 2)	100% D <sub>2</sub> <sup>18</sup> O
15	1.202798	1.195212	1.216786
20	1.202203	1.194598	1.216223
25	1.201216	1.193599	1.215256
30	1.199879	1.192253	1.213930
35	1.198226	1.190598	1.212282

## Results

The absolute viscosity of the D<sub>2</sub><sup>18</sup>O samples reported in Table II were determined by use of

$$\eta = A\rho\tau - B\rho/\tau \quad (1)$$

where  $\eta$  is the absolute viscosity (cP),  $A$  and  $B$  are instrument constants,  $\rho$  is the sample density (g cm<sup>-3</sup>), and  $\tau$  is the flow time. The flow times measured were in the range of 69,000–114,000 counts (~170–285 sec). The instrument constants were determined by a least-squares fit of the National Bureau of Standards values<sup>6</sup> for the absolute viscosity of natural water (H<sub>2</sub><sup>16</sup>O) together with the corresponding flow times measured in our study at the following temperatures: 15, 20, 25, 30, and 35°. The best values were found to be  $A = 1.08010 \times 10^{-4}$  cm<sup>2</sup>/sec<sup>2</sup> and  $B = -2.51220$  cm<sup>2</sup> (cf., Table II, column 4).

Density values for pure D<sub>2</sub><sup>18</sup>O have been reported by Steckel and Szapiro<sup>7</sup> and were calculated by means of a modified version of the empirical equation of Tilton and Taylor<sup>8</sup>

$$(1 - \rho/\rho_{\text{max}}) = F\delta^2 \left( 1.74224 + \frac{480.502}{\delta + 77.861} \right) 10^{-6} \quad (2)$$

where  $F = 1.0555$  (°C<sup>-2</sup>) for D<sub>2</sub><sup>18</sup>O and  $\delta = t - t_{\text{max}}$  (°C). The temperature corresponding to the observed<sup>7</sup> D<sub>2</sub><sup>18</sup>O density maximum,  $t_{\text{max}}$ , is 11.458° and the maximum density is  $1.21691 \pm 0.00008$  g cm<sup>-3</sup>. (The mean square deviation of the differences between their measured and calculated values is ±0.000020 g cm<sup>-3</sup>.) The density values corresponding to our multicomponent samples were calculated by means of

$$\bar{V}_m = \sum N_i \bar{V}_i \quad (3)$$

$$\rho = M/\bar{V}_m \quad (3a)$$

where  $N_i$  and  $\bar{V}_i$  are the mole fraction and molar volume of species  $i$ ,  $M$  is the mole average molecular weight of the mixture, and the subscript  $m$  refers to the mixture. The density values corresponding to D<sub>2</sub><sup>18</sup>O and our samples are listed in Table III.

The absolute viscosity values for pure D<sub>2</sub><sup>18</sup>O were determined by means of Eyring's<sup>9</sup> equations for the viscosity of mixtures of similar liquids

$$\eta_m = (hN/\bar{V}_m) \exp[\sum_i N_i \Delta G_i^\ddagger / RT] \quad (4)$$

$$\Delta G_i^\ddagger = \left[ RT \ln (\bar{V}_m \eta_m / hN) - \sum_{i \neq j} N_i \Delta G_i^\ddagger \right] / N_j \quad (4a)$$

and pure liquids

$$\eta_i = (hN/\bar{V}_i) \exp[\Delta G_i^\ddagger / RT] \quad (5)$$

$$\Delta G_i^\ddagger = RT \{ \ln (\bar{V}_i \eta_i / hN) \} \quad (5a)$$

where  $\Delta G_i^\ddagger$  is the free energy of activation for viscous flow of species  $i$ . The values for the mixture viscosity,  $\eta_m$ , and molar volume,  $\bar{V}_m$ , were substituted into eq 4a together with the values for  $\Delta G^\ddagger(\text{H}_2^{16}\text{O})$ ,  $\Delta G^\ddagger(\text{H}_2^{17}\text{O})$ , and  $\Delta G^\ddagger(\text{D}_2^{16}\text{O})$ , i.e., those calculated by means of eq 5a using the literature values (cf., footnotes in Table IV) for the viscosity and molar volume of the pure species. The values for  $\Delta G^\ddagger(\text{D}_2^{18}\text{O})$  (they decrease from 2.43 to 2.28 kcal/mol in the temperature range of 15 to 35°) thus found were in turn substituted into eq 5 to calculate the absolute viscosity of 100% D<sub>2</sub><sup>18</sup>O in the temperature range investigated. These values for D<sub>2</sub><sup>18</sup>O are reported in Table IV together with the corresponding values for D<sub>2</sub><sup>16</sup>O, H<sub>2</sub><sup>18</sup>O, H<sub>2</sub><sup>17</sup>O, and H<sub>2</sub><sup>16</sup>O.

## Discussion

The difficulty involved in analyzing the experimental data due to the presence of the HDO species may be dealt with in one of two ways.

(i) One may use the available viscosity and density data on H<sub>2</sub><sup>16</sup>O–D<sub>2</sub><sup>16</sup>O mixtures containing very high concentrations of HDO (50–5) mixtures) and extrapolate to determine the viscosity and density values for the hypothetical

TABLE IV: Viscosities of the Various Water Isotopes

$t, ^\circ\text{C}$	$\eta, \text{cP}$				
	$\text{D}_2^{16}\text{O}^a$	$\text{D}_2^{16}\text{O}^b$	$\text{H}_2^{18}\text{O}^c$	$\text{H}_2^{17}\text{O}^d$	$\text{H}_2^{16}\text{O}^e$
15	1.5057	1.4347	1.2008	1.1633	1.139
20	1.3150	1.2471	1.0564	1.0246	1.0020
25	1.1441	1.0966	0.9381	0.9105	0.8904
30	1.0140	0.9732	0.8400	0.8153	0.7975
35	0.9072	0.8710	0.7568	0.7353	0.7194

<sup>a</sup> 100%  $\text{D}_2^{18}\text{O}$  calculated by use of Eyring's theory of viscosity based upon data for sample 1. <sup>b</sup> F. J. Millero, R. Dexter, and E. Hoff, *J. Chem. Eng. Data*, 16, 85 (1971). <sup>c</sup> Reference 1. <sup>d</sup> Reference 2. <sup>e</sup> Reference 6.

TABLE V: Viscosities of Mixtures of  $\text{H}_2^{16}\text{O}$ - $\text{D}_2^{16}\text{O}$  at  $25^\circ$ 

$N_{\text{D}_2^{16}\text{O}}$	$\eta_m/\eta(\text{H}_2^{16}\text{O})$	$\eta_{\text{expt}}, \text{cP}$	$\eta_{\text{calcd}},^a \text{cP}$	$\Delta\%$	$\eta_{\text{calcd}},^b \text{cP}$	$\Delta\%$
(a) Reference 12						
0.206	1.046	0.9314	0.9294	-0.21	0.9263	-0.55
0.368	1.082	0.9634	0.9613	-0.23	0.9566	-0.71
0.550	1.123	0.9999	0.9985	-0.14	0.9931	-0.68
0.709	1.161	1.0338	1.0321	-0.16	1.0274	-0.62
0.848	1.195	1.0640	1.0624	-0.15	1.0593	-0.44
0.980	1.226	1.0916	1.0920	+0.04	1.0915	-0.01
(b) Reference 13						
0.0059	1.00132	0.8916	0.8915	-0.01	0.8914	-0.02
0.2216	1.04968	0.9346	0.9325	-0.22	0.9291	-0.59
0.4285	1.09703	0.9768	0.9735	-0.34	0.9684	-0.86
0.5390	1.12255	0.9995	0.9962	-0.33	0.9908	-0.87
0.7028	1.16078	1.0336	1.0308	-0.27	1.0260	-0.74
0.8268	1.18969	1.0593	1.0577	-0.15	1.0543	-0.47
0.9730	1.22380	1.0897	1.0904	+0.06	1.0898	+0.01

<sup>a</sup>  $\eta_m = (hN/\bar{V}_m) \exp[\sum N_i \Delta G_i^\ddagger / RT]$ . <sup>b</sup>  $\eta_m = 1/\sum N_i/\eta_i$ .

pure HDO. The concentration of the various species present in the solution can be calculated since the equilibrium constant for the reaction



is known ( $\sim 3.8$  at  $25^\circ$ ).<sup>10</sup> Having obtained the viscosity and density values for HDO, we determine the concentration of the various species present in our samples ( $\text{HD}^{16}\text{O}$  and  $\text{HD}^{18}\text{O}$  are assumed to be equivalent with respect to eq 6) and calculate the viscosity of pure  $\text{D}_2^{18}\text{O}$  by use of Eyring's theory.

(ii) We can simplify the analysis of the results to a great extent by neglecting the presence of the HDO species altogether and assume that we are concerned with a quaternary solution composed of  $\text{H}_2^{16}\text{O}$ ,  $\text{H}_2^{18}\text{O}$ ,  $\text{D}_2^{16}\text{O}$ , and  $\text{D}_2^{18}\text{O}$ . An assumption must be made concerning the concentration of each species present in solution. We assume that the mole fraction of each species is the product of the mole fraction of its component atoms.<sup>11</sup> This approach, in essence, is equivalent to assigning to the HDO species viscosity and density values equal to the arithmetic mean of the corresponding  $\text{H}_2\text{O}$  and  $\text{D}_2\text{O}$  values.

The use of the first approach is not advisable since it involves the extrapolation of values for a ternary system ( $\text{HDO}$ ,  $\text{H}_2\text{O}$ , and  $\text{D}_2\text{O}$ ) from a concentration of 50% HDO to the hypothetical pure species. It also further complicates our system by the addition of another component and at the same time neglects the oxygen isotope effect by considering  $\text{HD}^{16}\text{O}$  and  $\text{HD}^{18}\text{O}$  to be equivalent.

We have therefore decided upon the second approach to

the problem, *i.e.*, during the course of the analysis of our experimental results we neglect the presence of the HDO species. In reality,  $\sim 90\%$  of the hydrogen isotope H present, which is about 4% of the total hydrogen, in our samples exists in the form HDO.

We have tested the validity of this simplification by calculating the absolute viscosity values for  $\text{H}_2^{16}\text{O}$ - $\text{D}_2^{16}\text{O}$  mixtures, neglecting the presence of HDO, by means of Eyring's theory of viscosity and comparing them to the experimental values reported by Baker and La Mer<sup>12</sup> and by Jones and Fornwalt.<sup>13</sup> As a further check on this system, we have also calculated the mixture viscosity using<sup>9</sup>

$$\eta_j = N_j / \left[ \left( 1/\eta_m \right) - \sum_{i \neq j} N_i/\eta_i \right] \quad (7)$$

which assumes that the free energy of activation for viscous flow of each species is the same in the mixture as in the pure liquid, *i.e.*, ideal solution behavior. The results are listed in Table V. The agreement between the calculated and experimental values justifies our approach to this problem.

The values obtained using Eyring's theory are in better agreement than those calculated using the linear eq 7. Previously,<sup>2</sup> we have found the opposite to be the case, *i.e.*, eq 7 gave values in better agreement with the experimental data in the case of  $\text{H}_2^{17}\text{O}$  mixtures. This, we believe, reflects the greater deviation from ideal solution behavior for deuterium and hydrogen oxide solutions relative to solutions containing a mixture of oxygen isotopes.

To determine the extent to which the above assumption

TABLE VI: Ratios of the Viscosities of the Pure Isotopic Species of Water

<i>t</i> , °C	$\eta(\text{D}_2^{18}\text{O})/\eta(\text{H}_2^{16}\text{O})$	$\eta(\text{D}_2^{16}\text{O})/\eta(\text{H}_2^{16}\text{O})$	$\eta(\text{H}_2^{18}\text{O})/\eta(\text{H}_2^{16}\text{O})$	$\eta(\text{H}_2^{17}\text{O})/\eta(\text{H}_2^{16}\text{O})$	$\eta(\text{D}_2^{17}\text{O})/\eta(\text{H}_2^{16}\text{O})^a$
15	1.3220	1.2596	1.0543	1.0213	1.28
20	1.3124	1.2446	1.0543	1.0226	1.27
25	1.2849	1.2316	1.0536	1.0226	1.25
30	1.2714	1.2203	1.0520	1.0223	1.24
35	1.2611	1.2107	1.0520	1.0221	1.23

<sup>a</sup> Approximated by assuming  $\eta_{\text{rel}}(\text{D}_2^{17}\text{O}) = 1 + [\eta_{\text{rel}}(\text{D}_2^{16}\text{O}) - 1] + [\eta_{\text{rel}}(\text{H}_2^{17}\text{O}) - 1]$ .

and the use of Eyring's theory of viscosity is valid when applied to our multicomponent system, we calculated the viscosity of the less concentrated D<sub>2</sub><sup>18</sup>O sample 2, using eq 4. The values for  $\Delta G^\ddagger(\text{D}_2^{18}\text{O})$  used in this calculation are those extrapolated from the data for sample 1. The results are listed in Table II, column 7. The agreement between the experimental and calculated viscosity values is not as good as it is for H<sub>2</sub><sup>16</sup>O–D<sub>2</sub><sup>16</sup>O mixtures. The average deviation being 0.71% in the former case as opposed to 0.18% in the latter case. We conclude that the validity of our approach, while affording a convenient means for analyzing the isotope effect, diminishes as the complexity of the system increases.

The effect of isotope substitution on the viscosity is best shown by the viscosity ratios of the various water species. We have listed the relative viscosity,  $\eta_{\text{rel}}$ , values (based upon H<sub>2</sub><sup>16</sup>O) in Table VI. It is of interest to note that the values for  $(\eta_{\text{rel}} - 1)$  for D<sub>2</sub><sup>18</sup>O are very nearly equal to the corresponding sum of those for D<sub>2</sub><sup>16</sup>O and H<sub>2</sub><sup>18</sup>O, especially in the 25–35° range.

Density and viscosity values for D<sub>2</sub><sup>17</sup>O have not been measured and due to the high cost of <sup>17</sup>O it is unlikely that they will be done in the near future. In light of the above-mentioned observation concerning the sum of  $(\eta_{\text{rel}} - 1)$  with regard to D<sub>2</sub><sup>18</sup>O, we believe that we can apply this kind of approximation to obtain the  $\eta_{\text{rel}}$  values for D<sub>2</sub><sup>17</sup>O. *I.e.*

$$\eta_{\text{rel}}(\text{D}_2^{17}\text{O}) = 1 + [\eta_{\text{rel}}(\text{D}_2^{16}\text{O}) - 1] + [\eta_{\text{rel}}(\text{H}_2^{17}\text{O}) - 1] \quad (8)$$

where  $\eta_{\text{rel}}$  is based upon H<sub>2</sub><sup>16</sup>O. The values are listed in Table VI, column 6, and the error is probably no more than 1%.

We conclude that, in general, solutions of the various water isotopes conform very closely to ideal solution behavior and that the HD<sup>17</sup>O species is fairly well approximated by the mean of the H<sub>2</sub>C and D<sub>2</sub>O isotopes.

*Acknowledgment.* We are very much indebted to Dr. J. Borowitz for many fruitful discussions and helpful suggestions during the course of this investigation.

## References and Notes

- (1) A. I. Kudish, D. Wolf and F. Steckel, *J. Chem. Soc., Faraday Trans. 1*, **68**, 2041 (1972).
- (2) A. I. Kudish, D. Wolf and F. Steckel, *J. Chem. Soc., Faraday Trans. 1*, **70**, 484 (1974).
- (3) H. Cohen and H. C. Urey, *J. Amer. Chem. Soc.*, **60**, 679 (1938).
- (4) I. Dostrovsky and F. S. Klein, *Anal. Chem.*, **24**, 414 (1952).
- (5) D. Staschewski, *Ber. Bunsenges. Phys. Chem.*, **68**, 454 (1964).
- (6) (a) These values were calculated from empirical relationships derived from measurements (*cf.*, ref 6b and 6c) in viscometers calibrated with water at 20° (and 1 atm), modified to agree with the currently accepted value for the viscosity of water at 20° of 1.002 cP. The values are tabulated in the "Handbook of Chemistry and Physics," 52nd ed, The Chemical Rubber Co., Cleveland, Ohio, 1971–1972. (b) R. C. Hardy and R. L. Cottingham, *J. Res. Nat. Bur. Stand.*, **42**, 573 (1949); (c) J. F. Swindells, unpublished results.
- (7) F. Steckel and S. Szaciro, *Trans. Faraday Soc.*, **59**, 331 (1963).
- (8) L. W. Tilton and J. K. Taylor, *J. Res. Nat. Bur. Stand.*, **18**, 205 (1937).
- (9) S. Glasstone, K. Laidler, and H. Eyring, "Theory of Rate Processes," McGraw-Hill, New York, N.Y., 1941.
- (10) W. C. Duer and G. L. Bertrand, *J. Chem. Phys.*, **53**, 3020 (1970).
- (11) *E.g.*, the probability of finding a H<sub>2</sub><sup>16</sup>O molecule in our sample is proportional to  $[\text{H}_a][\text{H}_b][^{16}\text{O}]$ . Since we neglect the presence of HDO the probability of the second hydrogen atom, H<sub>b</sub>, reacting to form H<sub>2</sub><sup>16</sup>O is determined by H<sub>a</sub>, *i.e.*, we are concerned only with the "pure species" H<sub>2</sub>O and D<sub>2</sub>O and it follows that the probability of a H isotope reacting with HO is 1 whereas the probability of a D isotope reacting with HO is 0. This is equivalent to saying that the probability is proportional to  $[\text{H}_a][^{16}\text{O}]$ .
- (12) W. N. Baker and V. K. La Mer, *J. Chem. Phys.*, **3**, 406 (1935).
- (13) G. Jones and H. J. Forwalt, *J. Chem. Phys.*, **4**, 30 (1936).

## Chemical Relaxation Studies of Micellar Equilibria

J. Lang, C. Tondre, R. Zana,\*

C.N.R.S., Centre de Recherches sur les Macromolécules, 67083 Strasbourg-Cedex, France

R. Bauer, H. Hoffmann, and W. Ulbricht

Institute for Physical Chemistry I, University of Erlangen, Nuremberg, Erlangen, West Germany (Received July 5, 1974)

Publication costs assisted by Centre de Recherches sur les Macromolécules

Ultrasonic absorption, pressure jump, temperature jump, and shock tube measurements have been performed to investigate the relaxation processes present in solutions of purified sodium lauryl sulfate and laurylpyridinium chloride, bromide, and iodide. The results show the presence of two relaxation processes characterized by the relaxation times  $\tau_1$  and  $\tau_2$  with a ratio  $\tau_2/\tau_1$  over a hundred. Both relaxation times depend on concentration ( $C$ ) and ionic strength ( $\mu$ ). The slow process ( $\tau_2$ ) is more affected by  $\mu$  than the fast one ( $\tau_1$ ). The various models presented to account for these two processes are discussed. It is shown that the available experimental data can be qualitatively explained by assigning  $\tau_1$  to the exchange of detergent ions between the micellar phase and the bulk solvent and  $\tau_2$  to the micellization-dissolution equilibrium. The variation of  $\tau_1$  with the chain length of the detergent ion can be quantitatively explained by assuming the exchange reaction to be diffusion controlled. The interpretation of the variation of  $\tau_2$  with  $C$  at various ionic strength leads to the conclusion that at concentration only slightly above the critical micelle concentration both the aggregation number and the rate constants for the exchange equilibrium depend on  $C$ .

### I. Introduction

Since 1965 chemical relaxation techniques,<sup>1-9</sup> stopped-flow,<sup>6c</sup> nmr,<sup>10,11</sup> and epr<sup>12-14</sup> have been extensively used to study the kinetics of fast processes occurring in micellar solutions. A large number of papers have been now published in this field and briefly the situation is as follows.

(1) Ultrasonic absorption methods have shown the existence of two fast relaxation processes in micellar solutions of ionic surfactants.<sup>7-9</sup> One of these two processes, however, is only observed in fairly concentrated surfactant solutions<sup>7b,9</sup> and has been related to changes of micelle shape.<sup>7b</sup> This process will not be further considered in this paper. The other relaxation process was first assigned to association/dissociation of counterions to/from micelles.<sup>8</sup> However a study of the effect of the nature of the counterion and of the paraffinic chain length of the detergent enabled Graber, Lang, and Zana<sup>7</sup> to show that, in fact, the fast processes are associated to association/dissociation of amphiphilic ions to/from micelles (in the following, such processes are referred to as "exchange" reactions or equilibria). This assignment is in agreement with (a) nmr results for micellar solutions<sup>10,11</sup> which give an upper limit of the relaxation time for exchange reactions and (b) epr data<sup>12</sup> which have permitted the first direct measurement of the exchange rate of a spin-labeled amphiphilic ion between a micelle and the bulk of the solution. Ultrasonic absorption<sup>7b</sup> and epr<sup>12</sup> yield relaxation times of the order of a microsecond for solutions of ionic detergent with a paraffinic chain containing 12 carbon atoms. On the other hand, ultrasonic absorption measurements have shown that the relaxation time increases rapidly with increasing length of the amphiphilic ion.<sup>7b</sup>

(2) Temperature-jump (T jump), pressure-jump (P jump), and stopped flow studies have revealed the existence of a slow process, characterized by a relaxation time in the millisecond range.<sup>1-6</sup> The published results show that the slow process shares two characteristics with the fast one: (a) single relaxation times and not distributions of

relaxation times are associated with both processes and (b) the reciprocals of the long and of the short relaxation times increase linearly with the detergent concentration. In most studies<sup>2,3,6</sup> the slow process has also been assigned to exchange reactions.

Muller<sup>15</sup> was the first to emphasize the peculiarity of this situation where two relaxation times differing by as much as three orders of magnitude are assigned to the same chemical process. He also pointed out that the slow process is not detected when using nmr. To explain these apparent contradictions, Muller reexamined the assumption made in relaxation experiments, namely, that the perturbation of the chemical equilibrium is of sufficiently small amplitude to permit a linearization of the rate equation. He concluded to the nonvalidity of this assumption in the conditions of the T-jump experiments reported by Kresheck, *et al.*,<sup>2</sup> with the underlying consequence that the relaxation time measured by this technique should depend on the amplitude of the perturbation if the kinetic model postulated by these workers was correct. Muller attributed the slow relaxation process to the complete dissolution of the micelles and not to the exchange process.

More recently, Nakagawa<sup>16</sup> reviewed the kinetic results obtained for detergent solutions by means of chemical relaxation and by magnetic (epr and nmr) methods. He was led to postulate a model similar to that presented by Muller, *i.e.*, two reactions occur in micellar solutions, exchange and readjustment of micelles. However, Nakagawa assumed that most relaxation techniques are sensitive only to the exchange process. He proposed a method which makes use of the slope of the reciprocal relaxation time vs. concentration curves to reconcile at least in part the results of the various workers. Nevertheless, Table IV in his paper shows that differences as large as one to two orders of magnitude still persist between the rate constants so obtained for detergents of identical chain length.

The purpose of the present work is to show the following two essential points. (1) Detergent solutions are character-

ized by two relaxation times differing by two to three orders of magnitude. For several detergents both the long and short relaxation times have been measured by means of the same technique. Also, the relaxation time measured in T-jump experiments has been shown to be independent of the amplitude of the perturbation. (2) The relaxation times appear to be extremely sensitive to the ionic strength of the medium. This result has strong implications as regards the validity of the conclusions reached in previous studies where the effect of ionic strength was not thoroughly investigated.

Finally a dynamic model of micelle solution is proposed to explain the available data on the kinetics of micellization. This model is formally similar to that of Muller, but it is made more explicit.

## II. Experimental Section

The following compounds were investigated: laurylpyridinium iodide, bromide, and chloride (LPI, LPBr, and LPCI, respectively), sodium lauryl sulfate (NaLS), and potassium laurate. These compounds were purified by successive recrystallization in water or in mixtures of water and alcohol or acetone. Their critical micelle concentrations (cmc) are known.<sup>17</sup>

The relaxation times were measured by means of the following methods: (1) a T-jump apparatus with a uv absorption detection,<sup>18</sup> (2) a P-jump apparatus with conductivity detection,<sup>19</sup> and (3) a shock tube apparatus with conductivity and/or spectrophotometric detection.<sup>20</sup> In addition, the ultrasonic absorption of solutions of LPCI and LPBr was measured using a two crystal interferometer.<sup>21</sup>

All solutions were prepared with distilled, deionized water to which reagent grade KCl, KBr, or KI was added as specified in the text.

## III. Experimental Results

*1. Influence of the Amplitude of the Temperature Jump on the Relaxation Time Characterizing the Slow Process.* This study was performed on LPI and LPBr because of the large spectral changes associated with the transfer of the pyridinium ring from the micellar phase to the bulk of the solution which permits the observation of the relaxation process even with temperature jumps as small as 0.05°. The results are shown in Figure 1. Within experimental error the measured relaxation times are independent of the amplitude  $\Delta T$  of the temperature jump when  $\Delta T$  is increased from 0.1 to 8° for LPI and from 0.05 to 5° for LPBr. With  $\Delta T = 0.1^\circ$  the perturbation of the micellar solution is very small and eq 7 and 8 in Muller's paper<sup>15</sup> yield very slightly different values for  $(1 + z/[A]_e)^n$  and for its first approximation expansion  $1 + nz/[A]_e$  where  $n$  is the micellar number,  $[A]_e$  the critical micelle concentration (cmc), and  $z$  the change of free detergent concentration brought about by the temperature jump. On the contrary, with  $\Delta T > 5^\circ$  a better approximation of the relaxation time is given by eq 5 in ref 15 and a relaxation time very different from the preceding one should have been measured. That the relaxation time measured in T-jump experiments is independent of  $\Delta T$  implies the nonvalidity of the Krescheck, *et al.*,<sup>2</sup> model of micelle formation.

*2. Existence of Two Relaxation Times.* Two well-separated relaxation times have been detected for several detergent systems. Also, in many instances it has been possible to show that different techniques yield the same results. In view of their importance for the understanding of the ki-

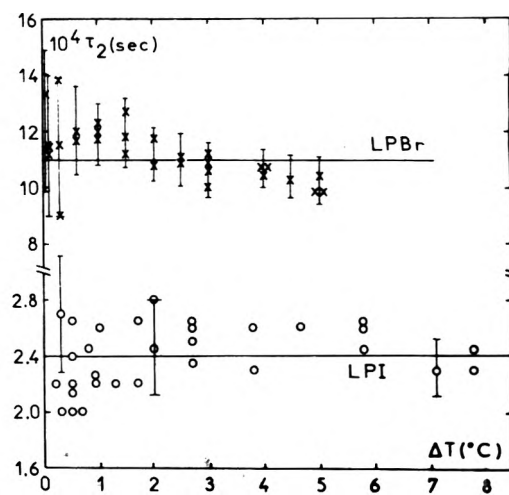


Figure 1. Plots of  $\tau_2$  vs. the amplitude  $\Delta T$  of the temperature jump: (O) LPI ( $C = 2.88 \times 10^{-3} M$ ),  $\lambda$  342 nm; (X) LPBr ( $C = 2 \times 10^{-2} M$ ),  $\lambda$  295 nm; final temperature  $25 \pm 0.2^\circ$ . Ionic strength  $\mu = 5 \times 10^{-2} M$  adjusted with KI and KBr, respectively.

netics of micellar solutions these results will be presented in details.

*a. Sodium Lauryl Sulfate.* The results are shown in Figure 2. The two relaxation times ( $\tau_1$  for the fast process and  $\tau_2$  for the slow process) are in a ratio of over 100 in the whole concentration range. The measurements were performed by means of shock tube ( $\tau_1$ ) and P jump ( $\tau_2$ ) with a conductivity readout. Owing to the vanishing amplitude of the relaxation effects, measurements of  $\tau_2$  could not be carried out at concentrations higher than 0.015 M.

The slow relaxation process has also been detected by other workers by means of P jump<sup>3,4</sup> and T jump with light scattering detection.<sup>6a,b</sup> Results on NaLS other than those reported in this work were generally in agreement. However, in a recent work Folger, Hoffmann, and Ulbricht<sup>22</sup> have shown that these results were probably obtained with samples of NaLS containing impurities and that for pure samples  $1/\tau_2$  does not increase linearly with the total detergent concentration  $C$  but rather goes through a flat maximum in the concentration range investigated (see Figure 2). The effect of impurities on  $1/\tau_2$  appears to be important mainly at concentrations close to the cmc.<sup>22</sup>

The fast relaxation process has also been detected by means of ultrasonic absorption.<sup>8a</sup> The agreement between the two sets of results has been shown to be satisfactory.<sup>22</sup>

*b. Laurylpyridinium Iodide.* Two relaxation times were found for LPI solutions by means of T jump and of P jump and shock tube, in disagreement with the results of other workers<sup>2</sup> who reported that only one relaxation was found in micellar solutions of LPI. However these authors used LPI solutions at an ionic strength of 0.1 M KCl, while KI was used in the present work. Thus, in work of Krescheck, *et al.*,<sup>2</sup> the excess of  $C_i^-$  with respect to  $I^-$  was so large that it may be considered that these authors studied LPCI in presence of KCl rather than LPI in presence of KCl. This point is further substantiated by the value of the cmc of LPI in presence of 0.1 M KCl reported by Krescheck, *et al.*<sup>2</sup> This value ( $6.5 \times 10^{-3} M$ ) is larger than that of LPI in salt free water ( $5.4 \times 10^{-3} M$ ) while a much lower value is expected on the basis of the well-known decrease of cmc at increasing ionic strength. On the other hand, the cmc value of LPCI in 0.1 M NaCl<sup>17</sup> is close to that found for LPI in 0.1 M KCl.

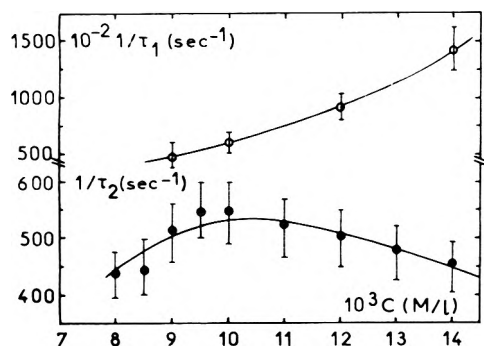


Figure 2. Variation of  $1/\tau_1$  (shock tube) and  $1/\tau_2$  (P jump) with NaLS concentration at  $20^\circ$  and without added salt.

Both relaxation times have been measured as a function of the total concentration  $C$ . The results are shown in Figure 3. Here again, the two relaxation times differ by a factor of over 100. Also the results obtained for the fast relaxation process by means of shock tube and T jump fall on the same curve.

As in the case of NaLS, impurities have been found to strongly affect the value of  $1/\tau_2$  at  $C$  close to the cmc.

*c. Laurylpyridinium Chloride and Bromide.* The measurements performed on these two compounds showed the existence of two relaxation processes. For the slow process, in the concentration range where measurements of the long relaxation time  $\tau_2$  were possible by means of both T jump and P jump, the two methods yielded results in good agreement (see Figures 7 and 11). Evidence of the existence of a fast process was obtained from shock-tube and ultrasonic absorption measurements performed as part of this work and also, for the second method, by other workers,<sup>23</sup> both for LPCl and LPBr. The ultrasonic absorption results are shown in Figure 4, where  $\alpha'/f^2$  ( $\alpha'$  = ultrasonic absorption,  $f$  = frequency) is plotted as a function of  $f$ . The excess absorption of the solution, with respect to water, is significant in the range 1–10 MHz and decreases as  $f$  is increased, thereby indicating a relaxation process with a relaxation frequency well below 1 MHz, *i.e.*, a relaxation time longer than  $0.2 \mu\text{sec}$ . This is in agreement with what is expected from shock tube measurements. Finally it must be pointed out that for the three laurylpyridinium halides investigated, both  $\tau_1$  and  $\tau_2$  increase in the order LPCl < LPBr < LPI, *i.e.*, in the order of decreasing cmc in the absence of added salt. This result appears to be a very general feature of micellar solutions. As for LPI and NaLS, the value of  $1/\tau_2$  is strongly affected by the presence of impurities. Thus the effect of the impurities present in solutions of insufficiently purified detergents (lauryl alcohol in the case of NaLS, and lauryl halides and pyridine in the case of laurylpyridinium halides) always results in a considerable acceleration of the slow process, in dilute micellar solutions. This result suggests that some kind of micelle nucleation is at the origin of this process.

The results of Figures 2 and 3 and those for LPBr and LPCl (see Figures 7 and 11) show that for well-purified detergents  $1/\tau_2$  and  $1/\tau_1$  are finite when measured at concentrations close to the cmc or extrapolated to cmc. Such a finding has been already reported in the case of  $1/\tau_1$  in an ultrasonic absorption study.<sup>7b</sup> For  $1/\tau_2$ , however, it is at variance with previous results as well as results obtained as part of this work on insufficiently purified detergents (see Figure 11) where the values of  $1/\tau_2$  were found to become

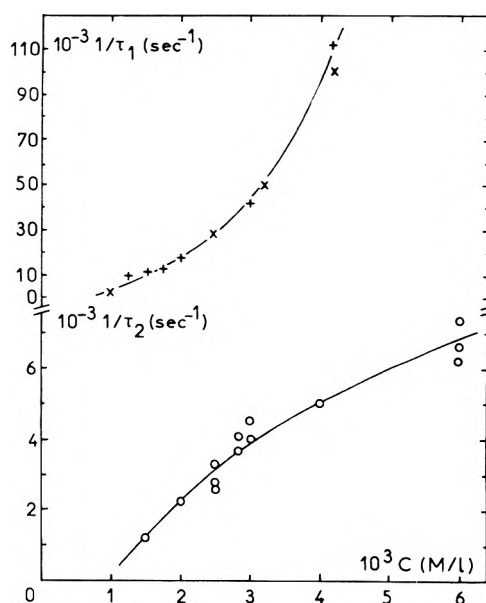


Figure 3. Variation of  $1/\tau_1$  and  $1/\tau_2$  with  $C$  for LPI solutions in 0.05 M KI at  $25^\circ$ : (+) shock-tube experiments; (O, X) T-jump experiments ( $\lambda$  342 nm).

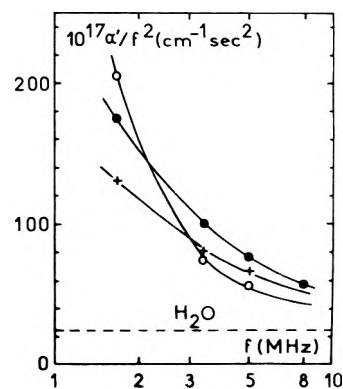


Figure 4. Variation of the ultrasonic absorption of LPCl: (O)  $C = 0.106 \text{ M}$  and ( $\bullet$ )  $C = 0.212 \text{ M}$ ; (+) LPBr  $C = 0.212 \text{ M}$ , as a function of frequency at  $25^\circ$ .

vanishingly small at  $C$  close to the cmc. These discrepancies are of course related to the effect of impurities.

The values of  $1/\tau_1$  and  $1/\tau_2$  at  $C = \text{cmc}$  have been collected in Table I.

*d. Potassium Laurate.* P-jump experiments with conductivity detection performed as part of this work showed the existence of a relaxation process characterized by a single relaxation time much longer than that determined by means of ultrasonic absorption in a previous study.<sup>7b</sup> Thus, as for the four preceding systems two relaxation processes appear to exist in potassium laurate solutions. With potassium octanoate (KOct) solutions the situation is clearly different. Indeed, a fast relaxation process has been detected in previous work by means of ultrasonic absorption<sup>7b,8b</sup> with KOct solutions at  $C/\text{cmc} < 2.5$ . On the contrary, P-jump and shock-tube experiments did not reveal any relaxation process with a time constant longer than  $1 \mu\text{sec}$ . Thus, the slow process is either absent or occurs with an amplitude smaller than the noise level in our experiments. These two possibilities are discussed at the end of section IV.

**TABLE I: Values of the Relaxation Times at  $C = \text{cmc}$** 

	NaLS <sup>a</sup>	LPI <sup>b</sup>	LPBr <sup>b</sup>
$\tau_1$ , $\mu\text{sec}$	29	12	<5
$\tau_2$ , msec	2.3	>100	0.4

<sup>a</sup> Results at 20°. <sup>b</sup> Results at 25°.

3. *Effect of Ionic Strength.* The curves  $1/\tau_2$  vs.  $C$  for LPI and LPBr at various ionic strength  $\mu$  are shown in Figures 5-7.

For the sake of comparison Figure 8 shows the variation of  $1/\tau_2$  with  $\mu$  (added KI) at a total LPI concentration  $C = 2\text{cmc}$ . The results indicate a 50-fold increase of  $1/\tau_2$  when  $\mu$  is increased from 0 to 0.075 M KI. It must be emphasized that this very large increase of  $1/\tau_2$  occurs in spite of a six-fold decrease of  $C$  of the solution. Indeed the cmc of LPI is decreased from  $5.2 \times 10^{-3} M$  in  $\text{H}_2\text{O}$  to about  $0.8 \times 10^{-3} M$  in  $\text{H}_2\text{O}-0.075 M$  KI. Figure 8 also indicates a levelling off of  $1/\tau_2$  at  $C_{\text{KI}} > 0.1 M$ . This result is in agreement with that of Krescheck, *et al.*,<sup>2</sup> who did not observe any change of  $1/\tau_2$  at ionic strength ranging from 0.1 to 0.5.

The results relative to LPBr (Figure 7) define a very complicated pattern. It can be seen that  $1/\tau_2$  may increase, decrease, or go through a maximum or a minimum with increasing  $\mu$ , depending on the value of the ratio  $C/\text{cmc}$ .

P-jump measurements with a conductivity readout performed as part of this work on NaLS and LPI in a limited range of ionic strength show that at a given  $C$ ,  $1/\tau_2$  decreases with increasing  $\mu$ .

The study of the effect of  $\mu$  on  $1/\tau_1$  has thus far been limited to NaLS. The results show a very small increase of  $1/\tau_1$  with  $\mu$ .<sup>22</sup>

#### IV. Discussion

1. *Assignment of the Two Processes.* As pointed out in the Introduction there is now enough qualitative evidence available to assign with certainty to exchange reactions the fast relaxation process detected thus far only by ultrasonic absorption<sup>7,8</sup> and epr,<sup>12</sup> and for the first time in the present work by means of T jump and shock tube. The calculation of the volume changes upon micellization<sup>7,16</sup> based on this assignment yields values in good agreement with the experimental ones,<sup>24</sup> thereby indicating that this assignment is also correct on a quantitative basis. For these reasons the fast relaxation process will not be further considered in this paragraph.

We are thus left with the task of assigning the slow process detected by means of T jump and P jump. As postulated by several authors<sup>2,15,16,22</sup> this process can be ascribed to reaction of micelle formation and dissolution. Our results make it possible to choose among the various mechanisms proposed for these reactions.

First of all, Krescheck, *et al.*,<sup>2</sup> have assumed the breakdown of one amphiphilic ion from the most stable micelle to be the rate-limiting step for micelle dissolution. As pointed out above this model disagrees with our finding that  $1/\tau_2$  is independent of the amplitude  $\Delta T$  of the temperature jump in the range  $0.05^\circ < \Delta T < 8^\circ$ . Another point of disagreement between this model and the experimental results lies in the fact that for LPI, P jump and T jump yield the same results. Indeed the quantity  $z$  in eq 7 of ref 15 takes opposite signs in these two types of experiments because a T jump brings about an increase of cmc in the case of LPI<sup>2</sup> and a P jump (which is in fact a decrease of pressure) always results in a decrease of cmc because the

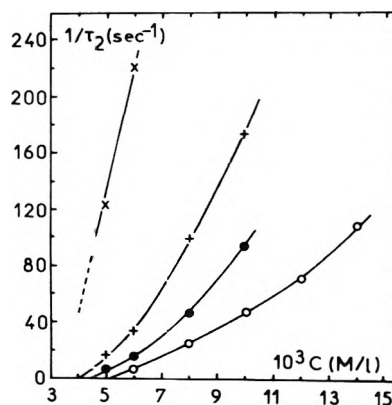


**Figure 5.** Variation of  $1/\tau_2$  for laurylpyridinium iodide with  $C$  at various ionic strengths for P-jump experiments at 25°: (O) no added KI; (●)  $C_{\text{KI}} = 10^{-3} M$ ; (+)  $C_{\text{KI}} = 2 \times 10^{-3} M$ ; (X)  $C_{\text{KI}} = 5 \times 10^{-3} M$ .

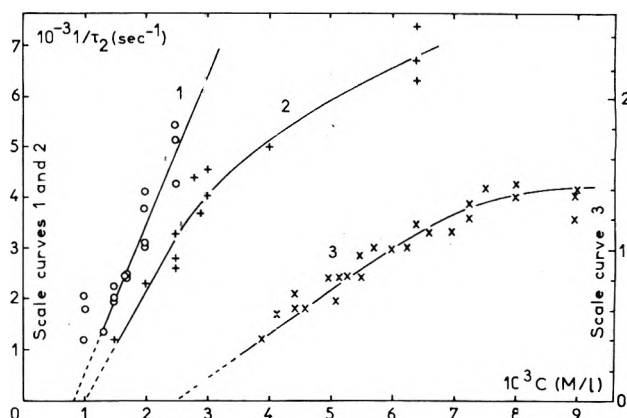


**Figure 6.** Variation of  $1/\tau_2$  for laurylpyridinium iodide with  $C$  at various ionic strengths for T-jump experiments, final temperature 25°,  $\lambda$  342-365 nm: (X)  $C_{\text{KI}} = 10^{-2} M$ ; (+)  $C_{\text{KI}} = 5 \times 10^{-2} M$ ; (O)  $C_{\text{KI}} = 7.5 \times 10^{-2} M$ .

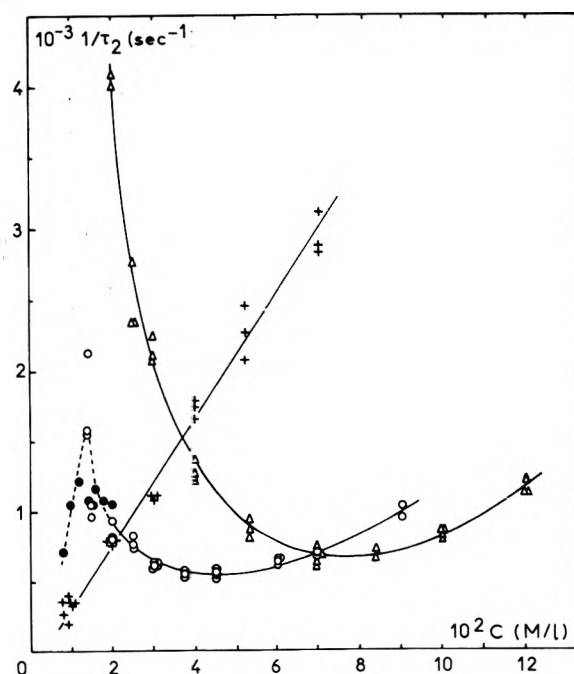


**Figure 7.** Variation of  $1/\tau_2$  for laurylpyridinium bromide with  $C$  at various ionic strengths, T-jump experiments, final temperature 25°,  $\lambda$  290-320 nm: (Δ) without added KBr; (O)  $C_{\text{KBr}} = 10^{-2} M$ ; (+)  $C_{\text{KBr}} = 5 \times 10^{-2} M$ ; (O) P-jump experiments at 25° and  $C_{\text{KBr}} = 10^{-2} M$ .

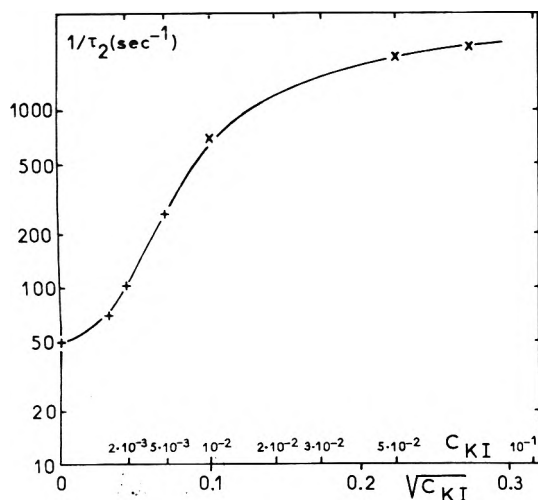


Figure 8. Variation of  $1/\tau_2$  for laurylpyridinium iodide with ionic strength at  $25^\circ$  and  $C/\text{cmc} = 2$ : (+) P-jump; (x) T-jump.

volume change upon micellization is positive.<sup>24</sup> Therefore very different values of  $\tau_2$  should have been measured by T jump and P jump. That such is not the case clearly indicates that model of Kresheck, *et al.*, must be discarded and that the conclusions drawn from studies where the results were interpreted in terms of this model must be reexamined.

Models of micelle equilibria have been recently proposed by Muller<sup>15</sup> and Nakagawa,<sup>16</sup> based on the fact that micelles are not monodispersed. The difference between these two models can be best illustrated by considering the changes of micelle size distribution curve (plot of the number  $N_j$  of micelles *vs.* the aggregation number  $j$ ) upon a perturbation. Although Muller does not explicitly discuss the changes of the micelle size distribution curve upon a perturbation these changes can be inferred from his paper. They are associated with the following two processes.

(a) One or a few amphiphilic ions dissociate from (or associate to) existing micelles, resulting in a shift of the distribution curve from the initial state 1 to state 2 in Figure 9. Nothing precise is said in Muller's work about this shift but it may be assumed that each stable micelle will undergo the same small reduction or increase of micellar number. Process a has been referred to as "exchange" reaction in the Introduction.

(b) A few micelles dissociate completely to (or are formed from) monomers. This reaction is much slower than process a and corresponds to a change in the distribution curve from state 2 to state 3 in Figure 9. In his paper Muller states that both processes can be detected by means of chemical relaxation techniques but that magnetic resonance methods are restricted to process a. It must be added that process b should be strongly affected by impurities since these can act as nuclei for micelle formation.

Nakagawa<sup>16</sup> also assumes the existence of process a. However, in contradistinction to Muller, he then assumes that state 2 relaxes by a slow process to state 4 whose distribution curve is shown in Figure 9 and discards the possibility of a direct passage from state 1 to 4. The passage from state 2 to 4 is presented as a "self-adjustment of micelle distribution, until the final equilibrium is attained." It is moreover assumed that this process is "undetectable by most techniques usually employed in relaxation method, the light scattering being an exception because of its high

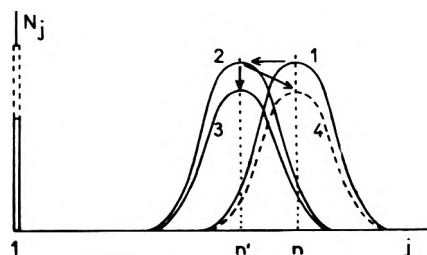
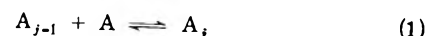


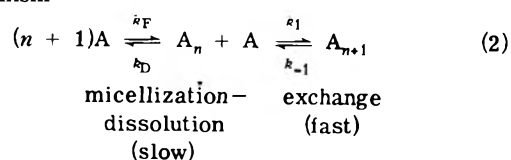
Figure 9. Changes of the distribution curve of micelle size, according to Muller (1  $\rightarrow$  2  $\rightarrow$  3) and Nakagawa (1  $\rightarrow$  2  $\rightarrow$  4).

sensitivity to the change of micelle size" and that it is process a which has been detected in all of the works reported thus far. Such a statement does not appear to be valid however as (i) measurements on NaLS by means of T jump with light scattering detection<sup>6a,b</sup> and P jump with conductivity detection<sup>3,4</sup> yielded very similar values of the relaxation time thereby indicating that the same process is detected by these two methods; (ii) the results given in section III.2 stand in clear disagreement with Nakagawa's approach where relaxations detected by means of ultrasonic absorption and epr on one hand, and by means of T jump and P jump on the other hand are both attributed to process a. Indeed our results show beyond any doubt the existence of two relaxation processes, with relaxation times in a ratio of 100 or more. These two points indicate that some of Nakagawa's assumptions are not valid. They do not however suffice to discard the possibility that an equilibrium between states 2 and 4 is at the origin of the slow relaxation process characterized by  $\tau_2$  and detected by T jump and P jump. This can be done on physical grounds. First, the "self-adjustment" from state 2 to state 4 seems to involve reactions between micelles which are very unlikely because of the strong electrostatic repulsions between so highly charged particles. Also, Nakagawa's model seems to assume an infinite lifetime for the existing micelles because the two processes considered by this author only result in small changes of the average aggregation number. However, a simple reasoning, such as that reported by Muller,<sup>15</sup> clearly shows that micelles have a finite lifetime which is related to the residence time of an amphiphilic ion into the micelle.

2. *Interpretation of the Dependence of the Two Relaxation Times on Various Parameters.* The kinetic model used for the interpretation of the results is very similar to that of Muller; micellization is assumed to proceed by a series of bimolecular steps such as



where  $A_{j-1}$  and  $A_j$  are two micelles of aggregation numbers  $j-1$  and  $j$ , respectively and  $A$  a molecule of free detergent. Exchange reactions are represented by eq 1 where  $j$  can take all of the values of the aggregation number of the stable micelles, *i.e.*, those found in the solution with finite concentration. The coupled exchange and micellization reactions can then be represented by the simplified reaction mechanism



$n$  is the average aggregation number (see Figure 9). According to this model, upon perturbation, one amphiphilic

ion dissociates from micelle  $A_{n+1}$  (or associates with micelle  $A_n$ ) and a few micelles  $A_n$  dissolve to monomers (or monomers associate to form a few  $A_n$ ).

a. *Exchange Process.* This process equilibrates much faster than the micellization-dissolution equilibrium. Therefore the expression of the relaxation time  $\tau_1$  for the exchange process can be derived without consideration to the slow process. This derivation has been attempted by several workers under various assumptions. The association rate constant  $k_1$  has been taken constant<sup>2-4,6,7</sup> or proportional to  $n$ ,<sup>9</sup> or proportional to  $n^{1/3}$ .<sup>16</sup> Whichever the assumption, it has been shown<sup>16</sup> that expressions of the type

$$\frac{1}{\tau_1} = k_{-1} \left( \alpha + \beta \frac{C - \text{cmc}}{\text{cmc}} \right) \quad (3)$$

are obtained where  $k_{-1}$  is the rate constant for the dissociation of one monomer from the most stable micelle;  $\alpha$  a constant equal to 1,  $1/3$ , or 2 according to the authors, and  $\beta = 1$  in most instances.

At the present time Nakagawa's derivation, which is based on the assumption that the rate of the reaction  $A_n + A \rightleftharpoons A_{n+1}$  is proportional to the total surface area of micelle per unit volume, appears to be the most reasonable one available. This derivation can be easily extended as to include the effect of any other parameter  $X$  (such as the surface potential, for example) affecting the kinetics of the exchange process provided that the dependence of  $k_1$  on  $X$  and also the dependence of  $X$  on the aggregation number are known. As shown by Nakagawa in such a case only the values of  $\alpha$  and  $\beta$  would be affected, but the expression of  $\tau_1$  remains unchanged.

On the other hand, it must be pointed out that  $k_{-1}$  is roughly proportional to  $(\text{cmc})^\gamma$  where  $\gamma$  is a constant larger than one. This can be shown in the following way. From the transition state theory one can write

$$k_{-1} \sim \exp(-\Delta G^\ddagger/RT) \quad (4)$$

Moreover, since exchange reactions are diffusion controlled<sup>22,25</sup>

$$\Delta G^\ddagger \approx \Delta G \quad (5)$$

where  $\Delta G$  is the free energy change upon transfer from micelle to water of one amphiphilic ion  $A$ . As a first approximation  $\Delta G$  can be set proportional to the number  $n_C$  of carbon atoms of  $A$ . Thus

$$\Delta G \approx n_C \delta RT \quad (5')$$

For micelles,  $\delta = 1.1$  to  $1.2$ .<sup>26</sup> Finally, it has been shown<sup>27</sup> both experimentally and theoretically that

$$\log \text{cmc} = P - Bn_C \quad (6)$$

where  $B \approx 0.3$ .<sup>27</sup> The combination of eq 4-6 yields

$$k_{-1} \sim (\text{cmc})^{\delta/2.3B} \quad (7)$$

with

$$\gamma = \delta/2.3B = 1.6 \text{ to } 1.8$$

Equations 3 and 7 will be now used to account for the experimental results presently available for the kinetics of the exchange process.

(i) Equation 3 predicts the linear behavior of  $1/\tau_1$  with  $C$ , which has been observed in several ultrasonic absorption studies<sup>7-9</sup> of a variety of ionic detergents. In the case of shock-tube studies (see this work and ref 22) the plots of

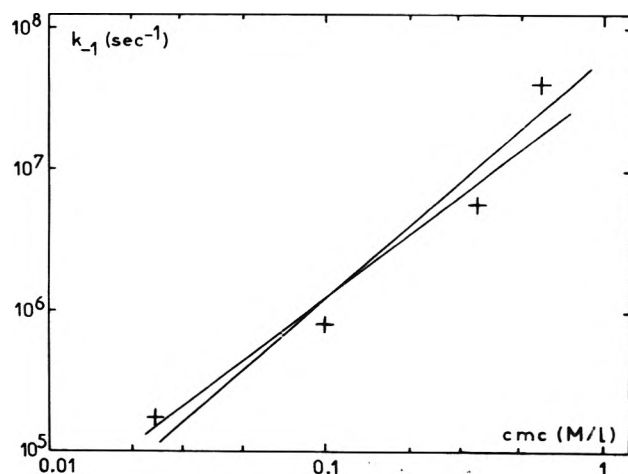


Figure 10. Variation of  $\log k_{-1}$  vs.  $\log \text{cmc}$  for potassium carboxylates. The values of  $k_{-1}$  are those from ref 7b.

$1/\tau_1$  vs.  $C$  show a slight upward curvature. However, these experiments were performed at concentration closer to the cmc ( $C/\text{cmc} < 2$ ) than ultrasonic studies. It is possible that in this concentration range the polydispersity of micelles is larger than at higher concentrations and affects the kinetics of the exchange process. This curvature may also be taken as an evidence of an increase of  $k_{-1}$  as the micelles build up upon increasing detergent concentration. We shall further discuss this point at a later stage.

(ii) Equations 3 and 7 account for the fact that the measured relaxation time may or may not depend on the counterion for a given ionic detergent. Indeed the cmc's of sodium, potassium, and cesium decanoates differ only little and the measured  $\tau_1$  at a given  $(C - \text{cmc})/\text{cmc}$  are very close for these three detergent, as expected from eq 3 and 7. On the contrary, laurylpyridinium halides have cmc's decreasing in the order  $\text{Cl}^- > \text{Br}^- > \text{I}^-$  and the  $1/\tau_1$  values have been found in this work to decrease in the same sequence.

(iii) Equation 7 accounts for the increase of  $k_{-1}$  with cmc reported in an ultrasonic study of potassium carboxylates.<sup>7b</sup> Although the plot of  $\log k_{-1}$  vs.  $\log \text{cmc}$  shows a positive curvature (see Figure 10) the two straight lines drawn through the experimental points yield values of the slope  $\gamma$  between 1.5 and 1.7, in surprisingly good agreement with the above estimate, despite the approximations made in deriving eq 7.

b. *Micellization-Dissolution Equilibrium.* In eq 2,  $k_F$  and  $k_D$  represent overall rate constants for the whole sequence of elementary steps. They are probably related to  $k_1$  and  $k_{-1}$  in a very complicated manner if one wants to take into account the variations of all the parameters which are involved in micelle formation and dissolution. For this reason the derivation of an (exact) analytical expression of  $\tau_2$  by means of the classical procedures of chemical relaxation is not possible at the present time without making drastic simplifying assumptions. There has been a very promising attempt to obtain an analytical expression of  $\tau_2$ , which makes use of the formalism of heat conduction.<sup>28</sup> For the purpose of the present work it suffices to point out that since exchange and dissolution are coupled reactions with the former much faster than the latter,  $1/\tau_2$  should be of the form<sup>29</sup>

$$\frac{1}{\tau_2} = k_D + \frac{k_F}{1/\tau_1} f(C, \text{cmc}) \quad (8)$$

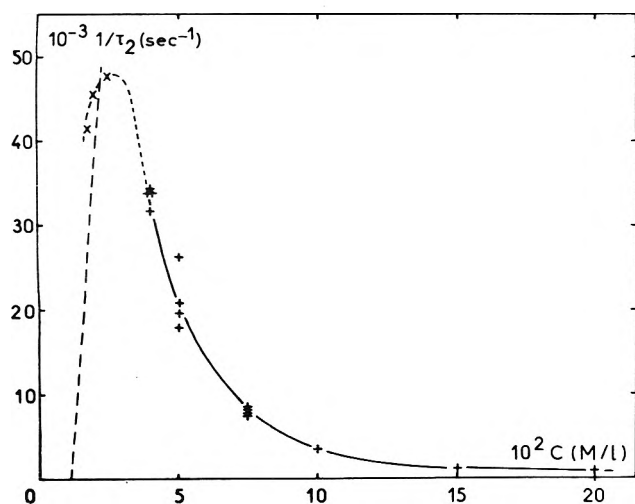


Figure 11. Variation of  $1/\tau_2$  with  $C$  for solutions of laurylpyridinium chloride at  $15^\circ$ : (X) P-jump; (+) T-jump,  $\lambda$  280 nm. The results given for the three higher concentrations are average values over four or five T-jump experiments. The curve in dotted line shows the results obtained by means of P-jump with the nonpurified detergent.

In this equation  $k_D$  is expected to be predominant at low concentration and the  $k_F$  term at high concentration. Muller<sup>15</sup> has shown that  $k_D$  is related to  $k_{-1}$  by the approximate relation

$$k_D = k_{-1}/n^2 \quad (9)$$

As will be shown now eq 8 and 9 can be used to account for the results concerning the variation of  $\tau_2$  with  $C$  and ionic strength.

First it must be pointed out that at concentration close to the cmc, an increase of  $C$  is likely to result in an increase of the average aggregation number  $n$ , and of the surface potential of the micelle. This in turn should result in an increase of  $k_{-1}$  because of the increased electrostatic repulsion between the amphiphilic ions constituting one micelle. It has been pointed out above that this increase may explain in part the positive curvature of the plots of  $1/\tau_1$  vs.  $C$  (see Figures 2 and 3). Thus, at concentrations close to the cmc, where the  $k_D$  term in eq 9 is predominant,  $1/\tau_2$  will go through a maximum or show a decrease as  $C$  is increased, depending on whether or not  $k_{-1}$  increases faster than  $n$ . At higher concentration both  $k_{-1}$  and  $n$  level off as the most stable micelles are constituted and only their number increases with  $C$ . The  $k_F$  term in eq 9 may then become comparable or larger than  $k_D$ , and bring about an increase of  $1/\tau_2$ . Various situations may therefore arise.

(i) In the most complicated one,  $1/\tau_2$  will go successively through a maximum at very low  $C$  and then through a minimum. This is the case for LPBr in 0.01 M KBr and probably also in the absence of added salt although the very low range of  $C$  was not investigated (see Figure 7). For NaLS a maximum is apparent at low  $C$  but the higher concentration range was not investigated.

(ii) If the build up of the micelles occurs in a very narrow concentration range the initial maximum or decrease yields to an increase of  $1/\tau_2$  with  $C$ . This appears to be the case for LPI at all ionic strength (Figures 5 and 6) and for LPBr in 0.05 M KBr (Figure 7). The examination of the results

for LPBr reveals that an increase of the ionic strength  $\mu$  brings about a passage from situation i to ii. This is understandable as indeed an increasing  $\mu$  results in a large increase of  $n$  and a decrease of  $k_{-1}$  because of the reduced electrostatic interaction. Thus the  $k_D$  term decreases very fast and the larger the ionic strength, the lower the concentration at which the influence of the  $k_F$  term in eq 8 is sensitive.

(iii) If the build up of micelles occurs in a wide range of concentration and/or if the  $k_F$  term in eq 8 remains small the curve  $1/\tau_2$  vs.  $C$  may show only a monotonous decrease, as for LPCI in the absence of added salt (Figure 11). This situation appears to occur for detergents with relatively high cmc.

Moreover, eq 7-9 indicate that  $1/\tau_2$  should decrease rapidly with increasing  $n_C$ . This increase should also bring about a passage from situation i to ii. Indeed it is known<sup>27</sup> that such a variation results in an increase of aggregation number and a decrease of cmc, and thus both  $k_{-1}$  and  $k_D$  should be decreased, with  $k_D$  more affected than  $k_{-1}$ , as indicated by eq 9. Results for sodium alkyl sulfates<sup>3,30</sup> and alkylpyridinium bromides<sup>31</sup> and chlorides<sup>30</sup> do indeed show that  $\tau_2$  becomes longer with increasing chain length.

Finally, the fact that only one relaxation process was found in solutions of potassium octanoate may also be explained in terms of the above model. Indeed, micelles formed by octanoate detergents are much smaller than those of LP halides or potassium laurate. It may be thought that the distribution curve of small detergents stretches from monomers to micelles through intermediate species in finite concentrations or that it shows only a narrow dip corresponding to unstable micelles. In the first case it would be possible to go from monomers to micelles through a series of exchange reactions between stable aggregates. The dissolution-micellization equilibrium should then disappear because in our model this equilibrium occurs between stable micelles and monomers, through intermediate species present only with very small concentrations. If the distribution curve shows only a narrow dip, the amplitude of the dissolution process may be very small since it involves mainly reactions between stable species and very few with unstable micelles. In addition its relaxation time may not differ very much from that of exchange reactions.

## V. Conclusions

The experiments reported in this work have definitely proved the existence of two relaxation processes related to micellar equilibria in solutions of ionic detergents, not taking into account the additional relaxation processes detected by means of ultrasonic absorption in more concentrated solutions. These processes have been assigned to exchange and micellization-dissolution equilibria. Using the model previously developed by Muller in a more explicit manner it has been possible to account for the dependence of the two relaxation processes on various parameters: concentration, nature of the counterion, ionic strength, and number of carbon atoms of the amphiphilic ion.

*Acknowledgments.* Three of the authors (R.B., H.H., and W.V.) thank the Deutschen Forschungsgemeinschaft (DFG) for a research grant in support of this work and the Fa. Henkel u. Cie GmbH, Düsseldorf, for the donation of the detergents used in this investigations.

## References and Notes

- (1) P. J. Minjlieff and R. Ditmarsch, *Nature (London)*, **208**, 889 (1965).
- (2) G. Kresheck, E. Hamori, G. Davenport, and H. Scheraga, *J. Amer. Chem. Soc.*, **88**, 246 (1966).
- (3) K. Takeda and N. Tatsunaga, *J. Colloid. Interface Sci.*, **40**, 127 (1972); **45**, 406 (1973).
- (4) T. Janjic and H. Hoffmann, *Z. Phys. Chem. (Frankfurt am Main)*, **86**, 322 (1973).
- (5) U. Herrmann and M. Kahlveit, *Ber. Bunsenges. Phys. Chem.*, **77**, 1119 (1973).
- (6) (a) B. Bennion, L. Tong, L. Holmes, and E. Eyring, *J. Phys. Chem.*, **73**, 3288 (1969); (b) B. Bennion and E. Eyring, *J. Colloid Interface Sci.*, **32**, 286 (1970); (c) J. Lang, J. Auburn, and E. Eyring, *ibid.*, **41**, 484 (1972); (d) J. Lang and E. Eyring, *J. Polym. Sci., Part A-2*, **10**, 89 (1972).
- (7) (a) R. Zana and J. Lang, *C. R. Acad. Sci., Ser. C*, **266**, 893, 1347 (1968); (b) E. Graber, J. Lang, and R. Zana, *Kolloid-Z. Z. Polym.*, **238**, 470, 479 (1970).
- (8) (a) T. Yasunaga, H. Oguri, and M. Miura, *J. Colloid Interface Sci.*, **23**, 352 (1967); (b) T. Yasunaga, S. Fujii, and M. Miura, *ibid.*, **30**, 399 (1969).
- (9) J. Rassing, P. Sams, and E. Wyn-Jones, *J. Chem. Soc., Faraday Trans. 2*, **69**, 180 (1973).
- (10) T. Nakagawa, H. Inoue, H. Jizimoto, and K. Horiuchi, *Kolloid-Z. Z. Polym.*, **229**, 159 (1969); T. Nakagawa and K. Tori, *ibid.*, **194**, 143 (1964).
- (11) N. Muller and F. Platko, *J. Phys. Chem.*, **75**, 547 (1971).
- (12) K. Fox, *Trans. Faraday Soc.*, **67**, 2802 (1971).
- (13) J. Oakes, *J. Chem. Soc., Faraday Trans. 2*, **68**, 1464 (1972).
- (14) T. Nakagawa and H. Jizimoto, *Kolloid-Z. Z. Polym.*, **250**, 591 (1972).
- (15) N. Muller, *J. Phys. Chem.*, **76**, 3017 (1972).
- (16) T. Nakagawa, *Colloid Polym. Sci.*, **252**, 56 (1974).
- (17) P. Mukerjee and K. Mysels, *Nat. Stand. Ref. Data Ser., Nat. Bur. Stand., No. 36*, (1971).
- (18) J. Sturm, R. Zana, and M. Daune, manuscript submitted for publication.
- (19) H. Strehlow and M. Becker, *Z. Elektrochem. Ber. Bunsenges. Phys. Chem.*, **63**, 457 (1959).
- (20) G. Platz and H. Hoffmann, *Ber. Bunsenges. Phys. Chem.*, **76**, 491 (1972).
- (21) R. S. Musa, *J. Acoust. Soc. Amer.*, **30**, 215 (1958).
- (22) R. Folger, H. Hoffmann, and W. Ulbricht, *Ber. Bunsenges. Phys. Chem.*, **78**, 986 (1974).
- (23) K. M. Lee, Daehan Hwahak Hwojee, **17**, 72 (1973); summary in *Chem. Abstr.*, **79**, 4798v (1973).
- (24) J. Corkill, J. Goodman, and T. Walker, *Trans. Faraday Soc.*, **63**, 768 (1967); M. Tanaka, S. Kaneshina, K. Shin-No, T. Okajima, and T. Tomida, *J. Colloid. Sci.*, **46**, 132 (1974); K. Shinoda and T. Soda, *J. Phys. Chem.*, **67**, 2072 (1963).
- (25) J. Brotherus and P. Tormälä, *Kolloid-Z. Z. Polym.*, **241**, 774 (1973).
- (26) P. Mukerjee, *Advan. Colloid. Interface Sci.*, **1**, 241 (1967).
- (27) K. Shinoda, "Colloidal Surfactants," Huchingson and Van Ryselberghe, Ed., Academic Press, New York, N.Y., 1963, pp 1-88.
- (28) E. Aniansson and S. Wall, *J. Phys. Chem.*, **78**, 1024 (1974).
- (29) M. Eigen, *Angew. Chem., Int. Ed. Engl.*, **3**, 1 (1964).
- (30) H. Hoffmann, R. Folger, and W. Ulbricht, unpublished results.
- (31) C. Tondre, J. Lang, and R. Zana, unpublished results.

## Depolarization Thermocurrents Study of Polymers above the Glass Transition Temperature

C. Lacabanne\* and D. Chatain

Laboratoire de Physique des Solides, Associé au C.N.R.S., Université Paul Sabatier, 31077 Toulouse Cedex, France

(Received September 24, 1973; Revised Manuscript Received June 11, 1974)

Publication costs assisted by Laboratoire de Physique des Solides

In polymers, below the glass transition temperature, molecular movements can be described by activated states theories. The depolarization thermocurrents (DTC) method has given interesting results on the associated relaxations. The aim of this paper is to show that this technique can also be applied to the study of nonactivated relaxations. Above the glass transition temperature, some molecular theories predict that the relaxation time would become infinite at a "critical" temperature. Then, this temperature could be deduced from the analysis of the corresponding DTC spectra. The DTC study of a semiaromatic polyamide, poly(ethyleneisophthalamide), shows the existence of such a critical temperature.

### Introduction

Owing its high sensitivity and resolving power, the depolarization thermocurrents method<sup>1-5</sup> has been used for the study of secondary relaxations in partially crystalline polymers.<sup>16-19</sup> Those mechanisms which involve rotations of side groups attached to the main chain or local motions within the chain backbone are observed at low temperatures and show a constant activation energy.

At higher temperatures, a relaxation region associated with the glass transition is observed: it is usually labeled the primary or glass-rubber relaxation.<sup>20,21</sup> From a molecular point of view, it has been widely accepted for many years that the glass-rubber relaxation results from large-scale conformational rearrangements of the polymer chain backbone.

In dielectric measurements, the criteria by which the primary dispersion can be distinguished from any other dispersions are as follows: the dispersion temperature should be in the vicinity or above the glass transition temperature; the strength of dispersion should increase with the increase in the fraction of the amorphous phase; the "apparent" activation energy should be relatively large and strongly temperature dependent.<sup>22</sup>

The analysis of the DTC method, presented in the first part of this paper, shows that it gives the dependence on temperature of the dielectric relaxation time without any assumption about the nature of the mechanism. Therefore, the "apparent" activation energy vs. temperature is obtained.

In the second part of this paper, the results of current molecular theories of the glass-rubber relaxation are brief-

ly outlined. The average relaxation time has been related either to the so-called "free volume," or to "quasistatic" properties; this relaxation time should become infinite for a "critical" temperature.

This critical temperature can be obtained from the analysis of the DTC spectrum observed above the glass transition temperature. The thermal expansion coefficient of the fractional free volume or the ratio, height of the potential energy barrier per monomer unit/difference in specific heat between the equilibrium melt and the glass, can also be estimated (third part).

In the last part, the DTC study of poly(ethyleneisophthalamide) above its glass transition temperature is presented.

## I. Principle of the Method

The sample to be investigated is polarized by an electric field at a temperature  $T_p$  for a period much longer than the relaxation time  $\tau(T_p)$ . After a rapid cooling to a temperature lower than  $T_p$ , the electric field is turned off. On warming the sample, the polarization is released.

*1.1. Single Relaxation Time.* We assume that, in the studied sample, we can define a single relaxation time  $\tau$  at a given temperature. We call  $N$  the number of units that can be polarized by an electric field.

The corresponding variation  $dN$  vs. time  $t$  is given by

$$dN/N = - dt/\tau$$

If one polarizes the sample at the temperature  $T_p$ , the polarization  $P$  would take on a value  $P_0$  after an infinite time.

This polarization is quenched at a sufficiently low temperature, and, the temperature of the sample is given by  $T(t)$ .

The corresponding depolarization is

$$P = P_0 \exp\left(-\int_0^t \frac{dt'}{\tau(T(t'))}\right)$$

and the depolarization current

$$j(t) = - dP/dt$$

so

$$j(t) = P(t)/\tau(t)$$

The last equation can be rewritten

$$\tau(T) = P(T)/j(T) \quad (1)$$

We see that the measurement of  $P(T)$  and  $j(T)$  from a DTC spectrum gives the variation of the relaxation time vs. temperature in the corresponding temperature range without any assumption about the nature of the studied mechanism.

If the temperature is a monotonic increasing function of time, the density of current is maximum for the temperature  $T_M$  such that

$$\left\{ \frac{d}{dT} \ln \tau \right\}_{T_M} = - \frac{1}{b\tau(T_M)}$$

where

$$b \equiv (dT/dt)_{T_M} \quad (2)$$

where  $b \equiv (dT/dt)_{T_M}$

This equation can be used for the determination of the different parameters which intervene in the variation law of the relaxation time.

*1.2. Discrete Distribution of Relaxation Times.* If the parameters of the various processes are not of the same

order of magnitude, there is no interaction among the responses of the various mechanisms: the thermocurrent spectrum will be resolved and each thermocurrent peak can be interpreted separately from the others. If the various processes are close, the thermocurrent spectrum is not resolved. However, the relaxation time is always a steeply decreasing function of temperature; so, the thermocurrent spectrum can be experimentally resolved into isolated "pure" peaks by an appropriate choice of the conditions of polarization.<sup>5,7,16,19</sup> Each "pure" DTC peak is then studied independently from the others.

*1.3. Continuous Distribution of Relaxation Times.* In the last case, the individual thermocurrents must pass through a maximum at a temperature which varies in a continuous manner with the polarization conditions (time and temperature of polarization). Nomura and Kojima<sup>23</sup> introduced in the theory of thermal stimulated currents (TSC) the distributing relaxation time. They considered a system of dipoles which has two alternative sites separated by a potential barrier. By taking the experimental data on the TSC into account, they deduced the order estimation on parameters which characterize the shape of potential barriers.

## II. The Williams, Landel, and Ferry Equation, the Free Volume Theory, and the Statistical Thermodynamic Theory

*II.1. The Williams, Landel, and Ferry Equation.* Williams, Landel, and Ferry have proposed an empirical equation which describes the temperature dependence of relaxation times in the glass transition region.<sup>24,25</sup> This equation is now well known as the WLF equation and can be written in the "universal" form

$$\log a_T = - \frac{c_1^g(T - T_g)}{c_2^g + T - T_g}$$

where  $T_g$  is the glass transition temperature.

The "universal" constants  $c_1^g$  and  $c_2^g$  have approximate values of 17.44 and 51.6°, respectively, for a wide variety of glass-forming materials.

This equation implies that, at a temperature  $T = T_g - c_2^g$ , the relaxation time of the polymer is infinite. This has led to the view that the WLF equation should be related at the molecular level to the temperature  $T = T_g - c_2^g$  rather than to the dilatometric glass transition  $T_g$ .

There have been two basic approaches along these lines. The free volume theory is modified so that the changes in free volume with temperature relate to a discontinuity which occurs at  $T_\infty = T_g - c_2^g$  rather than  $T_g$ . This is discussed in section II.2. The existence of a true thermodynamic transition temperature,  $T_2$ , has been shown. A modified transition-state theory is developed in which the frequency of molecular jumps relates to the cooperative movement of a group of segments of the chain. The number of segments acting cooperatively is then calculated from statistical thermodynamic considerations. This is the theory of Adam and Gibbs; the results are given in section II.3.

*II.2. The Free Volume Theory of Cohen and Turnbull.* Cohen and Turnbull<sup>26,27</sup> have proposed that the free volume,  $v_f$ , corresponds to that part of excess volume which can be redistributed without a change in energy.

The definition of the fractional free volume,  $f$ , is  $f \equiv v_f/v$  where  $v$  is the measured specific volume of the polymer at temperature  $T$ .

For small excess volume, the redistribution energy will be large and thus  $f \equiv 0$  for  $T < T_\infty$ .

At a sufficiently large excess volume, most of the volume added by thermal expansion will be available for redistribution. Accordingly, Cohen and Turnbull have written  $f = \alpha_f(T - T_\infty)$  for  $T \geq T_\infty$ , where  $\alpha_f$  has the dimensions of a thermal expansion coefficient.

This gives for the relaxation time

$$\tau(T) = \tau_0 \exp \frac{1}{\alpha_f} \frac{1}{T - T_\infty} \quad (3)$$

Note that letting

$$c_1^g = \frac{1}{2.30 \alpha_f (T_g - T_\infty)}$$

and

$$c_2^g = T_g - T_\infty \quad (4)$$

in the WLF equation gives us expression 3.

Free volume concepts are widely used but the free volume is ill defined operationally;<sup>28</sup> it cannot be associated with a real molecular volume and has to be interpreted in a hitherto undefined way on the basis of inter- and intramolecular interaction.

**III.3. The Statistical Thermodynamic Theory of Adam and Gibbs** Adam and Gibbs<sup>29</sup> define a cooperatively rearranging region as a subsystem of the sample which can rearrange into another configuration independently of its environment.

This theory explains the temperature dependence of relaxation phenomena in terms of the temperature dependence of the size of the cooperatively rearranging region. Gibbs and Di Marzio<sup>30</sup> proposed that the dilatometric  $T_g$  is a manifestation of a true equilibrium second-order transition at the temperature  $T_2$  where the configurational entropy vanishes. At this temperature, the cooperatively rearranging region must, of course, comprise the whole sample. At higher temperatures, however, the much larger number of configurations available to the system allows individual rearrangements into different configurations for microscopic cooperative regions. Now, there must be a lower limit to the size of a cooperative subsystem that can perform a rearrangement into another configuration. Adam and Gibbs have shown that the overwhelming majority of transitions are undergone by regions where size differs negligibly from the smallest size that permits a transition at all. Thus the relaxation time can be written

$$\tau(T) = \tau'_0 \exp \frac{s^* \Delta E}{k \Delta C_p} \frac{1}{T \ln (T/T_2)} \quad (5)$$

where  $\Delta E$  is largely the potential energy hindering the cooperative rearrangement per monomer segment;  $\Delta C_p$ , the difference in specific heat between the equilibrium melt and the glass at  $T_g$ ; and,  $s^*$ , the lower limit to the configurational entropy of a cooperative subsystem that can perform a rearrangement into another configuration.

A first approximation of this critical value is  $s^* = k \ln 2$ ;  $\Delta E$ ,  $\Delta C_p$ , and  $\tau'_0$  are assumed to be constant over the considered temperature range.<sup>31</sup>

### III. DTC Study of the Glass-Rubber Relaxation

**III.1. Identification of Relaxations with a Temperature Dependent "Apparent" Activation Enthalpy.** The relaxations described by thermally activated states theories have a relaxation time given by<sup>31</sup>

$$\tau(T) = \tau_0'' \exp \frac{\Delta H}{kT}$$

where the activation enthalpy,  $\Delta H$ , is a constant.

Then, the analysis of the DTC spectrum shows that  $\ln [P(T)/j(T)]$  is a linear function of  $1/T$  (cf. eq 1).

If  $\ln [P(T)/j(T)]$  is not a linear function of  $1/T$ , this can be due to a discrete or a continuous spectrum of relaxation times. Then, the temperature corresponding to the thermocurrent maximum will be strongly dependent on conditions of polarization.

A thermocurrent spectrum characterized by a temperature of thermocurrent maximum independent of the conditions of polarization and by a nonlinear variation of  $\ln [P(T)/j(T)]$  vs.  $1/T$  must be assigned to a single relaxation time with an "apparent" activation enthalpy

$$\Delta H = k \frac{d}{d(1/T)} \left\{ \ln \frac{P(T)}{j(T)} \right\}$$

which is a function of temperature. One can deduce from the DTC spectrum the variation of  $\Delta H$  vs. temperature.

If  $\Delta H$  is a decreasing function, theories of the glass-rubber transition may be used to fit the experimental results.

**III.2. DTC Spectrum above the Glass Transition Temperature.** If the results are interpreted on the basis of the theory of Cohen and Turnbull, one must find the temperature  $T_\infty$  such that  $\ln [P(T)/j(T)]$  plotted vs.  $1/(T - T_\infty)$  should be a straight line (cf. eq 1 and 3); then, the slope of this line is the thermal expansion coefficient of the free volume  $\alpha_f$ .  $\alpha_f$  can also be obtained from the characteristics of the maximum of thermocurrent. Indeed, 2 becomes

$$\alpha_f = \frac{bP(T_M)/j(T_M)}{(T_M - T_\infty)^2}$$

The results can also be described by the WLF equation. If  $T_g$  is known,  $c_1^g$  and  $c_2^g$  are given by eq 4. It is sometimes interesting to know the order of magnitude of  $T_g$ ; it can be obtained from eq 4 by adopting the empirical value for  $c_2^g$ .

The theory of Adam and Gibbs may also be used for the interpretation of the results; then, the variation of  $\ln [P(T)/j(T)]$  vs.  $1/T \ln (T/T_2)$  (cf. eq 1 and 5) and the slope of this line give an estimation of the ratio  $\Delta E/\Delta C_p$ .

### IV. Example DTC Study of Poly(ethyleneisophthalamide) above the Glass Transition Temperature

The experimental set-up we used has been described previously.<sup>5,16,18,19</sup> The depolarization thermocurrent was detected by means of a Cary Model 401 vibrating reed electrometer coupled to a two-pen recorder. The emf of a thermocouple located on one of the electrodes was recorded by one of the pens. The sample container allowed the work to be performed *in vacuo* or in a controlled atmosphere in the temperature range between liquid nitrogen temperature and 300°; the heating rate could be chosen in the range 0.02–0.2 deg sec<sup>-1</sup>.

The samples were synthesized and characterized by the method reported by Soulier, *et al.*<sup>33</sup> From differential thermal analysis experiments, the glass transition has been found at 190°. At some 60° higher, the thermocurrents isolated in this temperature range pass through a maximum. The analysis of this spectrum was performed using eq 1; Figure 1 shows that the plot of  $\ln \tau$  as a function of  $1/T$  is not a straight line. This response could be due to a discrete or a continuous spectrum of relaxation times.

In these cases, experiments performed with different polarization temperatures might give DTC peaks at different  $T_M$ ; this is not true here.

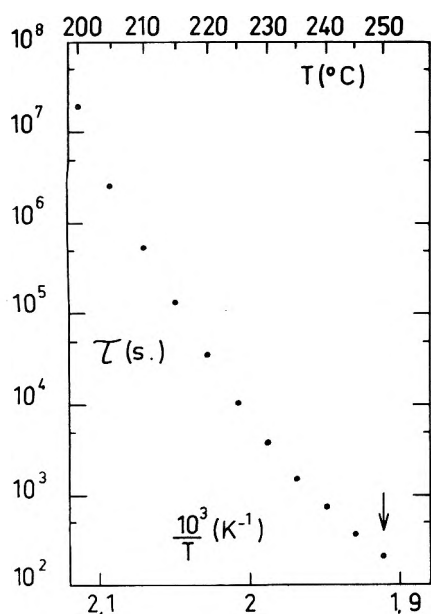


Figure 1. Plot of  $\ln \tau$  as a function of  $10^3/T$  from the DTC peak observed in poly(ethyleneisophthalamide) above the glass transition temperature. The arrow indicates the position of the maximum thermocurrent.

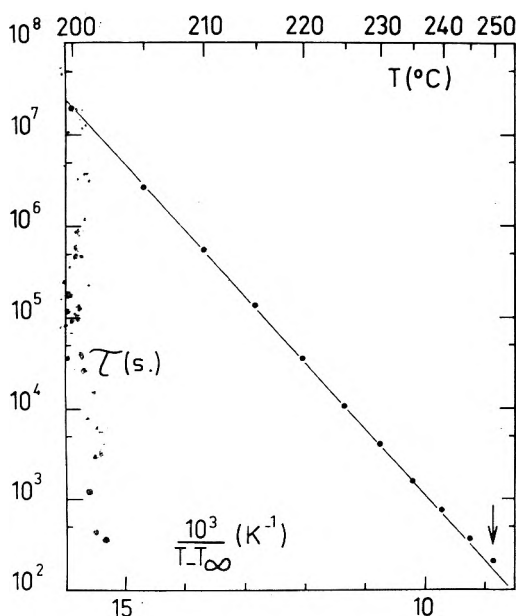


Figure 2. The plot of  $\ln \tau$  as a function of  $10^3/(T - T_\infty)$  where  $T_\infty = 410$  K from the DTC peak observed in poly(ethyleneisophthalamide) above the glass transition temperature. The arrow indicates the position of the maximum thermocurrent.

We have verified that this peak is always situated at the same temperature, independent of the polarization conditions, if the warming rate is held constant. Therefore, these thermocurrents must be due to a mechanism characterized by a *single* relaxation time with an "apparent" activation energy which is a function of temperature.

The results can be interpreted on the basis of the free volume theory of Cohen and Turnbull (*cf.* section II.2.); it is then necessary to find the temperature,  $T_\infty$ , such that  $\ln \tau(T)$  plotted against  $1/(T - T_\infty)$  will be a straight line. Figure 2 indicates that the experimental data were well described by the equation

$$\tau(T) = 6.8 \times 10^{-5} \exp\left(\frac{1660}{T - 410}\right) \quad (6)$$

By comparing eq 3 and 6, one obtains  $T_\infty = 410$  K and  $\alpha_f = 6 \times 10^{-4} \text{ deg}^{-1}$ .

A transition temperature can be associated with  $T_\infty$ , by using the WLF universal value of  $c_g^2$  (*cf.* eq 4):  $T_\infty + c_g^2 = 188.6^\circ$ .

Note that this temperature is comparable to the glass transition temperature deduced from DTA experiments performed on the same samples, using the same heating rates as for DTC experiments.

The results may also be fitted by the Adam and Gibbs theory (*cf.* section II.3). Again the plot of  $\ln \tau(T)$  vs.  $\{T \ln T/410\}^{-1}$  is practically a straight line; from its slope, one obtains  $\Delta E/\Delta C_p = 2410$  K.

Boyer<sup>34</sup> has summarized present views on transitions lying between the glass temperature and the melting point in polymers; he mentioned that more effort is needed to elucidate their exact nature.

## Conclusion

The DTC method gives the dependence on temperature of the dielectric relaxation time in the temperature range of the DTC peak without any assumption on the nature of the process.

The experiments are performed with no electric field. They permit a discrete or a continuous spectrum of relaxation times to be distinguished from a single relaxation time with an "apparent" activation enthalpy function of temperature. Thus, this technique seems to be well suited for the study of the glass-rubber transition in polymers. The results obtained on poly(ethyleneisophthalamide) are presented as an example. If the data are interpreted in the light of the free volume theory of Cohen and Turnbull, one obtains the thermal expansion coefficient of the free volume and the critical temperature  $T_\infty$ . If the statistical thermodynamic theory of Adam and Gibbs is adopted, one obtains the second-order transition temperature  $T_2$  with a good accuracy and an estimation of the ratio  $\Delta E/\Delta C_p$ .

## References and Notes

- (1) C. Bucci and R. Fieschi, *Phys. Rev. Lett.*, **12**, 16 (1964).
- (2) C. Bucci, R. Fieschi, and G. Guidi, *Phys. Rev.*, **148**, 816 (1966).
- (3) P. G. Bishop and J. W. Glen, "Physics of Ice," Plenum Press, New York, N.Y., 1969, p 492.
- (4) T. Nedetzka, M. Reichle, A. Mayer, and H. Vogel, *J. Phys. Chem.*, **74**, 2652 (1970).
- (5) C. LaJ, "Nonmetallic Crystals," S. C. Jain and L. T. Chadderton, Ed., Gordon Breach, London, 1970, p 77.
- (6) B. S. M. Royce and S. Mascarenhas, *Phys. Rev. Lett.*, **24**, 98 (1970).
- (7) P. Dansas, *J. Phys. Chem. Solids*, **32**, 2699 (1971).
- (8) J. P. Stott and J. R. Crawford, *Phys. Rev. B*, **4**, 668 (1971).
- (9) M. M. Perlman, *J. Appl. Phys.*, **42**, 2645 (1971).
- (10) J. Vanderschueren, *Polym. Lett.*, **10**, 543 (1972).
- (11) P. K. C. Pillai, K. Jain, and V. K. Jain, *Phys. Lett.*, **39A**, 216 (1972).
- (12) K. Shimada, K. Iwama, and I. Yamamuro, *Jap. J. Appl. Phys.*, **11**, 910 (1972).
- (13) J. Perret, R. Jocteur, and B. Fallou, *Rev. Gen. Elec.*, **81**, 757 (1972).
- (14) S. Unger and M. M. Perlman, *Phys. Rev. B*, **6**, 3973 (1972).
- (15) I. Kunze and P. Muller, *Phys. Status Solidi a*, **13**, 197 (1972).
- (16) D. Chatain, C. Lacabanne, and M. Maitrot, *Phys Status Solidi a*, **13**, 303 (1972).
- (17) D. Chatain, C. Lacabanne, M. Maitrot, G. Seytre, and J. F. May, *Phys. Status Solidi a*, **16**, 225 (1973).
- (18) D. Chatain, Thesis No. 581, Toulouse, 1974.
- (19) C. Lacabanne, Thesis No. 582, Toulouse, 1974.
- (20) N. Saito, K. Okano, S. Iwayanagi, and T. Hideshima, *Solid State Phys.*, **14**, 412 (1963).
- (21) N. G. McCrum, B. E. Read, and G. Williams, "Anelastic and Dielectric Effects in Polymeric Solids," Wiley, New York, N.Y., 1967, p 146.
- (22) G. Williams, *Trans. Faraday Soc.*, **60**, 1556 (1964).
- (23) S. Nomura and F. Kojima, *Jap. J. Appl. Phys.*, **12**, 205 (1973).

- (24) M. L. Williams, R. F. Landel, and J. D. Ferry, *J. Amer. Chem. Soc.*, **77**, 3701 (1955).  
 (25) J. D. Ferry, "Viscoelastic Properties of Polymers," Wiley, New York, N.Y., 1970, p 292.  
 (26) M. H. Cohen and D. Turnbull, *J. Chem. Phys.*, **31**, 1164 (1959).  
 (27) D. Turnbull and M. H. Cohen, *J. Chem. Phys.*, **34**, 120 (1961).  
 (28) A. J. Kovacs, *Fortschr. Hochpolym. Forsch.*, **Bd. 3**, 394 (1963).  
 (29) G. Adam and J. H. Gibbs, *J. Chem. Phys.*, **43**, 139 (1965).  
 (30) J. H. Gibbs and E. A. Di Marzio, *J. Chem. Phys.*, **28**, 373 (1958).  
 (31) I. M. Ward, "Mechanical Properties of Solid Polymers," Wiley, New York, N.Y., 1971, p 156.  
 (32) N. E. Hill, W. E. Vaughan, A. H. Price, and M. Davies, "Dielectric Properties and Molecular Behaviour," Van Nostrand-Reinhold, London, 1969, p 69.  
 (33) J. P. Soulier, B. Chabert, J. Chauchard, P. Berticat, and J. F. May, to be submitted for publication.  
 (34) R. F. Boyer, *Rubber Chem. Technol.*, **36**, 1303 (1963); *J. Polym. Sci. C*, **14**, 267 (1966).

## A Multiple-Equilibrium Model for the Micellization of Ionic Surfactants in Nonaqueous Solvents<sup>1</sup>

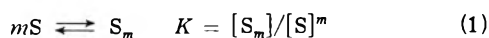
Norbert Muller

Department of Chemistry, Purdue University, West Lafayette, Indiana 47907 (Received March 18, 1974; Revised Manuscript Received October 29, 1974)

It is demonstrated that the reported concentration dependence of nmr chemical shifts for solutions of alkylammonium carboxylates in organic solvents can be reproduced equally well using either a single-equilibrium model where the micelle size is a disposable parameter or a multiple-equilibrium model where it is assumed that dimers and all higher species with even aggregation numbers coexist in each solution. The latter model is suggested by simple electrostatic energy calculations which show that trimers and other small odd-order aggregates should disproportionate to give the more stable even-order species. Although the available data do not suffice to determine which scheme is better, the multiple-equilibrium model seems more acceptable on physical grounds and avoids some difficulties encountered with the single-equilibrium interpretation. A major point of difference is that the single-equilibrium approach appears to show that only small micelles are present, but with the multiple-equilibrium model it is seen that the data are consistent with the presence, in the more concentrated solutions, of significant numbers of micelles with aggregation numbers of 20 or more.

### Introduction

Nuclear magnetic resonance spectroscopy has recently been used to study the formation of "inverted" micelles of alkylammonium carboxylate surfactants in organic solvents.<sup>2-5</sup> For each surfactant-solvent pair, the chemical shift,  $\delta$ , of a selected probe nucleus depends in a characteristic way on the total surfactant concentration,  $[S_0]$ , and the data can be rationalized on the assumption that monomers,  $S$ , are in equilibrium with micelles,  $S_m$ , having a fixed aggregation number,  $m$ , that is



and

$$\delta = \frac{[S]}{[S_0]} \delta(S) + \frac{m[S_m]}{[S_0]} \delta(S_m) \quad (2)$$

Here  $\delta(S)$  and  $\delta(S_m)$  are the chemical shifts for the monomeric and the micellar forms, evaluated by extrapolating the data to zero concentration, for  $\delta(S)$ , or to infinite concentration (*i.e.*,  $1/[S_0] \rightarrow 0$ ) for  $\delta(S_m)$ . The equilibrium constant  $K$ , defined subject to the assumption of unit activity coefficients, and the aggregation number are then evaluated by constructing a plot<sup>6</sup> of  $\log m [S_m]$  against  $\log [S]$ , which should yield a straight line with slope  $m$  and intercept  $\log mK$ . Once the parameters are thus fixed, this sin-

gle-equilibrium model leads to calculated values of  $\delta$  as a function of  $[S_0]$  which are in excellent accord with observations. The derived values of  $m$  are always small, ranging between about 3 and 8, but for a given surfactant  $m$  is by no means independent of solvent<sup>4</sup> or temperature.<sup>5</sup>

Several considerations prompt one to question whether or not the characterization of each surfactant-solvent pair at a given temperature by means of the four parameters,  $\delta(S)$ ,  $\delta(S_m)$ ,  $m$ , and  $K$ , represents the optimum procedure for interpreting these data. One disturbing feature is the occurrence<sup>4</sup> of nonintegral values of  $m$ . Another is the enigmatic variation of  $m$  with experimental conditions, since no attempt to visualize the aggregates in terms of structural models (see below) accounts in a reasonable way for the fact that small changes in temperature or solvent composition can apparently change the  $m$  value of the most stable micelle from 3 to 4 or 5. Moreover, it is inconvenient to compare results for a surfactant in different solvents, or in the same solvent at different temperatures, when each set of data refers to a different aggregation process. In particular, the thermodynamic relation

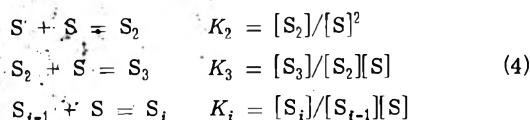
$$d \ln K/d(1/T) = -\Delta H^\circ/R \quad (3)$$

cannot be used to find the enthalpy of micellization when the micelle size is strongly temperature dependent.

It seems likely that these difficulties may be avoided if one turns to a multiple-equilibrium model of micellization,<sup>7-9</sup> explicitly recognizing that micelles of several different sizes coexist in each solution and that the derived values of  $m$  represent average aggregation numbers. Although a number of properties of such multiple-equilibrium systems have been derived and presented, the usefulness of these models has been restricted by the fact that far more parameters are needed to define the equilibria than can be evaluated experimentally. It is therefore necessary to make sweeping simplifications. Restricting considerations to micelles of a single size, as outlined above, is one way of doing this. The purpose of this work is to explore two simple alternatives.

### The Multiple-Equilibrium Model

It is generally agreed that aggregation probably occurs as a stepwise process involving addition of single monomers to already existing micelles, as suggested by the scheme



When all of these equilibrium conditions are satisfied simultaneously, the total surfactant concentration is given by

$$[S_0] = \sum_{i=1}^{\infty} i[S_i] \quad (5)$$

and the total concentration of surfactant in aggregated form is

$$[A] = [S_0] - [S] = \sum_{i=2}^{\infty} i[S_i] \quad (6)$$

If the chemical shift for species  $S_i$  is  $\delta(S_i)$  the observed shift is

$$\delta = \frac{1}{[S_0]} \sum_{i=1}^{\infty} i[S_i]\delta(S_i) \quad (7)$$

and the parameters which govern the dependence of  $\delta$  on  $[S_0]$  then consist of the entire set of equilibrium constants  $K_i$ ,  $i \geq 2$ , and the set of chemical shifts  $\delta(S_i)$ ,  $i \geq 1$ . If measurements are made at more than one temperature, a new set of parameters is required at each temperature, the  $K_i$ 's being related through a set of  $\Delta H_i^\circ$  values by eq 3.

No attempt to evaluate any of these variables experimentally offers any hope of success unless one can first reduce the number of unknowns by introducing suitable assumptions. If one is to rationalize data at all, the question is not whether or not to adopt simplifying assumptions but rather how they should be chosen. The single-equilibrium model described above represents one possible answer, since it may be regarded as a special case of (4) where the constants are assumed to have values which assure that  $[S_i] = 0$  except when  $i = 1$  or  $i = m$ . The set of parameters then shrinks to the four listed in the Introduction. Although good agreement between calculated and observed shifts can be produced with this model, it is desirable to find whether or not other assumptions generate models which fit the data equally well, and if so, which scheme forms the best approximate representation of the real systems.

*Case 1. Equal Association Constants.* It is mathematically very easy to deal with eq 4-7 when all the equilibrium constants are assigned a single value,  $K_2 = K_3 = \dots = K_i$ . The monomer concentration is given<sup>9</sup> by

$$[S] = \frac{1 + 2K_i[S_0] - \sqrt{1 + 4K_i[S_0]}}{2K_i^2[S_0]} \quad (8)$$

while the concentration of the  $n$ th micellar species is  $[S_n] = K_i^{n-1}[S]^n$ . Since the average chemical shift still depends on the whole set of micellar shift values, a further simplification is needed. An appealing possibility<sup>8</sup> is to assume that all aggregates with  $i \geq 2$  have the same chemical shift,  $\delta(A)$ , so that this shift and the monomer shift are the only additional variables to be evaluated. It then follows that

$$\delta = \delta(A) + \left\{ \frac{1 + 2K_i[S_0] - \sqrt{1 + 4K_i[S_0]}}{2K_i^2[S_0]^2} \right\} \{ \delta(S) - \delta(A) \} \quad (9)$$

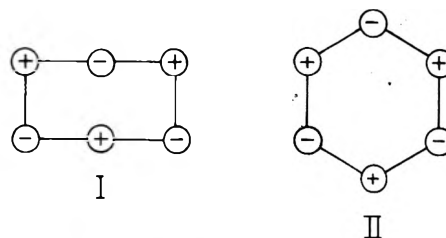
so that the dilution-shift curve is readily calculated.

Apart from any specific objections which might be raised against the plausibility of this model (see below), it suffers from the serious defect that the number of disposable parameters has been reduced to only 3, and thus it has one less degree of freedom than the single-equilibrium model. Available dilution-shift curves present such a variety of shapes that attempts to fit them using this model are not successful except in a few instances. It appears that no scheme will have sufficient flexibility to fit all of the data unless it provides at least four adjustable parameters.

*Case 2. Dimers and Even-Order Polymers.* When the stabilities of small aggregates of alkylammonium carboxylates are estimated on the basis of simple electrostatics it is quickly apparent that the assumption of equal association constants is far from realistic. Each monomer consists of an ion pair with the charges separated by a distance  $d$ , and its electrostatic potential energy in a medium of dielectric constant  $\epsilon$  is  $-e^2/\epsilon d$ . For a dimer the most stable form is a square planar one, and if the distance between adjacent charges is still  $d$  the energy is

$$V = (-e^2/\epsilon d)(4 - 2/\sqrt{2}) = -2.586e^2/\epsilon d \quad (10)$$

Two possible arrangements for the trimer are the rectangu-



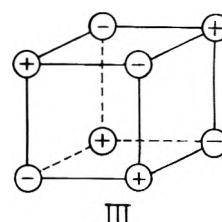
lar form I and the hexagonal form II. For the former

$$V = (-e^2/\epsilon d)(7 - 4/\sqrt{2} - 2/2 + 2/\sqrt{5}) = -4.066e^2/\epsilon d \quad (11)$$

while for the latter

$$V = (-e^2/\epsilon d)(6 - 6/\sqrt{3} + 3/2) = -4.036e^2/\epsilon d \quad (12)$$

The rectangular form is seen to be slightly favored. For the tetramer, the preferred arrangement is the cubic one, III,



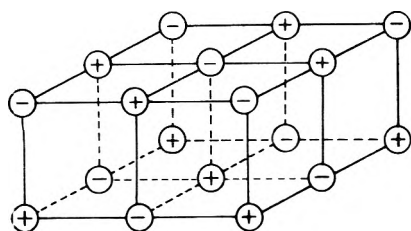
with

$$V = (-e^2/\epsilon d)(12 - 12/\sqrt{2} + 4/\sqrt{3}) = -5.824e^2/\epsilon d \quad (13)$$

The energy of a pair of trimers in units of  $e^2/\epsilon d$  is now seen to be  $-8.132$  while that for a dimer and a tetramer is  $-8.410$ , so that the disproportionation reaction



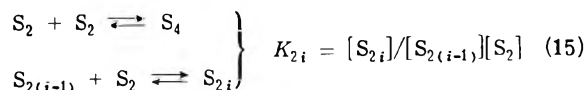
is energetically favorable by 0.288. Taking the dielectric constant as 2.28 and  $d = 5 \times 10^{-8}$  cm, the energy unit is 36 kcal/mol. Since the entropy change in the disproportionation is probably small, it appears that the concentration of trimers in the real system will be far less than that calculated with equal association constants. An extension of this reasoning suggests that other small polymers of odd order will also tend to disproportionate to give more stable even-order aggregates. The first exception is likely to be the nonamer, for which the array suggested by IV may repre-



IV

sent a relatively stable structure, but the error in predicted chemical shifts entailed by assuming that nonamers disproportionate to give octamers and decamers is not likely to be serious.

The following proposed modification of scheme 4 emerges from these considerations. Let dimerization occur as in (4) with an equilibrium constant  $K_2$ . In addition to dimers, consider only even-order polymers formed by processes



taking all values of  $K_{2i}$  to be identical when  $i \geq 2$ . It follows that

$$[S_{2n}] = K_2^n K_2^{n-1} [S]^{2n} \quad (16)$$

or introducing the abbreviation  $K_2 K_2^{n-1} = K_0$

$$[S_{2n}] = K_2 K_0^{n-1} [S]^{2n} \quad (17)$$

Then the concentration of surfactant in aggregated form becomes

$$[A] = \frac{K_2}{K_0} \sum_{n=1}^{\infty} 2n K_0^n [S]^{2n} = \frac{2K_2[S]^2}{1 - K_0[S]^2} \quad (18)$$

The total surfactant concentration is simply the sum of  $[S]$  and  $[A]$ , and if the assumption of equal chemical shifts for all micellar species is retained<sup>10</sup> this defines a four-parameter model with

$$\delta = \frac{[S]}{[S_0]} \delta(S) + \frac{[A]}{[S_0]} \delta(A) \quad (19)$$

It is not convenient to try to express  $\delta$  simply as a function of  $[S_0]$  alone as in eq 9, but the dependence of  $\delta$  on  $[S_0]$  with a given set of parameters is readily found by taking a series

of values of  $[S]$  and calculating first  $[A]$ , then  $[S_0]$ , and finally  $\delta$ .

When the desired parameters are initially unknown, evaluation of  $\delta(S)$  and  $\delta(A)$  by extrapolation using data for very dilute or very concentrated solutions yields values of limited reliability. At low concentrations, when the only significant associated species is the dimer, the chemical shift is given approximately by

$$\delta = \delta(S) + 2K_2[S_0]\{\delta(A) - \delta(S)\} \quad (20)$$

A plot of  $\delta$  against  $[S_0]$  should be linear in this region, with intercept  $\delta(S)$  and slope  $2K_2\{\delta(A) - \delta(S)\}$ . Since such linearity is not predicted with any single-equilibrium model having  $m > 2$ , it is possible in principle to determine which model is superior by collecting highly accurate data for very dilute solutions. When the only available data are for values of  $[S_0]$  larger than  $5 \times 10^{-3} M$ , as is often the case, there is apt to be considerable curvature even for the more dilute region, and extrapolation to  $[S_0] = 0$  will involve some uncertainty.

In concentrated solutions,  $[S_0]$  eventually becomes a very rapidly rising function of  $[S]$ , implying that  $[S]$  must remain roughly constant for moderate changes in  $[S_0]$ . Then  $\delta$  becomes a linear function of  $1/[S_0]$  approaching  $\delta(A)$  as  $1/[S_0]$  goes to zero. However, this result is again only approximate, and plots of  $\delta$  against  $1/[S_0]$  are not in fact found to be accurately linear when small micelles are present. Figure 4 of ref 11 shows that this is also a feature of the single-equilibrium model. Thus for either model, the value of  $\delta(A)$  obtained by linear extrapolation of a plot of  $\delta$  against  $1/[S_0]$  may be slightly in error.

A convenient procedure for fitting a particular dilution curve with the multiple-equilibrium model is to use these extrapolation methods to obtain trial values of  $\delta(S)$  and  $\delta(A)$  and to obtain a trial value of  $K_2$  from eq 20. The experimental curve can then be used to find the value of  $[S_0]$  for which two-thirds of the detergent is in the aggregated form, that is,  $[A] = \frac{2}{3}[S_0]$  and  $[S] = \frac{1}{3}[S_0]$  so that  $\delta = \frac{1}{3}\delta(S) + \frac{2}{3}\delta(A)$ , and with these values of  $[A]$  and  $[S]$  eq 19 yields a trial value of  $K_0$  consistent with the choice of  $\delta(S)$ ,  $\delta(A)$ , and  $K_2$ . One then calculates a trial dilution curve, which agrees with experiment at the two-thirds aggregation point. The parameters can then be adjusted iteratively to improve the fit until it is considered satisfactory over the entire range.

#### Application to the Association of Alkylammonium Propionates in Benzene

A numerical test of the single- and multiple-equilibrium models was undertaken using the data of ref 2 for butyl-, hexyl-, and octylammonium propionates in benzene. The three surfactants are designated by the abbreviations BAP, HAP, and OAP. Chemical shifts for the methyl protons of the propionate ions from ref 2 are given by the open circles in Figure 1. The filled circles represent calculated points using the single-equilibrium model with the parameters given in Table IA. These parameters are the same as those reported in ref 2 except that the values of  $K$  were adjusted to give a good fit. Only in the case of BAP does this require a value of  $K$  substantially different from that given in ref 2. The crosses in Figure 1 represent results calculated with the multiple-equilibrium model with parameters listed in Table IB. The values of  $\delta(A)$  were retained unchanged, but  $\delta(S)$  was varied, subject to the constraint that all three values of  $\delta(S)$  be identical (see below).

**TABLE I: Parameters for Model Calculations for the Association of Alkylammonium Propionates in Benzene**

Surfactant	$\delta(S)$	$\delta(S_m)$	$m$	$K, M^{1-m}$	
A. Single-Equilibrium Model					
BAP	0.868	0.987	4	$10.2 \times 10^4$	
HAP	0.830	1.027	7	$2.87 \times 10^{12}$	
OAP	0.826	1.079	5	$3.93 \times 10^8$	
Surfactant	$\delta(S)$	$\delta(A)$	$K_2, M^{-1}$	$K_0, M^{-2}$	$K_{2i}, M^{-1}$
B. Multiple-Equilibrium Model					
BAP	0.810	0.987	70	$2.12 \times 10^3$	30.2
HAP	0.810	1.027	60	$9.66 \times 10^3$	161
OAP	0.810	1.079	55	$15.27 \times 10^3$	278

**TABLE II: Calculated Concentrations of Selected Species in an Octylammonium Propionate Solution with Parameters in Table IB and  $[S_0] = 92.1 \text{ mM}$** 

$[S] = 7.00 \text{ mM}$	$[A] = 85.13 \text{ mM}$
$[S_2] = 2.70$	$2[S_2] = 5.40$
$[S_4] = 2.02$	$4[S_4] = 8.07$
$[S_6] = 1.51$	$6[S_6] = 9.05$
$[S_{10}] = 0.845$	$10[S_{10}] = 8.45$
$[S_{20}] = 0.199$	$20[S_{20}] = 3.97$
$[S_{30}] = 0.047$	$30[S_{30}] = 1.40$

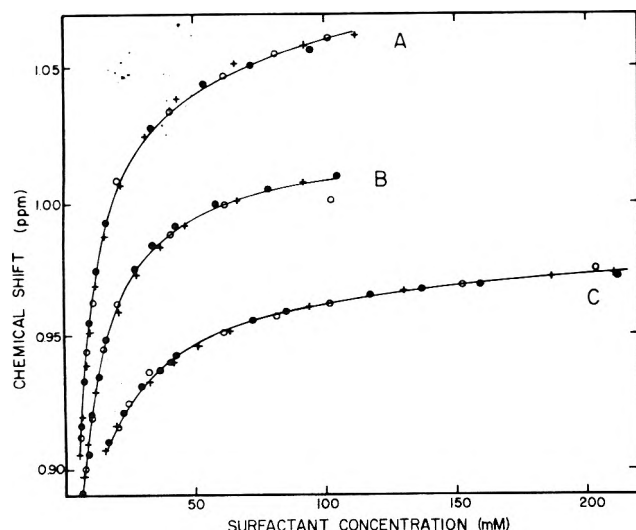


**Figure 1.** Chemical shifts as a function of surfactant concentration for the methyl protons of the propionate ions of octyl (A), hexyl (B), and butyl (C) ammonium propionates in benzene solution: open circles; experimental values from ref 2; filled circles; calculated values for a single-equilibrium model with parameters in Table IA; crosses; calculated values for a multiple-equilibrium model with parameters in Table IB.

It is evident that either model is able to provide excellent agreement between calculated and experimental dilution-shift curves. Thus the available nmr data do not suffice to indicate which model is to be preferred, nor to eliminate other models derived from scheme 4 with different simplifying assumptions (*e.g.*, equal association constants with unequal values of  $\delta(S_i)$  or unequal association constants with inclusion of odd-order aggregates). Arguments in favor of the particular multiple-equilibrium model presented here include the following.

(1) On the basis of the electrostatic energy calculations above, the present scheme appears more realistic than models which treat even- and odd-order aggregates as equally probable and more realistic than the single-equilibrium model. The latter is most emphatically true when the single-equilibrium analysis seems to show that the predominant aggregated species is the trimer.

(2) With the multiple-equilibrium model, every surfactant by assumption forms the same set of aggregated species, but with somewhat different relative concentrations, and the variation of  $m$  with chain length, including the unexplained maximum for HAP, is eliminated.

(3) It is expected *a priori* that at infinite dilution the shift for the methyl protons of the propionate ion should be independent of the size of the alkylammonium ion, and the multiple-equilibrium model shows that the data are compatible with this expectation.

With either model, it is probably best to deemphasize the concept of critical micelle concentration (cmc). It was shown long ago<sup>12</sup> that when small micelles are present there is no well-defined concentration at which aggregation abruptly sets in. Any definition of cmc then becomes arbitrary or ambiguous,<sup>8</sup> and it becomes preferable to base comparisons instead on appropriate equilibrium constants or free-energy changes. For this purpose the equilibrium constants which give the best fit with the multiple-equilibrium model are perhaps the best ones available, since they always refer to the same aggregation reactions, and since the assumptions used to make the model tractable are likely to introduce similar errors for similar systems.

The parameters in Table IB do not represent a unique best fit; the quality of fit is almost unaffected by small changes in  $\delta(S)$  together with compensating changes in  $K_2$ . Additional data for very dilute solutions would greatly help to reduce this ambiguity. In any case, it seems that the three values of  $K_2$  are essentially the same, but  $K_{2i}$  certainly increases with increasing chain length of the alkylammonium ion. The simple electrostatic energy calculations cannot provide an explanation of such a variation, since they do not provide for contributions due to van der Waals attractions, steric repulsions, or internal entropy changes associated with the hydrocarbon chains. Such contributions must become increasingly important as the structure of the surfactant ions becomes more elaborate.

Finally, attention should be drawn to the fact that *if the multiple-equilibrium model is even approximately correct* the more concentrated solutions contain appreciable amounts of surfactant in the form of rather large micelles. This is shown by calculated results in Table II for an OAP solution with  $[S_0] = 0.092 \text{ M}$ . These numbers should not be taken too literally, since the assumptions used in defining the model become progressively worse as the number of large micelles increases, but they show unequivocally that the nmr data *do not exclude* the possibility that higher aggregates may exist in these solutions in amounts far in excess of what one would expect after seeing only the single-equilibrium analysis. This result may have important implications for the interpretation of solubilization and catalytic effects<sup>13</sup> of these inverted micelles.

The question immediately arises of whether or not the results in Table II are compatible with measurements of colligative properties of these surfactant solutions. Little relevant information is available, but it has been reported that for tetradecylamine butyrate in benzene the freezing-point depression indicates that the average molecular

weight is 4.32 times the monomer molecular weight.<sup>14</sup> For the model defined above, the corresponding average degree of association is given by

$$\langle N \rangle = \frac{[S_0]}{[S] + \sum_{n=1}^{\infty} K_2 K_0^{n-1} [S]^{2n}} = \frac{[S_0]}{[S] + [K_2/K_0(1 - K_0[S]^2)]} \quad (21)$$

With the conditions used to calculate the values in Table II the result is  $\langle N \rangle = 4.33$ . The single-equilibrium approach with parameters given for OAP in Table IA and  $[S_0] = 0.096 M$ , leads to  $\langle N \rangle = 3.69$ . Again both models give rather similar values, but they are not identical, and thus there is some hope that decisive experiments might be performed using a combination of spectroscopic and colligative measurements, especially if chemical shifts are obtained for very dilute solutions (see above).

### References and Notes

- (1) Presented at the 8th Great Lakes Regional Meeting of the American Chemical Society, West Lafayette, Ind., June 1974. Financial support by the National Science Foundation under Grant No. GP 19551 is gratefully acknowledged.
- (2) J. H. Fendler, E. J. Fendler, R. T. Medary, and O. A. El Seoud, *J. Chem. Soc., Faraday Trans. 1*, **69**, 280 (1973).
- (3) E. J. Fendler, J. H. Fendler, R. T. Medary, and O. A. El Seoud, *J. Phys. Chem.*, **77**, 1432 (1973).
- (4) O. A. El Seoud, E. J. Fendler, J. H. Fendler, and R. T. Medary, *J. Phys. Chem.*, **77**, 1876 (1973).
- (5) N. Muller and B. J. Konieczka, unpublished results.
- (6) N. Muller and F. E. Platko, *J. Phys. Chem.*, **75**, 547 (1971).
- (7) J. M. Corkill, J. F. Goodman, and J. R. Tate, "Hydrogen Bonded Solvent Systems" A. K. Covington and P. Jones, Ed., Taylor and Francis, Ltd., London, 1968, p 181.
- (8) J. M. Corkill, J. F. Goodman, T. Walker, and J. Wyer, *Proc. Roy Soc., Ser. A*, **312**, 243 (1969).
- (9) K. H. Meyer and A. van der Wyk, *Helv. Chim. Acta*, **20**, 1321 (1937).
- (10) The appropriateness of this assumption is certainly open to question, but to abandon it would require introduction of at least one more parameter which would be hard to evaluate experimentally. Qualitatively, one expects that various values of  $\delta(S_i)$  should differ by less than the difference  $\delta(A) - \delta(S)$ , which is at most 0.27 ppm for the systems considered here. Also,  $\delta(S_i)$  should approach a limiting value as  $i$  increases, and in the more concentrated solutions much of the material exists as aggregates with  $i \geq 6$  (see Table II), so that the assumption should be reasonably good.
- (11) N. Muller and T. W. Johnson, *J. Phys. Chem.*, **73**, 2042 (1969).
- (12) J. Grindley and C. R. Bury, *J. Chem. Soc.*, 679 (1929).
- (13) E. J. Fendler, S. A. Chang, J. H. Fendler, R. T. Medary, O. A. El Seoud, and V. A. Woods, "Reaction Kinetics in Micelles," E. Cordes, Ed., Plenum Press, New York, N.Y., 1973, p 127.
- (14) S. R. Palit and V. Venkateswarlu, *Proc. Roy. Soc., Ser. A*, **208**, 542 (1951). See also A. Kihara, "Cationic Surfactants," E. Jungermann, Ed., Marcel Dekker, New York, N.Y., 1970 pp 298, 300.

## COMMUNICATIONS TO THE EDITOR

### Emission Spectra of Monochlorobenzene and Benzyl Chloride in Solid Matrix

Sir: Since McClure<sup>1</sup> reported the lifetimes of triplet states of halogenated benzene derivatives, the process due to halogen-induced spin-orbit interaction has been an attractive problem.<sup>2,3</sup> The emission spectra and the quantum yields,<sup>4a,b</sup> however, seem to have not been reported yet supposedly because of the experimental difficulty. In this paper the emission spectra of monochlorobenzene and benzyl chloride in solid matrices have been measured and the quantum yields of fluorescence and phosphorescence have been estimated.

A low-pressure mercury lamp was used as an excitation light source at 253.7 nm in conjunction with a monochromator of 25 cm focal length in order to eliminate the extraneous emission from the mercury lamp. The emission spectra were observed in CO<sub>2</sub>, ethane, propane, and *n*-butane matrices at 77°K. The sample vapor and the matrix gas were condensed on the surface of cold finger cooled with liquid nitrogen. The emission spectrum was recorded using a combination of a 50-cm monochromator and a photon-counting system with a photomultiplier (HTV R-585), which is described in previous paper.<sup>5</sup>

The recorded emission spectra were identical in the several matrices. The fluorescence and phosphorescence spectra of monochlorobenzene are shown in Figure 1a and 1b, respectively. The fluorescence predominantly consists of two progressions with the same frequency of 930 cm<sup>-1</sup>. The spacing between these two progressions is about 300 cm<sup>-1</sup>, probably due to the nontotally symmetric C-Cl bending vibration.<sup>6</sup> In the phosphorescence spectrum in Figure 1b vibrational mode of 1600 cm<sup>-1</sup> is assigned to be the ground state carbon vibration suggested by Sponer and Kirby-Smith.<sup>7</sup>

The fluorescence and phosphorescence of benzyl chloride, which are similar to those of monochlorobenzene, are shown in Figure 2a and 2b. The fluorescence intensity of benzyl chloride was very weak and maximum high sensitivity measurement caused the appearance of scattered line of a mercury lamp, so that the vibrational structure of the fluorescence could not be obtained. The phosphorescence spectrum in Figure 2b looks identical with that of monochlorobenzene in Figure 1b except for a slight red shift (~1 nm) of the spectrum and the contrast of the relative intensity of the first vibrational mode to the third one.

The quantum yield of the emission was obtained relative to that for benzene as a standard, 0.20 for both the fluorescence and the phosphorescence at 253.7-nm excitation.<sup>8</sup>

TABLE I: Quantum Yield and Lifetime of Emission

	$\Phi_F$	$\Phi_P$	$\tau_P$ , msec
$C_6H_5Cl$	$(1 \pm 0.5) \times 10^{-1}$	$(2 \pm 1) \times 10^{-2}$	4 <sup>a</sup>
$C_6H_5CH_2Cl$	$(1 \pm 0.5) \times 10^{-1}$	$(1 \pm 0.5) \times 10^{-2}$	4

<sup>a</sup> The datum obtained by McClure.<sup>1</sup>

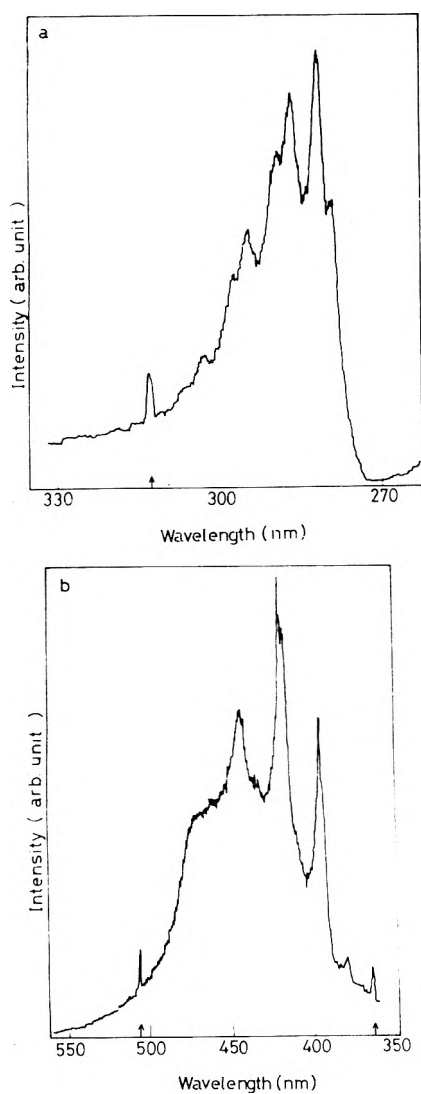


Figure 1. Recorded spectra of (a) the fluorescence and (b) the phosphorescence of monochlorobenzene in  $CO_2$  matrix at 253.7-nm excitation: slit width, 400  $\mu$ . The peaks marked by a vertical arrow are the scattered mercury line.

The values of the fluorescence quantum yield ( $\Phi_F$ ) and the phosphorescence quantum yield ( $\Phi_P$ ) are listed in Table I together with the phosphorescence lifetime ( $\tau_P$ ) through the flash photolysis.  $\Phi_P$  of monochlorobenzene is in good agreement with the value (0.02~0.05) obtained by McClure, *et al.*<sup>4a</sup> As is clearly shown in Table I,  $\Phi_F$  of benzyl chloride is much smaller than that of monochlorobenzene, while monochlorobenzene and benzyl chloride have similar values of  $\Phi_P$ . The much larger fluorescence quantum yield of monochlorobenzene in the solid matrix compared with that in the vapor phase,  $2.7 \times 10^{-3}$ , sharply contrasts with the benzyl chloride fluorescence quantum yield which has a slightly smaller value in the solid matrix than

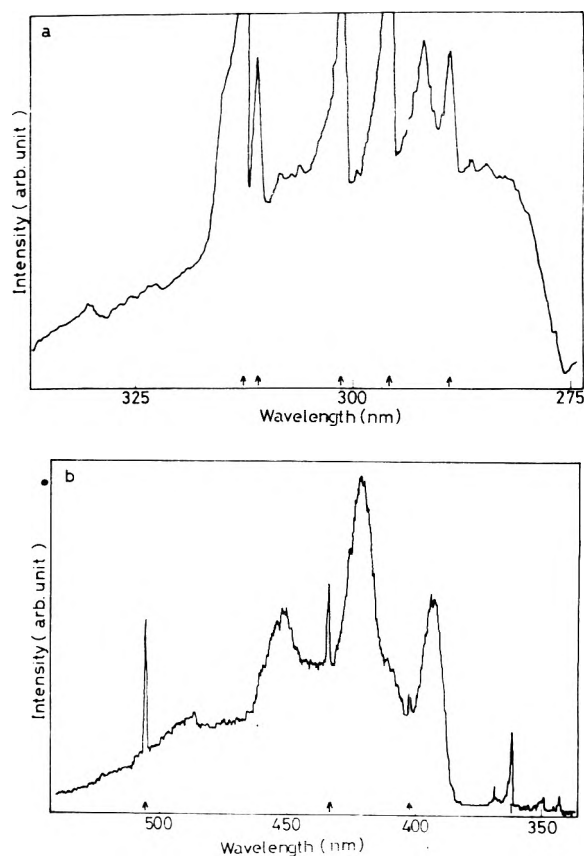


Figure 2. Recorded spectra of (a) the fluorescence and (b) the phosphorescence of benzyl chloride in  $CO_2$  matrix at 253.7-nm excitation: slit width, (a) 200  $\mu$ , (b) 350  $\mu$ . The peaks marked by a vertical arrow are the scattered mercury line.

in the vapor phase ( $\Phi_F$  (vapor) =  $4.5 \times 10^{-4}$ ).<sup>9</sup> The radiative decay rates of the lowest excited singlet states of monochlorobenzene and of benzyl chloride are estimated to be similar order of magnitude because of the close similarity of the absorption spectra. The smaller fluorescence quantum yield of benzyl chloride seems to suggest the much shorter lifetime of the excited singlet state of benzyl chloride compared with that of monochlorobenzene. On the other hand, the study of the vapor-phase photolysis have suggested a longer lifetime of photodecomposing excited state for benzyl chloride than that for monochlorobenzene.<sup>10,11</sup> This is due to the experimental results that the quantum yield of primary photodecomposition of benzyl chloride clearly decreased with the increase of foreign gas pressure while no such pressure effect was observed in the vapor-phase photolysis of monochlorobenzene. Therefore, the smaller  $\Phi_F$  (shorter lifetime) of benzyl chloride in vapor phase should be attributed to the strong coupling between the excited singlet state and the higher triplet levels. The higher triplet levels undergo decomposition to radicals and atoms or two body vibrational relaxation to lower triplet levels. The triplet level density at 253.7-nm excitation may be close to "intermediate" condition rather than "statistical limit." The decrease in the photodecomposition quantum yield at higher pressures indicates the vibrational relaxation of the photodecomposing triplet levels by two body collisions. The smaller  $\Phi_F$  of benzyl chloride in the solid matrix compared with that in the vapor phase may be explained by the increased triplet level density in the solid matrix, which rapid vibrational relaxation decreases the lifetime of excited manifold of benzyl chloride.

The excited singlet state of monochlorobenzene couples with the decomposing levels to give phenyl radicals and chlorine atoms and with the triplet manifold.<sup>11</sup> The probability of the transition from the excited singlet state to the decomposing levels should be dependent on the vibrational energy since the photodecomposition quantum yield increases with increasing the excitation energy. The vibrational relaxation in the solid matrix, being faster than radiationless decay processes from the excited singlet state, can transfer the molecule to the lowest excited singlet state which results in the increased fluorescence quantum yield in the solid matrix. Experiments in the vapor phase, such as wavelength and pressure effects on  $\Phi_F$ , must clarify complicated mechanisms mentioned above and are now undertaken.<sup>9</sup>

References and Notes

- (1) D. S. McClure, *J. Chem. Phys.*, **17**, 905 (1949).
- (2) D. S. McClure, *J. Chem. Phys.*, **17**, 665 (1949).
- (3) M. Kasha, *J. Chem. Phys.*, **20**, 71 (1952).
- (4) (a) Absolute quantum yield of the phosphorescence of monochlorobenzene was reported to be 0.02~0.05 at 39,400-cm<sup>-1</sup> excitation. (E. H. Gilmore, G. E. Gibson, and D. S. McClure, *J. Chem. Phys.*, **20**, 829 (1952).) (b) A fluorescence quantum yield of benzyl chloride in solution at 253.7-nm excitation was obtained to be 0.009. (V. B. Benefel'd and V. A. Krongauz, *Dokl. Akad. Nauk SSSR*, **162**, 1300 (1965).)
- (5) T. Hikida, T. Ichimura, and Y. Mori, *Chem. Phys. Lett.*, **27**, 548 (1974).
- (6) P. P. Barchewitz and M. Parodi, *J. Phys.*, **10**, 143 (1939).
- (7) H. Sponer and J. S. Kirby-Smith, *J. Chem. Phys.*, **9**, 667 (1941).
- (8) E. C. Lim, *J. Chem. Phys.*, **36**, 3497 (1962).
- (9) To be submitted for publication.
- (10) T. Ichimura and Y. Mori, *J. Chem. Phys.*, **57**, 1677 (1972).
- (11) T. Ichimura and Y. Mori, *J. Chem. Phys.*, **58**, 288 (1973).

Department of Chemistry  
Tokyo Institute of Technology  
Meguro-ku, Tokyo, Japan

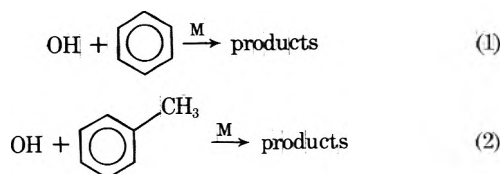
T. Ichimura\*  
T. Hikida  
Y. Mori

Received August 5, 1974

A Kinetics Study of the Reaction of the OH Free Radical with Aromatic Compounds. I. Absolute Rate Constants for Reaction with Benzene and Toluene at 300°K

Publication costs assisted by the Environmental Protection Agency

Sir: Whereas considerable work has been reported on the reaction of OH with paraffinic and olefinic hydrocarbons,<sup>1-8</sup> virtually no systematic study has been carried out on aromatics. We wish to report, therefore, a recent study completed in our laboratory involving the reaction of OH with two aromatic compounds, benzene and toluene.



To the best of our knowledge, the absolute rate constants given represent the first absolute rate constants reported for these organic species. The importance of these new measurements (in addition to their obvious fundamental

TABLE I: Rate Constant Measurements for Reaction of OH with Benzene at 298°K<sup>a</sup>

Helium, Torr	H <sub>2</sub> O, mTorr	Benzene, mTorr	Flash energy, J	k <sub>1</sub> , sec <sup>-1</sup>	10 <sup>12</sup> k <sub>bimolec</sub> , cc molecule <sup>-1</sup> sec <sup>-1</sup>
3	100	0	88	210	
3	100	2	88	267	
3	100	4	88	322	
3	100	8	88	430	0.849 ± 0.08
20	100	0	88	68	
20	100	0.5	88	87	
20	100	3	88	205	
20	100	5	88	295	
20	100	5	88 <sup>b</sup>	330	
20	100	5	45	290	
20	100	5	180	330 <sup>b</sup>	
20	100	8	88	420	1.36 ± 0.09
100	100	0	88	36	
100	100	3	88	190	
100	200	6	88	350	
100	100	9	88	500	1.59 ± 0.12

<sup>a</sup> CaF<sub>2</sub> window used in all experiments. <sup>b</sup> 150 flashes/gas filling (for all other experiments only 30 flashes/filling was used).

TABLE II: Rate Constant Measurements for Reaction of OH with Toluene at 298°K<sup>a</sup>

Helium, Torr	H <sub>2</sub> O, mTorr	Toluene, mTorr	Flash energy, J	k <sub>2</sub> , sec <sup>-1</sup>	10 <sup>12</sup> k <sub>bimolec</sub> , cc molecule <sup>-1</sup> sec <sup>-1</sup>
3	100	0	88	210	
3	100	1	88	325	
3	100	1.5	88	390	
3	100	2	88	450	
3	100	3	88	565	3.60 ± 0.26
20	100	0	88	68	
20	100	0.5	88	170	
20	100	1	88	240	
20	100	1.5	88	330	
20	100	1.5	88 <sup>b</sup>	310	
20	100	1.5	45	290	
20	100	1.5	180	350	
20	100	2	88	390	
20	100	3	88	555	
20	100	4.5	88	790	5.00 ± 0.18
100	100	0	88	36	
100	100	1	88	250	
100	100	2	88	425	
100	100	3	88	630	6.11 ± 0.40

<sup>a,b</sup> See corresponding footnotes to Table I.

significance to kinetics) lies in the fact that OH-aromatic reactions are of major concern in the combustion of non-leaded gasoline and in the formation of photochemical smog. For example, recent examinations of the emissions from cars running on regular nonleaded gasoline have shown that over 20% of the hydrocarbons emitted were aromatics.<sup>9</sup>

In this study the reaction of OH with benzene and toluene was followed by monitoring the concentration of OH as a function of time. The detection technique for OH was

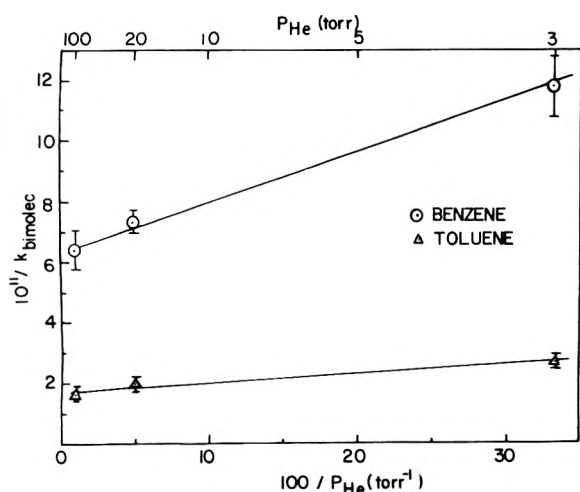


Figure 1. A  $1/k$  vs.  $1/p$  Lindemann plot showing the pressure dependence of the reaction of OH with benzene and toluene.

that of resonance fluorescence which has been discussed in detail in previous publications.<sup>10,11</sup> The photolysis of  $\text{H}_2\text{O}$  (in the region above the  $\text{CaF}_2$  cut off at  $1250 \text{ \AA}$ ) as a source of OH has also been described in earlier work.<sup>11</sup>

In all experiments reported here, gas mixtures were made up using an all-glass gas handling system. The toluene and benzene used in this study were from Fischer Scientific Co. and had a purity level of 99.96% or better. All low-pressure measurements of toluene, benzene, and  $\text{H}_2\text{O}$  were made using a MKS Baratron. High-pressure measurements (10–800 Torr) were made with a two-turn Bourdon gauge (Wallace and Tiernan Type FA145). The precision to which gas mixtures could be prepared, with the exception of  $\text{H}_2\text{O}$ , was estimated to be  $\sim 3\%$  or better.

The results from experiments performed at various total helium pressures are shown in Tables I and II. Of considerable interest here is the observed pressure dependence for the reaction of OH with both benzene and toluene; also there is the fact that for both compounds rather large  $k$  values were measured at 100 Torr He pressure,  $k_1 = 1.59 \pm 0.12 \times 10^{-12}$  and  $k_2 = 6.11 \pm 0.40 \times 10^{-12} \text{ cm}^3 \text{ molecule}^{-1} \text{ sec}^{-1}$ . In each case, the bimolecular rate constants reported were obtained from the slope of a plot of the pseudo-first-order rate constant  $k$  vs. the aromatic concentration. The nonzero value for  $k$  at zero reactant pressure represents the loss rate of OH due to diffusion out of the sampling region.<sup>10,11</sup> A close examination of the pressure dependence shown in Tables I and II for benzene and toluene indicates that over the pressure range studied in this work the reported rate constants are in the pressure fall off region for each reaction (e.g., the rate constant is not a true third-order rate constant nor is it a true bimolecular rate). The rate constant reported, therefore, is calculated in the form of a bimolecular rate constant at each total gas pressure employed. To better estimate the high-pressure limiting  $k$  value for these processes, a Lindemann plot ( $1/k$  vs.  $1/p$ ) is given for both aromatics in Figure 1. This figure clearly shows that benzene has a greater pressure dependency than toluene as might be expected; but, somewhat surprisingly, it also indicates that a very significant fraction of the total reaction of toluene with OH proceeds by the addition of OH to the aromatic ring. The evidence here is the fact that the change in the effective bimolecular rate constant from 3 Torr to 100 Torr is nearly a factor of 2. Since only the addition reaction would show a pressure dependence, it is

concluded that at least half of the total reaction is additions. Because of the weak benzyl carbon–hydrogen bond in toluene it is to be expected that some abstraction is also occurring although our data only indicate that the importance of this process is probably less than 50% of the total reaction. The dependence of the bimolecular rate constant on the total pressure for both reactions 1 and 2 can be explained on the basis of OH adding directly to the aromatic ring. A possible explanation for the observed difference in the pressure dependency for the two reactions is the larger number of degrees of freedom available in the case of toluene for stabilization of the transition complex. Figure 1 also indicates that toluene is more reactive than benzene by at least a factor of 4. This can be explained by the higher efficiency of the addition process for reaction 2, but also important, as indicated above, is the fact that reaction 2 can proceed by abstraction as well as by addition. The second process would involve abstracting a hydrogen atom from the methyl group on toluene.

There has been much speculation as to whether OH only abstracts the  $\alpha$  hydrogens of branched aromatics or whether addition to the ring is possible. This study indicates that the addition process is very important for toluene and will therefore have a very significant effect on the product distribution resulting from reaction 2.

Concerning the possible role of aromatics in smog formation, an examination of Figure 1 would indicate that at near atmospheric pressure (for the case of  $M = \text{He}$ ) the respective rate constants for processes 1 and 2 would probably be very close to their 100-Torr values,  $1.59 \times 10^{-12}$  and  $6.11 \times 10^{-12} \text{ cm}^3 \text{ molecule}^{-1} \text{ sec}^{-1}$ . Using an estimated OH steady-state concentration for the atmosphere of  $5 \times 10^6$  molecules/cc would therefore give a  $1/e$  lifetime for benzene and toluene of  $\sim 36$  and  $10$  hr under daylight conditions. (This would probably be even shorter if rate constants for  $M = \text{N}_2$  were to be used.) From these simple calculations, along with available concentration data, aromatic compounds would now appear to contribute to the formation of photochemical smog in areas involving heavy automobile traffic.

**Acknowledgment.** The authors of this paper thank Mr. Gene Machado and Mr. Steve Wagner for assisting in carrying out several of the experimental measurements reported in this work.

## References and Notes

- (1) N. R. Greiner, *J. Chem. Phys.*, **46**, 2795 (1967).
- (2) N. R. Greiner, *J. Chem. Phys.*, **53**, 1070 (1970).
- (3) E. D. Morris, Jr., D. H. Stedman, and H. Niki, *J. Amer. Chem. Soc.*, **93**, 3570 (1971).
- (4) N. R. Greiner, *J. Chem. Phys.*, **53**, 1284 (1970).
- (5) J. N. Bradley, W. Hack, K. Hoyerman, and H. Gg. Wagner, *J. Chem. Soc., Faraday Trans. 1*, **69** (11) 1889 (1973).
- (6) I. W. M. Smith and R. Zellner, *J. Chem. Soc., Faraday Trans 1*, **69**, 1617 (1973).
- (7) N. R. Greiner, *J. Chem. Phys.*, **46**, 3389 (1967).
- (8) R. A. Gorse and D. H. Volman, *J. Photochem.*, in press.
- (9) J. H. Seinfeld, T. A. Hecht, and P. M. Roth, EPA Report No. EPA-R4-73-031, Research Triangle Park.
- (10) D. D. Davis, R. Klemm, and M. Pilling, *Int. J. Chem. Kinet.*, **IV**, 367 (1972).
- (11) D. D. Davis, R. Schiff, and S. Fischer, *J. Chem. Phys.*, **61**, 2213 (1974).
- (12) This author wishes to acknowledge the support of this research by the Environmental Protection Agency.

Chemistry Department  
University of Maryland  
College Park, Maryland 20742

D. D. Davis\*<sup>12</sup>  
W. Bollinger  
S. Fischer

Received August 7, 1974

# From the borders of organic chemistry . . . To the borders of theoretical physics:

Inorganic Chemistry brings you a broad range of authoritative information presenting both experimental and theoretical studies in all phases of inorganic chemistry.

Each month, this rapidly growing journal brings you the data you need on synthesis and properties of new compounds, quantitative studies regarding structure, and thermodynamics of inorganic reactions.

When you've seen the 50 or more papers offered in each issue, you'll also want to look through the Notes and Correspondence sections for their concise exchange of scientific views and ideas.

To order INORGANIC CHEMISTRY today, just complete and return the form below.



... another ACS service

## Inorganic Chemistry



**Inorganic Chemistry**  
**American Chemical Society**  
1155 Sixteenth Street, N.W.  
Washington, D.C. 20036

**1975**

Yes, I would like to receive INORGANIC CHEMISTRY at the one-year rate checked below:

	U.S.	Canada	Latin America	Other Nations
ACS Member Personal-Use One-Year Rate	<input type="checkbox"/> \$18.00	<input type="checkbox"/> \$22.00	<input type="checkbox"/> \$22.00	<input type="checkbox"/> \$22.50
Nonmember	<input type="checkbox"/> \$72.00	<input type="checkbox"/> \$76.00	<input type="checkbox"/> \$76.00	<input type="checkbox"/> \$76.50
Bill me <input type="checkbox"/>	Bill company <input type="checkbox"/>	Payment enclosed <input type="checkbox"/>		

Name

Street  Home   
Business

City  State  Zip

Journal subscriptions start on January '75



# Transform your T-60 for <sup>13</sup>C spectra with a Nicolet TT-7 pulsed FT system.

You can update a T-60 for <sup>13</sup>C measurements at a fraction of the cost of a new, dedicated system with the Nicolet TT-7 pulsed FT nmr accessory. The sensitivity provided by this combined system is comparable to that of instruments specifically designed for <sup>13</sup>C spectroscopy. Features offered with the TT-7/T-60 combination include:

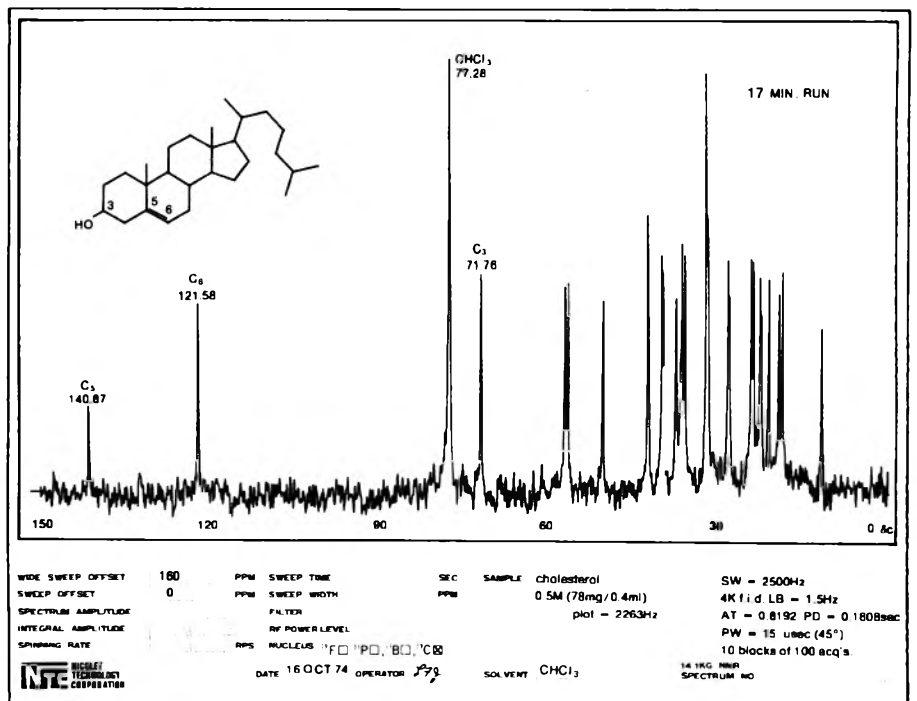
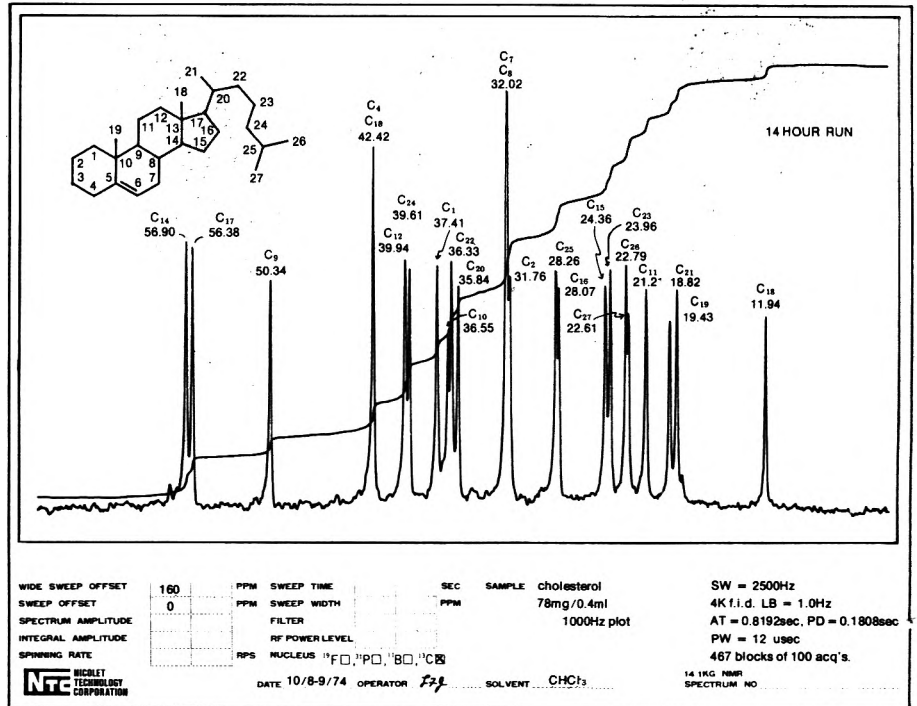
- <sup>13</sup>C spectra on 50 mg samples in 15 minutes;
- 6.5 mm sample size;
- no lock material required (expensive deuterated solvents are not required);
- long-term runs of 12 hours or more are made possible through computer peak registration techniques which compensate for field drifts;
- decoupling accessory for selective proton decoupling, noise decoupling, and gated decoupling;
- expandable to 16K transform size;
- optional T<sub>1</sub> (relaxation time) measurements unattended using multi-pulse inversion recovery techniques.

Signal input, accumulated free induction decays, or transformed spectra can be displayed on the TT-7's cathode ray tube for visual monitoring. The spectra can be plotted using the T-60 recorder and digital integration of spectra can be viewed or plotted as well.

The TT-7's ease of use is incomparable. Not only will it provide increased sensitivity and/or sample throughput of your T-60, but it will also provide an excellent Fourier transform training facility. The basic TT-7 system will provide computer calculations of theoretical nmr spectra of up to six spins.

Phone or write today for more detailed information.

**NTC NICOLET TECHNOLOGY CORPORATION**  
 145 East Dana Street  
 Mountain View, California 94041  
 Phone: 415/969-2076  
 (formerly Transform Technology Inc.)



7 13C 2518